

THE UNIVERSITY OF SHEFFIELD

**Polymersome Mediated Delivery of
Mitochondrial Therapeutics to
parkin Mutant Fibroblasts**

by

Guy Yealland

A thesis submitted in partial fulfillment for the
degree of Doctor of Philosophy

in the

Faculty of Pure Sciences
Department of Biomedical Sciences

March 2015

Declaration of Authorship

I, Guy Yealland, declare that this thesis titled, 'Polymersome Mediated Delivery of Mitochondrial Therapeutics to *parkin* mutant Fibroblasts' and the work presented in it are my own. I confirm that:

- This work was done wholly while in candidature for a research degree at this University.
- Where any part of this thesis has previously been submitted for a degree or any other qualification at this University or any other institution, this has been clearly stated.
- Where I have consulted the published work of others, this is always clearly attributed.
- Where I have quoted from the work of others, the source is always given. With the exception of such quotations, this thesis is entirely my own work.
- I have acknowledged all main sources of help.
- Where the thesis is based on work done by myself jointly with others, I have made clear exactly what was done by others and what I have contributed myself.

Signed:

Date:

*“THE MICROBE is so very small
You cannot make him out at all
But many sanguine people hope
To see him through a microscope.
His jointed tongue that lies beneath
A hundred curious rows of teeth;
His seven tufted tails with lots
Of lovely pink and purple spots,
On each of which a pattern stands,
Composed of forty separate bands;
His eyebrows of a tender green;
All these have never yet been seen—
But Scientists, who ought to know,
Assure us that it must be so...
Oh! let us never, never doubt
What nobody is sure about!”*

Hilaire Belloc

THE UNIVERSITY OF SHEFFIELD

Abstract

Faculty of Pure Sciences
Department of Biomedical Sciences

Doctor of Philosophy

by Guy Yealland

Mutations in *parkin* cause autosomal recessive Parkinsonism and mitochondrial defects. A recent drug screen identified a steroid like class of hydrophobic compounds able rescue mitochondrial function in mutant parkin fibroblasts. These included Ursolic Acid, Ursocholic Acid, and Ursodeoxycholic Acid. pH-sensitive polymersomes, nanoparticles composed of amphiphilic block copolymer, have been shown to encapsulate hydrophobic cargoes, enter cells without detriment to viability and release their cargoes therein. PMPC₂₅–PDPA₆₅ nanoparticles successfully encapsulating drugs were made by thin film rehydration, and purified by hollow fibre filtration. High encapsulation efficiencies were revealed by HPLC. Particle characterisation by and Transmission Electron Microscopy revealed a spectrum of morphologies, including spherical particles, branched tubular assemblies, and large high genus lyotropic structures. Morphological fractionation was achieved through stepwise centrifugation, and mass quantification showed drug encapsulation increased the relative proportion of tubular assemblies. Polymersomes were found to enter into parkin mutant fibroblasts without cytotoxic induction, or detriment to mitochondrial function as assessed by LDH release, mitochondrial membrane potential and cellular ATP levels. Drug loaded polymersomes of both spherical and tubular morphology increased cellular ATP levels of parkin mutant fibroblasts, and were found to deliver a fluorescent steroid at least as effectively as DMSO. The results presented here suggest PMPC-PDPA nanoparticles are suitable for use as a therapeutic vector in *parkin* mutant cells. The production of spherical and tubular nanoparticle morphologies would be of interest to *in vivo* applications, each being known to show distinct properties affecting nanoparticle distribution within the body.

Acknowledgements

A great many people have helped me through this project, both in academic and personal terms, and I would like to thank them all here. First and foremost, my thanks go to (in alphabetical order) Beppe, Heather and Oliver. I would thank them for taking me on, keeping me on and seeing me through to the end of the project. They greatly reduced the time I spent turning in work related circles, and kept me on track.

From the Battaglia group I would like to thank James, Mila, Gavin, Luca, Silvia, Margaret, Jackie, Russell, Priya, Jeppe, Carla, Adrain, Denis, Irene, Nick, Jens, Nisa, and Joe, all my friends, and all my mentors. It was an excellent melting pot of cultures I took a lot of pleasure in being a part of, and likely a wasted opportunity to improve foreign language skills.

From the Bandmann group I would like to thank Marcus, Lisa and Pip for their scientific input, and their ongoing friendship. From SITraN I would like to thank Dave, Alex, Lynn, Matt, Chris, Nadhim and Adrian for their many advices, and the rest of the institute for the sense of community, and friendship. They are an extremely personable collection of people, and one I would hope to keep contact with for a long time.

I would also like to thank Svet and Chris from the Biological Sciences EM suite, Sue from the Med schools FACs facility, and Rob from the department of Chemistry's Chromatography facility. Thanks of course also go to the technical team at SITraN, to Anne and Kim in particular, as well as Jackie, the Battaglia group technician.

Special thanks must be given to Jeppe Madsen and Nicholas Warren for synthesising and supplying all the copolymer used in this project, and to Heather Mortiboys for teaching and watching over my cell culture work.

I would also mention the philosophers, baker, yoga teacher and climbers who were so kind to me throughout. Finally, my thanks go to Laura, both for supporting me and for sharing me with this PhD.

List of Publications

Robertson, J. D., Yealland, G., Avila-Olias, M., Chierico, L., Bandmann, O., Renshaw, S. A, & Battaglia, G. (2014). pH-Sensitive Tubular Polymersomes: Formation and Applications in Cellular Delivery. *ACS Nano*, 8, 4650–4661.

Contents

Declaration of Authorship	iii
Abstract	v
Acknowledgements	vi
List of Publications	vii
List of Figures	xiii
List of Tables	xv
1 Introduction	1
1.1 Parkinson's Disease	1
1.1.1 Current clinical and experimental therapeutic strategies for Parkinson's Disease	2
1.1.2 The Mitochondria	4
1.1.3 Mitochondrial dysfunction in PD	9
1.1.3.1 The genetics of Parkinson's Disease implicate mitochondrial dysfunction	11
1.1.3.2 Rectifying the mitochondrial dysfunction in Parkinson's Disease	17
1.1.4 Ursolic acid, Ursodeoxycholic acid and Ursocholic acid	19
1.1.4.1 Drug distribution to the Brain	23
1.2 Polymersomes & Drug Delivery	30
1.2.1 Drug Delivery	31
1.2.1.1 Hydrophilic surface chemistry	31
1.2.1.2 Particle size	33
1.2.1.3 Particle tensile strength and shape	34
1.2.1.4 Nanoparticle ligand functionalisation	35
1.2.1.5 Targeting the CNS	36

1.2.1.6	Penetrating the cell membrane	40
1.2.1.7	Tuning nanoparticle for cellular uptake	42
1.2.1.8	Environmentally sensitive block co-polymers and intracellular cargo release	45
1.2.2	Controlling the shape and size of amphiphilic diblock copolymer assemblies	47
1.2.2.1	Packing factor determines assembly structure	48
1.2.2.2	Lyotropic phases	49
1.2.2.3	Copolymer size determines membrane properties	51
1.2.2.4	Method of formation determines vesicle size	51
1.3	Project aims and objectives	54
1.3.1	Objectives of Chapter 3: Drug Loaded Polymersomes	54
1.3.2	Objectives of Chapter 4: Suitability of PMPC-PDPA polymersome use in <i>parkin</i> mutant fibroblasts	55
1.3.3	Objectives of Chapter 5: Polymersome mediated delivery of mitochondrial therapeutics to <i>parkin</i> mutant fibroblasts	55
2	Materials and Methods	57
2.1	Materials	57
2.1.1	Block Co-Polymer	57
2.1.2	Organic Solvents	58
2.1.3	Small Molecules	59
2.1.4	Primary Human Dermal Fibroblasts	59
2.1.5	Cell Culture	60
2.1.6	Physiological Assays	60
2.2	Methods	61
2.2.1	Formation of Polymersomes by pH switch	61
2.2.2	Formation of loaded and unloaded Polymersomes by Thin Film Rehydration	61
2.2.3	Centrifugal Fractionation of PMPC-PDPA nanoparticles	62
2.2.4	Nanoparticle characterisation	62
2.2.4.1	<i>Dynamic Light Scattering</i>	62
2.2.4.2	<i>Transmission Electron Microscopy</i>	64
2.2.4.3	<i>Fluorescence emission spectrophotometry</i>	64
2.2.4.4	<i>High Performance Liquid Chromatography</i>	65
2.2.5	Purification by Hollow Fibre Filtration	68
2.2.6	Primary Fibroblast Culture	70
2.2.7	Physiological Assays	70
2.2.7.1	<i>Lactate Dehydrogenase release assay</i>	71
2.2.7.2	<i>Mitochondrial Membrane Potential assay</i>	72
2.2.7.3	<i>Cellular ATP Levels</i>	75
2.2.7.4	<i>Polymersome uptake assays</i>	76
2.2.8	Statistical analysis	77
3	Results: Drug Loaded Polymersomes	79

3.1	Aims	79
3.2	Background	79
3.3	Thin film rehydration of PMCP ₂₅ –PDPA ₆₅	80
3.4	Formation, purification and characterisation of PMPC ₂₅ –PDPA ₆₅ nanoparticles encapsulating tetracyclic and pentacyclic compounds	87
3.5	Discussion	94
3.6	Conclusion	99
4	Results: Suitability of PMPC-PDPA polymersome use in <i>parkin</i> mutant fibroblasts	101
4.1	Aim	101
4.2	Background	101
4.2.1	Exacerbation of mitochondrial defects in fibroblasts	104
4.3	Uptake of PMPC-PDPA polymersomes by <i>parkin</i> mutant fibroblasts	104
4.3.1	Characterisation of rhodamine labelled polymersomes	104
4.3.2	Uptake of polymersomes formed by pH switch and the effect of fibroblast metabolic state	106
4.3.3	Uptake of PMPC-PDPA nanoparticles formed by thin film rehydration	108
4.3.4	Uptake of polymersomes formed by thin film rehydration of PMPC ₂₅ –PDPA ₆₅ synthesised by RAFT	112
4.3.5	Inter-experimental comparison	117
4.4	Effects of PMPC-PDPA polymersomes on fibroblast viability and mitochondrial physiology	118
4.4.1	Polymersome characterisation	118
4.4.2	Assessment of potential polymersome induced toxicity	119
4.4.3	Fibroblast Mitochondrial Membrane Potential	121
4.4.4	Assessment of fibroblast ATP levels in the presence of polymersomes	124
4.5	Discussion:	127
4.6	Conclusions	131
5	Results: Polymersome mediated delivery of mitochondrial therapeutics to <i>parkin</i> mutant fibroblasts	133
5.1	Aim	133
5.2	Background	133
5.3	Rescue of <i>parkin</i> mutant fibroblast ATP levels using drug loaded polymersomes	136
5.3.1	Characterisation of drug loaded polymersomes	136
5.3.2	Therapeutic effect of drug loaded polymersomes	137
5.4	Delivery efficiency of steroid like compounds by PMPC ₂₅ –PDPA ₆₅ polymersomes	141
5.4.1	Characterisation of DHE loaded polymersomes	141

5.4.2	Polymersome mediated DHE delivery to fibroblasts	142
5.4.3	Discussion	147
5.5	Conclusions	152
6	Discussion & future directions	153
6.1	Project findings	153
6.2	Implications for the treatment of Parkinson's Disease	156
6.2.1	Therapeutic effect <i>in vitro</i>	156
6.2.2	Therapeutic effect <i>in vivo</i>	158
6.2.2.1	Potential of UA, UCA and UDCA in the treatment of Parkinson's Disease	158
6.2.2.2	Potential of tubular nanoparticles to enhance drug distribution to the brain	160
6.3	Conclusion	164
	Bibliography	167

List of Figures

1.1	Mitochondrial OXPHOS and ROS generation	6
1.2	Summary of pathogenic pathways in Parkinson's disease involving the mitochondria	12
1.3	Hexa-, Penta- and Tetra- cyclic mitochondrial therapeutics	24
1.4	The Blood Brain Barrier	26
1.5	Polymersome schematic	30
1.6	Endocytic pathways	43
1.7	pH sensitivity of Poly-(2methacryloyloxy -ethylphosphorylcholine)-poly(2 -(diisopropyl -amino)ethyl methacrylate) (PMPC-PDPA)	46
1.8	Amphiphile packing parameter correlates assembly morphology	49
1.9	Phase diagram of a diblock copolymer	50
1.10	Diblock copolymer membrane properties scale with amphiphile size	51
1.11	Vesicle size varies with methods of polymersome formation	53
2.1	Small molecules	59
2.2	R.6G-PMPC-PDPA fluorescence standard curves	65
2.3	HPLC Calibration curves	67
2.4	Example HPLC traces	68
2.5	Validation of purification techniques for PMPC-PDPA nanoparticles	69
2.6	Purification of micellar UA by HFF	70
2.7	Optimisation of TMRM incubation periods	74
2.8	Linearity of DNA quantification after ATP bioluminescence assay	76
3.1	Thin film rehydration of PMPC ₂₅ –PDPA ₆₅ produces mixed particle morphologies	83
3.2	Centrifugal fractionation of nanoparticles	86
3.3	Drug loaded PMPC ₂₅ –PDPA ₆₅ nanoparticles	88
3.4	Long term stability of drug loaded “Polymersomes” and “tubes”	89
3.5	Cholesterol incorporation alters PMPC ₂₅ –PDPA ₇₂ nanoparticle morphology	90
3.6	Relative masses of morphological fractions present within populations of drug loaded PMPC ₂₅ –PDPA ₆₅ nanoparticles during formation	92
3.7	Image analysis of empty and 5% cholesterol loaded PMPC ₂₅ –PDPA ₆₅ nanoparticles	93
4.1	Rhodamine labelled nanoparticle characterisation	105

4.2	Polymersome uptake in fibroblasts cultured in different sugar substrates	107
4.3	Growth curves of <i>parkin</i> mutant and control fibroblast	107
4.4	Effect of Polymersome concentration on internalisation	109
4.5	DNA content of fibroblasts incubated with polymersomes	111
4.6	Rapid binding, but slow internalisation of TFR formed PMPC-PDPA nanoparticles	113
4.7	Fibroblast internalisation of Rhodamine labelled polymersomes	115
4.8	Effect of cell number on nanoparticle internalisation	116
4.9	Inter-experimental comparison of TFR and pH switch formed polymersomes uptake in fibroblasts	118
4.10	PMPC-PDPA polymersomes characterisation	119
4.11	LDH release assay pilot	120
4.12	Effect of Polymersome incubation on fibroblast LDH release	121
4.13	Mitochondrial membrane potential assay pilot	123
4.14	The effect of Polymersomes on fibroblast MMP	124
4.15	Cellular ATP assay pilot	125
4.16	The effect of Polymersomes on fibroblast ATP levels	126
5.1	Characterisation of UA and UCA loaded polymersomes for therapeutic assays	137
5.2	Increased cellular ATP of healthy and <i>parkin</i> mutant fibroblasts following incubation with drug loaded PMPC ₂₅ –PDPA ₆₅ nanoparticles	139
5.3	DHE loaded nanoparticle characterisation	142
5.4	Flow cytometry settings for DHE delivery experiments	144
5.5	Delivery efficiency of nanoparticle formulated DHE to fibroblasts following 24 and 48 incubation	145
5.6	Comparison of “Polymersome” and “Tubular” fractions efficiency in delivering DHE	147

List of Tables

2.1	PMPC-PDPA batches	57
2.2	Fibroblasts	60
3.1	Drug loaded nanoparticle concentrations	87
4.1	Percentage of fibroblasts demonstrating Rhodamine 6G labelled PMPC-PDPA (R.6G-PMPC-PDPA) fluorescence	109
4.2	Linearity of polymersome concentration on magnitude of uptake	114
5.1	Intracellular ATP levels of <i>parkin</i> mutant fibroblasts following treatment with UA or UCA formulated in nanoparticles or DMSO	140
5.2	Percentage of cells demonstrating Rh.6G-PMPC-PDPA and/or DHE fluorescence following incubation with DHE formulations	146

- AD** Alzheimer's Disease
- ADP** Adenosine Diphosphate
- ALS** Amyotrophic Lateral Sclerosis
- APAF1** Apoptotic protease activating factor 1
- APP** amyloid precursor protein
- ATP** Adenosine Triphosphate
- ATRP** Atom Transfer Radical Polymerisation
- BBB** Blood-Brain Barrier
- BCB** Blood-CSF Barrier
- BSA** Bovine Serum Albumin
- CAC** Critical Aggregation Constant
- CCCP** carbonyl cyanide 4-(trifluoromethoxy)phenyl-hydrazone
- CNS** Central Nervous System
- CoQ10** Coenzyme Q10
- CSF** Cerebro Spinal Fluid
- DHE** Dehydroergosterol
- DLS** Dynamic Light Scattering
- DMEM** Dulbeccos Modied Eagle's Medium
- DMSO** Dimethyl Sulfoxide
- DPA** 2-(diisopropylamino)ethyl methacrylate
- DUA** dehydro (11,12) ursolic acid lactone
- EB** poly(ethylene oxide)copoly(butylene oxide)
- ELSD** Evaporative Light Scattering Detection
- EM** Electron Micrographs

-
- ENS** Enteric Nervous System
- EPR** Enhanced Permeability Retention
- ETC** electron transport chain
- FBS** Foetal Bovine Serum
- Fbxo7** F-box only protein 7
- FDA** Federal Drug Administration
- FXR** farnesoid X receptor
- GBA** beta-glucocerebrosidase
- GD** Gaucher's Disease
- GPC** Gel Permeation Chromatography
- GPCR** G Coupled Protein Receptor
- GPx-1** Glutathione peroxidase 1
- GR** Glucocorticoid Receptor
- GRE** Glucocorticoid Response Element
- GWAS** Genome Wide Association Studies
- HDF** Human Dermal Fibroblast
- HFF** Hollow Fibre Filtration
- HPLC** High Performance Liquid Chromatography
- IMM** inner mitochondrial membrane
- IMS** inter membranous space
- ISF** Inter-stitial Fluid
- KO** knock-out
- LB** Lewy Bodies
- LDH** Lactate Dehydrogenase

LDL Low Density Lipoproteins

Lf Lactoferrin

LHON Leber's Hereditary Optic Neuropathy

Log-P Octanol-Water Partition co-efficient

XLog-P predicted partition co-efficients

LRP LDL receptor-related protein

LRRK2 Leucine-rich repeat kinase 2

MAPT Microtubule Associated Protein Tau

MCCC1/LAMP3 Methylcrotonoyl-CoA Carboxylase 1/Lysosomal-Associated Membrane Protein 3

MELAS Myoclonus-Epilepsy-Lactic Acidosis-Stroke syndrome

MEM Minimum Essential Media

MeOH Methanol

MitoQ Mitoquinone

MMP Mitochondrial Membrane Potential

MOI Multiplicity of Infection

mPEG-PCL methoxy poly(ethylene glycol)poly(caprolactone)

MPTP 1-methyl-4-phenyl-1,2,5,6-tetrahydropyridine

MQ MilliQ filtered water

MRs Mineralcorticoid Receptors

mtDNA mitochondrial DNA

mtPTP mitochondrial permeability transition pore

MTS mitochondrial targetting sequence

MW Molecular Weight

- MWCO** Molecular Weight Cut Off
- NADP(H) Oxidase** Nicotinamide adenine di-nucleotide phosphate Oxidase
- NMR** Nuclear Magnetic Resonance
- NRF** Nuclear respiratory factor
- OMM** outer mitochondrial membrane
- OXPHOS** mitochondrial Oxidative Phosphorylation
- PARIS** Parkin interacting substrate
- PBS** Dulbecco's Phosphate Buffered Saline
- PD** Parkinson's Disease
- PDI** Polydispersity Index
- PDMS₆₀–PMOXA₂₁** poly(dimethylsiloxane)-poly(2-methyl-oxazoline)
- PEG-PCL** Poly(ethylene glycol)-poly(caprolactone) methyl ether
- PEG-PLA** poly(ethylene glycol)poly(lactic acid)
- PEG-PLGA** poly(ethylene glycol)-poly(lactic-co-glycolic acid)
- PEG** Polyethylene glycol
- PEO** Polyethylene oxide-poly 2-(diisopropylamino)ethyl methacrylate
- PGC1 α** Peroxisome proliferator-activated receptor gamma coactivator 1-alpha
- PGC1** PPR γ coactivator 1
- PINK1** PTEN-induced putative kinase 1
- pKa** acid dissociation constant
- PLGA** Poly(D,L-lactic-co-glycolic acid)
- PMPC** Poly-2-methacryloyloxyethyl phosphorylcholine
- PMPC-PDPA** Poly-(2methacryloyloxy -ethylphosphorylcholine)-poly(2 -(diisopropyl -amino)ethyl methacrylate)

POEGMA-PDPA poly(oligo(ethylene glycol) monomethyl ether methacrylate)-poly(2-(diisopropyl-amino)ethyl methacrylate)

PPAR- γ Peroxisome proliferator-activated receptor gamma

PS1 Presenilin-1

PTA Phosphotungstic acid

R.6G Rhodamine 6G

RAFT Reversible Addition-Fragmentation chain Transfer polymerisation

RCF Relative Centrifugal Force

RES Reticulo-endothelial System

R.6G-PMPC-PDPA Rhodamine 6G labelled PMPC-PDPA

ROS Reactive Oxygen Species

RT Room Temperature

SN Substantia Nigra

SOD Superoxide Dismutase

STK39 Serine Threonine Kinase 39

SYT11/RAB25 Synaptotagmin XI/ras-related protein Rab-25

TEM Transmission Electron Microscopy

TFA Trifluoroacetic Acid

TFR Thin Film Re-hydration

TMRM Tetramethyl rhodamine methyl ester perchlorate

TOM Translocase of the OMM

TTP triphenylphosphonium

UA Ursolic Acid

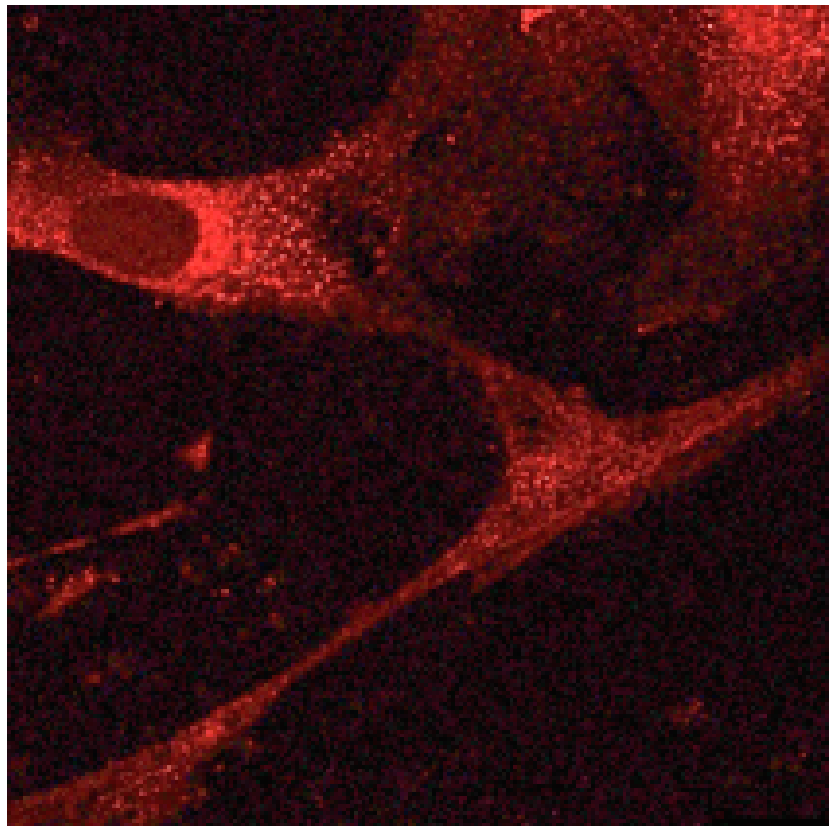
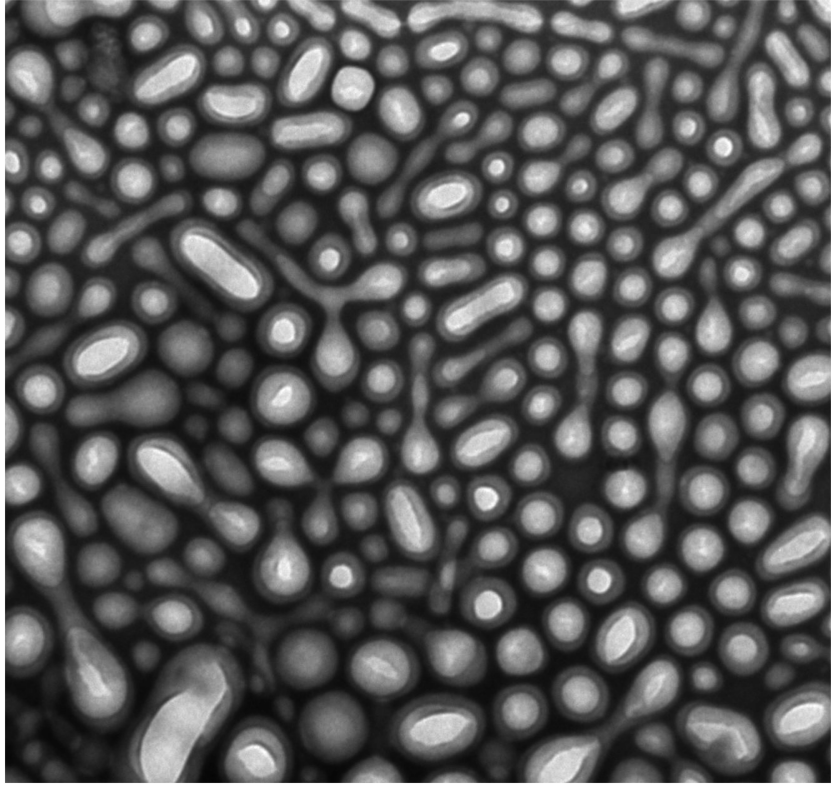
UCA Ursocholic Acid

UDCA Ursodeoxycholic Acid

UV Ultra Violet

wt *wild type*

For my parents



Chapter 1

Introduction

1.1 Parkinson's Disease

Parkinson's Disease (PD) is the second most common neurodegenerative disease, affecting 1% of the western world's population. It most commonly occurs in persons over 60 years of age, and subsequently its prevalence is projected to increase as the aged population continues to grow in the western world [1]. PD is characterised by the progressive loss of voluntary movement, balance, as well as the variable development of non-motor symptoms such as cognitive decline, compulsions and insomnia [2]. The life expectancy of patients is similar to those free of PD and the disease course is typically slow. As the symptoms worsen, increasing levels of therapy and care must be given to manage the disease, which, taken with its prevalence and duration, makes PD a substantial personal, social and economic burden. Currently therapies offer symptomatic relief only. However progress is being made towards understanding the underlying aetiology and developing treatments that will target this directly, to slow or halt the disease course.

Common to all PD is the loss of cells from the Substantia Nigra (SN) of the patient's midbrain, most markedly, pigmented dopaminergic neurons [3, 4]. These neurons form an important part of the basal ganglia, a series of circuits within

the brain that act to permit or deny the initiation of bodily movements. Their loss is believed to underly Parkinsonian impairment to movement. Histopathological studies have also revealed the presence of proteinacious inclusions known as Lewy Bodies (LB) and Lewy Fibrils within surviving neurons of the midbrain and other brain regions [5]. The specific role these play in PD is still debated. Whilst both loss of dopaminergic neurons and the presence of LB is necessary to the histopathological diagnosis of PD, their severity varies greatly between patients and may occur independently of one another. For instance, mutations in *parkin* cause a familial Parkinsonism typically absent of LB [6], whilst dementia with LB may present without Parkinsonian features [7].

1.1.1 Current clinical and experimental therapeutic strategies for Parkinson's Disease

Therapies in current clinical use for PD aim to replace or compensate the loss of dopaminergic neurons, which though failing to address the ongoing neurodegeneration, are effective in alleviating some PD symptoms. Medication artificially raising levels of dopamine, or inducing dopamine like activity in the brain has proven effective in relieving motor symptoms [8, 9]. However, long term administration can lead to diminishing therapeutic effect and motor, cognitive and systemic complications [9, 10].

Attempts have been made to replace those neurons lost in the SN. Transplants from neural progenitors to the patient striatum have yielded some positive, though variable results in symptomatic relief [11]. However evidence of true neuron replacement is currently lacking. Further, there is evidence that the existing PD pathology is able to spread from effected cells to those newly introduced, leading to the eventual re-emergence of disease symptoms [12]. Whilst work continues to resolve such issues [13], their complexity and the availability of stem cells will continue to hold back this approach.

Other currently experimental approaches aim to slow or prevent the on-going neurodegeneration in PD. Neurotrophic factors are small proteins that have long been recognised as a potential therapeutic agent for neurodegenerative disorders, exerting pro-survival effects and inducing neuronal growth [14]. As neurotrophic factors are unable to penetrate into the Central Nervous System (CNS) from systemic circulation, application directly into the brain is necessary. Whilst infusion via catheter to the striatum of PD animal models has proven effective in preventing loss of dopaminergic cells and motor function, similar attempts in humans have been inconsistent, possibly due to greater populations of neurotrophic factor receptors, greater brain volume and/or method of administration [15, 16]. New human trials are currently underway in which implants will be used to improve the delivery of promising neurotrophic factors to the desired site of action. It is hoped this will resolve previous inconsistencies in clinical trials [17].

Therapies that target the brain from routes of administration that avoid externally penetrating the brain will be both less dangerous to the individual and easier to implement. Recombinant genes packaged within modified viruses are being explored as a way to locally and specifically up- or down- regulate disease-modifying proteins *in vivo* [18]. Though the effects of gene therapies do vary, particularly in mitotic cells, their duration of effect and potential efficacy greatly exceeds many exogenous therapies. There are however certain safety complications associated with the use of modified viruses, including increasing immunogenicity with repeated use, infection of inappropriate tissue and cytotoxicity. Appropriate modifications and tailored dosing can limit or remove these and numerous human trials have proven various viral therapies to be both safe and therapeutically effective [19, 20]. Data from an ongoing clinical trial using lentiviral vectors loaded with three genes encoding dopamine synthesising enzymes has shown both good long term safety profiles and symptomatic improvement in PD patients, succeeding where single gene approaches have failed [19, 21]. Though administration occurred by direct injection into patient midbrains, benefits were seen 6 months after treatment, suggesting long term effects of gene translation. This approach again targets the loss of dopamine in

PD rather than the cause of neurodegeneration. Gene therapies for PD based on neurotrophic factors have so far proved safe in clinical trials, but lack the necessary therapeutic efficacy even following direct injection into the SN to be of clinical use [19].

Though PD is primarily a sporadic disorder with no one clear cause, investigation of environmental and genetic factors linked to the disease have brought to light a number of molecular pathways now implicated in the pathogenesis [22, 23]. Potential therapeutic targets that could slow or prevent the progressive neurodegeneration seen in PD have subsequently been identified. Great efforts have gone into finding small molecules that affect one or more of these targets, demonstrate therapeutic action, and which are able to penetrate the brain from systemic circulation. Whilst compounds may appear effective in disease models, they frequently fail to enter into clinical relevance. Two possible reasons for this are (1) the models of PD used do not accurately represent the disease in human patients, and (2) that the small molecules are unable to accumulate within the brain at therapeutically relevant concentrations. Herein the role of mitochondrial dysfunction in PD and the therapeutic potential of therapies that target this are discussed.

1.1.2 The Mitochondria

Mitochondria are a semi-continuous organelle found in almost all eukaryotic cells, whose predominant role is to enhance the cells Adenosine Triphosphate (ATP) production capacity, the cells primary “energy currency” [24]. They also regulate and/or take part in a number of physiological pathways. Mitochondria are double membraned compartments, the outer mitochondrial membrane (OMM) being planar and the inner mitochondrial membrane (IMM) extending tubular protrusions into the mitochondrial lumen, also known as the matrix. At

the μm scale, they appear throughout the cell as a highly dynamic network undergoing continuous “fusion”¹ and “fission”² [25, 26].

Mammalian cells are able to produce ATP by glycolysis, a series of cytosolic reactions that convert sugars such as glucose or lipid metabolites to pyruvate, generating ATP and NADH molecules in the process [27]. Following glycolysis, pyruvate can be transported into the mitochondrial matrix, where it, along with a number of other metabolites, enter the citric acid cycle (also known as the Krebs cycle) to produce NADH and FADH_2 . FADH_2 is also produced by β oxidation of fats. NADH and FADH_2 are respectively oxidised by complexes I (also known as NADH dehydrogenase) and II (also known as succinate dehydrogenase), protein complexes imbedded within the IMM, to NAD^+ and FAD. Their freed electrons are passed into the complexes initiating the mitochondrial electron transport chain (ETC). The respiratory complexes undergo a number of redox reactions, passing electrons along their subunits sequentially, driving the translocation of H^+ ions into the inter membranous space (IMS) as they do so. Electrons are then passed to Coenzyme Q10 (also known as ubiquinone), which in turn transfers them to Complex III (also known as coenzyme Q oxidoreductase), and a further series of redox reactions take place, driving more H^+ ions into the IMS. Complex III transfers electrons to cytochrome C which in turn passes them to Complex IV (also known as cytochrome C oxidase). Finally Complex IV transfers electrons to split O_2 molecules, producing two water molecules and driving the import of yet more H^+ cations into the IMS. The large proton gradient generated by the ETC, the Mitochondrial Membrane Potential (MMP), is utilised by Complex V (also known as ATP synthase) to generate ATP molecules. Protons diffuse into the IMS facing pore of Complex V and translocate through the complex into the mitochondrial matrix, driving conformational changes that catalyse the anabolism of Adenosine Diphosphate (ADP) and inorganic phosphate bound to the complex’s matrix face. This process is collectively known as mitochondrial Oxidative Phosphorylation (OXPHOS) (summarised in figure

¹Mitochondrial fusion; in which separate mitochondrial sections combine

²Mitochondrial Fission; in which a section of mitochondria splits and separates

1.1), and generates ATP with great efficiency. A single glucose molecule will for instance provides enough energy to generate 36 ATP molecules [27]. Some heat is also generated as a by product as a result of ineffective electron transfers, and electron flow back to the matrix when not through Complex V. Matrix ATP and cytosolic ADP are then exchanged, and the ATP is used throughout the cell where the catalysed transfer of its phosphates to various cell components induce conformational and chemical changes that regulate many physiological processes.

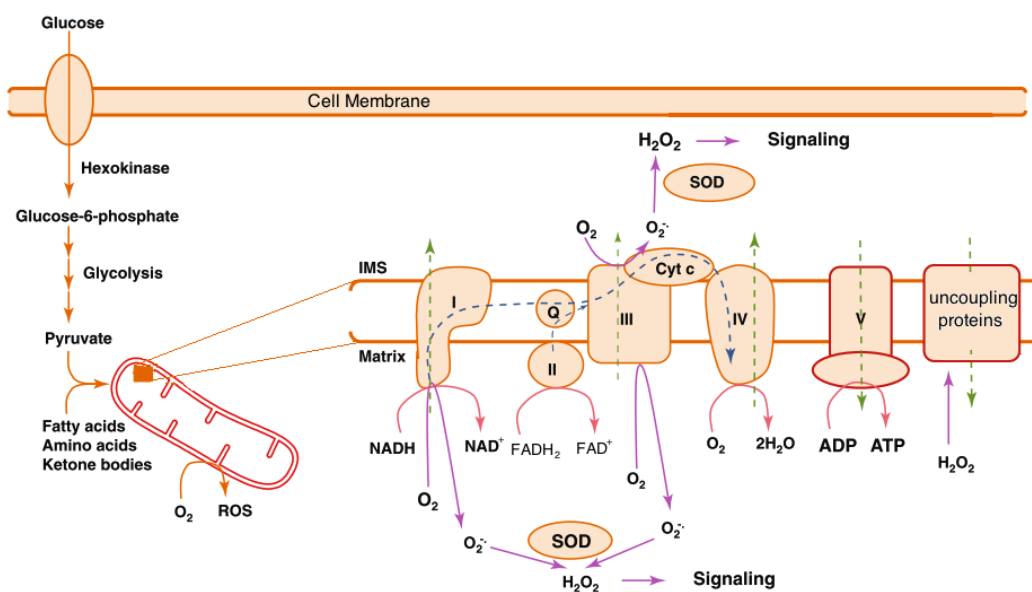


FIGURE 1.1: **Mitochondrial OXPHOS and ROS generation:** Orange arrows show glycolysis, purple arrows show ROS generation and handling, pink arrows show products of reactions with respiratory complexes, dashed blue line shows flow of electrons through the ETC, and dashed green lines show the flow of protons. Adapted from Mailloux and Harper 2012, with permission [33]

OXPHOS can be modified for specific cellular processes, for instance proteinaceous uncouplers may be inserted into the IMS, allowing protons to leak back into the matrix decreasing Complex V derived ATP production. Mitochondrial uncoupling increases the mitochondrial OXPHOS kinetics, and generates more heat than when the ETC is tightly coupled, as seen in thermogenic brown adipose tissue [28]. Uncoupling may also limit the production of Reactive Oxygen Species (ROS), Ca²⁺ of which the mitochondria are the primary generators.

Electrons transported through the respiratory complexes are capable of “leaking” out of the ETC, directly to oxygen creating O_2^- [29, 30]. This typically occurs from complexes I, III or coenzyme Q10. Mutations causing loss of OXPHOS capacity have been shown to increase mitochondrial ROS generation [31, 32]. Oxygen radicals can be converted into the less reactive H_2O_2 by Superoxide Dismutase (SOD) enzymes, which in turn can be converted to water by cytosolic or mitochondrial Glutathione peroxidase 1 (GPx-1). There are also a number of free radical scavengers present within the cell such as glutathione which sequester excesses of free radicals. Whilst ROS generation is natural and indeed plays important roles in signalling pathways, excesses beyond a cell’s antioxidant capacity can lead to cumulative damage to DNA among other cellular components and eventually lead to cell death [33]. Certain uncoupling proteins are activated by ROS and/or their by-products [34], inducing a proton leak that associates decreased ROS production, however the physiological relevance of this contentious [33, 35].

Mitochondria act as an important, though relatively small reservoir for Ca^{2+} ions, a second messenger that must be kept at low concentrations in the cytosol to correctly regulate its actions [36]. Mitochondria along with other calcium stores have been found in close apposition to sites of high calcium flux such as neural synapses, where its buffering role has a significant effect despite its limited capacity and calcium uptake kinetics [37]. Calcium is also known to induce ATP production, despite the MMP lowering effect of introducing a cation to the matrix, allowing Ca^{2+} to couple regions of high energy demand to high ATP production in the mitochondria [38]. Calcium overload in the mitochondria has, however been observed to lead to excess ROS generation and opening of the mitochondrial permeability transition pore (mtPTP), which allows the dissipation of matrix ions and the MMP, as well as the release of pro-apoptotic factors [39, 40].

Permeabilisation of the OMM results in the release of IMS proteins including pro-apoptotic factors such as cytochrome c and Apoptotic protease activating factor 1 (APAF1), which activate the caspase cascade that ultimately results

in “cell suicide” [41]. Mitochondria and mitochondrial health are thus essential to cell survival, even in cells relatively independent of OXPHOS generated ATP. Numerous proteins act as regulators of mitochondrial permeability including Bcl-2 and Bcl-XL [42]. It is also notable that both pro- and anti- apoptotic proteins are involved in other aspects of mitochondrial physiology [43].

During apoptosis, the mitochondrial network fragments as it undergoes extensive fission [42]. Numerous proteins are involved in the fusion and fission of the mitochondrial network, and mutations are seen to cause impaired energy production and specific neurodegenerative diseases [25]. There are indications mitochondrial dynamics play a part in normal energy metabolism. For instance widespread fusion is seen under cellular stress and accompanies increased intracellular ATP content, perhaps the result of improved distribution of various respiratory components [44]. Dynamics also play an important role in the mobility of mitochondria through the cell, such as in neurons where mitochondria must present at numerous distant locations of changing energetic need [45]. It also allows discrete sections of damaged mitochondria to be sequestered by fission from the bulk organelle, and targeted for autophagy in a process known as mitophagy [44, 46].

As defective sections of the mitochondria are removed, so to are new sections created to match the cells energetic needs. This is regulated by numerous factors and requires the concerted transport of lipids and proteins plus mtDNA replication. The PPAR γ coactivator 1 (PGC1) family of proteins are master regulators of mitochondrial biogenesis [47]. Upregulation of PGC1 $-\alpha$ and $-\beta$ have been shown to increase mtDNA synthesis and mitochondrial gene expression [48], whilst inactivation results in decreased expression and mitochondrial function [49]. The PGC family regulate a number of proteins involved in the regulation of mitochondrial genes including Nuclear respiratory factor (NRF) -1 and -2, Peroxisome proliferator-activated receptor gamma (PPAR- γ) which is also involved in lipid homeostasis and estrogen related receptors that also indirectly stimulate mitochondrial biogenesis [50, 51]. Numerous signalling pathways have been shown to induce mitochondrial biogenesis in an at least partly PGC1

dependent manner [52]. These include; the AMPK pathway triggered by low intracellular ATP levels, Ca²⁺ signalling, cAMP signalling, nitrous oxide signalling, and neurotrophic factors.

Though mtDNA encodes for 37 locally transcribed genes, including tRNAs and ETC proteins, the majority of mitochondrial genes are found in the nucleus [53, 54]. These are translated either with one of several mitochondrial targeting sequence (MTS) or close association with a chaperone protein. These are recognised by the Translocase of the OMM (TOM) complex, which initiates their import into the IMS, wherein further sorting occurs [55].

1.1.3 Mitochondrial dysfunction in PD

Many lines of evidence have linked mitochondrial dysfunction as a common point in the pathogenesis of sporadic and familial PD. Early evidence came from work that identified 1-methyl-4-phenyl-1,2,5,6-tetrahydropyridine (MPTP), a brain penetrant neurotoxin that induces atypical Parkinsonism, as an inhibitor of Complex I of the mitochondrial ETC [56, 57]. Subsequently, a specific Complex I deficiency was identified in the post mortem SN of PD patients [58]. Similar deficiencies have now also been identified in the frontal cortex, where evidence has also been found of oxidative damage to both mitochondrial and nuclear Complex I subunits [59, 60]. Complex I inhibitors such as MPTP and rotenone are frequently used to induce Parkinsonian-like loss of dopaminergic neurons in animals to model PD, as is paraquat, a compound found to increase the production of ROS. Indeed, epidemiological links have been established between Parkinsonism and the environmental presence of these and other compounds believed to impact on mitochondrial function, such as found in certain fruits and pesticides [23, 61, 62]. Evidence of mitochondrial deficiencies in tissue other than of the CNS has also been uncovered in a proportion sporadic cases, suggesting underlying genetic or environmental factors [63, 64].

It is notable both that ageing is the single greatest risk factor for PD, and that mitochondrial function declines with age as mutations accumulate within the mitochondrial DNA (mtDNA) [24, 65]. Though there is no strong evidence that mutations in mtDNA are causative of PD, there are indications of their involvement [23]. For instance, mutations in *POLG*, a DNA polymerase that plays an important role in proof reading mtDNA for replication errors, have been shown to co-segregate with PD in some families [66]. Mutations in this gene produce increased accumulation of mtDNA mutations over time. Post mortem analysis of SN from patients with pathogenic mtDNA mutations found widespread deficiencies in complexes I and IV, but marked neuronal loss only in patients with *POLG* mutations [67]. Post mortem analysis of neurons from PD patients has revealed increases in mtDNA mutations relative to controls of dopaminergic neurons of the SN, but not hippocampal or cortical neurons, suggesting a specific vulnerability and sensitivity [68, 69]. Seven of the subunits composing Complex I are encoded in mtDNA, more than double any other complex of the ETC, and could explain why it is more susceptible to mutations.

Mitochondria, as the primary centres for ATP anabolism, the formation and response to ROS, calcium buffering and apoptosis [24], have proven particularly involved in the physiology and pathogenesis of the SN's dopaminergic neurons [70, 71]. Firstly, like all neurons they have a high energy demand to sustain the continuous function of these very long post mitotic cells [70]. Dopaminergic neurons of the SN possess an atypically large and unmyelinated axonal arbor, at least ten fold larger than other dopaminergic neurons, for which it is predicted they have greater energetic demands [72]. It is also notable that mitochondrial biogenesis plays an important role in the maintenance and formation of dendritic processes [73].

Secondly, in contrast to neighbouring dopaminergic neurons, those in the SN are exposed to a continuous influx of calcium due to their spontaneous pace-making activities [74, 75]. It is recognised that calcium promotes mitochondrial oxidative phosphorylation, so may exacerbate mitochondrially related dysfunction [76]. In keeping, dopaminergic neurons of the SN have been shown to

possess greater ROS levels than their neighbours, and that this decreases with attenuated calcium flux [77, 78]. It is also notable that reliance on calcium channels for pace-making activity in the substantia nigra increases with age [77]

Thirdly, cytoplasmic metabolism of dopamine generates both ROS and quinones, though this is largely prevented by transporting dopamine into vesicles [79–81]. Mice with deficient dopamine uptake into presynaptic vesicles demonstrate age related nigrostriatal degeneration with signs of alpha-synuclein inclusions [80]. Mishandling of dopamine could also conceivably occur due to energy deficits. Partial Complex I activity has been shown to increase the presence of its substrate NADH, an inducer of dopamine biosynthesis, and increased susceptibility to toxin induced cytosolic release of dopamine [81–83].

1.1.3.1 The genetics of Parkinson's Disease implicate mitochondrial dysfunction

Whole genome sequencing and linkage analysis of families displaying heritable forms of PD have identified a number of single gene mutations that cause rare forms of PD, from which a number of physiological pathways are now been implicated in the disease pathogenesis (figure 1.2). Roles for the mitochondria and mitochondrial dysfunction have been implicated in almost all of these [23].

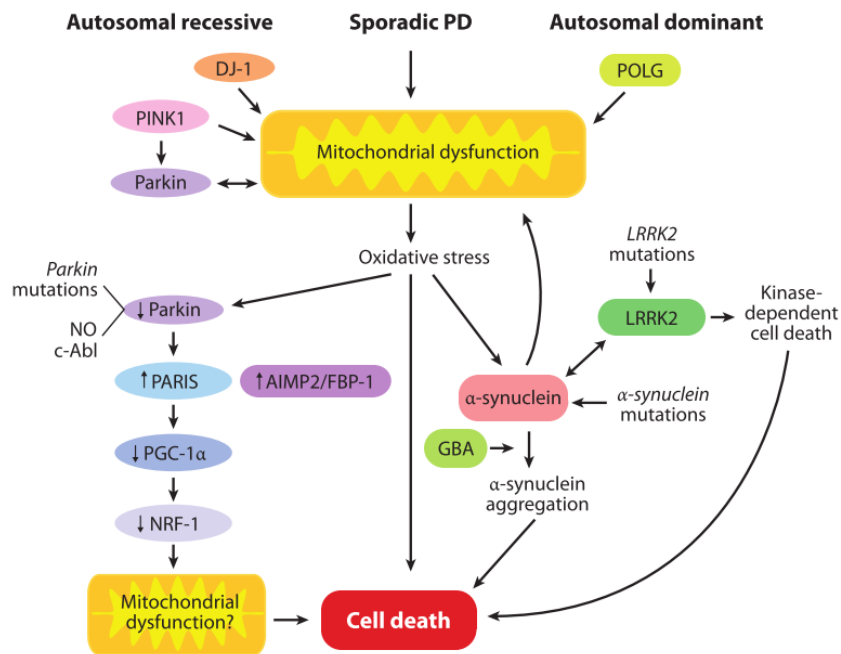


FIGURE 1.2: **Summary of pathogenic pathways in Parkinson's disease involving the mitochondria:** Taken from Martin et al. 2011, with permission [22].

Mutations in PTEN-induced putative kinase 1 (*PINK1*) cause an early onset, autosomal recessive Parkinsonian syndrome demonstrating a clear Complex I deficiency [84–86]. Studies have identified a role for PINK1 in maintaining the functional health of mitochondria. PINK1 is translocated to the IMM where it is degraded [87]. Where MMP is low, a key indicator of an ineffective ETC and mitochondrial dysfunction, PINK1 is instead integrated into the OMM where it plays a role in flagging the organelle for destruction by autophagy; known as mitophagy [88, 89]. PINK1 deficiencies in mice have been shown to enhance the susceptibility of dopaminergic neurons to death by MPTP, and that this can be prevented by expression of *parkin*, *DJ-1* or F-box only protein 7 (*Fbxo7*) [90, 91]. Mutations in *parkin* [92] *DJ-1* [93] and *FBXO7* [94] are also known to cause early onset, autosomal recessive Parkinsonian syndromes similar to those of PINK1.

Tissue from *parkin* mutant PD patients consistently show lowered ATP levels and altered mitochondrial morphology, as well as decreased activity of Complex I and a lowered MMP [95–98]. Oxidatively damaged and misfolded Parkin

has also been found in the brains of sporadic PD patients [99–102]. Parkin, an E3 ubiquitin ligase, is recruited to the mitochondria by PINK1 localised to the OMM, an event necessary for the mitophagy of damaged mitochondria, and which PD causing mutations in *parkin* compromise [103–105]. However the relevance of this to highly energetic cells is questionable. For instance it has been shown that rat midbrain neurons exposed to a highly effective mitochondrial uncoupler, failed to demonstrate Parkin translocation to the mitochondria on loss of MMP [106]. Similarly, while collapse of HeLa cell MMP lead to Parkin-mitochondrial co-localisation in glucose media, the same is not true when incubated in galactose media, an energy substrate which forces cells to depend heavily on mitochondrial OXPHOS for their ATP supply [106, 107]. More recent work has shown Parkin will translocate to depolarised mitochondria in mouse cortical neurons, but only in the absence of antioxidants within the culture media, suggesting a greater mitochondrial deficit is perhaps required to initiate this form of mitophagy in neurons [108].

Concordant to their roles in mitophagy induction, PINK1 and Parkin are also known to alter mitochondrial transport, effecting the dissociation of a number of transport proteins from dysfunctional mitochondria [109, 110]. Interestingly, a role for the PINK1-Parkin pathway in the selective turnover of mitochondrial respiratory complexes has also been described, suggesting wide roles in the maintenance of mitochondrial health [111]. It is also notable that mitophagy has been observed in the absence of *parkin* and *PINK1*

Though Parkin induced mitophagy is dependent on PINK1, *parkin* over-expression still rescues *PINK1* mutant phenotypes [23, 90, 112]. In keeping, an emerging role for Parkin in the maintenance of mitochondria outside of mitophagy is being uncovered. As an E3 ubiquitin ligase, it is involved in ubiquitination and subsequent proteosomal degradation of numerous substrates, one of which is Parkin interacting substrate (PARIS) [113]. PARIS is a transcriptional repressor to Peroxisome proliferator-activated receptor gamma coactivator 1-alpha ($PGC1\alpha$), a positive regulator of mitochondrial biogenesis [114]. PARIS over-expression was shown to induce dopaminergic cell death in the SN of adult mice, and was

mitigated by co-expression of either PGC1 α or Parkin [113]. Further, mice in whom Parkin was KO at 6-8 weeks demonstrated loss of Dopaminergic neurons in a PARIS dependent manner [113].

Recent work has shown that Fbxo7 also translocates to depolarised mitochondria, where it promotes mitophagy through multiple mechanisms, and that PD causing mutations interfere with this[91]. Fbxo7 was also found to interact directly with both PINK1 and Parkin, and it's over-expression to rescue Parkin null, though not PINK1 null, phenotypes. F-box containing proteins are known to recruit substrates to E3-ubiquitin ligase complexes [115], indicating a potential mechanism by which Fbxo7 may perform its roles in mitophagy, and raising the possibility of further interactions with the Parkin pathway.

DJ-1, a protein possessing structural similarities to a stress inducible chaperone protein, has been found to respond to and protect against oxidative stress in the cell [116, 117]. Cells deficient of DJ-1 demonstrate fragmented mitochondrial networks with deficient MMP, both of which are mitigated by exposure to antioxidants or *parkin* / *PINK1* over-expression, though neither has been shown to complex with DJ-1 [118, 119]. As with *parkin* or *PINK1*, over-expression of *DJ-1* protects against rotenone induced alterations to mitochondrial morphology, and does so even in the absence of *PINK1* indicating its actions are independent [119].

Though the above mutations produce highly penetrant forms of PD, they occur at exceptionally low frequencies within population and produce an early onset form of the disease, calling into question their relevance to the late onset sporadic forms of the disease [22]. Certain polymorphisms in genes already linked to autosomal dominant forms of PD on the other hand have also been identified as risk factors for the disease by unbiased Genome Wide Association Studies (GWAS) and/or association studies focussed on candidate genes.

Mutations, duplication and triplication in *SNCA* cause an aggressive autosomal dominant PD of earlier onset [120–122]. Genetic variants have also been

identified as risk factors [123–125]. *SNCA*'s protein, α -synuclein, is a negatively charged protein that is able to integrate into phospholipid membranes, and a major constituent of LBs [126, 127]. It is well expressed in the CNS, where it is believed to have roles in transcriptional regulations, and neurotransmitter release [128–130]. α -Synuclein polymerises into large fibrillar aggregates, intermediate structures of which are recognised as toxic to the cell [131]. α -Synuclein fibrils or protofibrils also appear to induce further aberrant α -Synuclein aggregation, and their transport between cells is believed to underlie the prion like spread such aggregates through the brain [12, 132]. α -Synuclein is found on and within mitochondria [128, 133, 134]. It is suggested to play a role in organising membrane dynamics, and in keeping, over-expression has been shown to induce mitochondrial fragmentation [126, 133, 134]. Models in which excessive mitochondrial fission is present are noted to show accumulation of mtDNA mutations, mtDNA depletion, and mitochondrial dysfunction [135]. Similarly, α -Synuclein overexpression has been shown to induce oxidative stress, bioenergetic defects and Complex I deficiencies [136–138].

Mutations in Leucine-rich repeat kinase 2 (*LRRK2*) number the most common known cause of autosomal dominant PD, and the only mendelian form of the disease to present with a typical age of onset and disease course [139, 140]. Like, *SCNA*, certain *LRRK2* haplotypes are also known to increase the risk of developing PD [123–125]. *LRRK2* is a large dimerising protein which functions as a kinase, GTPase and protein scaffold [23, 141]. While its function in health and PD are still unknown, disease causing mutations have so far been identified in regions relating to Kinase and GTPase activity suggesting mis-regulation of signalling pathways. Over-expression of PD causing *LRRK2* mutants causes cellular toxicity that can be rescued using kinase inhibitors [142, 143]. Fibroblasts derived from *LRRK2* mutant PD patients demonstrate lowered MMP and ETC linked ATP production [144]. *LRRK2* protein has been found localised at the mitochondria within rat brains, and links to functional roles here have been made [145–147].

There are also those genes that have been found to contribute toward PD in an entirely non-mendelian manner. Cumulatively, GWAS have identified more than 20 gene haplotypes associated with an increased risk of developing PD; typically with odds ratios of <1.5 [148]. Though their effect is small, these mutations must be present in $>5\%$ of the population to be detected by GWAS suggesting these might play a role in the more common forms of Parkinsonism. Gene variants of intermediate disease penetrance and population frequencies have also been identified, however these are rarely identified by GWAS. Identification thus relies on biased candidate gene association studies. It is widely speculated that sporadic PD occurs as the result of one or more genetic susceptibilities, plus certain environmental factors. In this regard it is notable that up to 30% of patients have a familial history of the disease [149].

A recent meta-analysis, in which multiple GWAS and candidate gene studies were combined to increase statistical power, has identified 12 common genomic loci associated with PD [125]. Of particular interest were *SCNA* and *LRRK2*, as already discussed, *MAPT*, a gene implicated in other neurodegenerative diseases such as Alzheimer's Disease (AD). It is also notable that research indicates other hits may interact with pathways responsible for mendelian forms of PD. For instance *SYT11/RAB25* interacts with Parkin, *MCCC1/LAMP3* is essential to autophagy, and *STK39* is involved in stress signalling and ion homeostasis [150, 151]. A polymorphism in beta-glucocerebrosidase (*GBA*) was also identified, a gene found by other candidate studies to be the strongest known genetic risk factor for PD [152].

Homozygous and compound heterozygous mutations in *GBA* result in the lysosomal storage disorder Gaucher's Disease (GD), a disease which manifests in a heterogenous fashion, and which is known to associate with typical Parkinsonism among other neurological deficits [153]. *GBA1* is found in the lysosome where it metabolises glucocerebrosidase. Decreased activity is associated with decreased lysosomal function. Post mortem analysis of sporadic and *GBA* mutant PD patient brain's revealed deficient *GBA* activity, most dramatically in the substantia nigra [154]. *In vitro* studies have also shown *GBA* activity

decreases with either increased α -synuclein or decreased PINK1 [154]. *GBA* knock-out (KO) mice demonstrated midbrain accumulation of α -synuclein aggregates, where deficient autophagic and proteosomal activity were also seen [155]. In both -/- and +/- *GBA* phenotypes, MMP and ETC efficiency were decreased and mitochondrial network morphology altered. Defective mitophagy was clearly established in *GBA* -/- neurons and astrocytes.

With the advent of next generation sequencing, the number of genes implicated in PD is expected to increase in the coming years.

1.1.3.2 Rectifying the mitochondrial dysfunction in Parkinson's Disease

Correcting mitochondrial dysfunction is a promising target for neuroprotective therapy in PD. The use of creatine in PD has received attention due to the role this compound plays in the rapid replenishing of intracellular ATP levels, the apparent bioenergetic deficit seen in PD, and the presence of creatine uptake transporters in the Blood-Brain Barrier (BBB) [156, 157]. Oral administration has been shown to protect nigrostriatal cell death in MPTP treated mice and cells [158, 159]. Early clinical trials in which creatine was administered to PD patients at 10g/day has proven safe, and indications of a therapeutic effect have been seen [160]. Given these promising initial results, a five year multi-center phase III clinical trial in which creatine will be orally administered daily to early symptomatic PD patients is presently underway [161].

Coenzyme Q10 (CoQ10) is a cofactor of the mitochondrial ETC, accepting electron from both complexes I and II, and with a potential antioxidant role in its reduced form [162]. It has proven protective against MPTP induced dopaminergic cell death *in vitro*, preventing the collapse of MMP and excess ROS production otherwise seen [163]. Dietary administration of CoQ10 reduces the loss of nigrostriatal neurons in MPTP treated mice and primates [164, 165]. While

an initial trial demonstrated therapeutic effects following high dose oral administration to early symptomatic PD patients [166], a follow up in mid-stage patients showed no difference from placebo [167]. CoQ10 possesses a Molecular Weight (MW) >500Da and is highly hydrophobic, both factors associated with reduced brain penetrance from systemic circulation [168]. Poor water solubility also leads to poor compound absorption from the gut, thus the clinical failures of CoQ10 in PD may result from the poor brain distribution.

In an attempt to improve its mitochondrial localisation, CoQ10 has been conjugated with the cation triphenylphosphonium (TTP), a molecule found to segregate into polarised (i.e. respiring) mitochondria [169]. Like CoQ10, this too has proved promising in animal and cell culture models of PD [170, 171], but has also failed to show a clinical benefits in a double blind trial with PD patients over a year [172, 173]. Poor brain penetrance is again a probable cause for this. Idebenone, a synthetic analogue of CoQ10 of lower MW may possess a greater ability to penetrate the brain from oral administration. It shows highly effective redox-cycling antioxidant activity and some promise in the treatment of Friedreich's ataxia, a rare neurological disorder, at early stages of the disease course [174, 175]. Subsequently its use has been considered for PD, though there is recent evidence that at μM concentrations it induces apoptosis in dopaminergic cells, though this could be attenuated by application of antioxidants [176]. A therapeutic dosing regime will thus require careful determination.

Pioglitazone is a specific agonist of PPAR- γ , marketed as a hypoglycaemic agent for use in type II diabetes [177, 178]. It has demonstrated partial protection from MPTP induced cell death, and increased mitochondrial respiratory function [179, 180]. Its use in 6OHDA treated rats was protective against loss of dopaminergic neurons in the SN. In MPTP treated primates, Pioglitazone has also shown clinical improvement of Parkinsonism like features, and a reduction in oxidative damage in the midbrain [181]. It was suggested Pioglitazone may produce its therapeutic effect by enhancing glucose metabolism within affected neurons, given the drugs ability to increase insulin sensitivity in other tissues and the increase in SN glucose demand produced by MPTP treatment

[182, 183]. Other work has shown that a separate PPAR- γ agonist increases mitochondrial biogenesis in mouse brains [184]. As it is already in clinical use, a randomised clinical trial testing the therapeutic effect of Pioglitazone in PD patients receiving MAO-B inhibitor therapy has been initiated.

Methylene blue, used to treat cyanide poisoning, is able to accept electrons from NADH and transfer them to mitochondrial cytochrome c, entirely bypassing Complex I [185–187]. It has been shown to protect against rotenone induced dopaminergic neuron loss in rat brains [187]. Its pharmacological profile is well established, and following observations that methylene blue delays senescence in fibroblasts [186], is currently under phase II clinical trial for AD, another neurodegenerative disorder in which mitochondrial dysfunction is also strongly implicated.

The female sex hormone oestrogen has been shown to increase the expression of nuclear and mitochondrially encoded ETC enzymes, as well as induce direct interactions between its cytosolic receptor and the mitochondria [188, 189]. Further, it also regulates a number of genes involved in neuronal survival, including Bcl-2, Bcl-xl and BDNF [190–192]. A recent short term clinical trial for the safety and tolerability of oestrogen replacement in menopausal women with PD showed a non-significant trend towards relief of motor symptoms [193]. Interestingly, links have been made between steroid deficiencies and the incidence of PD [194, 195], including oestrogen [196] and testosterone [197].

1.1.4 Ursolic acid, Ursodeoxycholic acid and Ursocholic acid

A recent drug screen performed in human dermal fibroblasts derived from *parkin* mutant PD patients, a well characterised model of mitochondrial dysfunction in PD [95, 96], identified a number of compounds that rescue the phenotypic deficiencies in mitochondrial membrane potential and cellular ATP levels [198].

Though PD obviously does not result from the cell death of fibroblasts, using primary patient tissue which expresses identified Parkinson's genes and which have experienced similar ageing to the effected regions provides advantages over models in which genetic manipulation is required [199]. As primary cells, their metabolic profile is also in closer keeping to that seen *in vivo*, immortalised cells by contrast often demonstrate a greatly increased dependance on glycolysis. Despite large differences in protein expression and energy utilisation, *parkin* mutant fibroblasts and dopaminergic neurons both demonstrate similar mitochondrial deficits, such as MMP and cellular ATP deficiencies, as well as significant alterations in mitochondrial morphology and OXPHOS respiration [95, 96]. The accessibility of fibroblasts makes them well suited to high content drug screening [198].

Two compounds in particular were selected for follow up studies owing to their efficacy, availability and known pharmacological profile. These were Ursocholic Acid (UCA), a bile acid derivative and dehydro (11,12) ursolic acid lactone (DUA), a pentacyclic triterpene. Literature searches identified structural analogues of these that were already under investigation for a number of medical conditions (figure 1.3). Ursolic Acid (UA) is a pentacyclic triterpene found in many plants. Ursodeoxycholic Acid (UDCA) is an endogenous bile acid, the use of which is already approved for use as a treatment for liver cirrhosis [200, 201]. Both, like DUA and UCA, were found to rescue the deficient ATP levels and MMP of *parkin* mutant fibroblasts to and beyond control levels, as well as increasing readings from controls [198].

UA and UDCA have previously been shown to modulate Akt activity [202, 203], and following this line UCA and DUA were found to significantly increase the Akt^{Ser473} phosphorylation in patients but not controls fibroblasts. Inhibition of PI3Kinase activity and Akt phosphorylation were also found to abolish the therapeutic effects of DUA and UCA in both patients and control fibroblasts, implicating PI3K/Akt signalling. Interestingly given their structural similarity to glucocorticoids, antagonisation or knockdown of the Glucocorticoid Receptor (GR) in *parkin* was shown to abolish the effects UCA and DUA, of note given research

that details interactions between the GR and PI3K signalling [204, 205]. Finally UCA and UDCA were successfully able to restore deficient ATP levels in both *parkin* knockdown mouse cortical neurons, and mutant *LRRK2* fibroblasts, heightening the relevance of these compounds for possible therapeutic use in PD. These four compounds of similar chemical structure became the primary focus of further investigation (figure 1.3).

UA and UDCA have previously been investigated for numerous biological actions in particular; anti-oxidant, anti-inflammatory, anti-apoptotic, anti-proliferative, anti-cancer, anti-hyperglycaemic, autophagy inducing and mild mitochondrial uncoupling activities. These are believed to result at least in part from modulation of the Akt, ERK1/2, JNK1/2, insulin, Nrf2, PPAR- α , mTORC1, GR, and NF κ B pathways as well as direct interactions with the mitochondrial and nuclear DNA [206–214]. Previous work also corroborates the affect of UA and UDCA on mitochondrial physiology, and anti-apoptotic effects are frequently reported [215–220]. Literature on the therapeutic effects of DUA is comparatively sparse as is the literature for UCA. UCA however shares strong structural similarities with hydrophobic bile acids [209, 221].

Bile acids have been shown to bind to intracellular nuclear steroid and bile acid receptors and an extracellular G Coupled Protein Receptor (GPCR); TGR5 [222, 223]. TGR5 is expressed throughout the body, including the CNS, Enteric Nervous System (ENS) and skin [224–227]. It is believed to be activated following extracellular binding, and is internalised once bound [228]. Activation is known to induce increased oxygen consumption and energy output in tissues co-expressing type II iododthyronine deiodinase (D2) such as human brown fat and skeletal muscle [224, 229, 230]. Notably, human brain expresses TGR5 and D2 at levels comparable to muscle [224, 225]. Whilst UA and UCA are both reported as TGR5 agonists [231, 232], UDCA shows only weak TGR5 activity [223, 233, 234]. It is notable that there is evidence that GPCRs can be activated whilst in intracellular locations [235]. Though also involved with energy metabolism, expression of intracellular bile acid receptors are restricted to visceral organs [227], thus cannot explain the therapeutic effects seen with

UA, UCA and UDCA in other tissues [198]. Nuclear steroid receptors on the other hand are expressed widely and are known to stimulate nuclear and mitochondrial genes involved in OXPHOS [236, 237], therefore could account for the effect these compounds exert in fibroblasts and neurons.

UA has been shown to directly bind cytoplasmic GR and increase its nuclear localisation without classical Glucocorticoid Response Element (GRE) transactivation [238–240], as have other pentacyclic triterpenes such as avicin D [241, 242]. Avicins have also been shown to directly interact with the mitochondria and to modulate cellular oxygen consumptions [243]. UDCA is also known to interact with the GR, though by an indirect mechanism [244–247]. Sola et al. [246, 248] demonstrated that UDCA's anti-apoptotic effects are dependent on the carboxy-terminus of the GR, and that UDCA increases the presence of GR in nucleus, which in turn mediates UDCA's nuclear entry. The same group also demonstrated UDCA interacts with mitochondria directly, and this is sufficient to prevent apoptosis related permutations in the MMP [249]. Many glucocorticoid like molecules show direct interactions with the mitochondria, and mild uncoupling of the ETC [207]. Lanosterol has been shown to prevent MPTP induced cell death in dopaminergic midbrain neurons through mild mitochondrial uncoupling, which promoted mitophagy of damaged mitochondria [250]. Mild ETC uncoupling and an enhanced antioxidant state are seen in cardiomyocytes following incubation with a UA rich plant extract, both of which were suggested as adaptive responses to increased mitochondrial ETC kinetics and local ROS generation [251–253]. Corticosterone has been shown to increase MMP in rat cortical neurons, and to induce the translocation Bcl-2, an anti-apoptotic protein that prevents permeabilisation of the OMM, to the mitochondria following complexation with the GR [254]. Overexpression of Bcl-2 has previously been shown to enhance mitochondrial calcium capacity [255], high levels of which induce higher ATP production [38]. Notably prolonged exposure of corticosterone at 1 μ M saw an eventual decrease in both MMP and mitochondrial Bcl-2 [254]. 1 μ M dexamethasone also causes GR translocation to the mitochondria in thermocytes, as well as decreases in MMP [256]. Glucocorticoid response

elements have been found within mtDNA, and the GR, among other steroid receptors, have been found in the mitochondria themselves underlining the coordinate mechanisms by which glucocorticoids are able to stimulate both nuclear and mitochondrial OXPHOS genes [237, 257]. Also of note, glucocorticoids are known to directly bind many cytoplasmic proteins such as the MAPK family, potentially connecting them to numerous other signalling pathways [207]. Thus there are multiple intracellular targets by which UA, UCA and UDCA might exert their effects in fibroblasts and neurons. One further consideration regarding the physiological actions of these steroid like compounds would be their incorporation into lipid membranes, the effect this will have on membrane organisation and the knock on effects to the cell [258–260].

1.1.4.1 Drug distribution to the Brain

UA, DUA, UCA and UDCA all possess therapeutic potential in PD by merit of their ability to enhance mitochondrial function in fibroblasts and neurons. Indeed UA and UDCA have previously been shown to exert neuroprotective effects against a range of cellular stresses. However, to treat diseases of the brain such as PD, they must be able enter into the CNS, for which several barriers must be traversed. A drugs pharmokinetic profile can broadly be defined by ADME; Absorption into blood circulation, Distribution to bodily tissues and fluids, potential Metabolisation of the compounds by an organism, and Excretion from the body. Certain predictions about a compounds pharmokinetics can be made based on its molecular properties. Lipinski et al. [261, 262] famously established the “Rule of Five”, a set of criteria that the majority of successful orally administered drugs adhere to. These include Octanol-Water Partition coefficient (Log-P)³ of <5, a MW <500Da, the possession of <5 H bond donors and <10 H bond acceptors; note all numbers are multiples of five. Accordingly, DUA, UA, UCA and UDCA are all likely to demonstrate poor absorption into

³LogP, determined by the relative partitioning of a compound within an immiscible mixture of octanol and water, is a measure of a compounds water solubility, where lower values indicate greater hydrophilicity, and higher values greater hydrophobicity

blood circulation following oral administration, so called bioavailability, owing to their high hydrophobicities; only UDCA possesses a predicted LogP of less than, though close to five (figure 1.3). This can be circumvented by intravenous administration directly into blood flow, however this requires solubilisation of the drug either within an organic solvent or formulation within solubility enhancing compounds collectively termed excipients. Formulation within excipients may also be used to enhance oral bioavailability. Once in systemic circulation, brain distribution requires penetration through the BBB [263].

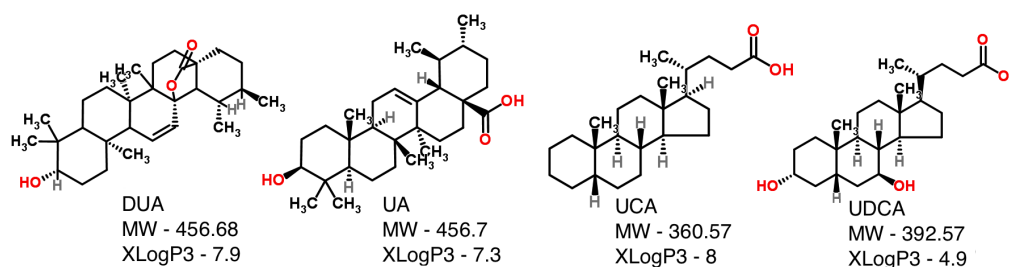


FIGURE 1.3: **Hexa-, Penta- and Tetra- cyclic mitochondrial therapeutics:** Dehydroursolic Acid Lactone (DUA), Ursolic Acid (UA), Ursocholic acid (UCA), Ursodeoxycholic Acid (UDCA). Molecular weights (MW) and LogPs estimated by XLOGP3 software (XLogP3) are indicated. Information taken from "pubchem.com", pictures taken from "chemspider.com".

The BBB is a continuous endothelial layer that regulates the exchange of material between the CNS and the micro-vessels that pass within the sub-arachnoid space and penetrate directly through the pia mater into the brain and spinal cord (schematised in figure 1.4) [263]. It is estimated that no neuron is further than 8-20 μ m distance from a capillary, and that the BBB covers \sim 20m² surface area [264]. Endothelial cells here are bound tightly together by tight junctions that prevent most para-cellular extravasation between cells, requiring materials to pass through the cells themselves. This may be achieved by diffusion through the lipid membranes, facilitated transported, or receptor and/or adsorption mediated transcytosis across the cells. Foreign materials entering the BBB may be effluxed back into circulation by P-glycoprotein and multi-drug resistant protein [265]. The presence of intra- and extra- cellular catabolic enzymes provides a further metabolic barrier that materials must overcome in passing into

the CNS. The high selectivity of material import and export to the CNS is essential for maintaining the correct nutrient and ion composition of the Interstitial Fluid (ISF) within the CNS, and is essential to brain function. Importantly it also prevents the entry of potentially pathogenic agents such as bacteria. Endothelial cells are surrounded by contractile pericytes and receive projections from astrocytes, forming the “neurovascular unit”, which co-ordinates blood flow and exchange of material with neural activity [263, 266]. Other routes of entry to the CNS ISF exist, including; intranasal administration, administration into the Cerebro Spinal Fluid (CSF) and passage through the choroid plexus, traversing the peripheral nervous system as some viruses are known to, and direct administration. However, the distribution to the brain from these limited to quite specific regions. The vasculature of the brain on the other hand is fully penetrant, and crossing the BBB would allow for unmatched accessibility to distinct brain regions.

To effectively and manageably treat PD, it is desirable that DUA, UA, UCA, and UDCA cross through the BBB, something that an estimated >98% of small molecules fail to do [267]. To diffuse through a cell membrane as must be done in passive transit of the BBB, a molecule must be able pass through the transitional spaces in the fluid mosaic cell membrane, something impeded by greater size/surface area, low lipophilicity and greater ability to hydrogen bond. The effect of these can be quite dramatic, for instance increases in a compounds MW from ~300 to 450 Da have been shown to limit brain penetrance by ~100 fold [268], and a decrease of ~10 fold is predicted each pair of hydrogen bonds a molecule makes [269]. Those compounds that can penetrate the brain are generally lipophilic, possess MWs <400-500Da and make <8 hydrogen bonds [168, 267, 270]. Whilst DUA, UA, UCA and UDCA fall within these hypothetical criteria, the margin by which they do so is notable. Of further consideration are the strong interactions these hydrophobic compounds are likely to make with tissues outside of the BBB and serum components, the latter of

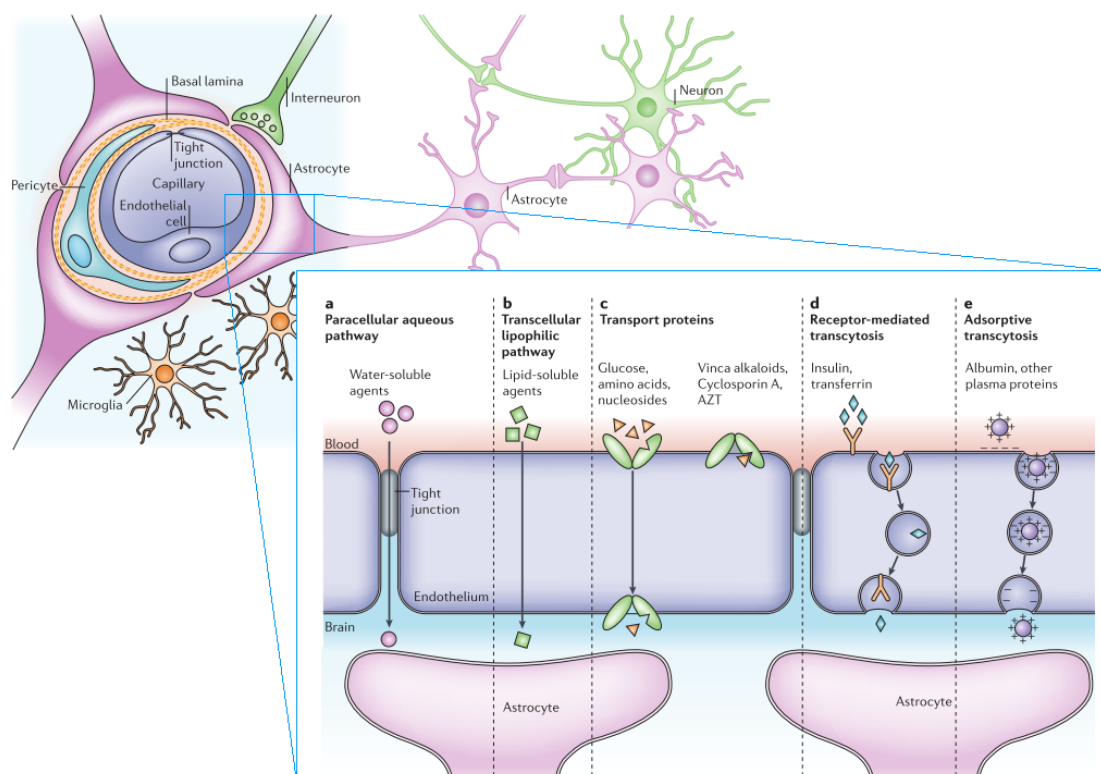


FIGURE 1.4: **The Blood Brain Barrier:** Cross section of the BBB depicting the association between endothelial cells, basement membrane, pericytes, projections from astrocytes, neurons and glia. (a-e) Enlargement depicts routes of crossing the BBB, and the materials that typical cross. Adapted from Abbott et al. 2006, with permission [263].

which has been experimentally shown to hinder the brain penetration of similar steroids [270]. Indeed it is recognised that the optimal LogP for the brain penetration of several classes of small molecule resides between 1.5 and 2.7, significantly lower than the those exhibited by the compounds here (figure1.3) [168]. Further consideration must also be given to the possible effects of drug metabolism within the organism and potential efflux from the BBB by transporters such as the P-glycoprotein. To treat diseases of the brain such as PD, it will be essential that these compounds both cross the BBB, and distribute to the brain in fractions large enough to provide therapeutic effects without producing harmful off target effects.

Dietary administration of UA to mice has demonstrated poor percentage distribution to the brain relative to other organs including the heart, liver, kidneys and

colon [271]. Brain penetrance in humans is currently unknown. Oral administration of UDCA has been shown to result in accumulations within the CSF [272]. However this should not be directly attributed to penetrance of the BBB, as the blood CSF barrier is leaky relative to the BBB, permitting entry, albeit slow entry, to almost all blood soluble molecules [267, 273]. Delivery from the CSF to the brain is also relatively unfavourable due to the convection flow towards venous circulation, and access to only ependymal surfaces [267, 274]. A separate trial in which UDCA formulated within “Yoo’s solution” was administered orally to Amyotrophic Lateral Sclerosis (ALS) patients also reported CSF penetration [275, 276]. “Yoo’s solution” is a non-covalent formulation of UDCA within certain carbohydrates that greatly enhances its water solubility and limits its accumulation within the liver, as typically seen with unformulated UDCA [276]. Brain penetrance of UDCA has been reported in models of stroke, [277, 278], however permeability of the BBB is increased in this condition.

Though certainly UA has shown therapeutic effects against neurotoxicity in animal models following systemic and oral administration, whether this results from actions in the brain or other systemic effects is not discerned, and the extent of systemic toxicity is mostly unreported [216, 217, 279]. It is also of note that most animal models used are of significantly smaller mass than humans, and that even with dose adjustment by weight, the differences in endothelial surface area and number of biological components present between the two makes distribution and toxicity studies difficult to translate. In humans, safety concerns have been raised over the long term use and/or high dosage of both UA [280–282] and UDCA [210, 275, 283]. It is desirable therefore that dosage be kept to a minimum, something which can be achieved by improving the compounds specific distribution to the brain.

Whilst the native properties of DUA, UA, UCA and UDCA may not perfectly lend themselves to BBB penetrance from systemic circulation, appropriate formulations could rectify this. By using excipients capable of carrying the compounds within aqueous environments, and releasing them at the desired site(s)

of action, inappropriate drug interactions can be limited. Indeed a number of evolutionary designs following this paradigm exist within mammals:

- Corticosteroid-binding globulin is a liver serum protein that interacts with, and carries ~80% of circulating glucocorticoids, a further ~15% associating with albumin them within systemic circulation [284]. Unbound glucocorticoids are cleared from the blood more rapidly. KO mice demonstrate impaired stress induced memory retrieval, which was rescued by direct injection of corticosterone to the brain [284]. This suggests corticosteroid-binding globulin plays an important role in mediating the brain delivery from blood. Corticosteroid-binding globulin is also expressed within the CNS where it may act as a glucocorticoid vector [285, 286].
- Lipoproteins are nanoparticles assembled within the intestine and liver, that encapsulate and transport cholesterol through blood and lymphatic systems [287]. They are composed of apolipoproteins and phospholipid encapsulating triglycerides and cholesterol, varying in composition, size and morphology. Notably, Low Density Lipoproteins (LDL) play a significant role in transporting cholesterol to extra-hepatic tissues, particularly adipose and adrenal tissues, which are able to utilise more cholesterol than is synthesised locally [287, 288]. It should be noted that peripheral cholesterol is not required by the CNS, which relies on instead on *de novo* cholesterol synthesis to produce all its cholesterol [289]. However there is evidence that other peripheral lipoproteins enter pass through the BBB, such as apolipoprotein A-1 containing high density lipoproteins [290, 291].

Though UA, UCA and UDCA maybe able to cross the human BBB, their distribution is likely to be fairly unspecific. Thus to attain therapeutically relevant concentrations within the CNS, high doses may be required, which may lead to increased adverse side effects. Formulations that could increase their specific distribution to the brain would allow for lower dosing, and a reduction in potential side effects. In addition, formulations that could also increase the plasma circulation times of these could increase their duration of effect. There are a number

of nanoparticles in existence that are able to package hydrophobic molecules in fashion akin to lipoproteins and cholesterol. These water soluble carriers possess surface chemistries that greatly limit their interaction with other materials. Further their shape and size can be tuned to enhance their non-fouling properties, as well as evade clearance by the RES. Finally they may be “functionalised” with receptor ligands, increasing their specific adherence, and initiating uptake into- or transcytosis across- the BBB.

1.2 Polymersomes & Drug Delivery

In the 1990s, synthetic, high MW amphiphilic block copolymers were shown to self assemble into a number of structure when exposed to water, including nano- and micro- scaled vesicles (figure 1.5) [292]. These later came to be known as polymersomes (*greek*; body of polymer) both for meaning, and for the analogy the name pays to liposomes, vesicles that self assemble from naturally occurring amphiphilic lipids [293]. Like liposomes, polymersomes are able to encapsulate hydrophilic molecules within their aqueous lumen, and amphiphilic and/or hydrophobic molecules within their membrane. When of appropriate size, shape and chemistry, they are also capable of entering cells and releasing their cargo therein. Unlike liposomes, polymersomes have been found to circulate in blood for much longer durations by merit of their tougher membranes and greater capacity for anti-fouling properties. Owing to their synthetic nature, a wide range of potential customisations such as environmentally sensitive drug release and variable morphologies are also available. For these reasons, polymersomes and other polymeric nanoparticles are being investigated as an alternative to liposomal drug formulation [294–296]. Indeed a number of copolymer assemblies have proven safe in humans and are now beginning to enter into the clinic [296–298]. Herein, the use of nanoparticles in drug delivery is discussed, and the advantages of polymersomes highlighted with particular consideration to brain penetration.

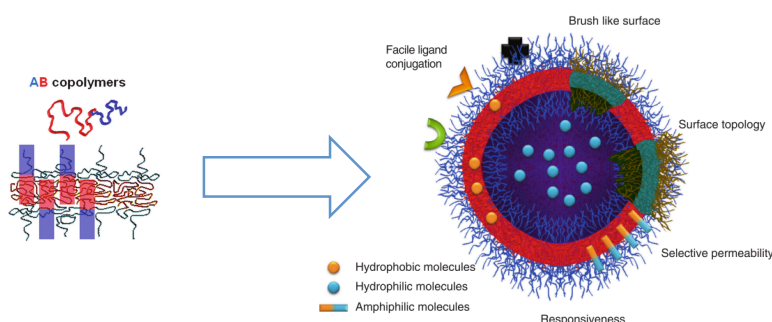


FIGURE 1.5: **Polymersome schematic:** Cartoon of an amphiphilic diblock copolymer membrane (left) and archetypal polymersome plus possible encapsulates, adornments and membrane characteristics. Adapted from Massignani et al. 2010, with permission [401].

1.2.1 Drug Delivery

Drug formulation within materials, collectively known as excipients, has long been performed to improve a compounds shelf life, and distribution within the body from a given route of administration. To take intravenous administration of a hydrophobic or amphiphilic compound as an example, compounds are solubilised prior to injection within a mixture that both solubilises the compound, and prevents its precipitation on contact with blood, something which may otherwise lead to potentially fatal embolisms. Typical formulation techniques include; the use of co-solvents that are both water miscible and solubilise the drug, drug complexation with water soluble molecules containing hydrophobic “pockets”, packaging compounds within micelles formed of amphiphilic surfactants, emulsification within oils and biocompatible surfactants, and encapsulation within vesicles composed of self-assembling amphiphiles. With the exception of co-solvation, these all form particulate, or semi-particulate systems.

A major goal of drug formulation is to enhance therapeutic properties, either by improving distribution to a given site, or prolonging a drugs effect. The body presents a number of barriers that limit both. The Reticulo-endothelial System (RES) is the collective name for opsonising proteins, immune cells and tissue filters, which together identify, filter and remove foreign bodies or dysfunctional plasma components from circulation [299, 300]. Except where it is the therapeutic target, evasion of the RES is desirable. A number of properties can help achieve this, as well as improve particle distribution to specific areas within the body.

1.2.1.1 Hydrophilic surface chemistry

Drug adsorption to plasma components can lead to altered bio-distribution, increases in particle size, and clearance from circulation. Opsonins are molecules that bind to foreign or damaged bodies in circulation, and enhance the ability of immune cells to target and phagocytose these. Certain opsonins are known

complement activators, agents that induce increased immune system activity for more effective clearance of foreign matter. As excessive complement activation can result in reduced therapeutic efficacy and even anaphylactic shock, it is essential that drug formulations are designed to limit or prevent such interactions with the immune system [301, 302]. One effective strategy to delay adsorption by serum components is to surround a drug containing particle with a hydrophilic material. As interactions with water are more energetically favourable than with larger molecules, an effective barrier of water is formed around the particle, buffing it against further interactions. Hydrophilic compounds possessing an overall charge will still readily interact with counter-ions and materials of complementary charge so charge neutral materials have proven the most effective [303, 304]. In this regard, non-ionic- and zwitterionic- polymers have received a lot attention, both for their relative ease of manufacture and, given their high MW, their large water holding capacities [305, 306].

Polyethylene oxide-poly 2-(diisopropylamino)ethyl methacrylate (PEO) (also known as Polyethylene glycol (PEG)) [307] is a charge neutral hydrophilic polymer that has famously been used to coat numerous nanoparticles, both synthetic and biological in nature, resulting in greatly improved circulation times [299, 305, 308]. Unlike many other hydrophilic polymers, PEO/PEG is also non-immunogenic, and is now considered the gold standard anti-fouling coating within biomedical applications [306]. A number of alternatives do however exist, including Poly-2-methacryloyloxyethyl phosphorylcholine (PMPC), a zwitterionic hydrophilic polymer composed of repeating phosphorylcholine groups. Phosphorylcholine groups are also found in the head groups of phosphatidylcholine and sphingomyelin, major lipid components of the cell membrane. PMPC is biocompatible, non-immunogenic, and highly resistant to adsorption by biological materials, for which it is now in use as a biocompatible coating for a number of long term medical implants [309, 310]. PMPC is the hydrophilic group of Poly-(2methacryloyloxy -ethylphosphorylcholine)-poly(2 -(diisopropyl -amino)ethyl methacrylate) (PMPC-PDPA), the diblock copolymer used throughout this thesis.

Anti-fouling properties are most effective where access to the drug by adsorbent material is minimised. Packaging drugs within particles totally surrounded in a hydrophilic surface achieves this without requiring modifications to drug chemistry that may otherwise alter therapeutic efficacy. PEG'ylated lipids have been used to package compounds, resulting in improved circulation times [299, 308, 311]. However, the covalent attachment of a large MW hydrophilic polymers to low MW lipids alters their self assembly properties, resulting in the formation of lipid micelles in place of liposomes. The packing density of micelles is markedly smaller than vesicles, resulting in a "thinned" hydrophilic "brush" border, and subsequently reduced anti-fouling properties. Lacking a lumen, these are also unable to encapsulate water soluble molecules. As copolymers can be synthesised at great MW, they are able to incorporate large non-fouling hydrophilic polymers whilst retaining their ability to form vesicles, and dense hydrophilic "brush" borders.

1.2.1.2 Particle size

There is evidence that increasing diameter of spherical PEG'ylated polymerosomes results in decreased circulation times [312, 313]. This is due, at least in part, to the particulate "filters" present within systemic circulation. Blood flows through a number of sites where anastomising capillaries lacking tight junctions and possessing large fenestrations, known as sinusoids, allow large molecules to pass out into tissue. These include the liver, spleen and bone marrow, all typical sites of large nanoparticle accumulation, particularly those of larger diameter [312, 314]. Spleen sinusoids have fenestrations typically 200-500nm \varnothing^4 , which block the passage of larger bodies. Flexible bodies larger than this such as μm scaled erythrocytes may however still pass through by merit of their deformability [312]. In this regard, it is notable that the supramolecular nature of polymersomes will permit a high degree of flexibility [293].

⁴ \varnothing = diameter

Fenestrated endothelia are present throughout the body including the pancreas, kidney and intestine, permitting the extravasation of material up to $\sim 80\text{nm}$ \varnothing [315]. Endothelia elsewhere, such as along the CNS, are continuous permitting only those molecules that pass through or between endothelial cells and their basement membrane to enter the surrounding tissue. Particles $<5\text{nm}$ are known to clear very rapidly from blood, either by renal clearance or extravasation [316], and particles designed for extravasation should generally be $<100\text{nm}$ [317]. All particles should be $<15\mu\text{m}$ to avoid potentially fatal occlusion of capillaries [318].

1.2.1.3 Particle tensile strength and shape

To prolong circulation times, nanoparticles should be designed to withstand the turbulent forces experienced within blood flow, something the high tensile strengths of solid nanoparticles fair well with. However, this same characteristic will also limit particle size owing to inflexibility and the presence of the aforementioned particulate “filters” present within mammalian systemic circulation. Their high tensile strengths may also prove incompatible and potentially damaging to “softer” supramolecular biological surfaces [319]. Supramolecular assemblies on the other hand are both deformable and possess tensile strengths more akin to those found in the body. Assemblies held together by “weak forces” do however possess tendencies to break apart under force and/or dilution, the cause of the low circulation times of liposomes demonstrate in blood [320]. Nanoparticles composed of self-assembling high MW copolymers such as polymersomes circumvent these issues, demonstrating markedly more robust membrane properties that also retain the deformable characteristics of other supramolecular assemblies [293, 305, 321].

The longest reported circulation time for a particulate system comes from flexible worm like micelles, or filomicelles, composed of a PEG^ylated diblock copolymer [322]. These were $22\text{-}60\text{nm}$ \varnothing and circulated in the the blood of mice with a half-life of up to five days, the duration of circulation scaling with particle length.

This is roughly ten times greater than the circulation times reported for spherical nanoparticles. Under flow, tubular particles have been shown to detach from surfaces with greater ease than spherical particles, due to the greater shear stress exerted on them [323, 324]. It has also been shown that tubes are less likely to enter endocytic cells if presented to the plasma membrane side-on, as a result of the slower membrane wrapping around elongated bodies [325, 326]. Notably, inhibited uptake of higher aspect ratios is also seen in phagocytes [327, 328]. Thus tubular particles of appropriate diameter appear able to effectively navigate the various tissue filters of systemic circulation and evade clearance by immune cells .

Nanoparticles holding cargo bound for the CNS will benefit most from those properties that prevent their extravasation into other tissues, or clearance by the RES. However it is also essential that they are able to interact with the endothelia of the BBB, something that can be achieved by coating/functionalising the nanoparticle with ligands against receptors/targets found on the BBB. Antibody functionalised nanoparticles of both spherical and elongated morphologies demonstrate enhanced endothelial binding specificity relative free antibodies, where the shear stress experienced by these particles likely acts prevent adhesion to sites of weak interaction [329–331]. Binding specificity and avidity is greater in elongated particles relative to spherical particles, by merit of their larger contact area to volume ratios, and greater shear forces experienced in flow [324, 326]. When in flow, it has also been shown that elongated nanoparticles align to flow and drift laterally toward vessel walls, aiding their endothelial interactions [324]. Particles of tube like morphology thus possess a number of properties advantageous to targeting the BBB by ligand functionalisation.

1.2.1.4 Nanoparticle ligand functionalisation

Within systemic circulation, it is possible to enhance the specificity of nanoparticle accumulation by decorating their surface with ligands known to interact with molecules specific to- or enriched in- given tissue types [332, 333]. These

may be molecules found on the cell surface, or the surrounding extracellular-matrix. Targeting may simply enhance a particles tissue affinity, or directly target them into the cell via receptor mediated endocytosis (discussed further bellow) . Particle functionalisation has shown success in targeting solid neoplasm, both when functionalised against tumour endothelia [334–336], and the tumour itself as direct extravasation through their leaky endothelia is possible [334, 336, 337]. A cautionary note should be taken regarding the effects receptor activated processes may have, ranging from receptor mediated endocytosis to receptor induced cell death [338].

Ligand decoration maybe rendered unnecessary where a polymers chemistry demonstrates an inherent affinity for certain receptor interactions. For instance, despite PMPC's highly non-fouling nature, polymersomes composed of the di-block co-polymer PMPC-PDPA have been found to enter cells much more readily than PEG-PDPA polymersomes of similar size [339, 340]. Recently, a major role for Class B scavenger receptors in mediating the uptake of PMPC-PDPA was identified [341], receptors known to recognise phosphorylcholine moieties such as found in PMPC [342]. Though widely expressed, Class B scavenger receptors are particularly concentrated in immune cells, adipocytes and a number of cancer cells; PMPC-PDPA nanoparticles may be well suited to targeting these.

1.2.1.5 Targeting the CNS

To treat diseases of the brain such as PD, nanoparticles must be able to deliver their cargo to the interstitial fluid of the brain, if not to individual cells of the CNS. As mentioned before, the BBB is a continuous endothelia that prevents the passage of all but selective material to and from the CNS, presenting a major hurdle the greater number of potential CNS therapeutics fail to cross [263, 267]. However, as systemic circulation perfuses rapidly and fully throughout the CNS, with neurons being no further than an estimated 8-20 μ m distant from a capillary [264], drug delivery from blood would provide the greatest accessibility to the

brain, and in many cases the most direct route to disease affected regions. Numerous endogenous ligands, unable to directly penetrate the BBB, cross into the CNS via receptor mediated transcytosis (discussed further below) through the BBB endothelium, and there are multiple examples where nanoparticles have been able to hijack this mechanism [296].

Poly(ethylene glycol)-poly(caprolactone) methyl ether (PEG-PCL) polymersomes decorated with a monoclonal antibody (OX26-PO) against a transferrin receptor (CD71), were able to enhance the brain accumulation and therapeutic effect of a poorly brain penetrant therapeutic (NC-1900, a vasopressin fragment peptide) in rats with toxin induced brain damage [343]. Notably, this study found an optimal ligand density, above or below which brain accumulation was detrimented. Transferrin receptors are responsible for the transcytosis of iron to the CNS and advantageously are highly expressed along the BBB [344, 345]. Using antibodies against epitopes of transferrin receptor distinct from the transferrin binding region circumvents the issue of competitive antagonism with the high blood concentrations of transferrin [345, 346]. Notably, work has shown that nano-rods decorated with monoclonal transferrin demonstrate a ~ 7 fold improvement in targeting brain endothelia relative to spheres [330]. Liposomes have also employed this strategy, though the improved stability and circulation times of polymersomes present a distinct advantage over these [345, 346].

Lactoferrin (Lf), another receptor involved in the transcytosis of iron, is of particular interest to Parkinson's Disease (PD). Lf-PEG-PLA nanoparticles with fluorescent cargo have demonstrated marked distribution to the cortex, SN, third ventricle and periventricular region [347]. When loaded with therapeutics, such particles have shown therapeutic effects over free drug in toxin induced models of PD (6-OHDA rats) [348]. Therapeutic Lf-poly(ethylene glycol)poly(lactic acid) (PEG-PLA) polymersomes have also been used to effectively treat mouse models of Alzheimer's Disease [349] and Lf nanoparticles to treat glioma [350]. However like transferrin receptors, lactoferrin receptors are expressed more widely than at the BBB alone.

Recently polymersomes decorated with des-octanyl ghrelin showed improved accumulation in mouse brain, as well as decreased liver and spleen accumulation relative to unadorned polymersomes [351]. These successfully delivered soluble cargoes to the brain, and therapeutic actions related to these were seen. Des-octanyl ghrelin blood concentration is much lower than lactoferrin and transferrin, and has been observed to move from blood to CNS and not the reverse [351].

LDL receptor-related protein (LRP) is a scavenger receptor expressed highly expressed in both the BBB and the cells of the CNS, and is involved in receptor activated bidirectional transcytosis to and from the brain [352]. Angiopep-2 is a small peptide able to bind and induce LRP-1 mediated transcytosis [353, 354], and has been used to functionalise drug loaded nanoparticles targeting gliomas, which showed enhanced specific accumulation and tumour reduction [355]. Recently, Angiopep-2-poly(oligo(ethylene glycol) monomethyl ether methacrylate)-poly(2-(diisopropyl-amino)ethyl methacrylate) (POEGMA-PDPA) copolymers have been synthesised and blended into POEGMA-PDPA polymersomes. These were found to successfully cross a 3D BBB model, with relatively little accumulation in the endothelial cells themselves [356, in preparation]. They and their antibody cargoes if present, were also found to accumulate within mouse brain in significantly higher concentration than unadorned polymersomes, and found to accumulate at numerous locations distant to fluorescently labelled capillaries again indicative of true penetrance into brain parenchyma. Interestingly, LRP-1 was found to be associated with a form of endothelial transcytosis in which no compartmental acidification takes place, evident by the presence of intact polymersomes within the brain ISF; PDPA possessing assemblies disassemble at pHs <6.3 (discussed further below) [357, 358].

Another mechanism by which nanoparticles may induce transcytosis to the CNS is by adsorption to the negatively charged surface of the BBB, as achieved by a number of positively charged serum proteins [263]. As cationic nanoparticles generally induce a higher level of toxicity, this method seems a poor option [359]. However one study relevant to the work here used chitostatin-PLGA

nanoparticles loaded with the highly hydrophobic antioxidant co-enzyme Q10, and administered them to a transgenic mouse model of AD where a therapeutic effect was seen [360]. Thus where orally administered co-enzyme Q10 has previously failed to evoke a disease modifying effect, carriers that increase its concentration within the brain are still promising [167].

It is however notable that none of the above nanoparticles have or are likely to show brain specific accumulation. Further, though improvements in brain distribution are noted, total brain concentrations achieved are typically less than 1% of the injected dose per unit weight of the *in vivo* model, and a large amount of off-target distribution still occurs. A number of studies have indicated that inter-nasal administration of large molecules allowed them to pass through the nasal mucosa and into the brain, particularly the olfactory bulb, and medical effects have been demonstrated in animal models of disease as well as humans [361]. Transport to the brain can occur by one of three potential mechanisms; by diffusion between or within axons from the olfactory bulb both resulting in accumulation in the olfactory bulb, or along the trigeminal nerve projecting to the midbrain. A meta-analysis in 2007 found only two of approximately one hundred publications presented data indicative of feasible distribution of molecules from the nose to the deep regions of the human brain, highlighting the difficulty in translating therapies from animal studies, and the need for highly efficient delivery in this mode [362]. Since, a number of nanoparticles functionalised with lectins that interact with the nasal mucosa's highly glycosylated surface have been developed [296]. Wheat germ agglutinin decorated nanoparticles have shown successful accumulation in the brain along olfactory and trigeminal nerve paths following intranasal but not intravenous administration [363, 364]. Nasal administration of lectin decorated poly(ethylene glycol)-poly(lactic-co-glycolic acid) (PEG-PLGA) nanoparticles loaded with therapeutics showed improved therapeutic effects in a toxin induced rat model of PD [363, 365], suggestive of the therapeutic potential for this route of administration as well as the improved efficiency of delivering lectins impart. However the feasibility of this approach in humans is still questionable.

Nanoparticles targeting the BBB's transcytotic machinery may be able to achieve one of two things. They may release their cargo within the BBB, greatly increasing their proximity to the brain, or, they may be able to traverse through to the brain's ISF intact. In the latter case, it may be possible for nanoparticles to exert a second level of targeting, delivering their cargo directly into certain cells, or to release their cargo directly into the ISF, allowing it to diffuse to its targets. Once robust brain delivery with a system has been established, it will be essential to establish the safety of this system with regard to cell viability and potential microglial activation, the CNS primary immune cell, among other factors.

1.2.1.6 Penetrating the cell membrane

For many delivery vectors, it is essential that their cargo is delivered into their target cell, either to produce enhanced therapeutic effects associated with the delivery of large drug loads [341, 366], or to yield a therapeutic effect in the first instance. Nanoparticles are of a scale that allows them to enter cells along those routes used to import materials essential to cell physiology. Cells utilise a number of mechanisms, collectively termed endocytosis, to internalise and appropriately process materials of various sizes (summarised in figure 1.6) [367, 368]. Materials bound or proximate to the cell surface are engulfed by the plasma membrane, which is then pinched off into the cytosol. The resulting vesicles are trafficked within the cell, typically to endosomes for further processing and distribution, lysosomes for degradation or the adjacent cell membrane in a process termed transcytosis⁵.

Phagocytosis (*greek*; cell eating) is a receptor activated internalisation mechanism that occurs predominantly within phagocytes [367]. Actin re-organisations extend membrane collars around and over $>1\mu\text{m}$ bodies such as bacteria and cell debris until enclosed [369]. The resulting phagosome typically fuses with lysosomes/late endosome. Macro-pinocytosis (*greek*; large cell drinking) also re-organises actin to indiscriminately extend the cell membrane around large

⁵Transcytosis is also known to occur from endosomal compartments

volumes of extracellular fluid, producing cytosolic vesicles up to several μm in diameter [369]. Though not directly cargo-receptor activated, macropinocytosis is inducible by for instance growth factors [370]. Once formed, the internalised macropinosome matures along cell specific paths. Typically, they undergo shrinkage and develop an elongated/tube like morphology before transitioning to smaller spheres, whilst taking on late endosomal markers and/or merging with the late endosome or lysosome.

Micro-pinocytosis (*greek*; small cell drinking), is a continual process in which small sections of plasma membrane are invaginated and internalised, drawing both lipids and extracellular fluids/materials into $\sim 40\text{-}300\text{nm}$ \varnothing vesicles [367]. Pits/invaginations in the plasma membrane that result from high concentrations of certain structurally ordering proteins, lipids or cytoskeletal reorganisations are pinched off into the cytosol, and typically trafficked to endosomal compartments or the adjacent cell membrane. This process is matched by a homeostatic addition of lipid to the plasma membrane from exocytotic vesicles, maintaining cell volume. The rate of pinocytosis varies with cell type, macrophages internalising 25% of their own volume per hour, where fibroblasts internalise just 1% [367]. Receptor activated endocytosis allows for specific extracellular molecules to be actively internalised along a bespoke route, dramatically increasing their accumulation within the cell despite possibly low extracellular concentration.

A classic example of receptor mediated endocytosis is the uptake of cholesterol containing LDLs. LDL receptors are found either in pits or dispersed across the cell membrane. In the latter case, pit formation is induced on LDL binding. Pits are formed by coating the cytosolic face of the cell membrane with the membrane deforming protein, clathrin. On receiving a cargo these pits bud inwards and are cut from the plasma membrane by the catalysed actions of multiple proteins, and the resulting vesicle is trafficked to early endosomal compartments. Interestingly, clathrin coated pits can vary in size, $\sim 10\text{-}300\text{nm}$ \varnothing having been observed [371, 372]. Links have been drawn between cargo size and the size of clathrin coated vesicle, wherein membrane deformations induced by the cargo

are proposed to guide the ordering of clathrin cages around the membrane [372]. Currently, 200nm \varnothing is the reported upper limit of cargo size admissible by clathrin mediated endocytosis. Larger entities are known to bind receptors affiliated with clathrin mediated endocytosis, and to assemble the machinery required of it, though whether their subsequent internalisation requires inputs from further internalisation mechanisms is unknown, though probable [373].

Pinocytotic mechanisms independent of clathrin are also known of, the best studied of which is caveolae mediated endocytosis. Caveolae (latin; little caves) are 50-80nm \varnothing “flasks” enriched with cholesterol, glyco-sphingolipids and most frequently calveolin proteins. Receptor mediated endocytosis through these is linked to cargo trafficking to a number of intracellular locations including the endosome, as well as a form of transcytosis [374, 375]. Despite their relatively small size, caveolae have reportedly mediated the endocytosis of 100nm \varnothing nanoparticles [376].

Whilst it is possible to target materials towards particular endocytic pathways and subsequent intracellular locations by merit of their physical characteristics and ability to bind receptors that activate endocytosis, the concurrent activity of internalisation mechanisms likely means uptake occurs by multiple routes. Indeed there is evidence that nanoparticles enter cells by more than one form of endocytosis [377, 378].

1.2.1.7 Tuning nanoparticle for cellular uptake

A nanoparticle’s size, tensile strength, shape and adherence to biological surfaces dictate their cellular interactions. Particles of identical chemistry but differing diameter [379–381], shape [340, 378] and/or stiffness [377] show altered cellular internalisation kinetics. This is a result of both the strength of attraction between the particle and cell membrane, and the particles ability to deform the cell membrane [382, 383]. It has been shown that solid spherical gold or silica nanoparticles co-incubated with liposomes are found engulfed in phospholipid

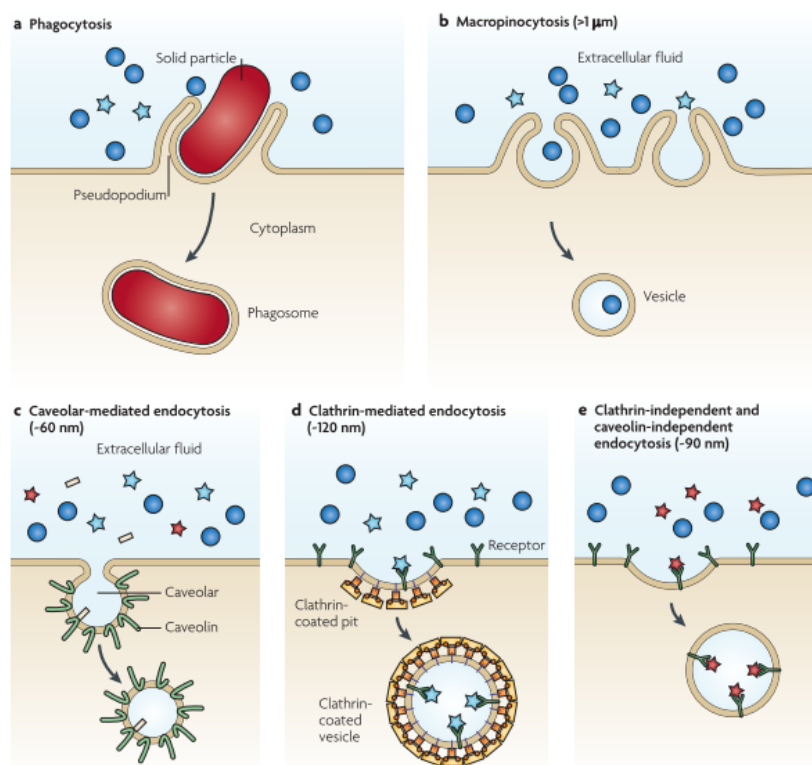


FIGURE 1.6: **Endocytic pathways:** Representations of (a) Phagocytosis, (b) macropinocytosis, (c) caveolae mediated endocytosis, (d) clathrin mediated endocytosis, (e) receptor mediated endocytosis independent of clathrin and caveolae. Typical cargo sizes are indicated. Taken from Petros and Desimone 2010, with permission [313].

vesicles found within the lumen of the latter despite the absence of active endocytosis [384, 385]. Other work has shown that mesoporous silica nanoparticles $\sim 600\text{nm}$ \varnothing are able to deform erythrocyte membranes and enter into these endocytically inactive cells [386]. Studies with spherical solid nanoparticles have identified optimum sizes for cellular uptake [380, 381, 387] and in close agreement numerous computer models have identified diameters of 40-60nm as the most effective at inducing plasma membrane wrapping [325, 382, 388]. Below the optimum, the high bending requirement of the plasma membrane slows or prevents membrane deformation, and above greater cell-particle adhesion must be developed for membrane wrapping, for instance by the diffusion of more receptors to the site of particle adhesion. Strength of adhesion is also significant, wherein increasing attraction theoretically increases the size optimum for membrane wrapping, with the converse being true of increasing repulsion [382, 383, 388]. For instance PMPC-PDPA polymersomes have been found to

enter cells more readily than PEG-PDPA polymersomes likely due to the specific interaction between PMPC and phosphorylcholine binding class B scavenger receptors [341]. The uptake of both declines with diameters increasing from 100nm [339, 340]. Interestingly, polymersomes composed of both these diblock copolymers were found to enter fibroblasts in a manner apparently independent of vesicle diameter. Characterisation of these particles revealed the two copolymers segregated into discrete regions of the membrane, creating patches. This will establish regionalised interaction strengths between patchy polymersomes and the cell membrane perhaps approaching the membrane wrapping ideals noted above.

It is interesting to note that many naturally occurring delivery vectors, whose design has been guided by billions of years evolution, display small protrusions from their surface enriched with molecules that interact with the cell surface, and arranged in a clear topological order. Many of these are also larger than the ideal diameter noted above, spherical/icosahedral viruses for instance are most commonly found with diameters of ~ 60 -150nm [389]. Theoretical work has demonstrated that clustering of nanoparticle induced deformations on the cell membrane lowers the energy threshold to membrane wrapping, meaning such topologically arranged cell membrane deformations could be an effective strategy to improve cell entry [388]. Enhancing the ability of larger vectors to enter cells is significant, as the volume and subsequent payload contained within these will be larger than in smaller particles. It is also important to reinforce that whilst effective entry to the cell is important, entrance into a specific subset of cells is often equally or more important for a medical molecular delivery vector, thus particles should not necessarily be designed for effective entry into all cell types.

As noted previously, particles of increased aspect ratio tend to show increased circulation times, and enhanced ligand specific interactions *in vivo*. In keeping, a number of studies have shown that shapes with increased aspect ratios, such as nano-rods, are internalised less effectively by cells even where particle volumes are matched [322, 378, 387]. This is also true of phagocytotic cells [327, 328].

Vector designs that carefully enhance certain cellular interactions may allow for cell specific internalisation. One study, for instance, found apolipo-protein peptides conjugated to lipid micelles selectively entered one type of endothelial cell among a mixture endothelial cells, using clathrin mediated endocytosis [390]. Liposomes or the peptide alone by contrast were internalised by all cells through a number of routes. In another study, when incubated with both neurons and glia, gold nano-rods preferentially entered endocytic neurons where “spiky” gold nano-particles entered phagocytic glia [391].

1.2.1.8 Environmentally sensitive block co-polymers and intracellular cargo release

Though many particles are able to enter into cells via receptor mediated endocytosis, their sub-cellular locations are often limited initially to the endosome, from which they are later trafficked to the lysosome. This has been known to limit and/or prevent therapeutic actions of nanoparticles acting as therapeutic vectors. Development has subsequently gone into discovering methods by which nanoparticles can be released into the cytosol, either by altered entry to the cell, or escape from the endosome.

PMPC-PDPA polymersomes have been shown to enter cells via an endocytic route and localise within the endosome [392, 393]. In this regard it is interesting to note that class B scavenger receptors, which play a major role in the internalisation of these particles [341], have been connected to both clathrin, and caveolae mediated endocytosis [394, 395]. On entering the endosome, these particles will experience environments of increasing acidity as they progress through the endolysosomal pathway. Owing to the tertiary amine groups present in the hydrophobic DPA block, PMPC-PDPA polymersomes are pH sensitive with a $pK_a \sim 6.3$ [357, 396]. Below this, DPA units become protonated, causing both units of the diblock copolymer to become water soluble and subsequently losing the hydrophobicity that held the self assemblies together (figure 1.7) [358, 396]. This feature is of particular relevance to PMPC-PDPA polymersomes $\sim 100\text{nm}$

in diameter, which are internalised along an endocytic pathway in which they are exposed to the mildly acidic environment of the early endosome. Here PMPC-PDPA polymersomes disassemble rapidly, causing an osmotic shock that drives the escape of soluble cargoes into the cytosol, and hydrophobic cargoes into neighbouring apolar environments [339] (further details on endosomal escape can be found in the introduction of Chapter 4). The eventual sub-cellular locations of the copolymer and its cargo, whether polar or apolar, will result from their specific properties and the manner in which the cell interacts with them, fluorescent cargoes having been observed both throughout the cell and concentrated within certain organelles such as the nucleus and mitochondria [392].

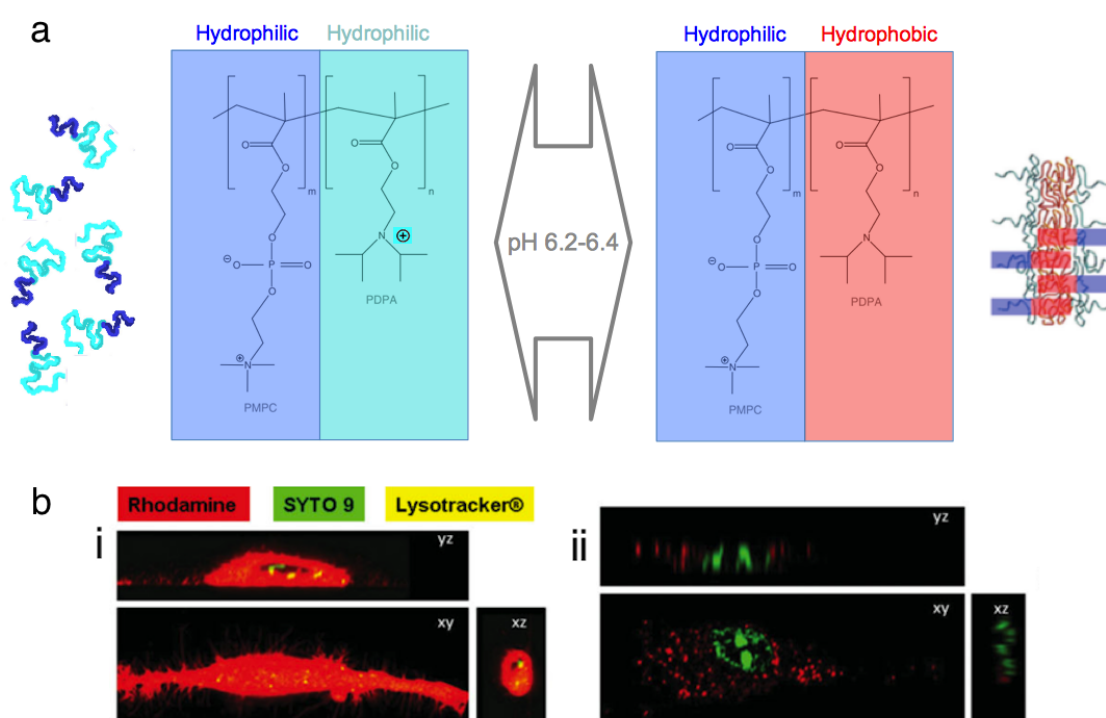


FIGURE 1.7: **pH sensitivity of PMPC-PDPA:** (a) PMPC-PDPA possesses a $pK_a \sim 6.3$, PDPA's tertiary amine group being protonated in mildly acidic concentrations, allowing it to interact with water molecules. (b) intracellular distribution of rhodamine B following delivery by polymersomes composed of (i) PMPC-PDPA and (ii) PEG-PBG, a non pH sensitive diblock copolymer.

Adapted from Massignani et al. 2009, with permission [338].

Other examples of polymersomes that disassemble or degrade in reductive

environments also show effective release of soluble cargoes from the endolysosomal compartment and delivery to the cytosol [397, 398]. A number of environmentally responsive copolymers beside these also show promise for medical applications. Polymersome that degrade after fixed periods could allow for better temporal control of drug dosing [399, 400]. Oxidation sensitive polymers could permit cargo release only in tissues generating high ROS levels, both for diagnostic and therapeutic reasons [401]. Temperature and light sensitive copolymer have also been synthesised, the latter being perhaps of particular interest as lasers could be focussed at points in which cargo release is desired [402]. Certain copolymers show specific permeabilities [403], and others have been used to incorporate proteins within their membranes, something that would allow mimicry of specific cell properties and functions [295].

Some of the above possess biodegradable groups, such as reductively sensitive disulfide bonds. Developing co-polymers that may be totally degraded, broken down and incorporated into a cells chemistry, or that are safely expelled from the body remains an important goal for medical delivery vectors. The long term biological effects of PMPC-PDPA have yet to be fully addressed, though early studies indicate it is biocompatible, non-immunogenic, and well tolerated in cells for at least a week [339, 358, 404].

1.2.2 Controlling the shape and size of amphiphilic diblock copolymer assemblies

So far, a number of properties that enhance the ability of nanoparticles to deliver therapeutic compounds within the body have been listed. Herein, methods by which these properties can be achieved using diblock copolymers are discussed.

1.2.2.1 Packing factor determines assembly structure

When hydrated, an amphiphile population of sufficient concentration will order into structures due to the introduction of the hydrating forces and the hydrophobic effect, which overcome the ordering imparted by other weak forces [405, 406]. Water molecules will attempt to orientate their dipoles away from apolar molecules they immerse. However, such ordering is energetically unfavourable in a liquid state, so water instead drives the association between apolar groups to maximise entropy, producing interactions markedly stronger than those imparted by other weak forces [406]. Hydrophilic molecules by contrast may interact with water molecules sufficiently to effectively dissolve within them. Interactions with water are believed generate more disorder than with other polar molecules, so hydrated polar entities will effectively “repel” one another [406]. When polar water solubilities are combined in a single molecule in an amphiphile, water will exert both attractive and “repulsive” forces that drive their self assembly into higher order structures. The balance of forces can be formalised using the dimensionless packing factor, p :

$$p = \frac{v}{a_0 l}$$

Where “ v ” is the molecular volume of the hydrophobic chain, “ l ” is the amphiphile length, and “ a_0 ” is the optimal area that is occupied by an amphiphile in an assembly that has reached equilibrium [406]. This is also known as Israelachvili’s parameter. Where $p \leq 1/3$ micelles (solid spherical particles) are most typical, $1/3 \leq p \leq 1/2$ worm like micelles (solid tubular particles) and $1/2 \leq p \leq 1$ lamellar membranes (planar sheets) (figure 1.8). Only the first of these can exist in water without further modification, their size being determined purely by the amphiphile’s character. Worms must form energetically frustrated end caps to prevent exposing their hydrophobic core to water, and will continue to lengthen until they do so. In membranes, curvature is generated from the energetic frustration of exposed hydrophobic edges plus local membrane fluctuations, wrapping this sheet into closed structures, typically vesicles. Except at very small diameters,

the energetic penalty for vesicle formation is mathematically equal at all sizes, and so final diameter is determined by the local availability of copolymer and thermodynamic state at the time of formation. Thus vesicle size varies with the method of preparation, and may differ significantly between vesicles formed at the same time. Material is not exchanged between vesicles due to the great insolubility of amphiphilic copolymers, the number of molecules present within the inner and outer leaflets being fixed at the time of membrane closure. The formation of discs instead of vesicles is unfavourable owing to the large number of molecules that must exist in an energetically frustrated state to cap the 360° of exposed membrane core.

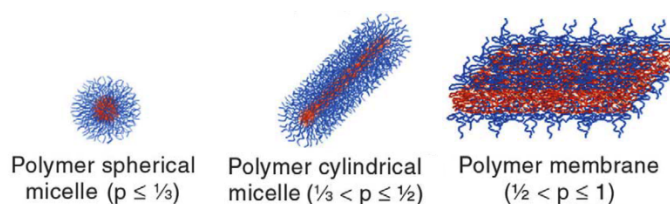


FIGURE 1.8: **Amphiphile packing parameter correlates assembly morphology:** Adapted from Smart et al. 2008, with permission [294].

1.2.2.2 Lyotropic phases

As water is the primary driver for amphiphile self assembly, another key determinant of aggregate structure is the amphiphile concentration in water [407]. At very low concentrations, amphiphile chains remain separately dissolved in water. Past a threshold, the Critical Aggregation Constant (CAC), amphiphile chains are able to interact with one another, where the combination of the hydrophobic effect and hydration forces drive their self assembly. It is notable that amphiphiles of high MW, such as block copolymers, have CACs close to zero. Thanks to both this and their low membrane fluidity (discussed further below) [408], copolymer assemblies will not readily disassemble on dilution as, for instance, occurs on entry to human blood.

Membrane forming amphiphiles order into disperse isotropic structures such as vesicles at low concentrations, and structures possessing long range order at

high concentrations (figure 1.9). The latter are metastable lyotropic phases, assemblies which though locally stable, are capable of ordering into structures of lower energy within a permissive environment. From a dry amphiphilic copolymer, initial film hydration results in the formation and/or swelling of planar membranous sheets known as lamellae [409]. There is evidence this occurs directly from films possessing a semi-crystalline order, whilst disordered copolymer films initially transition through a hexagonal rod phase prior to forming lamellae [407] (figure 1.9). As copolymer concentration in water continues to decrease, lamellae continue to swell until the changing balance of hydrating and hydrophobic forces results in membrane unbinding and the formation of “sponge” phases. Further dilution results in the formation of further structures, ever more closely approximating energetic equilibrium until the transitioning to isotropic/ergodic morphologies. All these phases are encountered when forming polymersomes by Thin Film Re-hydration (TFR), if only transiently [407, 409].

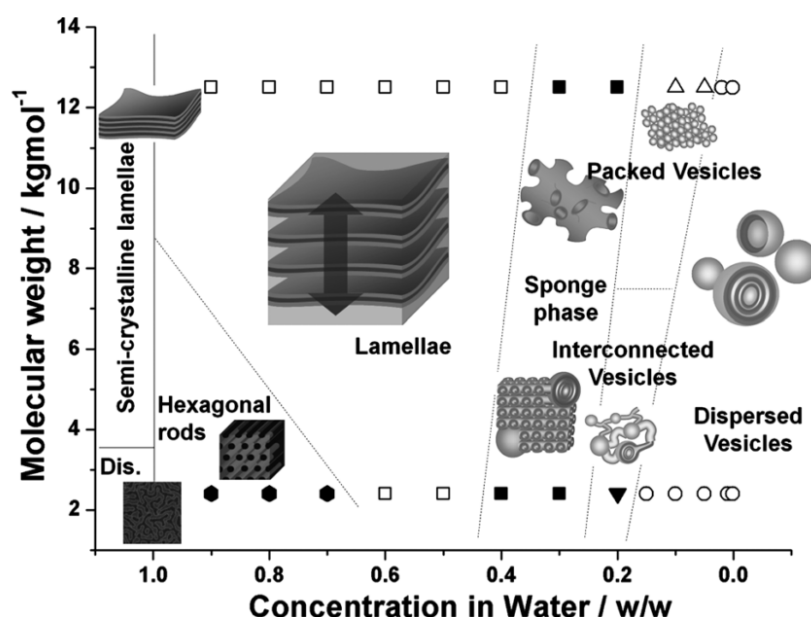


FIGURE 1.9: **Phase diagram of a diblock copolymer:** Phases formed by membrane forming PEO-PBO with increasing MW and water content. Figure taken from Battaglia and Ryan 2006, with permission [406].

1.2.2.3 Copolymer size determines membrane properties

Another key component to the nature of amphiphilic assemblies is amphiphile size (figure 1.10). Amphiphile membranes show increasing bending rigidity and mechanical properties with increasing MW. For instance, polymersomes composed from high molecular weight diblock copolymer have been shown to resist rupture at forces greater than ten times that required to rupture liposomes formed of low MW lipids [293]. Membrane thickness also scales with MW, though past a threshold, interdigitation between the hydrophobic chains of copolymers from opposing membrane leaflets can occur, resulting in an apparent decrease in thickness [410]. Concordantly, membrane fluidity / chain exchange kinetics decrease with amphiphile size. Relative membrane permeabilities also decrease with amphiphile size, though still remain specific to amphiphile chemistry. Membrane elasticity remains independent of MW, and is comparable to that of liposomes [293, 411].

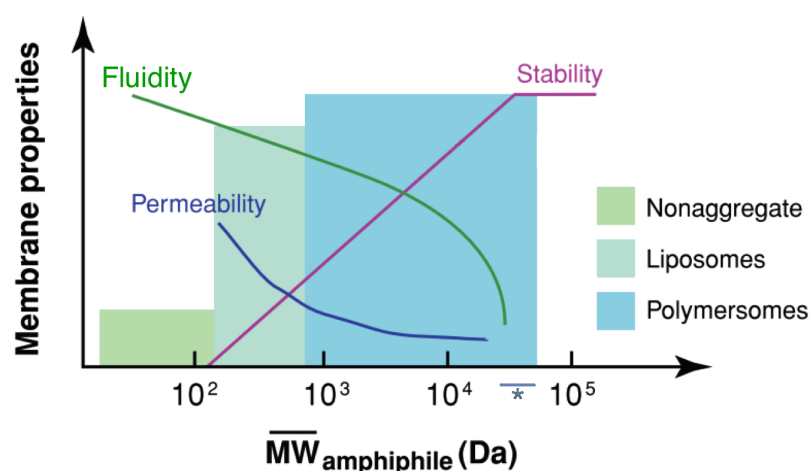


FIGURE 1.10: **Diblock copolymer membrane properties scale with amphiphile size:** *Relative position of PMPC₂₅–PDPA_{65–78} is indicated along the x axis. Adapted from Discher and Ahmed 2006, with permission [320].

1.2.2.4 Method of formation determines vesicle size

As mentioned earlier, for membrane forming amphiphiles, the method of formation is key to the size of vesicles produced. As amphiphilic diblock copolymers

have CAC close to zero, once energetically stable closed structures are formed, the copolymer chains within are fixed and only externally applied energy can disrupt this. The specific constraints placed on the copolymer at the time of formation will dictate the size and morphology of the particle they will assemble into [409]. For instance, electro-formation, a process in which an electrical current is passed through a thin film of, in this instance, membrane forming diblock copolymer at the time of hydration, results in giant (μm scaled) unilamellar vesicles. TFR by contrast, a method in which a thin film of the same membrane forming diblock copolymer is exposed to water in the presence of mechanical energy, will form nano-scaled vesicles, the mutual diffusion of copolymer and water into one another being slower than with the more energetic electro-formation [412]. Applying exogenous energy can further transform vesicle size post formation. Sonication for instance is routinely used to reduce average vesicle size and narrow size distribution. TFR and electro-formation are examples of top down nanoparticle formation, in which a bulk amphiphile transitions to dispersed particles. Bottom up approaches, in which particles are formed from molecularly dissolved amphiphile chains, tend to form smaller particles. Bottom up approaches typically utilise a switch in amphiphile solubility. PMPC-PDPA may for instance be dissolved in acidic water, which when raised to a neutral pH will cause this pH sensitive copolymer to precipitate as the PDPA block loses its charge and gains a hydrophobic nature, resulting typically in vesicle and micelle formation [357, 358]. Figure 1.11 lists some common methods of formation and post processing, along with the range of vesicles sizes expected from them.

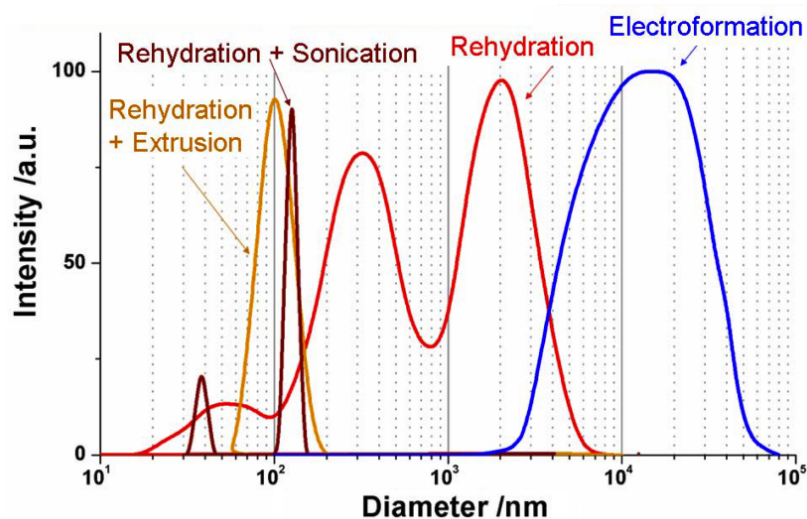


FIGURE 1.11: **Vesicle size varies with methods of polymersome formation:** DLS determined size distributions of E₁₆B₂₂ vesicle produced by different methods of formation and post formation processing. Adapted from Battaglia 2006, Amphiphilic polymeric membranes (thesis), with permission.

The specific structural character of nanoparticles self assembled from diblock copolymers can be controlled by determining block lengths, overall molecular weight, concentration and the method of formation. As a thermodynamic process, temperature will also be a key determinant. Further customisation, such as ligand functionalisation, can be achieved either at the point of copolymer synthesis, or following particle formation.

1.3 Project aims and objectives

UA, UCA and UDCA have been shown to improve the mitochondrial function of *parkin* mutant fibroblasts [198]. In these experiments, fibroblasts were incubated with serum supplemented media, to which DMSO formulated compounds were added (final concentration of 0.1% DMSO). As UA, UCA and UDCA are all highly hydrophobic, they risk adsorption to serum proteins and cell culture plastic. Previous work has shown encapsulation of hydrophobic therapeutic compounds within non-fouling PMPC-PDPA polymersomes produces enhanced *in vitro* drug efficacy relative to “free” drug [341]. This is believed to result from the high concentration polymersomes can house, and the resulting high drug “pay loads” delivered to a cell by each polymersome [341, 366]. PMPC-PDPA polymersomes have also been shown to encapsulate large loads of hydrophobic compounds with high efficiency [341, 413]. Further, they are known to enter into fibroblasts more rapidly than other copolymer chemistries [340, 341].

Thus one could hypothesise delivery of hydrophobic compounds such as UA, UCA and UDCA by PMPC-PDPA nanoparticles could improve the drugs therapeutic efficacy in fibroblasts. This project aims to create PMPC-PDPA loaded nanoparticles loaded with UA, UCA or UDCA of biologically relevant size and morphology, the suitability of PMPC-PDPA polymersomes to use in *parkin* mutant fibroblasts, and the therapeutic potential of drug loaded PMPC-PDPA nanoparticles relative to “naked” drug.

1.3.1 Objectives of Chapter 3: Drug Loaded Polymersomes

- Create empty PMPC-PDPA polymersomes by TFR, and characterise their shape and morphology over time with continuing formation.
- Assess the ability of centrifugation to separate out the unique particle morphologies formed by TFR.

- Create UA, UCA and UDCA loaded as well as unloaded polymersomes by thin film rehydration, and characterise their morphology and encapsulation efficiencies before and after hollow fibre filtration purification.
- Isolate “tubular” and “spherical” drug loaded nanoparticle fractions, and assess their stability after long term storage.
- Assess the effect of drug load on nanoparticle formation and final morphology.

1.3.2 Objectives of Chapter 4: Suitability of PMPC-PDPA polymersome use in *parkin* mutant fibroblasts

- Investigate the kinetics of polymersome uptake in *parkin* mutant fibroblasts under different bioenergetic conditions, relative to *wild type (wt)* fibroblasts.
- Assess the effect of concentration on the uptake of TFR formed nanoparticles, and the relation between initial particle binding kinetics (over minutes), and later nanoparticle accumulation (over days).
- Determine the effect of PMPC-PDPA nanoparticle concentration on the viability and mitochondrial function of *parkin* mutant fibroblasts and controls, using reproducible high content plate reader assays.

1.3.3 Objectives of Chapter 5: Polymersome mediated delivery of mitochondrial therapeutics to *parkin* mutant fibroblasts

- Assess the therapeutic potential of UA and UCA loaded nanoparticles of “polymersome” or “tubular” morphology in *parkin* mutant fibroblasts, relative to drug formulation within DMSO. The effect of concentration and incubation time are to be investigated.

-
- Assess the ability of DMSO, “Polymersomes” and “Tubes” to deliver sterol like compounds into *parkin* mutant fibroblasts and controls, with increasing concentration and incubation times.

Chapter 2

Materials and Methods

2.1 Materials

2.1.1 Block Co-Polymer

Block co-polymer PMPC-PDPA was synthesised by Dr. J. Madsen using Atom Transfer Radical Polymerisation (ATRP) and by Dr. N. Warren using Reversible Addition-Fragmentation chain Transfer (RAFT). Co-polymers were characterised by gel permeation chromatography (GPC) and ^{13}C Nuclear Magnetic Resonance (NMR) as previously described [357, 414]. Rhodamine-6G labelled PMPC-PDPA was synthesised by Dr. J. Madsen as previously described [415]. Details of all polymers used can be found in table 2.1.

TABLE 2.1: PMPC-PDPA batches

Copolymer	Polymerisation	MW
PMPC ₂₅ -PDPA ₇₀	ATRP	22.3kDa
PMPC ₂₅ -PDPA ₇₂	ATRP	22.7kDa
PMPC ₂₅ -PDPA ₇₆	RAFT	23.5kDa
PMPC ₂₅ -PDPA ₆₅	RAFT	21.2kDa
R.6G-PMPC ₂₅ -PDPA ₇₀	ATRP	22.7kDa

Limited polymer supplies required that several batches of PMPC-PDPA be utilised during this project. However, the great majority of work reported here was performed using PMPC₂₅-PDPA₆₅, and where appropriate R.6G-PMPC₂₅-PDPA₇₀. This work includes characterisation of nanoparticle formation with and without hydrophobic cargoes, measurement of empty and DHE loaded nanoparticle entry into fibroblasts, and assessment of cell viability and mitochondrial physiology following incubation with empty and drug loaded nanoparticles over a range of concentrations. The consistent use of PMPC₂₅-PDPA₆₅ throughout these key experiments allows conclusions to be drawn over the affects nanoparticles composed of this polymer produce. Work with other polymers comprise early pilot and validation studies only; corresponding figures are listed below:

- Figure 3.5; Cholesterol incorporation alters PMPC₂₅-PDPA₇₂ nanoparticle morphology
- Figure 4.1; Rhodamine labelled nanoparticle characterisation
- Figure 4.2; Polymersome uptake in fibroblasts cultured in different sugar substrates
- Figure 4.4; Effect of Polymersome concentration on internalisation
- Figure 4.1; Percentage of fibroblasts demonstrating Rhodamine 6G labelled PMPC-PDPA (R.6G-PMPC-PDPA) fluorescence
- Figure 4.5; DNA content of fibroblasts incubated with polymersomes
- Figure 4.9; Inter-experimental comparison of TFR and pH switch formed polymersomes uptake in fibroblasts
- Figure 4.10; PMPC-PDPA polymersomes characterisation
- Figure 4.12; Effect of Polymersome incubation on fibroblast LDH release
- Figure 4.15; Cellular ATP assay pilot

2.1.2 Organic Solvents

Analytical grade chloroform (99.8% purity) and absolute ethanol (99.8% purity) were purchased from Fisher Scientific UK Ltd. HPLC grade chromasolv[®] methanol (99.9% purity) was purchased from Sigma-Aldrich Ltd.

2.1.3 Small Molecules

UA, UDCA, UCA and cholesterol were all purchased from Sigma-Aldrich Ltd. at the highest available purity. Dehydroergosterol (DHE) was purchased from Avanti polar lipids inc. at the at the highest available purity. Compounds were dissolved, without further purification in ethanol or DMSO Dimethyl Sulfoxide (DMSO), for polymersome encapsulation and cell culture purposes respectively.

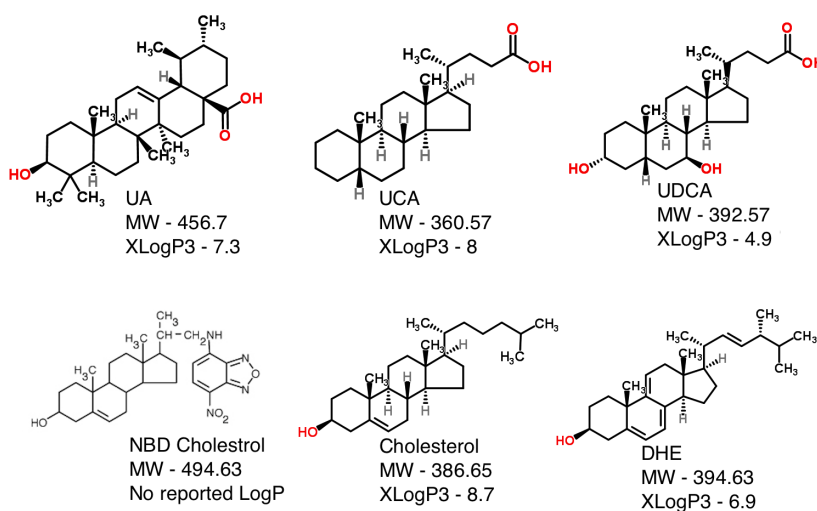


FIGURE 2.1: **Small molecules** LogPs estimated using ACD labs Physchem suite. Information taken from “chemspider.com”

2.1.4 Primary Human Dermal Fibroblasts

Human dermal fibroblasts were derived from punch skin biopsies of PD patients possessing compound heterozygous mutations in *parkin*, (initial biopsies were taken by Dr S. Klaffke and cell culture established by the Sheffield Children’s Hospital cell culture service headed by Dr S. Olpin) [95]. Healthy fibroblasts possessing *wt parkin* were purchased from the Coriell Cell Repository (Cambden, New Jersey). Mutant and wild type fibroblasts were paired by sex and age (± 3 years age at time of biopsy).

TABLE 2.2: Human Dermal Fibroblasts

Name	Age	Gender	1st <i>parkin</i> mutation	2nd <i>parkin</i> mutation
Ctrl1	37	F	<i>wt</i>	-
PD1	38	F	het202-203delAG(exon2)	hetExon2del
Ctrl2	45	F	<i>wt</i>	-
PD2	48	F	het202-203delAG(exon2)	hetExon4del
Ctrl3	32	M	<i>wt</i>	-
PD3	33	M	het255delA(exon1)	hetExon5del
Ctrl4	36	M	<i>wt</i>	-
PD4	39	M	c.101-102delAG(exon1)	c.1289G>A(exon11)
Ctrl5	12	M	<i>wt</i>	-

2.1.5 Cell Culture

Cells were cultured in 75cm² flasks made of tissue culture treated polystyrene (Nunc[™]). Minimum Essential Media (MEM) and Foetal Bovine Serum (FBS) gold were purchased from PAA Laboratories GmbH (now a subsidiary of GE healthcare). Dulbeccos Modied Eagle's Medium (DMEM) without glucose was purchased from Gibco[®] (Life technologies[™]). MEM vitamins, non-essential amino acids, and Penicillin-Streptomycin were purchased from Lonza. Sodium pyruvate was purchased from Sigma-Aldrich. Uridine was purchased from Alfa Aesar[®].

2.1.6 Physiological Assays

Flat bottomed clear and white walled well plates were purchased from greiner bio-one. CyQUANT[®]-NF cell proliferation assay kit was purchased from invitrogen[™]

(Eugene, OR, USA). CytoTox-ONE™ Homogeneous Membrane Integrity Assay was purchased from Promega (Madison, WI, USA). ATPLite™ kit was purchased from Perkin Elmer (Boston, MA, USA). MycoAlert™ Mycoplasma Detection Kit was purchased from Lonza Walkersville, inc. (MD, USA). Tetramethyl rhodamine methyl ester perchlorate (TMRM), carbonyl cyanide 4-(trifluoromethoxy)phenyl-hydrazone (CCCP) was purchased from Sigma-Aldrich Ltd. at the highest purity and respectively dissolved in DMSO and ethanol with no further purification.

2.2 Methods

2.2.1 Formation of Polymersomes by pH switch

PMPC-PDPA was dissolved in PBS [pH2-4] at 10mg/mL. The solution was slowly titrated to pH7-7.5 by drop-wise addition of 0.1M NaOH. Turbidity confirmed the formation of polymersomes.

2.2.2 Formation of loaded and unloaded Polymersomes by Thin Film Rehydration

In glass, PMPC-PDPA was dissolved in a mixture of chloroform and methanol (2:1). Hydrophobic small molecules dissolved in a miscible solvent (ethanol) were added at this point. Where sterility was required, the solution was filtered through 0.2 μ m nylon filters into a sterile glass vial in a class II laminar flow hood, and a 0.2 μ m nylon membrane secured over the vials opening. Solvents were evaporated under vacuum for 24hrs, leaving a thin film of polymer and hydrophobic small molecule(s). This was then rehydrated with Dulbecco's Phosphate Buffered Saline (PBS) - made up to a concentration of 10mg/mL - and left to stir by magnetic bar for 4 - 8 weeks. Following this, a 20 minute sonication was performed at ambient temperature (Water-bath Sonicator, S-100 from

Sonicator Instrument Corporation; 3 litre capacity, 100W output, pulse frequency 40kHz). The process is referred as TFR.

2.2.3 Centrifugal Fractionation of PMPC-PDPA nanoparticles

Polymersomes were centrifugated at 2000 Relative Centrifugal Force (RCF) for 20 minutes, the supernatant removed by pipette, and the resulting pellet resuspended in a volume of PBS equivalent to the original volume. The procedure was then repeated at 15,000RCF. Separation was confirmed by DLS.

2.2.4 Nanoparticle characterisation

2.2.4.1 *Dynamic Light Scattering*

DLS measures the scattering of monochromatic light within an equilibrated suspension of particles over time, which can be used to assess particle size. Fluctuations in light scattering result from the brownian motion of particles, where the larger a particle, the slower its movement and ergo the slow scattered light signal fluctuates. By recording the intensity of scattered light at a fixed point and plotting the decay of this signal normalised to total photon count over time, a samples auto-correlation function is acquired. The larger a particle the longer it will take for its DLS correlation function to decay. For a mono-disperse sample of spherical objects that do not interact with one another, a single exponential decay will be seen. By contrast polydisperse samples will produce variable exponents. Multi-modal samples may also be measured, these being suspensions of particles in which there are two or more particulate populations whose size centre around two distinct means, and which are discontinuous with one another. These will produce auto-correlation functions with a stepped appearance, in which at least two patterns of signal decay are superimposed onto one another.

Assuming a mono-disperse sample, a diffusion coefficient that is proportional to the duration of exponential decay can be calculated, and particle spherical hydrodynamic diameter derived using the 'Stokes-Einstein equation', for diffusion of spherical particles through a liquid with low Reynolds number [416]:

$$D = \frac{k_B T}{6\pi\eta r}$$

Where D is the diffusion constant, k_B is Boltzmann's constant, T is absolute temperature, η is viscosity and r is radius of spherical particle. For polydisperse samples, the measured correlation function will be the sum of intensity correlations measured - meaning the auto-correlations of larger particles will predominate in these measurements - and data fitting models are required to estimate the variance between multiple measurements. Data fitting of this kind is a so called an "ill posed" problem, being a mathematical problem to which there are multiple valid solutions that subsequently require certain assumptions to be made to give the most valid data fit. The Constrained Regularisation Method for Inverting Data (CONTIN method), developed by Stephen Provencher [417], is commonly used to estimate size variance in multimodal nano-particle populations. This technique aims to reveal "the least amount of detail or information that was not already known or assumed, providing smooth distributions between multiple centres of variance" and is routinely used to estimate the size distribution of polydisperse nanoparticle suspensions.

DLS measurements were performed on a Zetasizer nano zs (Malvern Ltd.) at copolymer concentration of 0.25mg/mL. Unless otherwise stated, 3 measurements at 25°C were taken - each consisting of 12 subruns - and averaged to give correlation functions, Z-averages achieved through cumulants analysis and size intensity distributions and Polydispersity Index (PDI) following the CONTIN method of analysis. A 633nm HeNe laser was used at a scattering angle of 173°. Using both a low concentration of nanoparticles and a highly acute angle of detection helps to reduce the effect of multiple scattering, this being the scattering of light, already scattered by one particle, by further particles. Multiple

scattering increases the probability that light will encounter larger particles in a suspension, so decreasing measurements of multiply scattered light increases the signal received from smaller particles.

2.2.4.2 *Transmission Electron Microscopy*

In Transmission Electron Microscopy (TEM), a beam of electrons is emitted by an electron gun and focussed onto a camera detector by magnetic fields. As the beam passes through a sample placed within its path, electron dense regions will prevent electrons passing, creating regions of absent signal on the camera, and from which a two dimensional image of electron dense material can be resolved.

Copper grids (Agar Scientific) were carbon coated and glow discharged. 5 μ L of PMPC-PDPA nanoparticles at 1mg/mL were then applied to these and left to adsorb for 60 seconds. Unattached polymersomes and PBS were removed by blot. Grids were then exposed to 0.75% (w/w) Phosphotungstic acid (PTA)(aq) (pH corrected to 7.4 and sterile filtered through a 0.2 μ m membrane for 5 seconds, and again blotted dry. Excess liquid was removed by vacuum. Stained Electron Micrographs (EM) were then imaged using a FEI Tecnai G2 Spirit electron microscope. EM were captured at 120 keV and analysed using Gatan Digital Micrograph and Image J (version 1.44o) software packages.

2.2.4.3 *Fluorescence emission spectrophotometry*

Fluorescence emission spectrophotometry excites fluorescent materials with defined wavelengths of light, and measures the magnitude of fluorescent light subsequently emitted. Where the amplitude of emitted fluorescent light remains linear to a materials mass, standard curves can be created to determine the mass of an unquantified sample.

R.6G-PMPC-PDPA plus PMPC-PDPA, in the same proportions as found in rhodamine labelled polymersomes, was dissolved in acidified PBS [pH4] and serial dilutions performed to create a standard curve. Samples of rhodamine labelled polymersomes were then taken, and their R.6G-PMPC-PDPA concentration calculated by interpolation from standard curve.

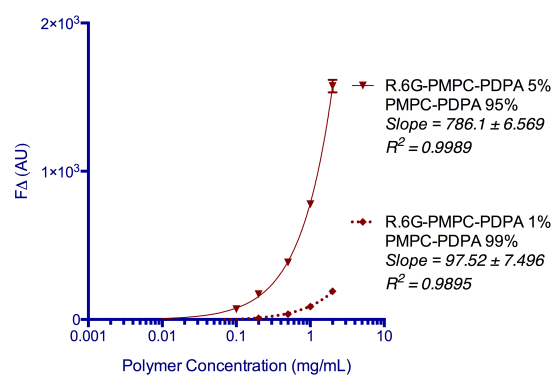


FIGURE 2.2: **R.6G-PMPC-PDPA fluorescence standard curves:** Standard curves produced by serial dilution of R.6G-PMPC-PDPA plus PMPC-PDPA in acidified PBS [pH4].

2.2.4.4 *High Performance Liquid Chromatography*

In reverse-phase High Performance Liquid Chromatography (HPLC), solubilised samples are injected into a mobile phase, typically a mixture of organic and inorganic solvents. This passes through a column packed with modified silica beads that eluted compounds within a sample will adsorb to with varying avidities. Compounds are subsequently retained within the column for durations dependent on their charge, solubility and where MW is great enough to retard passage between packed beads, size. Mixtures of compounds can thus be separated from one another. The mobile phase can then carry the temporally separated materials to a detectors which are used to measure the magnitude of compound present. Coupled with standard curves, this technique is used to quantify the mass of compounds within samples of a known volume.

Samples of PMPC-PDPA nanoparticles suspended in PBS were taken and dried under vacuum over night. Compounds were then re-solubilised in a mixture of acidified MeOH and water (4:1 plus 0.1% Trifluoroacetic Acid (TFA)) equal to one and half times their original volume, so as to solubilise the copolymer, hydrophobic encapsulates and the salts found within PBS. This was most effective where MeOH was added prior to water. Samples were left at 37°C for 30 minutes to assure solubilisation. Where turbidity was seen, the sample was diluted in half its own volume again until clarity was achieved. Only clear solutions were used for HPLC analysis.

Reverse-phase HPLC of samples containing UA, DHE, or cholesterol was performed on a Dionex ultimate 3000 system, using a C₁₈ analytical column (phenomenex[®] Jupiter; octadecylsilyl ultrapure silica, C₁₈, 300Å, 150 x 4.6 mm, 5µm). Samples Ultra Violet (UV) absorbance and 205nm was measured using a UV detector. Data was analysed using Dionex Chromeleon software. Reverse-phase HPLC of samples containing UCA, or UDCA was performed on a Shimadzu UFLC XR system, using a C₁₈ analytical column (phenomenex[®] Jupiter; octadecylsilyl ultrapure silica, C₁₈, 300Å, 150 x 4.6 mm, 5µm). PMPC-PDPA UV absorbance was measured at 205nm on a diode array detector, and small molecules light scattering measured using a Evaporative Light Scattering Detection (ELSD). Data was analysed using Shimadzu Labsolutions LCSolution software. Column temperature was set to 30°C in both sets of equipment.

UA and UDCA containing samples were injected into an initial mobile phase of 60% MilliQ filtered water (MQ) and 40% [0.1% TFA] (eluent A) Methanol (MeOH) [0.1% TFA] (eluent B). The following multistep gradient was then used at a flow rate of 1mL/min; 0 minutes 30% eluent B, 5 minutes 30% eluent B, 12 minutes 100% eluent B, 20 minutes 100% eluent B, 21 minutes 30 % eluent B, 26 minutes 30 % eluent B. The column was cleaned with 20 column volumes (1mL/min flow for 30 minutes) of 100% methanol and 5% methanol.

UCA, DHE and cholesterol containing samples were injected into an initial mobile phase of 60% MQ and 40% [0.1% TFA] (eluent A) MeOH [0.1% TFA] (eluent

B). The following multistep gradient was then used at a flow rate of 1mL/min; 0 minutes 30% eluent B, 5 minutes 30% eluent B, 12 minutes 100% eluent B, 22 minutes 100% eluent B, 23 minutes 30 % eluent B, 28 minutes 30 % eluent B. The column was cleaned with 20 column volumes (1mL/min flow for 30 minutes) of 100% methanol and 5% methanol.

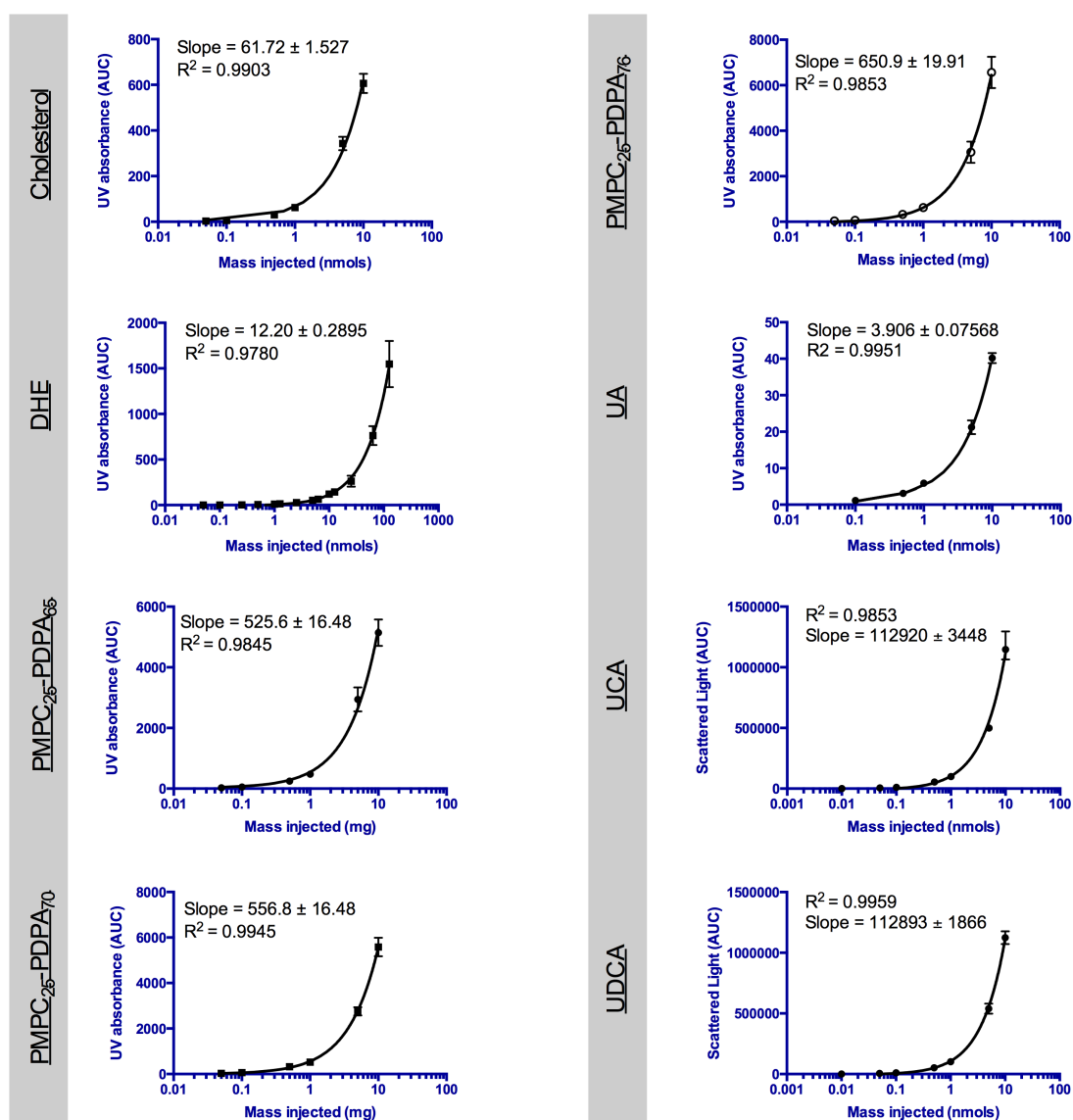


FIGURE 2.3: **Calibration curves of known standards:** Calibration curves of known standards following HPLC. Sample UV absorption at 205nm of light scattering was measured, and area under curves (AUC) calculated, from which calibration curves were constructed.

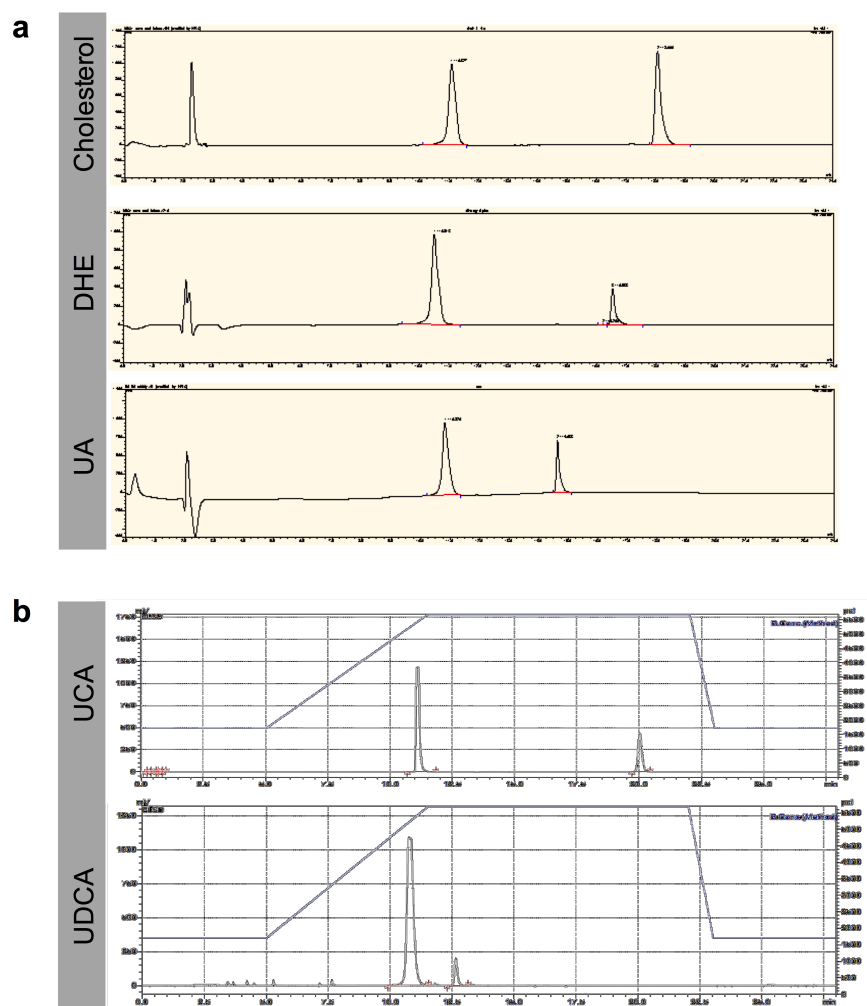


FIGURE 2.4: **Example HPLC traces:** HPLC traces of solubilised PMPC-PDPA plus compounds. (a) UV detection (205nm) and (b) ELSD detection.

2.2.5 Purification by Hollow Fibre Filtration

In Hollow Fibre Filtration (HFF), solutions are passed through hollow fibres possessing pores of distinct size / Molecular Weight Cut Off (MWCO), tangential to the direction of flow (figure 2.5a). This allows particles and/or molecules of low enough size to pass out whilst continuously moving larger particles onwards, preventing their lodging within these pores, retarding the filtration process. The extent of flow required for complete filtration of TFR formed poly-mersomes from unencapsulated material was assessed using Bovine Serum Albumin (BSA). 1mM BSA (69.3kDa) was added to a 10mg/mL solution of

TFR formed PMPC-PDPA nanoparticles and dilute either 50, 100 or 150 times. These were passed through porous hollow fibres (MWCO 500kDa, $\sim 20\text{-}50\text{nm}$ \varnothing) at $15\text{mL}/\text{min}$, until the original volume was reached. For comparison, BSA nanoparticle solutions were also purified by Gel Permeation Chromatography (GPC). Sepharose-4B beads ($45\text{-}165\mu\text{m}$ \varnothing , $35\text{-}50\text{kDa}$ pores) were packed into a 10mm \varnothing column to 75mm in height, and to which $200\mu\text{L}$ of nanoparticle plus BSA solution was added from the top. As BSA molecules are close in size, they will in part enter sepharose pores where they will temporarily be retained, and so will exit the column after larger nanoparticles which pass between beads without retention (figure 2.6b). Fractions were collected in a 96 well plate, each $\sim 100\mu\text{L}$ in volume (two drops), and turbid fractions combined. A second round of GPC was used to confirm full separation. UV-HPLC was used to determine BSA and copolymer concentrations of samples before and after purification steps (figure 2.5c).

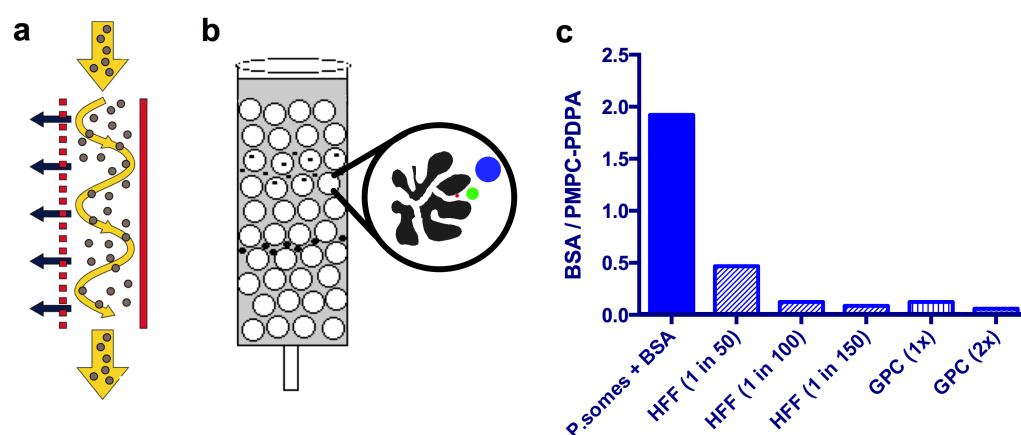


FIGURE 2.5: **Validation of purification techniques for PMPC-PDPA nanoparticles:** Cartoons of (a) HFF and (b) GPC. (c) BSA : PMPC-PDPA ratios (w/w) of polymersome plus BSA suspension, following purification by HFF, or GPC Images adapted from the Wikimedia Commons with permission

The ability of HFF to remove micellar UA was also validated. An UA thin film was solvent cast from a 1mM stock (ethanol), rehydrated to 1mM in PBS and agitated by magnetic stirrer (700rpm) for 4 weeks. The resulting solution was added to TFR formed polymersomes ($10\text{mg}/\text{mL}$), which were then diluted 1 in 100, and purified by HFF using $\sim 20\text{nm}/500\text{kDa}$ pores until the original volume

was re-established. Quantification by UV-HPLC reveals a decrease in UA concentration following HFF (figure 2.6).

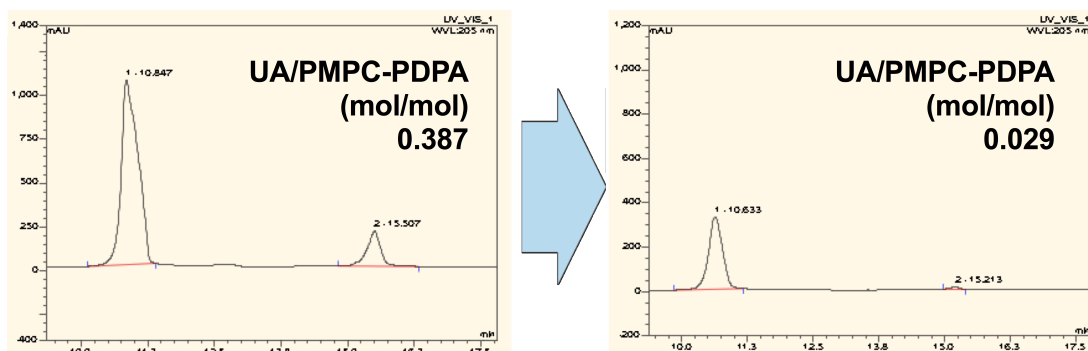


FIGURE 2.6: **Purification of micellar UA by HFF:** HPLC traces of polymer-some plus micellar UA before and after HFF at a 1 in 100 dilution. UA to PMPC-PDPA ratios (mol/mol) are indicated.

2.2.6 Primary Fibroblast Culture

Fibroblasts were kept at 37°C and 5% CO₂, and fed three times a week in MEM supplemented with; 10% FBS, L-glutamine (2 mM), sodium pyruvate (1mM), penicillin (100 IU/mL), streptomycin (100µg/mL), uridine (50µg/mL), and 1x MEM vitamins. Cells were subcultured at 80-90% confluence by chemical detachment (1x Trypsin plus EDTA or versene). Mycoplasma testing was performed fortnightly using the MycoAlert™ Mycoplasma Detection Kit (assay performed by Mrs. H. Crewe)

2.2.7 Physiological Assays

For physiological assays, cells were seeded into well plates at the required number and left to grow in media for 24 hours. 48 hours prior to physiological assays, cells were washed and left in galactose media consisting of; MEM (without glucose), supplemented with 10% FBS, sodium pyruvate (1mM), penicillin (100 IU/mL), streptomycin (100µg/mL) and 0.9 mg/mL galactose, as described before. 24 hours prior to physiological assays cells were changed into

fresh galactose media containing desired testable conditions (small molecules, polymersomes or appropriate controls). Testable conditions were applied in triplicate unless otherwise specified. Physiological assays comparing healthy and *parkin* mutant fibroblasts utilised cells matched by sex and subject age to within three years at time of biopsy. Cells were matched to within one passage of one another, and no fibroblasts were assayed passed passage 14.

2.2.7.1 *Lactate Dehydrogenase release assay*

Lactate Dehydrogenase (LDH) is a ubiquitous and highly stable cytosolic protein. An increased presence in extracellular LDH is good indication of increased membrane permeability, itself a sign of cellular toxicity. LDH release was assessed in fibroblasts using the CytoTox-ONE™ Homogeneous Membrane Integrity Assay kit (Promega, Madison, WI) according to the manufacturers instructions. Briefly, fibroblasts were seeded in a clear 96 well plate at 5000 cells per well and cultured as described above, except that conditions were applied to six wells instead of three. Cells were equilibrated to room temperature, and a 100% lysis solution was added to three of the six wells assigned to each tested condition. 100µL of "assay buffer" was applied to all wells containing cells plus media only "blanks", and shaken at 700rpm for 10minutes. The presence of LDH linearly catalyses the process leading to resazurins - present in the "assay buffer" - conversion to the fluorescent resorufin . 50µL of "stop solution" was then added to all wells, and shaken at 700rpm for 10 seconds. Resorufin fluorescence (excitation = 560nm, emission = 590nm) was then measured was then measure on a plate reader (Omega Fluostar, bottom reading). LDH release was expressed as:

$$\left(\frac{MeanFluorescence - Blank}{Mean Fluorescence 100\% Lysis - Blank} \right) \times 100 = LDH Release (\%)$$

2.2.7.2 *Mitochondrial Membrane Potential assay*

In order to produce ATP, the mitochondria must establish a proton gradient across its inner membrane. Decreases in the electrochemical potential are a good indicator of a dysfunctional ETC. MMP was assessed as previously described [95, 418]. Briefly, cells were seeded in clear 96 well plates at 5000 cells per well and cultured as described above, except that conditions were applied to six wells instead of three. CCCP - a chemical uncoupler of the mitochondrial respiratory chain - was applied to half the wells of each experimental condition 1.5 hours prior to the assay (final concentration 10 μ M). One hour later, media is removed from all cell and blank wells, and replaced with 100 μ L of 150nM TMRM made up in standard assay buffer (80mM NaCL, 75mM KCl, 25mM d-glucose, 25mM HEPES, solution corrected to pH7.4) and left to incubate for 30 minutes at 37° C. TMRM, a "Nernstian dye", is known to accumulate within cells and organelles in a membrane potential dependent manner [419], though also strongly adsorbs to the polystyrene of 96 well plates. Thus TMRM is removed and wells are washed 3 times with 150 μ L PBS - to remove excess TMRM - and left in 100 μ L PBS. TMRM fluorescence (excitation = 530, emission = 580) is then read on a plate reader (Omega Fluostar, bottom reading). Mean TMRM fluorescence of cells in the presence of CCCP (i.e. lacking the MMP) and without (i.e. whole cell membrane potential) can then be calculated for each condition. 50 μ L of CyQUANT[®]-NF solution, made up as per the manufacturers instructions, is then added to all wells and left to incubate at 37°C for 1 hour. CyQUANT[®]-NF fluorescence (excitation = 485nm, emission = 530nm) was read on a plate reader (Omega Fluostar, bottom reading), and is used as an inference of cell number:

$$\frac{\text{Mean TMRM Fluorescence} - \text{TMRM Blank}}{\text{Mean CyQUANT}^{\text{®}} \text{Fluorescence} - \text{CyQUANT}^{\text{®}} \text{Blank}} = \text{MMP / DNA (a.u.)}$$

$$\text{Membrane Potential} - \text{Membrane Potential with CCCP} = \text{MMP/DNA (a.u.)}$$

The MMP assay has previously been performed using 10 minute TMRM incubation periods, however this was found to produce weak signal to noise ratios. Incubation of 150nM TMRM over 30 minutes was selected as reliable following optimisation studies (figure 2.7a). Confocal microscopy at consistent laser exposure and gain settings confirmed loss of mitochondrial TMRM staining in cells pretreated with 10 μ M CCCP persisted after 30 minutes (figure 2.7b).

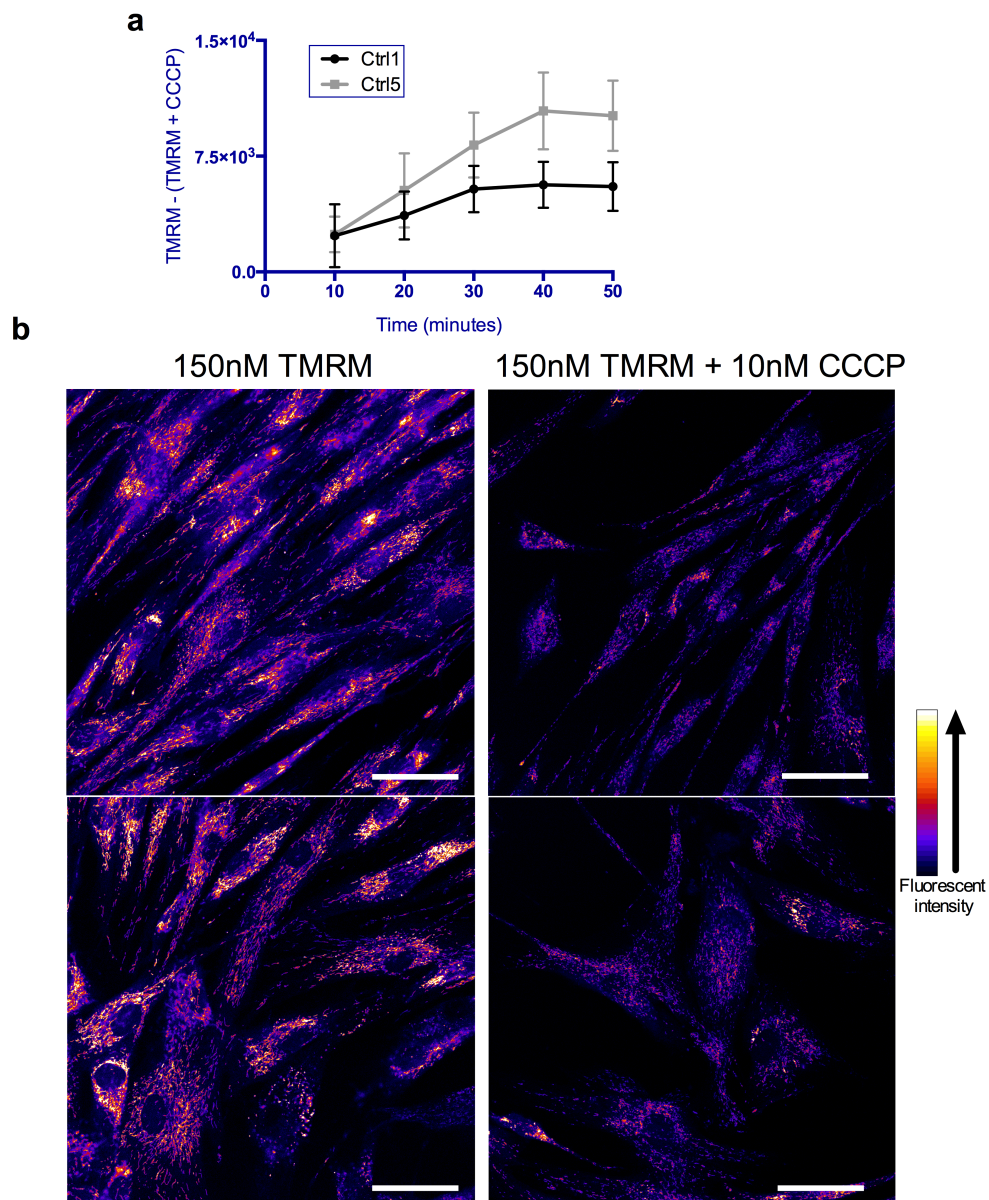


FIGURE 2.7: **Optimisation of TMRM incubation periods:** Ctrl1 and Ctrl5 were incubated with 150nM TMRM in standard assay buffer for 10, 20, 30, 40 and 50 minutes. Matched conditions including 1 hour incubation with 10 μ M CCCP were included. (a) Fibroblast TMRM fluorescence minus TMRM plus CCCP fluorescence ($n = 3$). (b) Confocal microscopy images of fibroblasts and fibroblasts pretreated with CCCP following 30 minute incubation with TMRM (taken with Zeiss 510 LSM confocal microscope; 60x objective, scale bars = 50 μ m).

2.2.7.3 *Cellular ATP Levels*

Cellular Adenosine Triphosphate (ATP) levels were measured using the the Perkin Elmer™ ATPlite kit™ according to the manufacturers instructions. Briefly, fibroblasts were seeded in a white walled 96 well plate at 5000 cells per well and cultured as described above. Cells and blank wells were then equilibrated to room temperature, and their media was removed and replaced by 50µL of lysis buffer. Plates were shaken at 700rpm for 5 minutes on an orbital shaker, following which 50µL of ATP substrate - containing luciferin and luciferase - was added to each well, and shaken for a further 5 minutes. 100µL of PBS was added to every well, and the plate removed from all sources of light to dark adapt for 10 minutes. In the presence of ATP and O₂, luciferase catalyses the conversion of luciferin to oxyluciferin and a number of other products including light. Luminescence was measured on a plate reader (Omega Fluostar, bottom reading). Plates were then removed and 50µL of CyQUANT-NF® - made up as per manufacturers instructions - was added to all wells, and left to incubate at 37°C for 1 hour. The CyQUANT®-NF solution contains a cell permeabilisation agent and a DNA binding dye whose fluorescence greatly increases when bound. CyQUANT® fluorescence (excitation = 485nm, emission = 530nm) was read on a plate reader(Omega Fluostar, bottom reading), and is used as an inference of cell number. Cellular ATP levels calculated as follows:

$$\frac{\text{Mean ATPlite}^{\circledR} \text{ Luminescence} - \text{Blank}}{\text{Mean CyQUANT}^{\circledR} \text{ Fluorescence} - \text{Blank}} = \text{ATP/DNA (a.u.)}$$

Cellular ATP and DNA assays produce signals independent of one another, and both of which show good linearity over a wide range of cell number [420–422]. However as assays are performed sequentially on the same lysed fibroblast population, it is possible that aspects of the ATP assay may interfere with the linearity of the DNA assay. To test this, healthy and *parkin* mutant fibroblasts were detached and aliquoted in PBS at 500, 1000, 5000, 10,000 and 20,000 cells per well. Both assays were then performed sequentially as before. A

linear positive correlation between cell number, ATP and DNA signal was seen in all fibroblasts tested (figure 2.8 a,b,c).

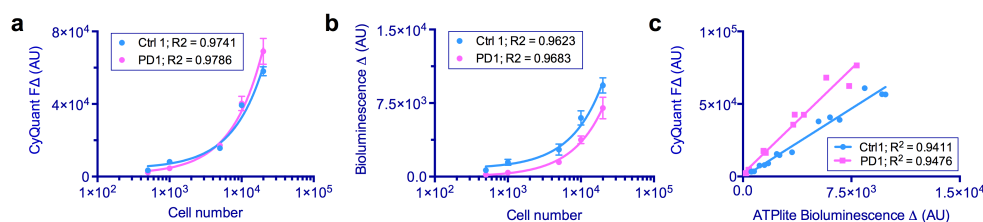


FIGURE 2.8: Linearity of DNA quantification after ATP bioluminescence assay: Fibroblasts were detached, resuspended in PBS and aliquoted into a 96 well plate at 500, 5000, 10,000 and 20,000 cells per well. (a) CyQuant and (b) ATP assays were then performed sequentially and linearity between cell number, and (c) each over tested (error bars = SD derived from three technical repeat within a single experiment i.e. $n = 1$).

2.2.7.4 Polymersome uptake assays

Cells were seeded in 12 well plates at 33,000 cells per well and cultured as described above with some exceptions. 24 hours prior to the application of polymersomes, wells were changed into galactose media. Fluorescent polymersomes were then applied directly to cell wells at the desired concentration, and left to incubate for the desired time. Application of polymersomes was staggered so that the varied incubation times would be reached concurrently, and so polymersome uptake could be assayed in parallel. A control population incubated with no polymersomes was also included and one technical repeat was performed for each condition per assay. Following polymersome incubation, cells were washed five times and detached (1% trypsin). Cells were centrifuged at 1000RCF in 1.5mL eppendorfs for 5 minutes and resuspended in 400 μ L cold PBS (4°C). Flow cytometry was then performed using either a BD FACSAarray™ Bioanalyzer, a Life technologies Attune® autosampler or a BD™ LSRII as indicated. Forward scatter, side scatter fluorescence lasers were calibrated before each experiment according to the manufacturers instructions. Size gating was determined using a control population of fibroblasts, one for each fibroblast

set. The fluorescent emissions of Rhodamine 6G labelled PMPC-PDPA fluorescence (excitation = 538nm, emission = 575nm) and where present DHE (excitation = 325nm, emission = 375nm) were measured in 10,000 size gated cells. Laser intensity was calibrated to produce a signal for the weakest signal/shortest incubation time, and kept constant within all experiments in a series. Data was analysed using the software local to the equipment in use.

2.2.8 Statistical analysis

All statistics were calculated using Graphpad Prism[®] version 5. Where appropriate, statistical significance was determined using p values as follows; $p \leq 0.05 = *$, $p \leq 0.01 = **$, $p \leq 0.001 = ***$, $p \leq 0.0001 = ****$.

- Student's t-test was used to assess the probability that the mean of two populations was different where data did not, or could not be assumed to possess a normal distribution.
- The Mann-Whitney test was used to assess the probability that the mean of two large data sets ($n > 100$) was different, where data did not fit a Gaussian distribution according to the "D'Agostino and Pearson omnibus normality test".
- One-way Analysis Of Variance (ANOVA) was used to assess the probability that the mean outputs from varied instances of the same treatment group (e.g. polymersome concentrations) within a single cell line were different.
- Two Way Analysis Of Variance (ANOVA) was used to assess the probability that the mean outputs produced by two categorically independent conditions (e.g. polymersome concentration and cell type) were different and to what extent these two conditions interacted with one another. Multiple comparisons were made following the Bonferoni correction, to assess for specific statistical differences between two groups within the same condition.
- Regression analysis was used to assess the correlation between a measured output and a scalable variable, as well as the linearity of any relationship.

Except where stated, results constitute three independent experiments, in each of which three measurements were taken.

Chapter 3

Results: Drug Loaded Polymersomes

3.1 Aims

To form and purify cePMPC25-PDPA65 nanoparticles encapsulating UA, UCA, UDCA, cholesterol, or nothing. The size, shape and encapsulation efficiencies of these are to be characterised, and the nature of their pathway to formation investigated.

3.2 Background

PMPC-PDPA, a pH sensitive diblock co-polymer self-assembles into nano- and micro-scaled structures on hydration owing to hydrophobic and hydrating forces. PMPC₂₅⁻ PDPA₇₀ is a membrane forming diblock copolymer that tends to assemble into energetically stable isotropic vesicles known as polymersomes [358]. The membranes of these are able to retain hydrophobic compounds, allowing polymersomes to act as water soluble vectors to insoluble molecules [341, 404].

Polymersomes are also capable of delivering hydrophobic compounds into endocytically active cells [402, 404].

The hydrophobic small molecules UA, UCA and UDCA¹ were recently identified as potential PD disease modifying agents (figure 2.1) [198]. UCA and UDCA are both tetracyclic triterpenes and bile acid derivatives [423], whilst UA is a pentacyclic triterpene found in a number of plants [271]. They bear similarities to cholesterol, a compound that in mammals is packaged into nanoscopic lipoproteins so it may be effectively transported through systemic circulation to numerous locations [287, 288]. Due to their hydrophobicity, UA, UCA and UDCA have previously been conjugated to water soluble compounds where they acted as the hydrophobic component of amphiphilic molecules designed to self assemble into nanoscopic micelles [424–426]. UA and UDCA have also been packaged within liposomal membranes, which demonstrated enhanced mechanical properties over empty liposomes [427–429].

Here UA, UCA and UDCA loaded polymersomes are formed by TFR of pre-mixed polymer-drug films at a final concentration of 10mg/mL in PBS. These were purified by tangential flow filtration, following which cargo encapsulation efficiencies, particle morphologies and particle size distributions were characterised. Encapsulation of these compounds was found to alter the morphology of polymersomes in a fashion akin to previous observations with NBD-Cholesterol encapsulation. The nature of these morphological changes is investigated further with UA, UCA, UDCA and Cholesterol by morphological fractionation and mass quantification.

3.3 Thin film rehydration of PMCP₂₅—PDPA₆₅

In TFR, nanoparticles are formed from a thin film of amphiphile and the desired encapsulate. Hydration of this film in the presence mechanical energy results in the formation of nanoparticles and the highly efficient encapsulation

¹Predicted logPs; UA = 7.3, UCA = 8 and UDCA = 4.9

of hydrophobic compounds [341, 413]. Use of high MW diblock copolymer has proven particularly effective in this regard, likely owing to the large membrane cores and robust nature of the nanoparticles they form [321, 341].

A PMPC₂₅–PDPA₆₅ film was solvent cast and rehydrated in PBS to a concentration of 1% w/w. Agitation by magnetic stirrer was applied over four weeks and the resulting particulate suspension was sonicated for 20 minutes. This produced dispersed particles of heterogenous morphology, ranging from isotropic particles resembling typical polymersomes to large lyotropic and high genus² structures with tube like protrusions (figure 3.1a,c). No multi-lamellar assemblies were apparent. This contrasts with the isotropic dispersed particles that would be expected at this concentration when using similar copolymers [409, 412], and indeed, which particles formed using the pH switch method of formation possessed (figure 3.1 b). Concordantly, those particles produced by pH switch were of smaller average size and size distribution compared to those particles formed by TFR (figure 3.1 c). Small particles <50nm were seen with both methods of formation, either representing micelles formed during TFR or more probably the result of vesicles that "burst" during drying steps required of the staining procedure (figure 3.1 a,b)[430].

During TFR, water and membrane forming amphiphile films diffuse into one another developing a concentration gradient of water [412]. At the interface, hydrophilic blocks hydrate and begin to effectively "repulse" one another, whilst the insoluble blocks are pushed away from water and driven together. Studies with large MW poly(ethylene oxide)copoly(butylene oxide) (EB) have shown membrane forming copolymers arrange themselves into planar sheets known as lamellae or long rods that later transition to lamellae [407, 409]. As the lamellae continue to swell with water, the effects of hydrophobic and hydrating forces become stronger, eventually resulting in membrane unbinding events that occur with thermodynamic fluctuations, and from which "sponge phases" are formed [407, 409]. As water continues to diffuse into these and alter the balance of

²"Genus" is used in its topological sense, and refers to particles possessing holes within their bulk that do not break the membrane

forces holding such assemblies together, copolymer amphiphiles continue to unbind into more energetically favourable structures, until particles of energetic uniformity are created. TFR subsequently generates a wide “spectrum” of initial metastable and stable morphologies, which all typically transition into isotropic structures with the addition of further external energy, such as ongoing stirring or sonication (figure 3.1e) [[412](#), [431](#)].

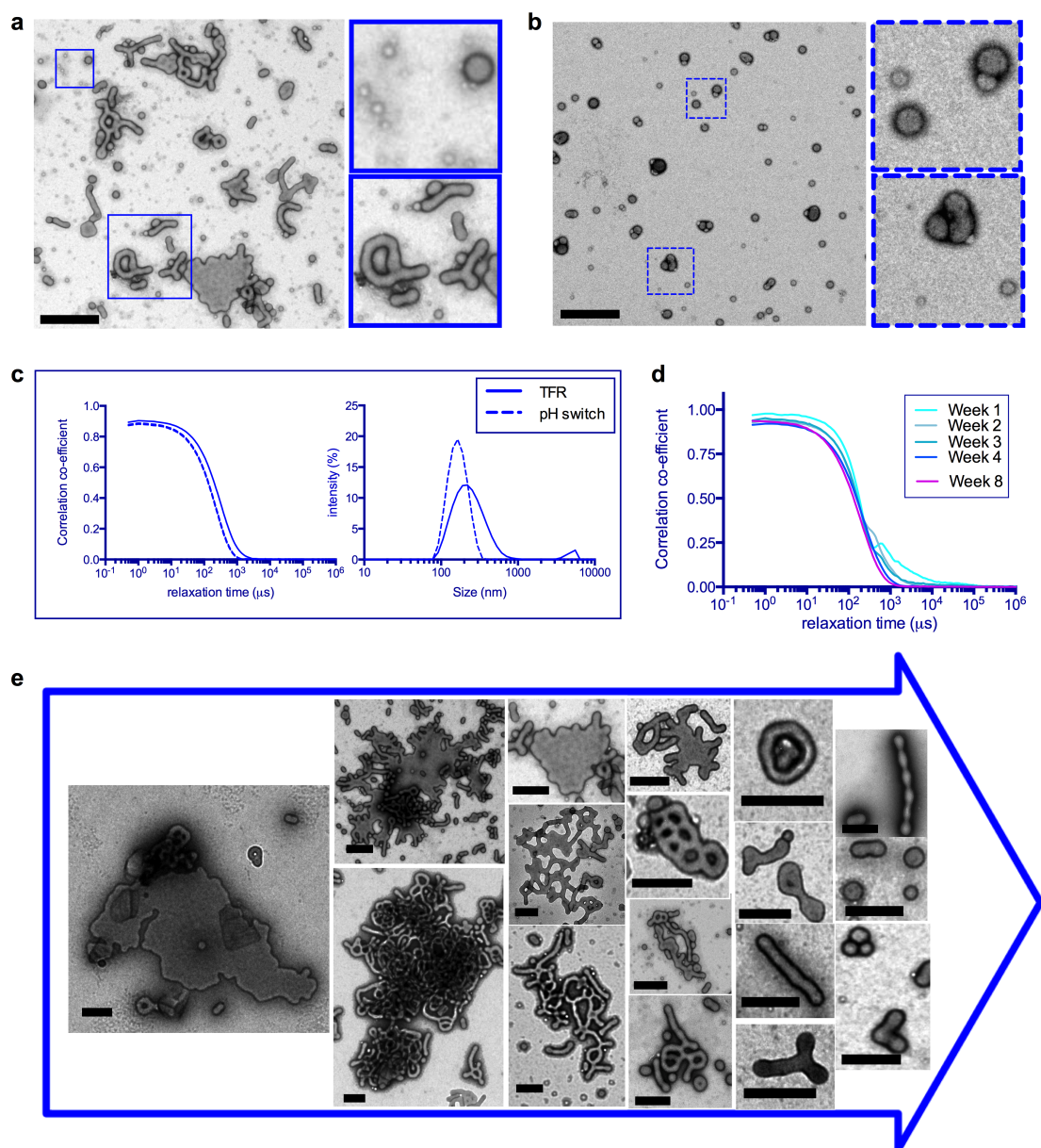


FIGURE 3.1: Thin film rehydration of $\text{PMPC}_{25}\text{-PDPA}_{65}$ produces mixed particle morphologies: EMs of $\text{PMPC}_{25}\text{-PDPA}_{65}$ nanoparticles formed by (a) TFR over 4 weeks and (b) pH switch methods of formation, both following 20 minutes sonication (scale bar = 500nm, magnified sections indicated by boxed selection). (c) DLS determined auto-correlation functions (left) and calculated size distributions by intensity (CONTIN algorithm) (right) for both nanoparticle suspensions. (d) DLS auto-correlation functions of TFR formed nanoparticles over 8 weeks formation. (e) Proposed transitional pathway of from bulk film to isotropic dispersed particles during TFR; images taken from multiple fields of view of the same electron micrograph

(scale bar = 200nm).

The presence of “lyotropic structures” after four weeks stirring that were resilient to sonication was unexpected. Diblock copolymers possess CACs close to zero, so once an assembly is closed, the number of amphiphile chains within is essentially fixed and non exchangeable [408, 432]. Thus morphological changes must occur by membrane fission/unbinding. The long lived nature of large, metastable particles here may be due to the high viscosity large MW copolymer membranes possess, and the formation of surprisingly stable initial metastable assemblies owing perhaps to unique polymer chain arrangements in bulk film [410, 433]. None the less, DLS over time reveals a particulate population tending towards smaller and more uniform sizes over weeks (figure 3.1d), indicating the presence of metastable assemblies slowly re-arranging into smaller, more energetically favourable structures. Arranging particle morphologies by order of size reveals a possible transitional pathway (figure 3.1e). Large intact planar structures are visible throughout the nanoparticle suspension. As open ended membrane sheets cannot exist in water, and end capping of discs only occurs only at great energetic cost with diblock copolymers, these are likely enclosed structures [434]. It is also notable that they possess irregular/non-uniform morphologies, another indication of the surprising stability presumably metastable structures in this particle population demonstrate. These planar structures appear to evolve holes that expand to form large interconnected tubular networks, which break from the bulk to form dispersed tubes and high genus structures. Tubes, branched tubes and tori of smaller scale are observed, and evidence of “pearling” is seen within these, instabilities which can result in budding and the formation of smaller tubes and/or vesicles. The absence of multi-lamellar structures is notable, and suggests bulk $\text{PMPC}_{25}\text{-PDPA}_{65}$ may evolve directly into the large suspended structures seen here.

By contrast, when $\text{PMPC}_{25}\text{-PDPA}_{65}$ were formed by a bottom up approach, the pH switch method, the great majority of particles produced were vesicles (figure 3.1b). This utilises the rapid switch in $\text{PMPC}_{25}\text{-PDPA}_{65}$ solubility above and below its acid dissociation constant (pKa), allowing molecularly dissolved amphiphile chains to freely assemble without prior ordering. That only vesicles and

micelles form underlines the energetic and entropic favourability these structures possess, and that PMPC₂₅–PDPA₆₅ assemblies will ideally tend towards arrangements of energetic uniformity. Vesicles produced by both methods are of similar size (figure 3.1 a,b).

Work in collaboration with James Robertson [435] showed PMPC–PDPA nanoparticles could be separated on the basis of size and density using stepwise centrifugal fractionation, without marked morphological changes. Centrifugation at 2000RCF, separation of supernatant and pellet, and further centrifugation of this supernatant at 15000RCF was found to reliably produce fractions enriched with larger “lyotropic aggregates”, “tubular” and high genus assemblies or smaller tubular and spherical “polymersomes” (figure 3.2a). Polymersomes were created by TFR, and samples taken and sonicated at weekly intervals up to four weeks, and a final sample taken after 8 weeks formation. These were split into the described morphological fractions and their relative masses determined using UV-HPLC (figure 3.2b, validation of HPLC method in Chapter 2). An initial transition from larger “lyotropic aggregates” to “tubes” and “polymersomes” is seen over the first 4 weeks, after which the presence of “polymersomes” overtakes the predominance of “tubes” indicating a transition of the former into the latter. This further supports the presence of long lived large metastable structures within the nanoparticle suspension.

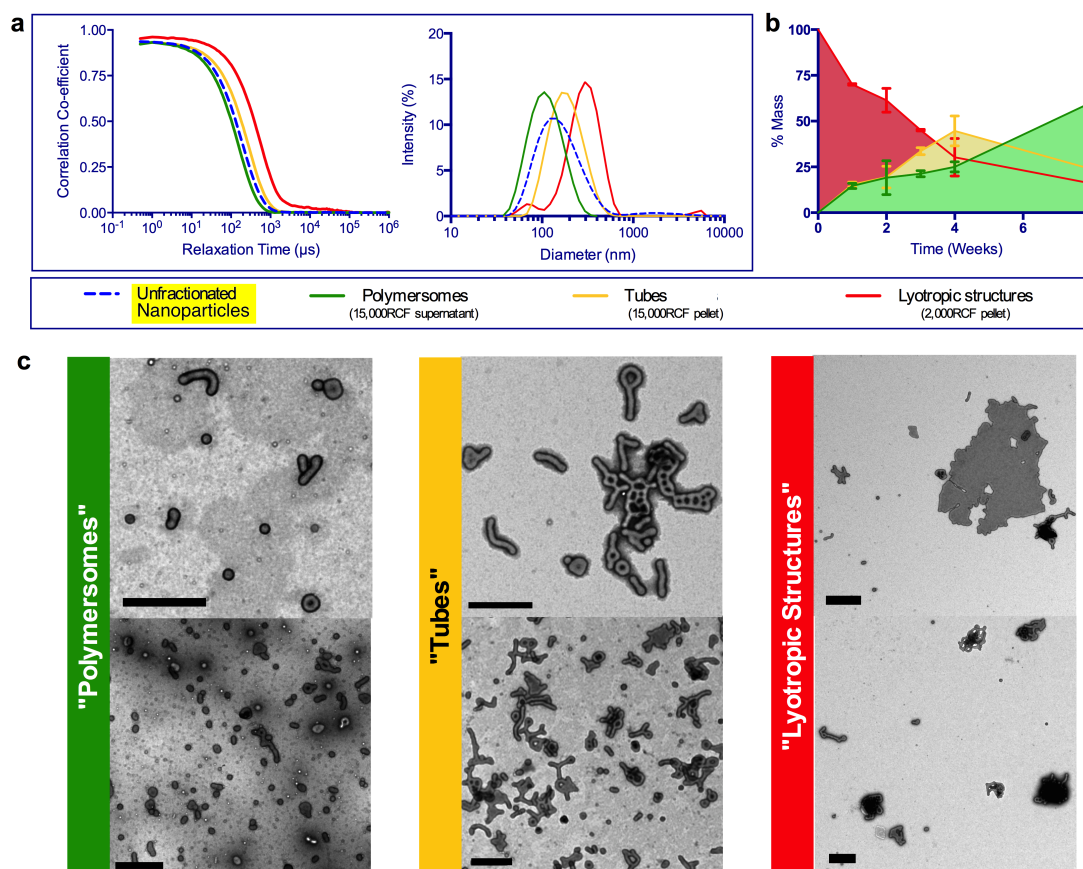


FIGURE 3.2: **Centrifugal fractionation of nanoparticles:** TFR of $\text{PMPC}_{25}\text{-PDPA}_{65}$ proceeded for 8 weeks under continuous agitation by magnetic stirrer. Samples were taken at weekly intervals, sonicated, and centrifugally fractionated. (a) DLS auto-correlation profiles and CONTIN calculated size distribution for of each centrifugal fraction, plus un-fractionated particles after 8 weeks formation. (b) The relative masses of each fraction during continuing agitation were determined by UV-HPLC (mean 3 separately prepared samples; error bars = SD). (c) Two separate fields of view from EM supporting nanoparticles from "Polymersome", "Tube" or "Lyotropic Structure" fractions, following 8 weeks formation (scale bar = 500nm).

3.4 Formation, purification and characterisation of PMPC₂₅–PDPA₆₅ nanoparticles encapsulating tetracyclic and pentacyclic compounds

PMPC-PDPA polymersomes encapsulating hydrophobic compounds have previously been prepared by TFR, with high resulting encapsulation efficiencies following purification by GPC [341]. Encapsulation of UA, UCA and UDCA within PMPC₂₅–PDPA₆₅ nanoparticles was trialled with films designed to produce a 10 μ M (low concentrations) or 1 mM (high concentration) drug solution, at copolymer concentrations of 10 mg/mL. Following 4 weeks formation, nanoparticles were characterised by DLS, TEM and drug/copolymer concentrations quantified by UV-HPLC (figure 3.3 and table 3.1). Nanoparticles were then purified by HFF, following which drug and polymer concentrations were re-quantified (table 3.1).

<i>Low Drug Conc. (10 μM)</i>					
		Copolymer (mg/mL)	Drug (nmol/mL)	Drug EE (% initial)	Drug/Copolymer (mol/mol)
	Initial Conc.	10	10	100.00%	0.0212
Pre HFF	Empty	7.8 \pm 0.42	N/A	N/A	N/A
	UA	8.8 \pm 0.12	8.2 \pm 1.46	82.05%	0.020
	UCA	8.4 \pm 0.55	8.5 \pm 0.75	85.48%	0.021
	UDCA	8.7 \pm 0.2	7.9 \pm 2.93	79.93%	0.019
Post HFF	Empty	5.8 \pm 0.93	N/A	N/A	N/A
	UA	6.4 \pm 0.63	5.9 \pm 2.27	59.27%	0.019
	UCA	5.9 \pm 0.86	6.4 \pm 1.56	64.56%	0.023
	UDCA	6.8 \pm 0.76	6.5 \pm 0.35	65.35%	0.020
<i>High Drug Conc. (1 mM)</i>					
		Copolymer (mg/mL)	Drug (nmol/mL)	Drug EE (% initial)	Drug/Copolymer (mol/mol)
	Initial Conc.	10	1000	100.00%	2.12
Pre HFF	Empty	7.8 \pm 0.42	N/A	N/A	N/A
	UA	8 \pm 0.71	667.6 \pm 4.9	66.77%	1.754
	UCA	8.6 \pm 0.7	703.2 \pm 7.1	70.31%	1.719
	UDCA	7.9 \pm 1.11	614.3 \pm 9.9	61.44%	1.646
Post HFF	Empty	5.8 \pm 0.93	N/A	N/A	N/A
	UA	5.3 \pm 0.75	392.7 \pm 3.2	39.28%	1.549
	UCA	5.9 \pm 0.24	442.5 \pm 4.5	44.25%	1.584
	UDCA	5.1 \pm 0.58	352.6 \pm 8.5	35.27%	1.449

TABLE 3.1: Copolymer and drug concentrations (mean of 3 measurements \pm SD), drug encapsulation efficiency (EE, % initial drug present) and drug : copolymer ratios (mol/mol) of nanoparticles after formation and HFF. Post HFF values are corrected for differences in volume.

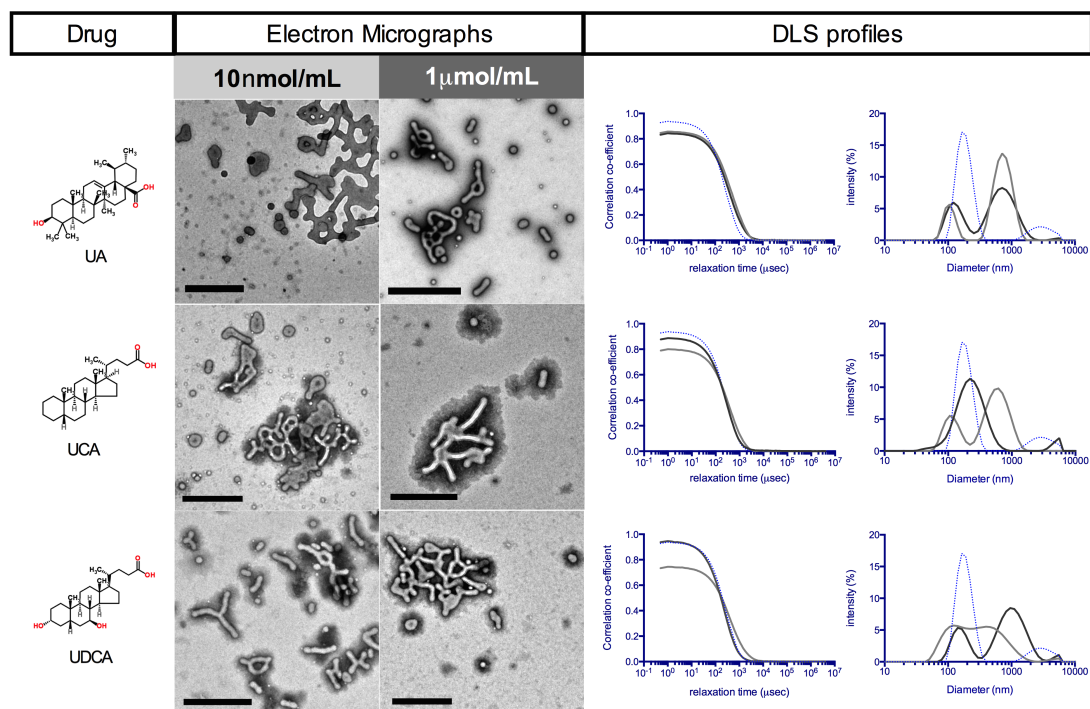


FIGURE 3.3: **Drug loaded PMPC₂₅–PDPA₆₅ nanoparticles:** (Top) Electron micrographs and DLS auto-correlation functions, and size distributions by intensity of drug loaded nanoparticles are shown for each compound in rows. Light grey = 10nmol/mL drug per 10mg/mL copolymer, Dark grey = 1 μ mol/mL drug per 10mg/mL copolymer, and for reference dotted lines = 10mg/mL copolymer alone.

Drug loaded nanoparticles took on a spectrum of morphologies similar to those seen with unloaded nanoparticles, though possessed larger size distributions (figure 3.3). Drug and copolymer quantification after formation revealed neither drug loaded or pristine copolymer films formed into nanoparticles with 100% efficiency (table 3.1), reflected by a visible unsuspended / insoluble mass within these samples. Following purification by HFF, the proportion of drug encapsulated is essentially unchanged at the low concentration, indicating almost all drug is present within co-polymer particles (table 3.1). At the high drug concentration, a slight though marked drop in % drug and drug:copolymer ratio is seen. It is unknown whether this results from the loss unencapsulated material or as a result of the purification, between \sim 20-30% of copolymer being lost by the HFF process.

Nanoparticles were next centrifugally fractionated, and separation confirmed by DLS (figure 3.5). ELSD/UV-HPLC revealed a greater proportion of drug within the “tube” fraction, relative to copolymer. The “polymersome” and “tube” fractions were stored at 4°C for 6 months and size distributions re-assessed. Drug loads were also re-characterised following purification by GPC to remove any freed drug (figure 3.5). Little deviation was seen in particle size distribution, indicating good long term stability. The appearance of slight bimodal distributions in some particles indicates that some larger particles were present after 6 months storage, though notably the particle suspensions still had not visibly precipitated. Similarly, drug loads did not significantly alter between the two time-points, again indicating all the compounds readily sit within the PMPC-PDPA membranes.

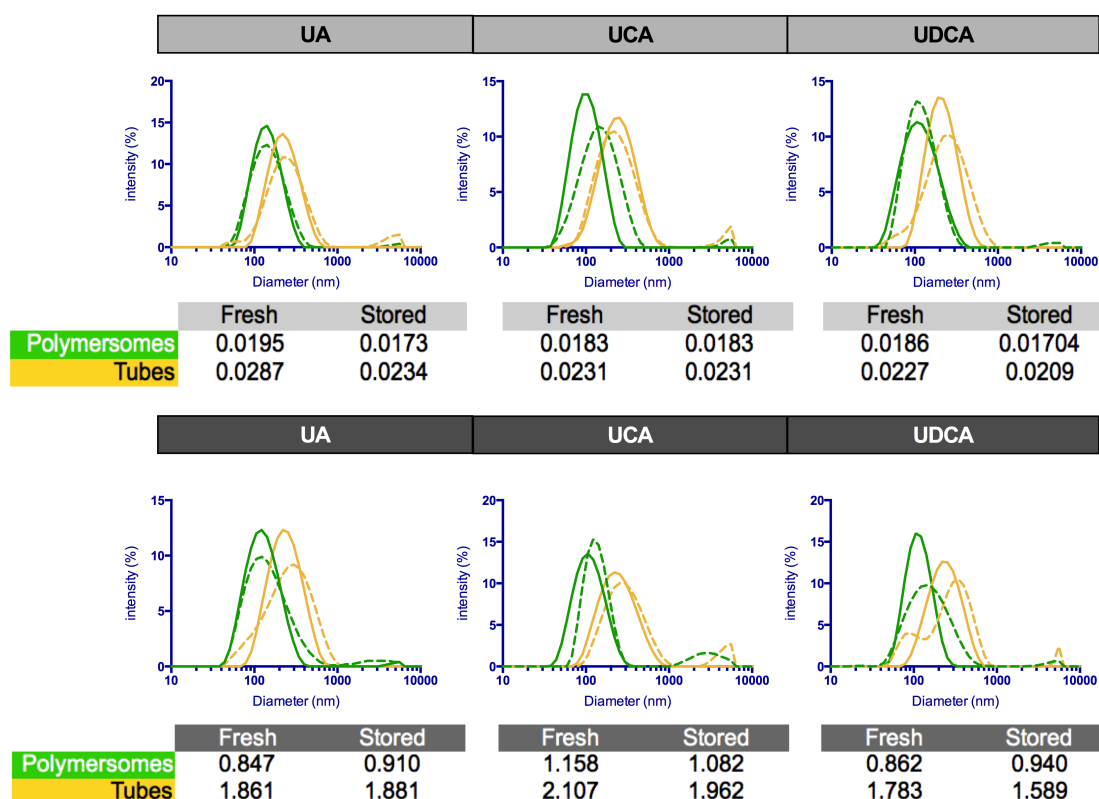


FIGURE 3.4: **Long term stability of drug loaded “Polymersomes” and “Tubes”**: Size distributions for nanoparticles after 8 weeks formation (solid lines) and 6 months storage at 4°C (dashed lines) are shown. The drug concentration within copolymer (w/w% from 3 measurements) at each time point is listed.

In earlier work aiming to assess the delivery of sterol like compounds into fibroblasts (not presented in this thesis), PMPC₂₅–PDPA₇₂ nanoparticles encapsulating the fluorescent NBD-cholesterol were formed by TFR. It was noted the presence of “tubular” morphologies increased with cholesterol loads (figure 3.5). Like NBD-cholesterol, UA, UCA and UDCA possess rigid cyclic backbones and high hydrophobicities. Thus it was of interest to assess whether these too would affect the morphologies of nanoparticles formed of PMPC₂₅–PDPA₆₅, the block copolymer used throughout this thesis. The affects of cholesterol encapsulation on nanoparticle morphology were also of interest, both for it’s similar structure and the extensive works conducted on this molecules affects in both lipid and copolymer membranes [436, 437]. As cholesterol is used widely in many fields, this work may also have greater relevance to other research.

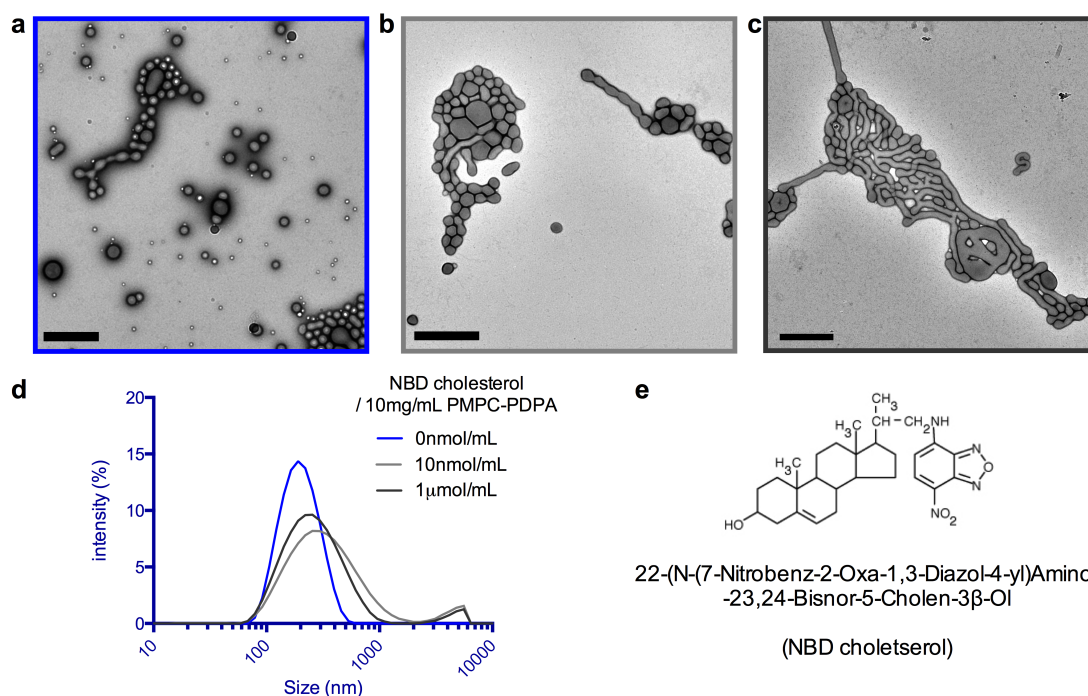


FIGURE 3.5: Cholesterol incorporation alters PMPC₂₅–PDPA₇₂ nanoparticle morphology: TFR formed nanoparticles formed from ATRP synthesised PMPC₂₅–PDPA₇₂ with target concentrations of 10mg/mL copolymer plus (a, blue border) 0, (b, light grey border) 10nmols/mL and (c), 1μmols/mL NBD-Cholesterol (dark grey border). (d) DLS determined size distributions by intensity. (e) Structure of NBD cholesterol.

The effect of encapsulating tetra- and penta- cyclic compounds within PMPC₂₅-PDPA₆₅ nanoparticles was assessed by centrifugal fractionation and quantification of each fractions relative mass. Copolymer films with 0, 0.05, 0.5 and 5% (w/w) cholesterol were solvent cast, and rehydrated under the TFR protocol. Samples of the resulting polymer/drug suspensions were taken at 1, 2, 3, 4, and 8 weeks and sonicated for 20 minutes. Centrifugal fractionation was performed, separation confirmed by DLS and copolymer/encapsulate concentrations quantified by UV-HPLC. It is worth noting that during centrifugal fractionation the supernatant and pellet were separated by hand, something that will have introduced a level of variability. The experiment was later repeated with UA, UCA and UDCA at the same concentrations, and with samples taken at 1, 4 and 8 weeks formation. In a concentration dependent manner all compounds tested increased the prevalence of “tube” structures, both increasing their initial prevalence and apparently stabilising them against transitions into smaller “polymer-somes” (figure 3.6) when compared to empty PMPC₂₅-PDPA₆₅ nanoparticles (figure 3.2b).

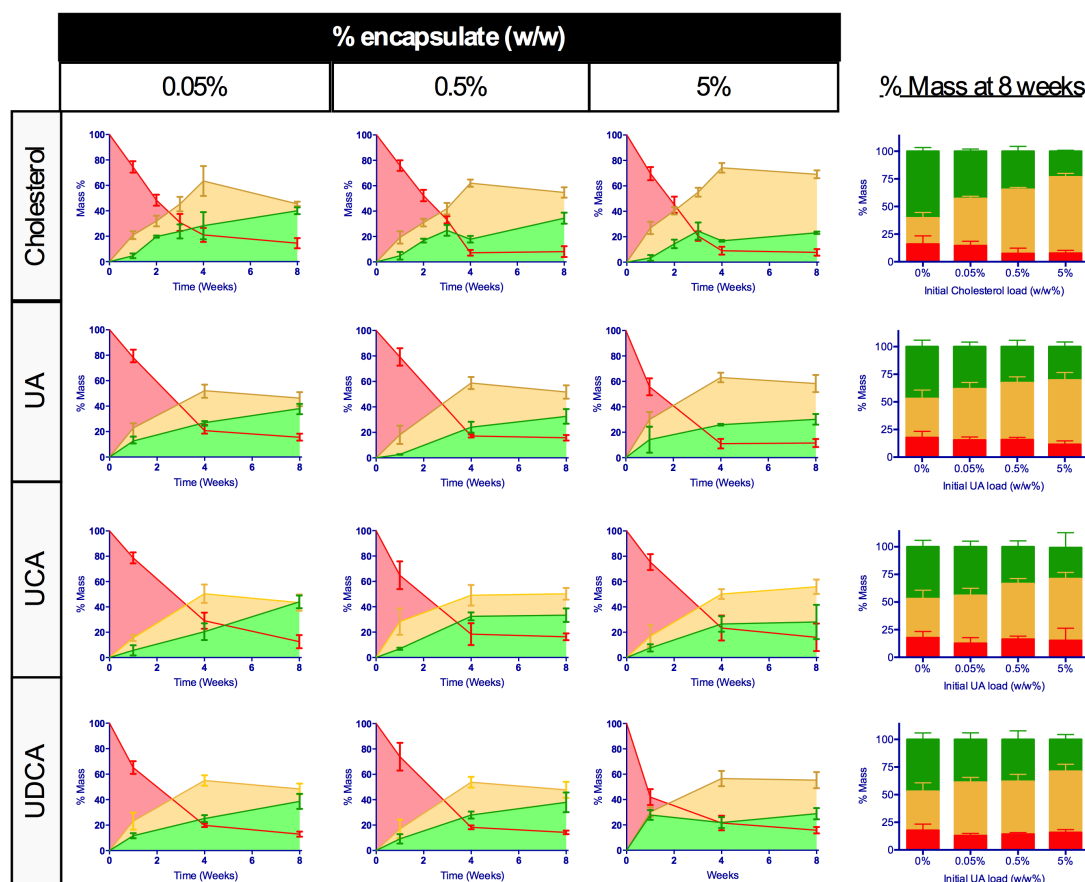


FIGURE 3.6: Relative masses of morphological fractions present within populations of drug loaded PMCP₂₅–PDPA₆₅ nanoparticles during formation: Drug loaded nanoparticles were made by TFR for fixed durations, sonicated, centrifugally fractionated and total volumes plus drug polymer concentrations quantified. Line graphs show the relative % of “polymersomes” (green), “tubes” (yellow) and “lyotropic aggregates” (red) fractions at given drug loads, and bar charts compare relative masses between the drug loads after 8 weeks of formation (error bars = SD from 3 individual nanoparticle populations).

If the load of tetra- / penta- cyclic encapsulate does increase the presence of tubular particles, one would might expect to find morphological differences. Indeed, DLS analysis suggests the unfractionated, drug loaded nanoparticles possess wider size distributions and greater average sizes when compared with unloaded nanoparticles. However, DLS analysis can only provide accurate estimation of particle hydrodynamic diameter for relatively mono-disperse populations, where the presence of larger particles will skew size distribution toward larger average diameters. The size distribution calculations also assume spherical particle morphology. Thus, DLS calculated size distributions for highly

heterogenous particle can only be considered qualitative. Image analysis was undertaken to provide a more accurate measurement of particle size and morphology. Unfractionated empty and cholesterol loaded (5% w/w) nanoparticles PMPC₂₅–PDPA₆₅ were imaged by TEM (29000x magnification). One full field of view possessing an even spread of all observable particle morphologies was selected as representative of the particle population. Particle two dimensional perimeter, area, persistent length and branch number were measured. All particles in a field of view were measured to limit selection bias.

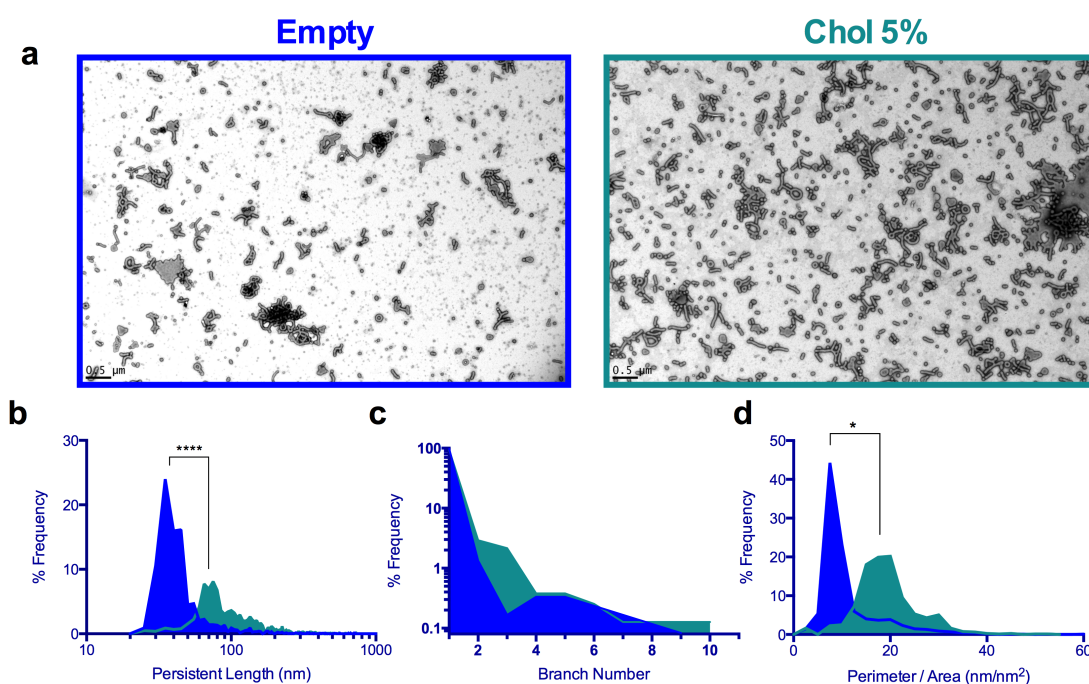


FIGURE 3.7: **Image analysis of empty and 5% cholesterol loaded PMPC₂₅–PDPA₆₅ nanoparticles:** (a) EM fields of view used for particle analysis. (b) Histogram of measured persistent lengths. (c) Histogram of particle branch numbers. (d) Histogram of particle perimeter divided by area. (statistic performed by unpaired, two tailed Mann-Whitney test).

Mean persistent length was greater in the cholesterol loaded nanoparticles ($p = <0.0001$) (figure 3.7b). Though the greater majority of structures in both samples were single branched a non-significant increase in branch number was seen in the cholesterol loaded nanoparticles ($p = 0.1465$) (figure 3.7c). Cholesterol loaded particles also possessed a significantly larger perimeter to surface area ratio, indicative of longer tubular morphologies ($p = 0.0482$) (figure 3.7d).

Taken together, this data corroborates the notion that cholesterol increases the relative presence of tubular structures. However, the relatively small sample size here is of note, as is the analysis of only one field of view for each sample. To increase the throughput of this technique, attempts were made to automate image analysis. This however was hampered by the mixture of positive and negative particle staining, and particle clustering, both of which made it harder to discern individual particles in quantitative terms. Progress in the image analysis of particles captured by electron microscopy have been made elsewhere [438].

3.5 Discussion

At 1% in water (w/w), TFR of PMPC₂₅–PDPA₆₅ produced a range of co-existing nanoparticle morphologies, including dispersed polymersomes, large lyotropic structures, and branched tubular assemblies intermediate of the two (figure 3.1a). This contrasts the purely spherical morphologies seen at the same concentrations when formed by pH-switch (figure 3.1b) [358, 430], and the TFR of other membrane forming diblock copolymers which too readily form into vesicles from film [407, 409]. Continued agitation by magnetic stirrer resulted in declining nanoparticle size, size distribution and particle density over the course of weeks, indicating the presence of metastable entities, slowly transitioning into smaller, more energetically favourable assemblies. Work conducted by James Robertson used confocal laser scanning microscopy to image the initial phases of thin PMPC₂₅–PDPA₆₅ film decomposition on hydration in PBS at the micron scale [435]. Consistent with other amphiphiles, the copolymer film swelled and wrinkled, extending finger like protrusions and developing holes which expand to create micron scaled bicontinuous networks [407, 439, 440]. However, unlike previous studies, large intact sections of these networks broke off directly into solution. This is most likely the origin of the large, flat, irregular lyotropic structures found in suspension, from which it is probable the observed,

nm scaled bicontinuous tubular networks and high genus assemblies evolved. Membrane unbinding within these would produce the smaller genus, and tubular structures. In turn, evidence is seen of pearling instabilities within tubular assemblies, from which smaller tubes and vesicles should bud. The presence of small spherical particles $\leq 50\text{nm } \varnothing$, possibly micelles, is notable [430], as is the absence of multi-lamellar assemblies despite the persistence of other large lyotropic phases.

The long lived nature of the lyotropic particles seen here, and their resistance to sonication indicates that, though metastable, they possess a high degree of stability, likely at least in part due to the high viscosity of copolymer membranes [410, 411, 433]. As $\text{PMPC}_{25}\text{-PDPA}_{65}$ is a diblock copolymer from which discs of a non-uniform shape are very unlikely to form, the observed large irregular structures are likely enclosed. Their irregular geometries might result from either interactions between the opposing membranes, or an uneven distribution of polymer chains between the inner- and outer- leaflet, either of which could limit membrane re-arrangements into more uniform shapes. If the latter is true, as the number of copolymer chains present within a membrane leaflet is essentially fixed at the time of membrane closure, the structures these evolve/unbind into will also possess fewer amphiphiles within their inner leaflet. In this regard it is notable that unequal distribution of amphiphile chains between membrane leaflets have previously been shown to produce outwardly curving, tubular and/or branched stable vesicles [441]. Whilst other long lived, metastable assemblies have been seen following a TFR of diblock copolymers, these rapidly broke into vesicles on addition external force [431]. It is also interesting to note that genus, non-uniform structures similar to those seen here have also been generated by pH switch, using $\text{PMPC}_{25}\text{-PDPA}_{94}$ at room temperature and $\text{PMPC}_{25}\text{-PDPA}_{77}$ at $\leq 15^\circ\text{C}$, a condition found to lengthen the PDPA_{77} chain [430]. As greater hydrophobic volumes increase an amphiphile's packing factor, these assemblies are unlikely to be the result of worm like micellar assembly. Future work may aim to look at the affect of copolymer block length,

thin film thickness and temperature on the formation of particular nanoparticle morphologies by TFR.

Thin films of PMPC₂₅–PDPA₆₅ plus UA, UCA or UDCA successfully formed into nanoparticles on rehydration. At the lower/10 μ M drug concentrations, purification by HFF did not markedly lower the drug to polymer ratios of particles, indicating the majority of drug existed within PMPC-PDPA nanoparticles. At the higher/1 mM concentration, a small though more marked decrease is seen, indicating drug enriched particles were removed either by filtration through 500kDa pores, or entrapment within the HFF system. Though these drugs are highly hydrophobic, limited solubility in water is seen particularly for UDCA as the least hydrophobic of the compounds [442, 443]. It is possible that during the TFR process, drug concentrations high enough to permit micellarisation may be achieved, resulting in the loss of compound from the bulk film. However, TEM of un-purified polymersomes did not reveal a discrete morphological population of micelles or crystal like structures under 500kDa (approximately 20nm \varnothing) as might be expected if this were the case (figure 3.3) [444, 445]. Also, drug loss from nanoparticle suspensions does not appear to correlate with compound hydrophobicity, the difference between drug:copolymer concentrations before and after HFF being approximately equal. This might indicate that particularly drug rich particles demonstrate an increased propensity to become entrapped within the HFF system, to which it is notable that a correlation between drug load and particle size was also noted (3.6). However, the possibility that a fraction of drug is lost as micelles or drug polymer micelles, of sizes unresolvable by TEM, cannot be excluded.

Characterisation of drug loaded polymersomes and tubular nanoparticle fractions before and after six months storage revealed little deviation in copolymer to drug ratios, indicating an absence of freed drug. The size distributions of these particles was also relatively undisturbed indicating good long term stability. This could be taken as indication the compounds readily integrate with PMPC-PDPA membranes, as poor compound miscibility within membranes is known to lead to phase separations between the membrane forming

amphiphiles and their hydrophobic cargo, resulting in loss of particle stability [437, 446]. As a hydrophobic poly-base [357], PDPA should be able to interact with hydrophobic acids UA, UCA and UDCA, hypothetically permitting their presence throughout the membrane core. Differential scanning calorimetry, nuclear magnetic resonance, and/or X-ray scattering experiments would however be necessary to confirm this. Other studies have also indicated good miscibility between copolymer membranes, and sterol like compounds. For instance, high encapsulation efficiencies have been reported of UA loaded, high MW methoxy poly(ethylene glycol)poly(caprolactone) (mPEG-PCL) nanoparticles [447, 448]. Similarly, dual fluorescence cross correlation spectrometry has been used to show that TFR of cholesterol plus poly(dimethylsiloxane)-poly(2-methyl-oxazoline) (PDMS₆₀-PMOXA₂₁) copolymer films (1:1 mol/mol) produce polymersomes composed exclusively of both substances [436]. No evidence of micro-domains was seen within these, and the particles remained stable for at least four weeks.

In a non-linear, concentration dependent manner, encapsulation of cholesterol was found increase the persistence of small genus, and tubular PMPC₂₅-PDPA₆₅ nanoparticles, apparently limiting their transition into smaller tubular and spherical “polymersomes”. Image analysis of cholesterol loaded particles (5% w/w) suggested nanoparticles were longer and more branched than control, again suggesting larger more heterogenous structures were stabilised. Concordantly, a separate image analysis in which tubular polymersomes alone were sampled found a small increase the persistent length and a clear increase in the branch number of cholesterol loaded nanoparticles relative to empty ones [435]. UA, UCA and UDCA encapsulation produced similar increases in the prevalence of the tubular fraction of TFR formed PMPC₂₅-PDPA₆₅ nanoparticles. UA, UCA, UDCA and cholesterol, all possess rigid cyclic backbones, and were all found to concentrate within the tubular fraction, indicative of a stabilising role within these particle morphologies. Precisely how this might be achieved is however unclear.

Previous work has investigated the effect of chloroform, a water immiscible organic solvent, on the TFR poly(ethylene oxide)copoly(butylene oxide) ($E_{16}B_{22}$), a membrane forming diblock copolymer [449]. As chloroform is soluble within $E_{16}B_{22}$ and not water, it will readily incorporate into $E_{16}B_{22}$ membranes, where it acts both to decrease water permeability and increase the free-volume between copolymer chains as well as decreasing entanglement, from which improved fluidity results. Indeed the presence of chloroform decreased the rate at which the $E_{16}B_{22}$ films swelled, and increased the speed and frequency with which tubular protrusions were extended. These protrusions possessed a smaller diameter, and showed signs of eased transition into μm scaled uni- and multi-lamellar vesicles. Assuming they are freely dissolved within the membrane, the compounds tested here may produce similar effects within $PMPC_{25}-PDPA_{65}$ membranes, easing initial transitions from bulk film to more stable assemblies. However one might then also expect eased transitions to nm scaled vesicles with improved membrane fluidity. One possible reason why this does not occur would be the increased hydrophobic membrane volume produced by the incorporation of hydrophobic compounds in the absence of a concomitant increase in hydrophilic volume. This could shift the balance of hydrating and hydrophobic forces, and produce re-arrangements effectively decreasing membrane curvature to accommodate them [450].

An alternative explanation by which tubular structures might be stabilised is altered membrane packing. Winzen et al. [436] showed using static- and dynamic- light scattering, that incorporation of 5 and 50% (mol/mol) cholesterol increased MW of isotropic $PDMS_{60}-PMOXA_{21}$ polymersomes in a concentration dependent manner whilst producing particles of slightly smaller diameter, indicating increased membrane density. It was speculated that this may be achieved in a fashion analogous to cholesterol's role in phospholipid membranes. Cholesterol possesses a rigid cyclic backbone, which when aligned with disordered hydrophobic phospholipid tails, acts to straighten these, reducing their free volume and producing lipid membranes of increased density in

their liquid crystalline phase [437, 451]. In their gel phase by contrast, cholesterol acts to increase the free volume between closely packed phospholipids, increasing membrane fluidity. Despite their more polar nature, incorporation of UA [260, 427] and UDCA [429] have been shown to produce analogous effects in lipid membranes, as have other hydrophobic bile acids similar to UCA [452]. A similar phenomena is harnessed in plastics. The incorporation of small molecules known as plasticisers, into bulk polymers, acts to reduce the entanglement between neighbouring polymer chains and increasing their freedom of movement. This results in the reduction of the materials glass transition temperature, the temperature at which plastics transition from a brittle- to a more malleable- state.

Large MW copolymer membranes are highly entangled within their hydrophobic core [410]. Hypothetically, the incorporation of small rigid cyclic compounds like UA, UCA, UDCA and cholesterol within and throughout the membrane core may interfere with this entanglement, resulting in somewhat straightened polymer chains, and increased polymer-polymer packing. It is also, again, notable that polymersomes formed by pH switch from PMPC₂₅–PDPA₉₄ formed high genus structures at room temperature, as did PMPC₂₅–PDPA₇₀ when the PDPA chain was stretched [430]. Again the increase in the membranes hydrophobic volume would also likely be an important factor. In the future it will be important to determine where these compounds sit in the membrane, how they interact with it, and how they alter its properties using techniques such as differential scanning calorimetry, nuclear magnetic resonance and X-ray scattering.

3.6 Conclusion

UA, UCA and UDCA were successfully encapsulated within purified PMPC₂₅–PDPA₆₅ nanoparticles with high efficiency and are subsequently promising as therapeutic vectors. Distinct spherical, tubular and large lyotropic morphologies were successfully fractionated into enriched populations. UA, UCA and UDCA

were found to favour segregation into the tubular fraction, and their incorporation into PMPC₂₅–PDPA₆₅ nanoparticles increased the proportion of these tubular and genus particles. As nanoparticles of different morphologies are known to have distinct biological interactions (Chapter 1), and given the different drug loading efficiencies seen in the morphological fractions, later work has aimed to compare the therapeutic effects of spherical “polymersome” and “tube” fractions (Chapter 5).

Chapter 4

Results: Suitability of PMPC-PDPA polymersome use in *parkin* mutant fibroblasts

4.1 Aim

To demonstrate the ability of PMPC-PDPA polymersomes to enter *parkin* mutant fibroblasts, and to assess their suitability as a drug vector to treat the mitochondrial dysfunction of *parkin* mutant fibroblasts.

4.2 Background

For PMPC-PDPA nanoparticles to be effective as a therapeutic vector, they must both enter the target cell and cause no adverse effects therein. Whilst PMPC-PDPA polymersomes are known to enter many healthy cell types without loss of viability [339, 358, 404], their entry into cells with a known mitochondrial defect has not yet been investigated. In this chapter, the uptake of fluorescently labelled polymersomes by healthy and *parkin* mutant fibroblasts is assessed

using flow cytometry and fluorescence microscopy. In addition, fibroblast viability following incubation with empty polymersomes are assessed by assays of cytotoxicity, intracellular ATP and MMP.

Massignani et al. [339] demonstrated PMPC-PDPA polymersomes of $\sim 100\text{nm}$ \varnothing are able to enter a large range of endocytically active primary and immortalised cells. In human dermal fibroblasts, internalisation was prevented by pre-incubation with chloroquine or cooling cells to 4°C both known to prevent or limit endocytotic processes [453, 454]. Pre-incubation with nocodazole, an agent known to disrupt microtubule assembly and interfere with intracellular trafficking [455], limited accumulation of polymersomes to the surface membrane only. Similarly, cell fixation prior to polymersome exposure also limited accumulation to the cell surface [393, pg.138]. Taken together, this suggests polymersomes are endocytosed by the cell. Recent work from Colley et al. [341] has shown antagonisation of class B scavenger receptors significantly reduces the uptake of PMPC-PDPA polymersomes in fibroblasts. Class B scavenger receptors are known to bind and mediate the internalisation of a wide range of ligands, including those bearing phosphorylcholine motifs such as PMPC [342, 456] and have been linked to both caveolae- and clathrin- mediated endocytosis [394, 395]. Though polymersomes appear to accumulate on the cell surface in abundance, they do not limit endosomal function, as demonstrated by the effective uptake of transferrin - a known cargo of clathrin mediated endocytosis - after pre-incubation with 50nM PMPC-PDPA polymersomes (approximately 1.15mg/mL) in serum containing media [393, pg.136].

Following internalisation, evidence shows PMPC-PDPA polymersomes enter the endolysosomal pathway [392? , 393, pg.139,141]. Here, polymersomes are exposed to a progressively more acidic environment, as H^{+} pumps work to acidify the endosomal compartments, the early endosome being typically pH 6.2-5.4, and the late endosome typically pH 5.6-5.4, depending on cell type [457, 458]. PDPA, possessing an pK_a of around 6.2-6.4 [357, 430] accepts protons at its tertiary amine groups whilst in mildly acidic conditions. Thus PMPC-PDPA becomes positively charged in the early endosome, increasing its

water solubility and initiating polymersome disassembly with subsequent cargo release.

Unlike non-pH sensitive analogues, PMPC-PDPA and its cargoes distribute widely throughout the cell, indicating both polymersome disassembly and endosomal escape [339, 404, 459]. The latter is believed to occur by transient osmolytic disruptions within the endosomal membrane. Below its pKa, nanoscopic PMPC-PDPA polymersomes have been shown to disassemble within milliseconds, wherein the number of water soluble entities sharply increases. For instance, a 200nm \varnothing PMPC₂₅-PDPA₇₀ polymersome formed in 100mM PBS is estimated to be formed from 1.7×10^3 copolymer chains, and encapsulate $\sim 5 \times 10^5$ ionic species [404]. The rapid release of both on particle disassembly will dramatically increase the osmotic potential of the endosomal compartment, the pressure of which is believed to result in localised destabilisations and the rapid flux of materials across the endosomal membrane [358, 404]. Other polymersomes known to disassemble within the endosomal environment also show cytosolic delivery of hydrophilic cargoes [397, 398]. The gain of cationic charge, a property that can induce phospholipid membrane disruptions, may also contribute to endosomal escape of PMPC-PDPA, as suggested in other systems [460, 461]. PMPC-PDPA polymersome disassembly and escape from the early endosome is believed to underly its apparent lack of toxicity relative to other vectors which escape from later, and more acidic endosomal locations.

At 1.15mg/mL, PMPC-PDPA polymersomes are able to enter a wide range of cell types without significant loss of cell viability [339]. Further, they fail to activate immune responses in fibroblasts or immune cells [358, 392, pg.135]. Fibroblasts have been shown to tolerate 48 hours incubation with polymersomes, and concentrations up to 5mg/mL without more than a 10% loss in metabolic viability [358, 393, 404, pg.129]. Fibroblasts exposed to rhodamine loaded polymersomes daily show now apparent decline in cell number after one week, further demonstrating the biocompatibility of this chemistry [339].

4.2.1 Exacerbation of mitochondrial defects in fibroblasts

Except where stated, experiments were undertaken with fibroblasts cultured in glucose free media supplemented with galactose, 24 hours prior to experimental conditions. Fibroblasts normally produce the majority of their ATP by cytosolic glycolysis when cultured in glucose media, utilising little mitochondrial OXPHOS [107]. However in galactose media, a sugar that is entered into the glycolytic pathway at a much slower rate, mitochondrial OXPHOS is relied on to a much greater extent to meet the energetic demands of fibroblasts [107]. It has previously been shown that cells possessing mitochondrial deficiencies demonstrate reduced growth and loss of viability when grown in galactose media as a consequence of their increased reliance on mitochondrial OXPHOS [462–464]. The mitochondrial defects in *parkin* mutant fibroblasts are also enhanced in galactose media [95]. Thus by using galactose media will exacerbate phenotypes related to mitochondrial defects in fibroblasts.

4.3 Uptake of PMPC-PDPA polymersomes by *parkin* mutant fibroblasts

4.3.1 Characterisation of rhodamine labelled polymersomes

Uptake of polymersomes in fibroblasts was assessed using polymersomes composed of PMPC-PDPA and R.6G-PMPC-PDPA (1% or 5% w/w), formed by either pH switch or TFR methodologies [339, 415]. Figure 4.1 details the concentrations, morphologies and size distributions of the Rhodamine 6G (R.6G) labelled polymersome batches used in this section. Rhodamine labelled polymersomes attained morphologies and size distributions typical to the method of formation [358, 435] (Chapter 3). Batches 1 and 2 were composed of an ATRP synthesised copolymer whilst batch 3 was composed predominantly of RAFT

synthesised PMPC₂₅–PDPA₆₅. The pH switch formed Batch 1 showed the narrowest size distribution and smallest average particle size. Batch 3 initially possessed a much greater size distribution relative to Batch 2, both of which were formed by TFR. Batch 3 was subsequently centrifuged at 10,000RCF, and the resulting supernatant was found to have a smaller size distribution more akin to Batch 2.

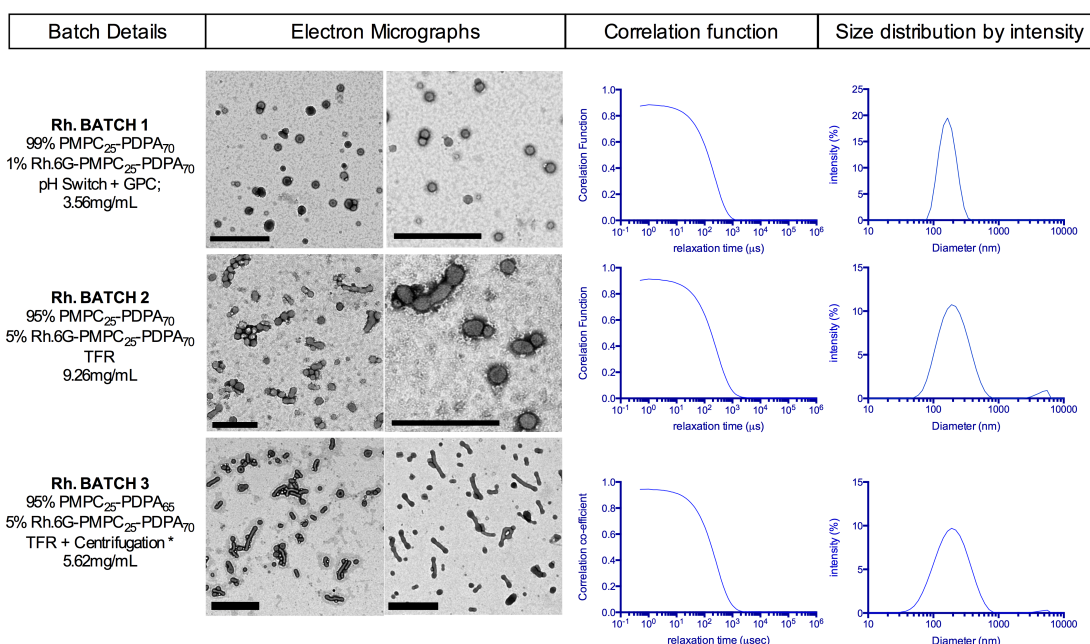


FIGURE 4.1: Rhodamine labelled nanoparticle characterisation: Batch details, two separate fields of view from EMs supporting nanoparticles, and DLS auto-correlation functions and size distributions for each batch of rhodamine labelled nanoparticles used in uptake studies. Batch details list; batch number, copolymers used, their proportions, method of nanoparticle formation plus purification step, and copolymer concentration. Polymer concentrations calculated using fluorometry and known standards of matching polymer composition (1 or 5% R.6G-PMPC-PDPA w/w; see methods 2). *Batch 3 possessed a very large size distribution after formation, so was centrifuged at 10,000RCF and the resulting supernatant used for experiments.

4.3.2 Uptake of polymersomes formed by pH switch and the effect of fibroblast metabolic state

To assess the ability of fibroblasts to internalise polymersomes, rhodamine labelled polymersomes formed by pH switch (1% w/w; figure Rh. BATCH 1 4.1) were incubated with *parkin* mutant fibroblasts plus controls (Ctrl1 plus PD1) for 1, 3, 12, 24 and 48 hours, in either glucose or galactose media. Cells were washed, detached and passed through a flow cytometer to measure R.6G-PMPC-PDPA fluorescence from individual cells. Results were gated firstly by size and granularity to include only intact fibroblasts (red "P1"; Forward Scatter vs Side Scatter), and secondly by endogenous fluorescence, to demarcate those cells that have certainly received polymersomes from those that have not (green "P2"; R.6G-PMPC-PDPA fluorescence)(figure 4.2a) [341].

Following 24 hours incubation, all fibroblasts tested demonstrate R.6G-PMPC-PDPA fluorescence greater than maximal endogenous levels, in either media (figure 4.2b). This indicates that at 1mg/mL, the polymersome to cell ratio is great enough to ensure all cells are able to receive a measurable number of polymersomes. Median R.6G-PMPC-PDPA fluorescence in fibroblasts increases with time for all cells tested, though to a significantly greater extent in Ctrl1 relative to PD1 (figure 4.2c; Ctrl1 gal vs PD1 gal, $p < 0.0001$; Ctrl1 glu vs PD1 glu, $p = 0.0007$). Where accumulation continues with approximate linearity to 48 hours in glucose media, a threshold is reached between 24 and 48 hours in galactose media. This might be due a depletion of polymersomes from the media, however that uptake is greater and remains linear in glucose media suggests otherwise. Further, fibroblasts have been shown to grow slower in galactose media both here (figure 4.3) and elsewhere [107, 464], suggesting a less favourable nanoparticle to cell ratio, or dilution of R.6G-PMPC-PDPA signal on cell division, are not reasonable explanations. Though galactose media reduces ATP levels in *parkin* mutant fibroblasts, it has no effect in healthy control's [95]. The effect of altered fibroblast physiology in galactose media on endocytic processes thus warrants further consideration.

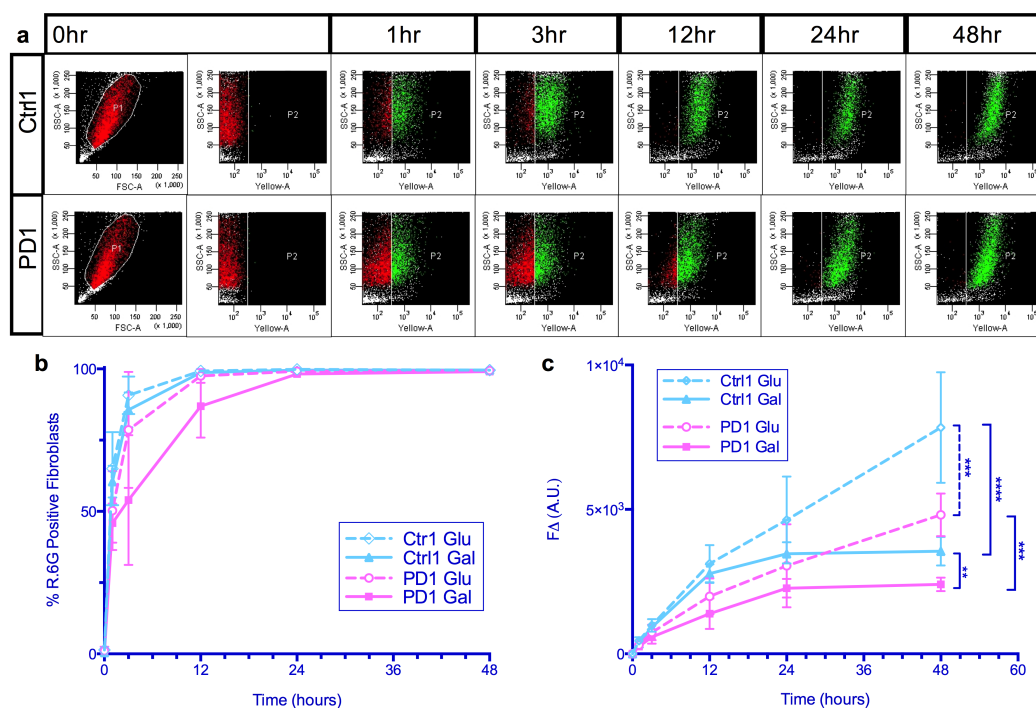


FIGURE 4.2: **Polymersome uptake in fibroblasts cultured in different sugar substrates:** Rhodamine labelled polymersomes were incubated with *parkin* mutant fibroblasts (pink; PD1) or healthy controls (blue; Ctrl1) for 1, 3, 12, 24 and 48 hours in either a glucose or galactose based media (dashed and solid lines respectively), and their fluorescence assessed by flow cytometry. (a) Representative dot plots and gates used in flow cytometry experiments (SSC-A = Side Scattering; FSC-A = Forward Scattering; Yellow-A = fluorescent light intensity, ex. 532nm, em. 564-606nm) (b) Percentage of R.6G-PMPC-PDPA positive cells as assessed by the p2 gate. (c) Magnitude of R.6G-PMPC-PDPA absorption in fibroblasts, as assessed by median P1 gate fluorescence (n=4; error bars = SD; two-way anova performed for glucose and galactose conditions separately, ** = p < 0.01, *** = p < 0.001, **** = p < 0.0001).

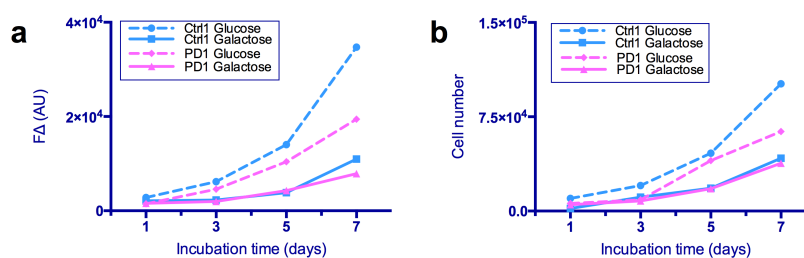


FIGURE 4.3: **Growth curves of *parkin* mutant and control fibroblast:** Fibroblasts were seeded at 5000 cells in 6 well plates in glucose, then switched into fresh glucose or galactose medias 6 hours later. (a) Fibroblast cellular DNA content as assessed by a DNA binding fluorophore (CyQuant™) and (b) cell number as assessed by cell counting on a haemocytometer were measured in parallel following 1, 3, 5, and 7 days incubation. (n = 1)

4.3.3 Uptake of PMPC-PDPA nanoparticles formed by thin film rehydration

PMPC-PDPA polymersomes encapsulating hydrophobic compounds such as UA, UCA and UDCA, are formed by TFR, a method found to produce polymersomes more tubular and genus¹ in nature when compared to pH switch method of formation (chapter 3 and figure 4.1). As size and shape are known to affect the cellular uptake of polymersomes, the uptake of TFR formed polymersomes was investigated. Also, as earlier data indicated *parkin* mutant fibroblasts may possess a deficient ability to accumulate polymersomes, a second patient derived *parkin* mutant fibroblast was studied. Healthy and *parkin* mutant fibroblasts (Ctrl1 plus PD1, and Ctrl2 plus PD2) were incubated with 0.1, 0.5 and 1mg/mL rhodamine labelled polymersomes (5% R.6G-PMPC-PDPA w/w; Rh.BATCH 2 figure, 4.1) for 1, 3, 12, 24 and 48 hours in galactose media. Median fluorescence was again assessed by flow cytometry (figure 4.4).

¹“Genus” is used in its topological sense, and refers to particles possessing holes within their bulk that do not break the membrane

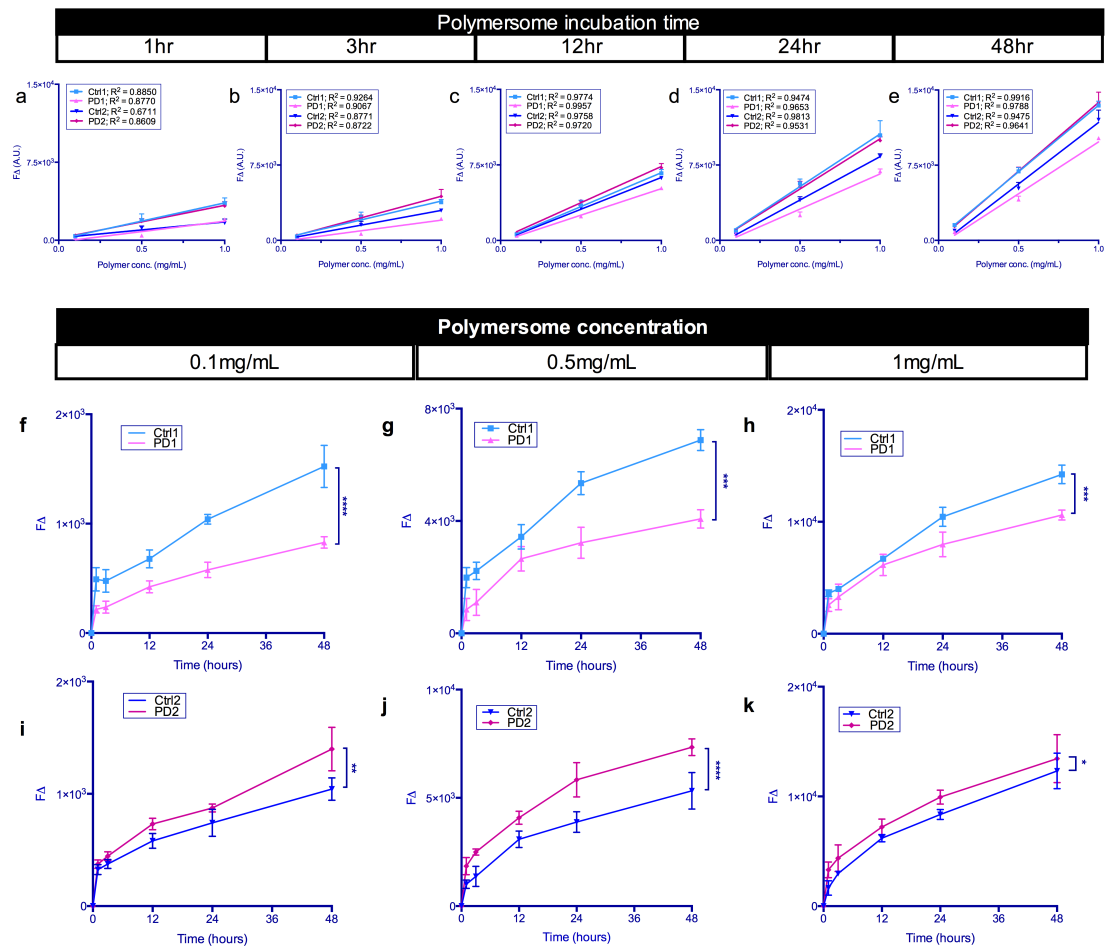


FIGURE 4.4: Effect of Polymersome concentration on internalisation: *parkin* mutant fibroblasts plus controls (PD1 + Ctrl1; PD2 + Ctrl2) were incubated with 0.1, 0.5 and 1mg/mL rhodamine labelled polymersomes (Rh.BATCH 2 4.1) for 1, 3, 12, 24 and 48 hours in galactose media. Fluorescence was assessed by flow cytometry. (a-e) The effect of polymersome concentration on median cell fluorescence at each time-point, with linear regressions (R^2 indicated). (f-k) Time course of polymersome uptake at concentrations of 0.1, 0.5 and 1mg/mL (f-h, Ctrl1 vs PD1; i-k, Ctrl2 vs PD2). (n=3; error bars=SD; statistics performed by two way anova, * = $p < 0.05$, ** = $p < 0.01$, *** = $p < 0.001$, **** = $p < 0.0001$).

	Ctrl1			PD1			Ctrl2			PD2		
	0.1mg/mL	0.5mg/mL	1mg/mL									
0 hours	0.7	0.4	0.3	0.3	0.5	0.5	0.2	0.4	0.6	0.3	0.4	0.2
1 hour	47.5	21.4	93.7	43.9	48.7	89.2	53	94.3	91.6	43	98.7	98.1
3 hours	51.1	95.1	96.8	46.5	61.1	99.8	52	99.8	97.3	55.8	98.2	98.3
12 hours	76.1	98.7	98.8	68.7	91.4	99.4	68	98.8	99.5	72.6	99.6	99.4
24 hours	93.9	98.7	98.7	86.2	96.9	99.7	84.2	99.8	99.4	86.6	99.8	99.7
48 hours	97.6	99.6	99.4	90.6	99.6	99.6	87.4	99.3	99.9	92.9	99.1	99.9

TABLE 4.1: Percentage of cells exhibiting fluorescence greater than maximal endogenous levels (P2 gate). Percentages higher than 95% are indicated in blue (data supplemental to figure 4.4)

R6.G-PMPC-PDPA fluorescence increased linearly with polymersome concentration at all time points studied (4.4a-e). Following 48 hour incubation, approximately all cells incubated with either 0.5 or 1 mg/mL polymersome demonstrated R.6G-PMPC-PDPA fluorescence greater than maximal endogenous levels (P2 gate). A substantial shift was also seen with 0.1 mg/mL concentrations though levels greater than 95% were not achieved (table 4.1). It is worth noting only 5% of the PMPC-PDPA possesses a Rh.6G conjugate, thus fluorescence signal represents only a proportion of polymer accumulated in fibroblasts.

The time-course of polymersome internalisation reveals a rapid increase in fluorescence at one hour, after which R.6G-PMPC-PDPA accumulates within the cell more slowly (4.4 f-k), something not seen, or at least not as apparent with pH switch formed polymersomes. This might depict the rapid binding of nanoparticles to the surface of the cell, followed by slower internalisation. Between 1 and 48 hours, internalisation is linear, suggesting an excess of nanoparticle is still available for internalisation, though there are some slight signs of saturating uptake. It is notable that accumulation of pH switch formed polymersomes had saturated by this time-point under identical conditions (figure 4.2c).

Where PD1 was significantly less able to accumulate R.6G-PMPC-PDPA than its control, PD2 was significantly more able (figure 4.4), implying the mutant *parkin* phenotype does not directly effect uptake. A possible explanation for these differences would be different growth rates however, quantification of cellular DNA content, a measure closely tied to cell number, demonstrates controls consistently have greater cell numbers than *parkin* mutant fibroblasts at the time of assay (Two way anova, Ctrl1 vs PD1, $p < 0.0015$; Ctrl2 vs PD2, $p = 0.0015$) (figure 4.5). Differences in uptake may possibly arise from variance of polymersome receptors number at the cell surface.

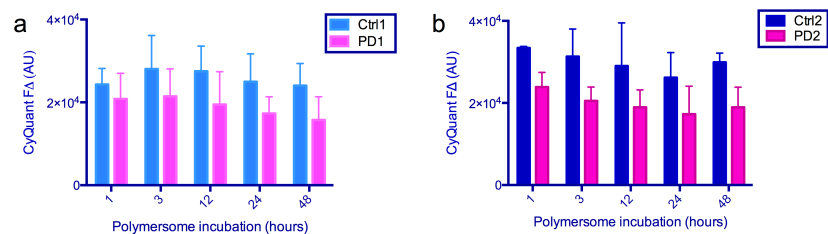


FIGURE 4.5: **DNA content of fibroblasts incubated with polymersomes:** *parkin* mutant fibroblasts plus controls (PD1 + Ctrl1; PD2 + Ctrl2) seeded at 30,000 cells a well in a 12 well plate. Cells were washed, placed in galactose media for 24 hours, then incubated with 1mg/mL rhodamine labelled polymersomes (Rh.BATCH 2 4.1) for an additional 1, 3, 12, 24 or 48 hours. (a,b) Fibroblasts were washed, incubated with a cell membrane perforant DNA stain (CyQuant™), and fluorescence read using a plate reader. (n=3; error bars = SD).

4.3.4 Uptake of polymersomes formed by thin film rehydration of PMPC₂₅–PDPA₆₅ synthesised by RAFT

The majority of work performed for this thesis utilised polymersomes formed by TFR of a RAFT synthesised PMPC₂₅–PDPA₆₅, which was found to produce polymersomes more heterogeneous and tubular than seen with other polymer batches (Rh.BATCH 3, figure 4.1, Chapter 3). Uptake of rhodamine labelled PMPC-PDPA nanoparticles (5% w/w) was again assessed in three *parkin* mutant fibroblasts plus controls. Two previously untested *parkin* mutant fibroblasts were introduced to further investigate whether alterations in polymersome uptake are associated with this phenotype. Availability of equipment required that these experiments were performed on a different flow cytometer to that used previously (population gating used shown in 4.6l). Fibroblasts were incubated with 0.1, 0.5 and 1mg/mL nanoparticle concentrations. Early binding of polymersomes was assessed with 1, 10 and 60 minute time points, whilst later uptake was determined at 24 and 48 hours (figure 4.6a-j).

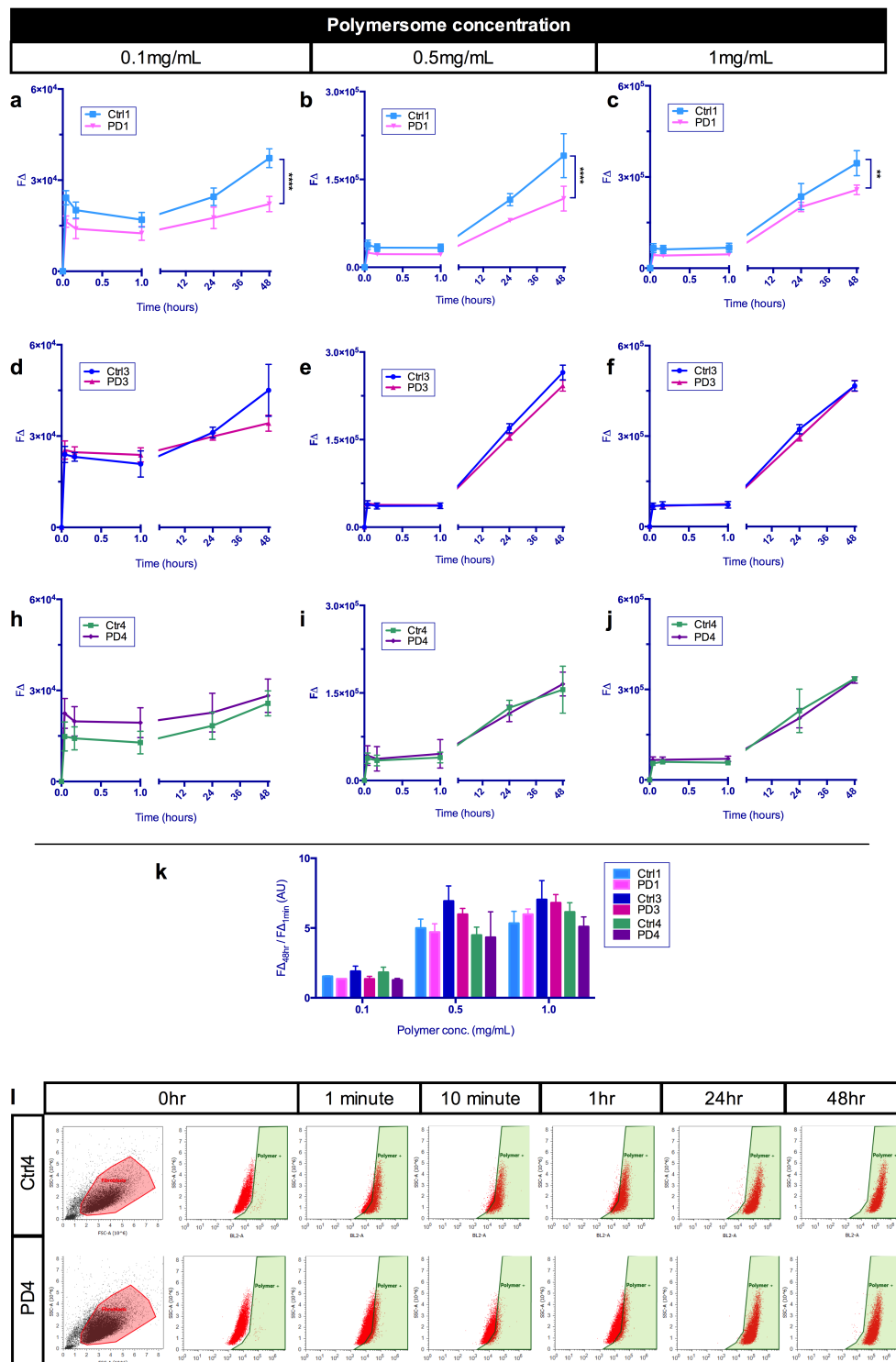


FIGURE 4.6: Rapid binding, but slow internalisation of TFR formed PMPC-PDPA nanoparticles: Rhodamine labelled polymersomes (Rh.BATCH 3 4.1) were incubated with *parkin* mutant fibroblasts plus controls for 1 and 10 minutes, 1, 24 and 48 hours. They were then washed, detached and passed through a flow cytometer (BD Attune[®] Autosampler). (a-j) Median R.6G-PMPC-PDPA fluorescence of fibroblast population with increasing incubation time. (k) R.6G-PMPC-PDPA accumulation at 48 hours normalised by accumulation after 1 minute. (l) Representative dot plots from flow cytometry experiments (SSC-A = Side Scattering; FSC-A = Forward Scattering; BL2-A = fluorescent light intensity, ex. 488, em. 561587) (n=3; error bars = SD; statistics performed by two way anova, ** = p < 0.01, *** = p < 0.001, **** = p < 0.0001)

	1minute		24hours		48hours	
	Slope	R ²	Slope	R ²	Slope	R ²
Ctrl1	45218	0.715	232940	0.937	465841	0.988
PD1	31238	0.979	207154	0.978	480586	0.995
Ctrl3	48955	0.885	323371	0.993	339433	0.949
PD3	49780	0.909	295570	0.995	263911	0.982
Ctrl4	54830	0.908	228244	0.882	326468	0.995
PD4	68230	0.842	203496	0.965	314845	0.984

TABLE 4.2: Linearity of polymersome concentration on magnitude of uptake. For each fibroblast biopsy, R.6G-PMPC-PDPA fluorescence at 1 minute, 24 and 48 hours was plotted as a function of polymersome concentration, from which linear regressions and R^2 values were calculated.

After one minute, there is a dramatic accumulation of R.6G-PMPC-PDPA in fibroblasts, the magnitude of which scales with polymer concentration (figure 4.6a-j, table 4.2). No apparent increase is seen up to one hour later. This likely represents the rapid binding of nanoparticles to scavenger receptors on the cell surface, followed by slow particle endocytosis. Though not seen with spherical polymersomes (figure 4.2 c), long cell surface dwelling times have also been observed with purified tubular polymersomes in other cell types [435]. From 1 to 10 minutes, a decrease in R.6G-PMPC-PDPA signal is notable at 0.1 and 0.5mg/mL concentrations, possibly the result of fluorescence quenching as polymersomes are enveloped/wrapped by phospholipid membrane prior to endocytosis [325, 326].

Following the initial binding step, a linear increase in signal is seen between 1 and 48 hours, also in a concentration dependent manner (table 4.2). At 0.1mg/mL, the increase in R.6G-PMPC-PDPA signal following the initial binding step is slight, most notably in Ctrl4 and PD4. This might suggest that very few polymersomes actually enter the cell. However other factors must also be considered; loss of signal through cell growth and polymer excretion, the possibility that R.6G-PMPC-PDPA fluorescence is quenched on internalisation, and the low percentage of polymer possessing a Rh.6G conjugate (5% w/w) . Fluorescent microscopy provides further evidence that these polymersomes are internalised and distribute within the cell (figure 4.7). Here there is evidence of

fluorescence throughout the cell, as well as contained within distinct puncta perhaps reminiscent of the tubular morphologies macro-pinosomes assume during their maturation [370].

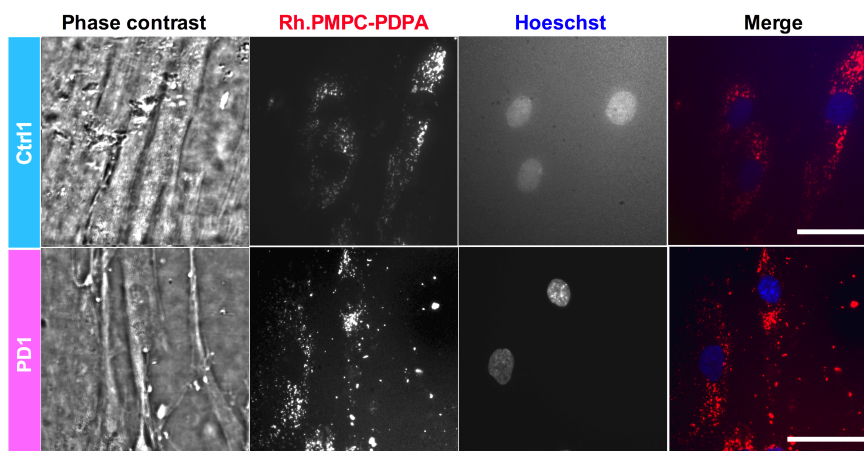


FIGURE 4.7: **Fibroblast internalisation of Rhodamine labelled polymersomes:** Healthy fibroblast incubated with polymersomes (RhBATCH 3) at 0.5mg/mL for 48 hours in galactose media. Cells were washed and imaged using the InCell Analyzer (60x objective; scale bar = 50 μ m).

Though, as in experiments with other polymersome batches (figures 4.2 and 4.6), a significant deficiency is seen in the ability of PD1 to accumulate polymersomes relative to Ctrl1 ($p = 0.0011$, <0.0001 and <0.0001 at 0.1, 0.5 and 1mg/mL concentrations respectively), this is not replicated in the other *parkin* mutant fibroblasts (4.6a-j). PD1 accumulates a notably smaller R.6G-PMPC-PDPA signal after one minutes incubation, relative to Ctrl1 . As no apparent increase in R.6G-PMPC-PDPA signal is seen between 1 and 60 minutes, the one minute time point could be taken as an approximate gauge of a fibroblast's ability to bind polymersomes, and would suggest PD1 has fewer polymersome receptors. In figure 4.6l, the R.6G-PMPC-PDPA signal accumulated after 24 and 48 hours has been divided by signal after one minute to give a hypothetical normalisation of polymer internalisation per bound receptor (i.e. the rate of internalisation itself). Here, there is no significant difference between *parkin* mutants or controls at any of the concentrations tested ($p = 0.6622$).

The effect of cell number on polymersome uptake was also investigated. Fibroblasts were plated at 7,500, 15,000, 30,000 and 60,000 cells a well, and grown

for 24 hours. They were then incubated with rhodamine labelled polymersomes (Rh.BATCH 3, figure 4.1) for 48 hours in galactose media. Cells were washed, detached, and the population was split in two. R.6G-PMPC-PDPA accumulation was assessed by flow cytometry with one half, and the DNA content quantified with the other (figure 4.8). If nanoparticle number were a limiting factor, a negative correlation between uptake and cell number would be expected, as greater cell numbers would effectively decrease the number of nanoparticles available to each cell for internalisation. A slight negative correlation between polymer-some accumulation and cell number is seen at lower concentrations, though the impact is not great, suggesting overall cell number had little impact, and that a saturation of nanoparticles bound to the fibroblast surface is achieved throughout the 48 hour experiment.

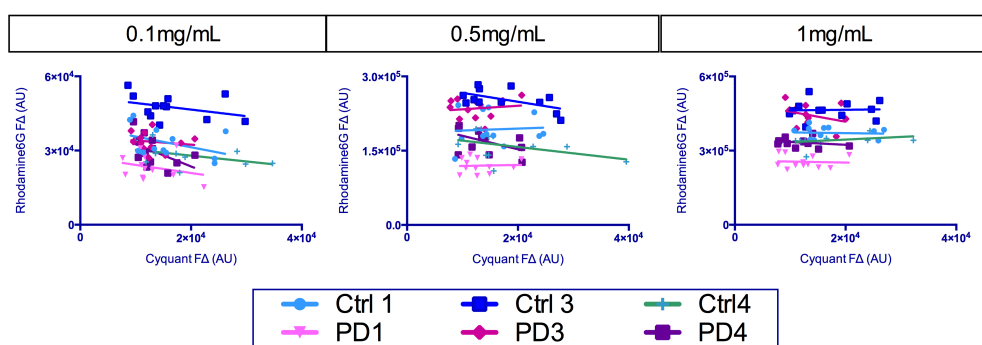


FIGURE 4.8: Effect of cell number on nanoparticle internalisation: Fibroblasts were seeded at 7,500, 15,000, 30,000 and 60,000 cells a well, grown in glucose media for 24 hours, then in galactose media for a further 24 hours, and then incubated with rhodamine labelled polymersomes for 48 hours. Cells were washed, detached and resuspended. Half the population was passed through a flow cytometer where R.6G-PMPC-PDPA fluorescence was assessed, and the other's cell number estimated using a cell perforant fluorescent DNA stain (CyQuantTM NF). Median Rh-PMPC-PDPA fluorescence is plotted against cellular DNA content for individual repeats, and lines of regression shown. Polymersome concentrations are indicated ($n = 3$).

4.3.5 Inter-experimental comparison

To compare the cellular uptake of each batch of rhodamine labelled polymersome, an inter-experimental normalisation was performed. Polymersome uptake in Ctrl1 and PD1 following 1, 24 and 48 hour incubation with 1mg/mL polymersomes in galactose media has been tested in all uptake experiments described. Median fibroblast R.6G-PMPC-PDPA fluorescence at 24 and 48 hours incubation was normalised by signal at 1 hour (figure 4.9). This corrects for differences in the gain settings of fluorescence measurements, and varied composition of R.6G-PMPC-PDPA in polymersomes. It also assumes that the accumulation of polymersomes on cell surface is similar between nanoparticle batches at one hour, which is unlikely, with pH switch polymersomes demonstrating signs of early internalisation. Therefore this normalisation must be considered qualitative only. Accumulation of polymersomes formed by pH switch is more than two fold greater than that of TFR formed nanoparticles in both fibroblasts after 24 hours incubation (figure 4.9a), the point at which pH switch polymersome uptake reached saturation (figure 4.2c). After 48 hours incubation, uptake of TFR formed polymersomes is still markedly less than pH switch polymersomes (figure 4.9b). If pH switch polymersomes have begun entering fibroblasts by the 1 hour time-point, then the difference in uptake between the two methods of formation is likely greater than even shown here. This reinforces other work which shows particles of larger sizes, and larger aspect ratios enter into cells more slowly [322, 340, 378].

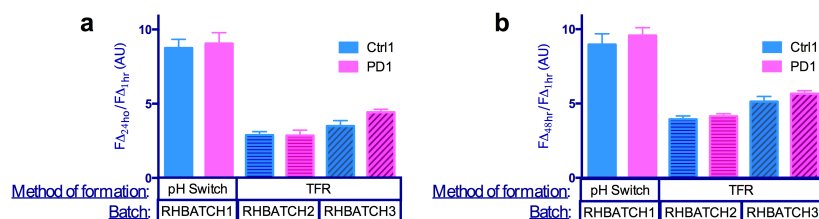


FIGURE 4.9: **Inter-experimental comparison of TFR and pH switch formed polymersomes uptake in fibroblasts:** Median R.6G-PMPC-PDPA fluorescence of Ctrl1 and PD1 following 24 (a) and 48 (b) hour incubation with rhodamine labelled polymersomes was divided by median R.6G-PMPC-PDPA fluorescence at 1 hour. Method of polymersome formation and primary polymer batch they were formed from are indicated along the x axis. (error bars = SD)

4.4 Effects of PMPC-PDPA polymersomes on fibroblast viability and mitochondrial physiology

4.4.1 Polymersome characterisation

The experiments described in this section used polymersomes formed by Thin Film Re-hydration (TFR). Assay pilots used polymersomes made from ATRP synthesised polymer (Batch 1 and 2, figure 4.10) and the polymersome dose response experiments used polymersomes formed from RAFT synthesised polymer (Batch 3, figure 4.10). Each batch demonstrated similar size distributions and polymersome morphologies.

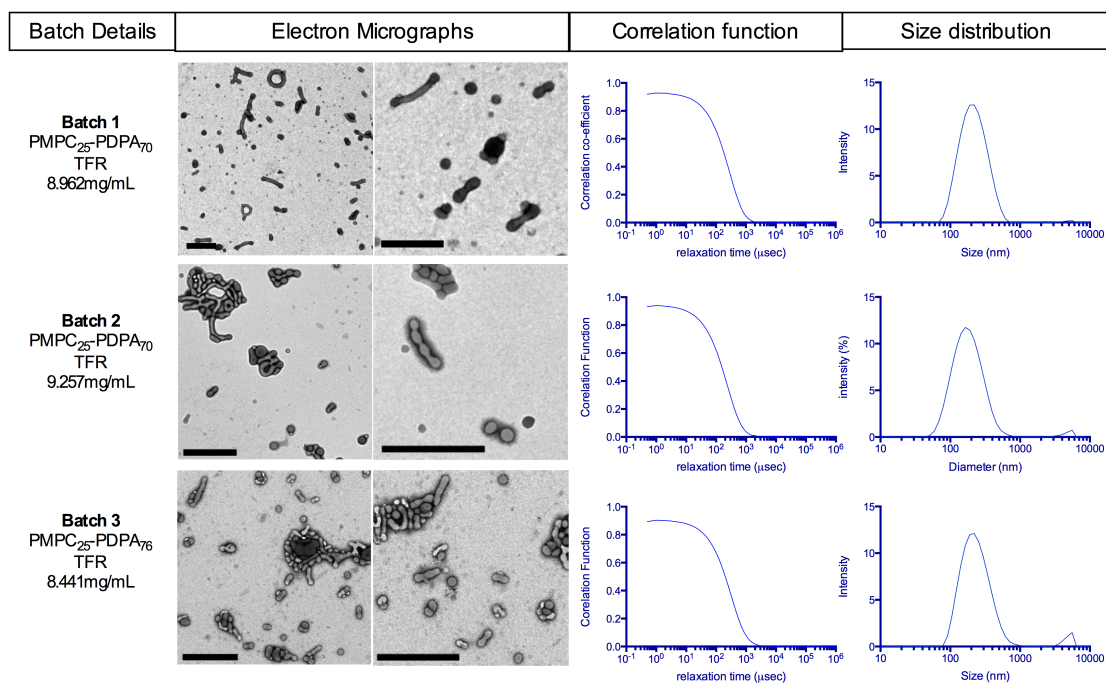


FIGURE 4.10: **PMPC-PDPA polymersomes characterisation:** All polymer-somes used to assess potential toxicity in fibroblasts were formed by TFR. Batch details list batch number, polymer used, method of formation and concentration (determined by UV-HPLC). Two separate fields of view from EMs of polymersomes, plus their DLS auto-correlation functions and size distribution by intensity are shown.

4.4.2 Assessment of potential polymersome induced toxicity

Potential polymersome induced cytotoxicity to fibroblasts was assessed by measuring extracellular levels of LDH, a highly stable cytosolic enzyme. Increased levels of cytosolic components outside the cell are a good indication that plasma membrane integrity may be compromised, something known to result from cell necrosis, apoptosis and other forms of cell death [465]. Fibroblasts from healthy controls were incubated with 1mg/mL polymersomes (polymersomes used; figure 4.10a) for 24 hours in either glucose or galactose media, and the LDH release assay performed in a 96 well plate according to previous protocol [95] (Chapter 2). (figure 4.11).

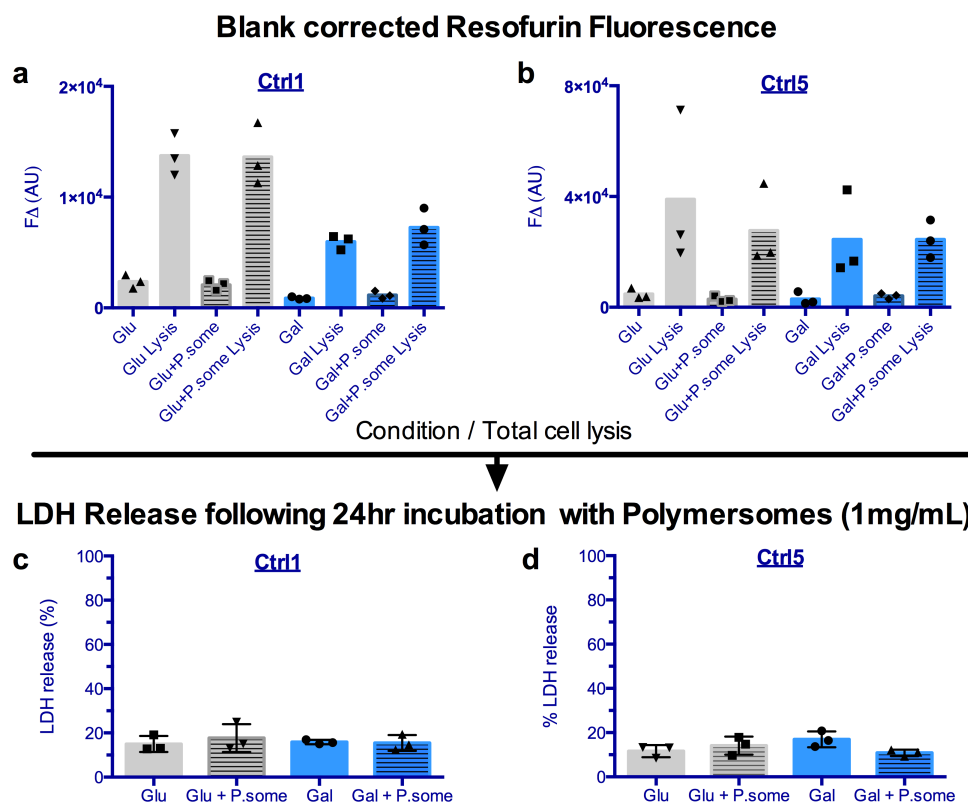


FIGURE 4.11: **LDH release assay pilot:** Fibroblasts from healthy controls were incubated in either a glucose (grey bars) or galactose (blue bars) medias in the absence (solid bars) or presence of 1mg/mL polymersomes (lined bars). The top graphs (a,b) show the background subtracted resofurin emitted fluorescence of intact and lysed cells, where the bottom graphs (c,d) show the signal from intact cells as a percentage of that from lysed cells ($n=3$; error bars = SD; individual data points shown).

No significant differences were found in % LDH release between conditions (Ctrl1 $p = 0.446$, Ctrl5 $p = 0.175$), suggesting neither incubation in galactose media for 48 hours, nor incubation with polymersomes for 24 hours induces deviation from baseline cell membrane integrity. As shown in figure 4.4, at 1mg/mL polymersomes accumulate into fibroblasts linearly over 24 hour and are internalised by $\approx 100\%$ of cells, so is a suitable point at which to assay for loss of membrane integrity caused by nanoparticle uptake. Though the half-life of LDH is approximately nine hours [466], the lack of even small deviations from baseline LDH release during continuous accumulation of polymersomes suggest little or no toxic insult has taken place and that signal loss due to LDH degradation is negligible. Also, the well matched 100% lysis signals between conditions with

and without polymersomes indicates that cell number is also unaffected. Visual inspection by light microscopy prior to the assay confirmed similar cell morphologies between conditions. It is interesting to note the apparent decrease in the 100% lysis levels between the glucose and galactose conditions in Ctrl1 (37 year old female), indicating a smaller amount of LDH present in cells grown in galactose media and perhaps reflecting a down-regulation of glycolysis or a reduction in cell growth, which indeed was seen previously (figure 4.3). This was not apparent in Ctrl5 (12 year old male).

The effect of polymersome concentration (polymersomes used; figure 4.10c) on LDH release from two *parkin* mutant fibroblast lines and their controls was tested (4.12). No apparent cytotoxicity was seen at polymersome concentrations up to 2mg/mL after 24 hours incubation (Ctrl1 vs PD1, $p=0.4102$; Ctrl2 vs PD2, $p=0.9968$) (figure 4.12).

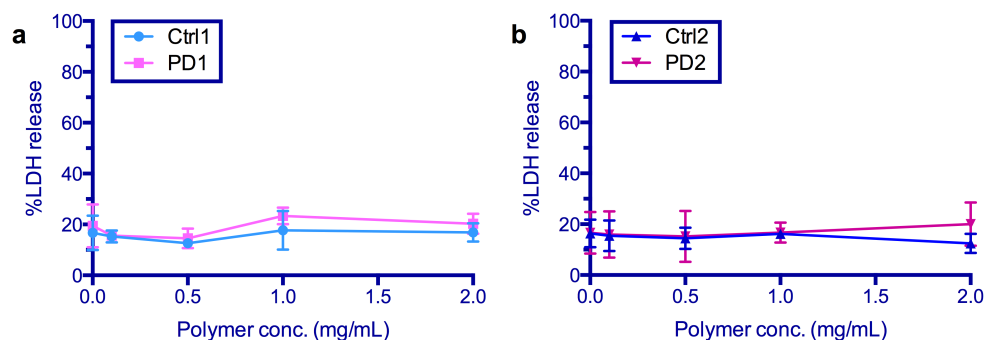


FIGURE 4.12: **Effect of Polymersome incubation on fibroblast LDH release:** LDH release from Ctrl1 and PD1 (a), plus Ctrl2 and PD2 (b) was assessed following 24hr incubation with PMPC-PDPA polymersomes at 0.1, 0.5, 1 and 2 mg/mL in galactose media. (n=3; error bars = SD; statistics performed by two way anova)

4.4.3 Fibroblast Mitochondrial Membrane Potential

To produce ATP by OXPHOS, mitochondria must generate a large electrochemical gradient across the inner mitochondrial membrane by translocating protons from the matrix to the IMS, something achieved by the ETC. This Mitochondrial Membrane Potential (MMP) can be perturbed at almost any point along the ETC

and is subsequently a useful indicator of mitochondrial health. Loss of MMP is also one of the first steps seen in apoptosis [465]. MMP has previously been assessed in intact fibroblasts using a TMRM based plate reader assay [95, 418]. It relies on three factors. First is the accumulation of a cationic and lipophilic fluorescent dye, TMRM, within cellular compartments of electrochemical potential difference, the most charged of which is the mitochondria [467]. Second is the specific disruption of the MMP using an ETC uncoupler, CCCP. Finally, a measure of cell number is necessary to normalise per cell the difference between whole cell membrane potential with and without the MMP. It is noteworthy that the rigorous washing regime this assay employs to remove noise causing excess TMRM, causes some fibroblast to detach, making normalisation by cell number essential. All assay reagents are cell penetrant.

Using optimised incubation times (see Chapter 2), the TMRM assay was piloted in two sets of apparently healthy fibroblasts (figure 4.13). The addition of polymersomes (polymersomes used; figure 4.10c) caused no significant alteration to MMP in either. It is interesting to note Ctrl5 demonstrated a higher MMP than Ctrl1.

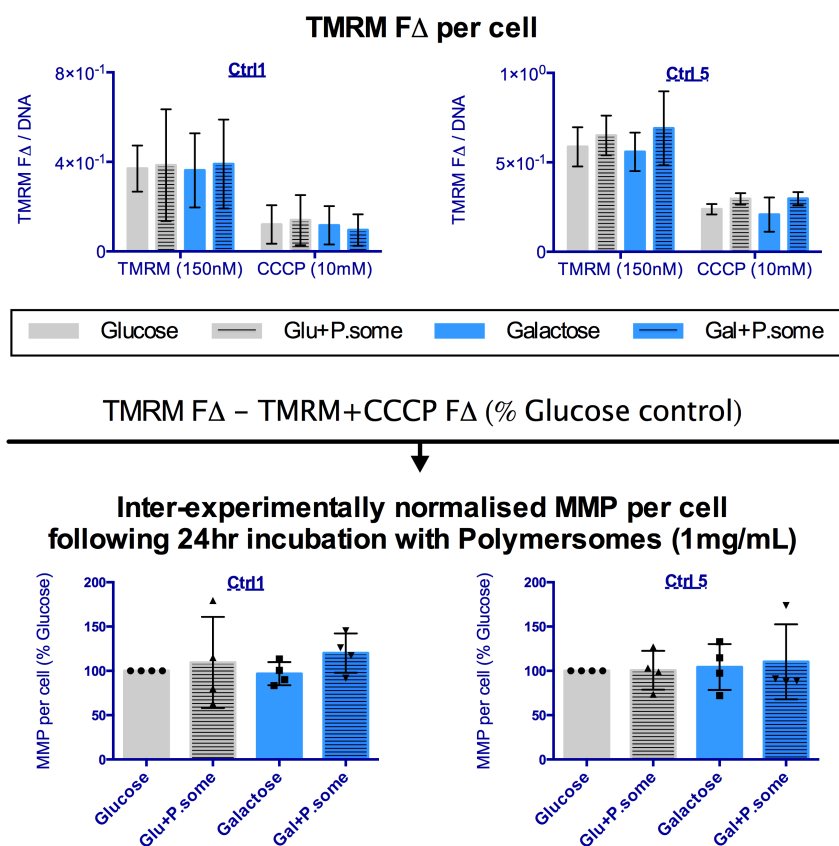


FIGURE 4.13: **Mitochondrial membrane potential assay pilot:** Fibroblasts derived from two separate healthy biopsies were incubated in either a glucose (grey bars) or galactose media (blue bars) in the absence (solid bars) or presence of 1mg/mL polymersomes (lined bars). Cells were incubated with TMRM in standard assay buffer (150nM) and washed three times with PBS. Additionally, replicates of each condition were incubated with CCCP (10nM) for 1 hour prior. TMRM fluorescence was read on a plate reader (ex. 544nm em. 590nm). (a,b) Background subtracted TMRM signals normalised by background corrected CyQuant[®] signal. (c,d) MMP, calculated as TMRM signal per cellular DNA minus TMRM signal per cellular DNA in the presence of CCCP, normalised by glucose only condition. (n=4; error bars = SD; individual data points shown)

Next the MMP of two *parkin* mutant fibroblasts plus controls was assessed following 24 hour incubation with PMPC-PDPA polymersomes (0-2mg/mL) (polymersomes used; figure 4.10c) was assessed.

No significant deviation from baseline levels were seen with increasing polymer-some concentration (unpaired one-way ANOVA; Ctrl1, $p=0.9721$; PD1 $p=0.9212$;

Ctrl2, $p=0.9721$; PD2, $p=0.9212$). A significant deficiency in MMP was seen relative to age-sex matched controls (Ctrl1 vs PD1 $p = 0.0058$; Ctrl2 vs PD2 $p = 0.0027$) [95].

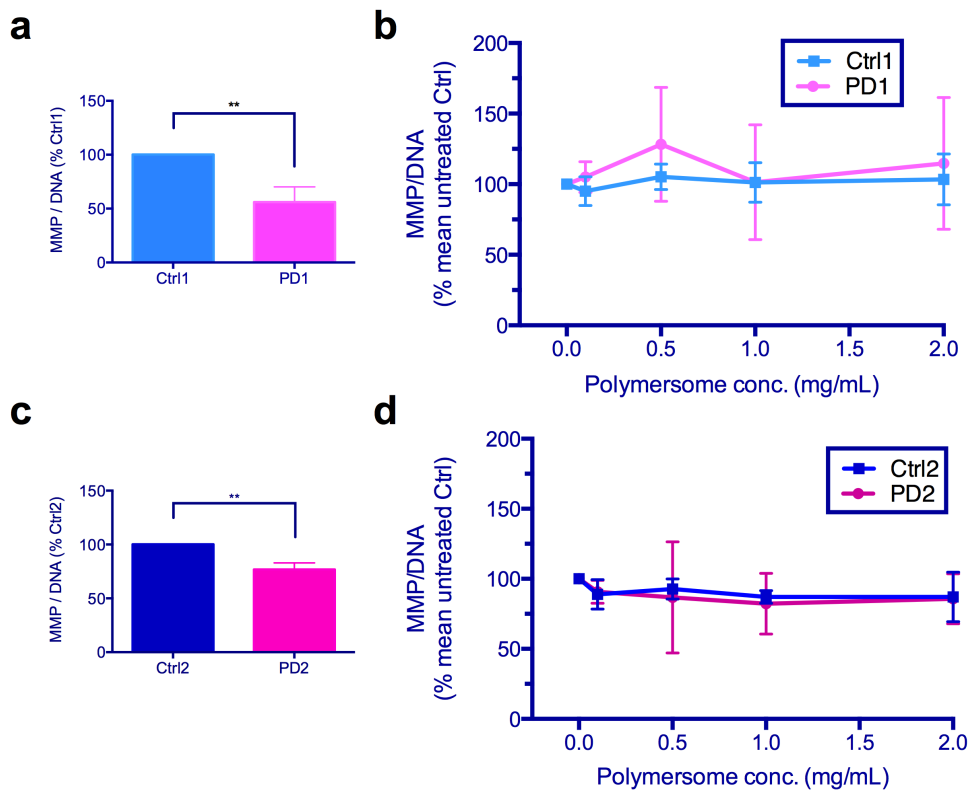


FIGURE 4.14: **The effect of Polymersomes on fibroblast MMP:** MMP of Ctrl1 and PD1 (a,b) plus Ctrl2 and PD2 (c,d), was assessed following 24hr incubation with polymersomes at 0.1, 0.5, 1 and 2 mg/mL. a,c) *parkin* mutant fibroblast MMP normalised to age-sex matched control. (b,c) MMP normalised to fibroblast matched untreated controls ($n = 3$; error bars = SD; Statistics performed by unpaired two-tailed t-test, ** = $p < 0.01$).

4.4.4 Assessment of fibroblast ATP levels in the presence of polymersomes

Intracellular ATP levels are routinely used to assess cell viability as they closely correlate to cell number and metabolic capacity [468]. As the great majority of ATP anabolism occurs by mitochondrial OXPHOS when fibroblasts are cultured in galactose media, ATP levels per cell give a good indication of mitochondrial function [95, 107]. Here, intracellular ATP levels of lysed fibroblast populations

are assessed by the luciferin luciferase assay, which produces bioluminescence proportional to ATP, and normalised by intracellular DNA content, a close correlate of cell number [420, 421](Chapter 2).

Fibroblasts from healthy controls were incubated with 1mg/mL polymersomes (Batch 2, figure 4.10) for 24 hours in either glucose or galactose media. Cell lysis was confirmed by light microscopy, and the intracellular ATP and DNA quantification assays performed sequentially on the same fibroblast populations (figure 4.15a,b). Cellular ATP levels were normalised by cellular DNA content to give ATP level per cell. This was then further normalised against the ATP per fibroblast incubated in glucose media alone, so as to compensate for inter-experimental variation and reduce variance within the conditions (figure 4.15c,d). It is interesting to note the higher ATP levels of Ctrl5 relative to Ctrl1 (figure 4.15a,b).

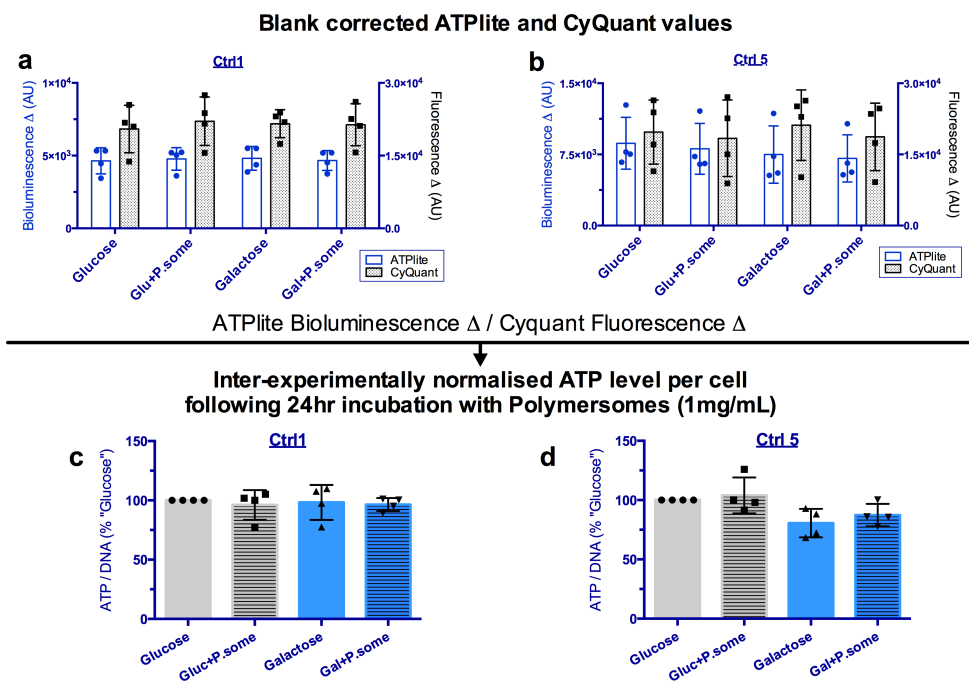


FIGURE 4.15: **Cellular ATP assay pilot:** Fibroblasts derived from two separate healthy biopsies were incubated in either a glucose (grey bars) or galactose (blue bars) medias in the absence (solid bars) or presence of 1mg/mL polymersomes (lined bars). Cells were then washed twice in PBS and lysed. (a,b) Background subtracted bioluminescence derived from ATP content (white filled bars) and background subtracted fluorescence derived from DNA content (dotted bars). (c,d) Cellular ATP per DNA content, normalised by glucose only condition (n=4; error bars = SD; individual data points shown).

Next, the effect of polymersome concentration (polymersomes used; figure 4.10c) on intracellular ATP levels was tested in two *parkin* mutant fibroblasts plus controls. As previously reported, a deficiency *parkin* mutant fibroblasts relative to controls was observed in the absence of polymersomes (figure 4.16, a, Ctrl1 vs PD1, $p=0.0004$; c, Ctrl2 vs PD2, $p=0.0049$) [95, 96]. Polymersome concentrations of 0.1, 0.5, 1 and 2mg/mL caused no significant deviation from baseline intracellular ATP levels in any fibroblasts tested (unpaired one-way ANOVA; Ctrl1, $p=0.9529$; PD1, $p=0.7213$; Ctrl2, $p=0.9301$; PD2, $p=0.8257$).

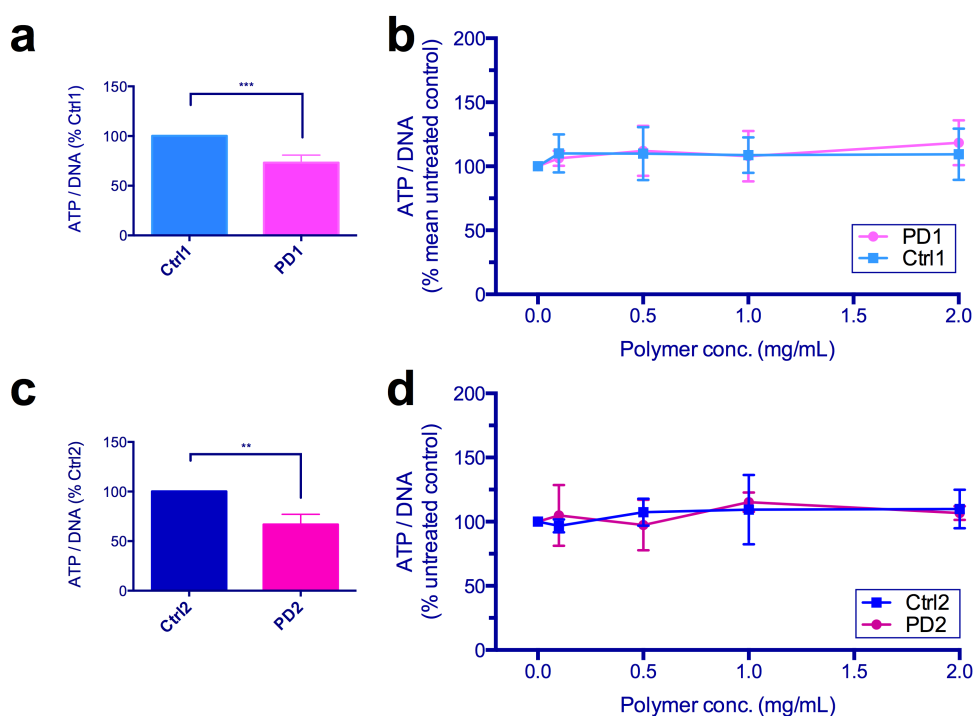


FIGURE 4.16: **The effect of Polymersomes on fibroblast ATP levels:** Cellular ATP levels were determined in Ctrl1 and PD1 (a,b), plus Ctrl2 and PD2 (c,d) following 24hr incubation with PMPC-PDPA polymersomes at 0.1, 0.5, 1 and 2 mg/mL in galactose media. (a,c) *parkin* mutant fibroblast cellular ATP levels normalised to age-sex matched control. (b,c) Cellular ATP levels normalised to fibroblast matched untreated controls ($n = 3$; error bars = SD; statistics performed by unpaired two-tailed t-test, ** = $p < 0.01$, *** = $p < 0.001$)

4.5 Discussion:

PMPC-PDPA polymersomes made by pH switch and TFR have been shown to accumulate on and within *parkin* mutant fibroblast in galactose media, which forces fibroblasts to rely more heavily on mitochondrial OXPHOS for ATP anabolism. Variation was seen between all fibroblasts tested and appeared independent of mutant *parkin* or wild type phenotypes. It was determined with polymersomes made by TFR of RAFT synthesised polymer (RhBATCH3, figure 4.1) that faster fibroblast growth rate did not significantly contribute to individual fibroblasts ability to accumulate polymersomes at the concentrations studied. A correlation between ability to bind polymersomes after one minute and ability to accumulate polymersomes at 24 and 48 hours was seen (figure 4.6). This ratio was similar between all fibroblasts studied suggesting the rate at which control and *parkin* mutant fibroblasts endocytose PMPC-PDPA nanoparticles is approximately the same, and that differences in uptake might mostly depend on varied nanoparticle receptor levels. There is evidence that class B scavenger receptor protein levels are altered in the brain and liver of *parkin* knock-out mice, and that this correlates with reduced lipid uptake [469]. However, much of this phenotype requires a high fat diet to manifest. The galactose media used here exposed fibroblasts only to those fats present in the FBS used, which though sadly a “black box” regarding exact lipid content, is derived from bovine fed on a low fat grass diet, thus plasma levels are perhaps unlikely to exceed a specific high fat diet. Over-expression of *parkin* was shown to increase lipid uptake, something also largely dependent on class B scavenger receptors, and this was mitigated by deletion of the ubiquitin like region, primarily coded for in exon 2 of PARK2 [469]. Interestingly the fibroblast demonstrating lowest polymersome uptake relevant to control was also the only to possess mutations effecting exon 2 in both copies of PARK2 (table 2.2, PD1). Similarly, *parkin* mutant transformed B cells possessing mutations on both PARK2 alleles effecting the ubiquitin like region also showed reduced lipid uptake [469, 470]. Quantification of class B scavenger receptor protein levels in *parkin* mutant fibroblasts was piloted, however

interpretable western blot or immuno-cytochemical data was difficult to acquire, perhaps due to the relatively low expression of class B scavenger receptors in fibroblasts and the low specificity of currently available commercial antibodies. Work elsewhere has successfully detected SRB1 and CD36 in fibroblasts respectively using a commercially available and patent protected antibody [341].

Whilst *parkin* mutant fibroblasts possess deficient cellular ATP [95, 96], the effect this might have on receptor-mediated and -independent endocytosis is not entirely clear. ATP depletion studies in cancerous cell lines have shown ATP is required for true receptor mediated endocytosis, and that this inhibition is fully reversible within minutes of partial ATP level recovery [471]. Somewhat confoundingly, ATP depletion in fibroblasts was shown not to directly correlate their ability over one hour to internalise LDL [472] whose internalisation is, like PMPC-PDPA polymersomes, mediated by class B scavenger receptors [473, 474]. However, this study did not clearly distinguish deeply invaginated but still exterior cargoes from those truly internalised, which may in part explain this disparity [471]. Macropinocytosis, being an actin regulated process is also ATP dependent, and there is evidence that ATP depletion causes a reduction, though the correlation between the two at modest reductions in ATP is not clearly documented [475, 476]. That healthy fibroblasts showed reduced polymersome uptake in galactose media similar to that seen in *parkin* mutant fibroblasts (figure 4.2), though only the latter's cellular ATP is reduced in this condition [95] suggests that in these conditions the ATP levels of both fibroblast phenotypes are sufficient to maintain normal endocytosis and macropinocytosis.

The uptake of TFR formed polymersomes in galactose media remained linear between the initial binding step and 48 hours at all concentrations tested, suggesting an excess of polymersomes was present down to 0.1mg/mL. By contrast, pH switch polymersomes saw an uptake plateau after 24 hours in galactose media (figure 4.2). As uptake of pH switch formed polymersomes remained linear up to 48 hours in glucose media, a condition which also produced faster cell growth, this is unlikely to have resulted from total polymersome

depletion. Another possibility is antagonisation of polymersome uptake by components of the galactose media not found in glucose media, though none of these are known class B scavenger receptor ligands. It has been shown in caco-2 cells cultured in high glucose or galactose that cholesterol uptake is increased [477]. Glucose was more efficacious in this respect, and antagonisation of SRB1 mitigates the effect of both media types. Increasing concentrations of glucose have also been found to increase protein levels of class B scavenger receptors in dendritic cells, endothelial cells, caco-2/15 cells, vascular smooth muscle, mesangial cells and macrophages [478–483]. Enhanced expression of polymersome receptors in glucose media relative to galactose could explain the increased uptake. Future work quantifying the presence of class B scavenger receptors may shed light on this situation.

Work, currently in preparation, from the Battaglia group has also shown that neutrophils both absorb polymersomes, and that reducing polymersome concentration results in a loss of polymer from the cell [484]. This indicates that both polymer entry and exit from the cell happens concurrently, and explains why saturated uptake might occur while there is still an excess of polymersomes in solution, as seen in many cell types [404, 413, 435]. The reduced rate of uptake seen in galactose media might thus result from decreased polymersome entry or increased polymer secretion. It is therefore interesting to note that high glucose concentration has also been found to reduce protein levels of cholesterol exporters in caco-2/25 and mesangial cells [480, 482]. Again, future work quantifying the presence of class B scavenger receptors and identification of components involved in polymersome secretion may shed light on this situation.

TFR formed PMPC-PDPA nanoparticles were generally larger and more tubular than pH switch formed polymersomes (figure 4.1). They also demonstrated a reduced ability to enter fibroblasts (figure 4.9), in close keeping with previous research demonstrating slower uptake of PMPC-PDPA particles with increasing

size over 100nm \varnothing [339, 340], and of tubular morphologies relative to spherical particles [435]. It is interesting that where uptake of pH switch polymersomes occurs linearly at early time-points, TFR polymersomes show a rapid initial accumulation (1-60 minutes) then slow internalisation, reminiscent of the long surface dwelling times seen with purified tubular polymersomes [435]. Evidence that isolated tube like “intermediate” particles accumulate in healthy and *parkin* mutant fibroblasts as a function of incubation time is shown in Chapter 5 (figure 5.5), suggesting these larger morphologies are also truly internalised. Though the TFR formed nanoparticles used here are a mixture of quickly and slowly internalised morphologies [387, 435], the longer receptor occupancy and greater surface area of the more tubular morphologies will impede the uptake of further nanoparticles more greatly than faster internalised particles. Further, the slower wrapping of cell membrane around tubular particles may also impede the uptake of spherical particles clustered closely to it on the cell surface [325, 326, 388]. Thus the presence of even a small proportion of slowly internalised particles may have a disproportionately large impact on the uptake of a nanoparticle population. Future experiments aiming to discern the endo- and phago- cytic routes by which polymersomes of varying size and shape are internalised by fibroblasts may shed light on the different uptake kinetics seen here.

PMPC-PDPA nanoparticles formed by TFR demonstrated no noxious effects towards healthy or *parkin* mutant fibroblasts as assessed by measures of cell membrane integrity, metabolism, and mitochondrial function. TFR formed rhodamine labelled nanoparticle have demonstrated effective binding and internalisation into fibroblasts at all concentrations tested here (figure 4.6 and 4.7), inferring these results relate to the presence of PMPC-PDPA both on and within cell. These are the first cells possessing a known mitochondrial defect to be tested with PMPC-PDPA nanoparticles has. Whilst the mitochondrial dysfunction of *parkin* mutant fibroblasts is mild relative to fibroblasts derived from patients of mitochondrial syndromes such as MELAS and LHON [95, 96, 462], the lack of obvious alteration to mitochondrial physiology or cytotoxic induction is promising

for the use of PMPC-PDPA nanoparticles in more severe mitochondrial disorders.

It must be noted that fibroblasts are known to show slow internalisation kinetics relative to other cell types, and that cells which internalise polymersomes more effectively tend to show larger reductions in viability at equivalent polymersome concentrations [339, 341]. There is evidence that fibroblasts show a loss of viability at concentrations greater than 2mg/mL, though never by more than 10%, slight in comparison to many other delivery vectors [358, 393, 413, pg. 129]. The nanoparticles used here are markedly more tubular than those used previously and assessment of their viability in fibroblasts was conducted in galactose media, both factors shown to decrease PMPC-PDPA nanoparticle uptake (figure 4.9 and 4.2). Studies in which PMPC-PDPA nanoparticle accumulation is greater could possibly identify disparate concentrations of toxic induction between cells with healthy and dysfunctional mitochondria.

As mitochondria are known to express class B scavenger receptors on their OMM [485], and the amphiphilic nature of PMPC-PDPA at pHs >6.3 forces it to associate with non-polar environments, as well as its overall cationic charge under this, the possibility of an interaction between PMPC-PDPA and the mitochondria is feasible and merits further study.

4.6 Conclusions

The ability of *parkin* mutant fibroblasts and their controls to accumulate and internalise PMPC-PDPA polymersomes whilst dependent on mitochondrial ATP anabolism has been demonstrated at 0.1-1mg/mL concentrations. TFR formed PMPC-PDPA polymersomes showed no significant noxious effect on cellular ATP production, MMP, or membrane integrity at concentrations of 0.1-2mg/mL. Together, the suitability of polymersomes as a therapeutic for *parkin* mutant fibroblasts has been demonstrated.

Chapter 5

Results: Polymersome mediated delivery of mitochondrial therapeutics to *parkin* mutant fibroblasts

5.1 Aim

To assess the therapeutic potential of UA, UCA, and UDCA loaded polymer-somes on the mitochondrial function of *parkin* mutant fibroblasts, and investigate the effectiveness with which steroid like compounds are delivered to fibroblasts when formulated in PMPC₂₅–PDPA₆₅ nanoparticles.

5.2 Background

Mortiboys et al. [198] recently identified a number of compounds capable of improving the mitochondrial dysfunction seen in *parkin* mutant and *LRRK2* mutant fibroblasts, as well as *parkin* knock-down cortical neurons. These included

UA, UDCA and UCA, respectively a naturally occurring triterpene found in many plants [271] a secondary bile acid and a bile acid derivative (figure 2.1). These all possess high hydrophobicity and molecular weights <500Da, indicating they may penetrate the BBB [168, 262]. However brain penetrance is proportional to plasma concentration, something that greater hydrophobicity will limit as the compound rapidly accumulates within any non-polar environment encountered. Dietary UA demonstrates relatively poor percentage distribution to the brain of rats [271]. Though distribution to the CSF is reported, evidence of true brain penetrance by UDCA is currently lacking [272, 275, 278].

Poor distribution to the brain would require increased dosage, creating an increased possibility for adverse side effects. UA and UDCA for instance have been studied extensively in other medical research fields for various therapeutic effects. However, both have known adverse effects *in vivo*, and concerns have been raised over their use at high doses or with prolonged use [210, 282]. Thus, though these compounds possess therapeutic potential in at least some forms of PD, *in vivo* effects could benefit from formulations that improve their brain specific distribution, something for which polymeric nanoparticles such as polymersomes show potential.

Polymeric nanoparticle such as polymersomes have previously been used to deliver hydrophobic cargoes *in vitro*, *in vivo*, and have recently entered into early clinical testing [296]. Delivery of hydrophobic chemotherapeutics have shown enhanced efficacy when encapsulated in polymersomes, attributed to improved tumour penetration/targeting, and the simultaneous delivery of large drug “payloads”, as opposed to the diffusion of single molecules into the cell [341, 366]. Progress has also been made in targeting polymersomes across the BBB. Intravenous administration of Poly(D,L-lactic-co-glycolic acid) (PLGA) nanoparticles (c.150nm \varnothing) coated with a cationic molecule known to enhance absorptive-mediated BBB transcytosis successfully delivered the highly hydrophobic antioxidant CoQ10 to the brains of transgenic mouse model of AD, where a disease modifying effect was seen [360]. Similar brain penetrance and therapeutic

effects have also been described for nanoparticles decorated with ligands targeting receptor mediated transcytosis across the BBB [351, 356], including Lactoferrin (Lf) which led to accumulation of particles in the SN, the region of midbrain particularly effected in PD [348](further details in Chapter 1).

UA has previously been formulated in lipid nanoparticles and administered topically and intravenously, the former of which was recently tested clinically in cancer patients [280, 282]. UA has also been encapsulated within PLGA polymeric nanoparticles and shown to enhance its anticancer properties, though the empty nanoparticles were also shown to alter cell metabolism [447]. The successful encapsulation of UA, UCA and UDCA in PMPC₂₅–PDPA₆₅ “polymersomes” and “tubes” has been discussed in detail in Chapter 3, and the innocuous effects of empty PMPC₂₅–PDPA₆₅ nanoparticles on *parkin* mutant fibroblast viability and mitochondrial function in Chapter 4. PMPC₂₅–PDPA₆₅ polymersome have also demonstrated the delivery of hydrophobic dyes that then distribute to multiple sub-cellular locations in fibroblasts [404]. Tubular PMPC₂₅–PDPA₆₅ polymersomes have been investigated in less detail, though their cellular uptake, slower relative to polymersome, has been demonstrated, as has their ability to deliver hydrophilic proteins to a cell’s intracellular space [435]. Thus PMPC-PDPA nanoparticles appear an appropriate delivery vehicle for UA, UCA and UDCA, to fibroblasts.

As PMPC-PDPA nanoparticles deliver their cargoes intracellularly, it is desirable that encapsulated therapeutics are able to elicit their desired response from inside the cell or cell membrane. Though precise targets have not yet been described, inhibitor studies have revealed roles for GR activation and PI3K/Akt signalling in mediating the mitochondrial effects of UCA and DUA, an analogue of UA [198]. Increased Akt phosphorylation was also demonstrated in UCA and UDCA treated *parkin* knock-down neurons. Thus the GR is a probable molecular target. However a number of other possibilities exist by which these compounds may exert their effects on the mitochondria, both intracellular and on the cell surface (discussed further in Chapter 1). This includes TGR5, a cell surface GPCR linked to increased mitochondrial activity [229]. Notably, both

UA and UCA are known TGR5 activators [231, 232]. UDCA on the other hand shows little efficacy for TGR5 activity [233, 234].

Herein the effect of UA- and UCA- loaded “polymersomes” and “tubes” on the intracellular ATP levels of *parkin* mutant fibroblasts, and their ability to deliver steroid like cargoes to these cells, is investigated.

5.3 Rescue of *parkin* mutant fibroblast ATP levels using drug loaded polymersomes

5.3.1 Characterisation of drug loaded polymersomes

Drug loaded polymersomes were made by TFR of PMPC₂₅–PDPA₆₅ with the addition of chosen drugs over one month. UA and UCA films were prepared to produce 10 μ M (low drug load) and 1mM (high drug loads) concentrations in PBS, should 100% of material form into drug loaded nanoparticles. Suspensions were split into polymersome, tubular and large lyotropic structure fractions using stepwise centrifugation. Drug plus polymer concentrations were determined by UV-HPLC as previously described (Chapter 3). Successful fractionation was confirmed by TEM and DLS studies (figure 5.1).

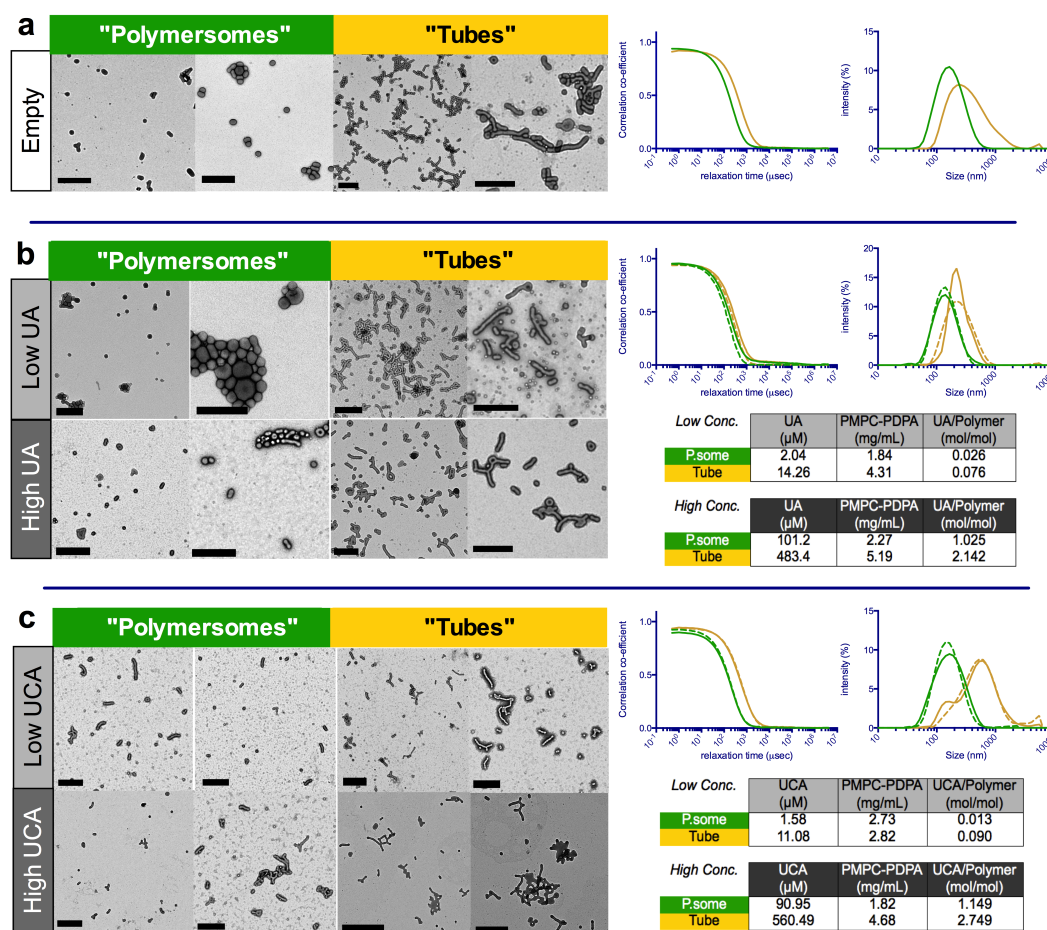


FIGURE 5.1: **Characterisation of UA and UCA loaded polymersomes for therapeutic assays:** (a) empty, (b) UA and (c) UCA loaded PMPC₂₅–PDPA₆₅ nanoparticles. Two separate fields of view from EM supporting either polymersome and tubular fractions, encapsulating the high or low drug loads, are shown (scale bars = 500nm). DLS correlation functions (right) and size distributions (left) are shown (green indicates “polymersome” fractions, yellow “intermediate” fractions, solid lines high drug loads, and dashed lines low drug loads). Tables indicate ELSD-HPLC determined drug and polymer concentrations in PBS, and nanoparticles drug composition by percentage weight.

5.3.2 Therapeutic effect of drug loaded polymersomes

The ability of UA and UCA formulated within PMPC₂₅–PDPA₆₅ “polymersomes” or “tubes”, at high or low concentrations (<3 or <0.1 drug:polymer (mol/mol) respectively), to increase the intracellular ATP levels of *parkin* mutant fibroblasts toward control levels was investigated relative to drug formulations in 0.1%DMSO. Previous work has determined the EC₅₀ of UCA to be 350nM, and both UA and

UCA were shown to be competent of increasing *parkin* mutant fibroblast ATP levels to control levels at 100nM [198]. Concentrations of 10, 100 and 1000nM were chosen for investigation, allowing comparison of the polymer based formulations of UCA against DMSO based formulations known respectively to be “therapeutically” ineffective, effective and highly effective. It is notable that a full dose-response in which the EC50 of UA is identified has not yet been performed. Though the purpose of these experiments were to test if polymer based formulations effected UA’s therapeutic efficacy, the possibility of loss of signal due to close proximity to the EC100 would need to be considered if increased dosing produced little apparent effect.

Fibroblasts were cultured for 24 hours in galactose media, and then incubated with all five formulations of UA and UCA formulated in 0.1% DMSO for 24 and 48 hours, following which cellular ATP levels were measured (figure 4.16). DMSO formulations were first diluted into galactose media, mixed and then applied to fibroblasts at a final concentrations of 0.1% DMSO. Nanoparticle formulations were diluted as appropriate into 10 μ L PBS, before application to fibroblasts so that the mix constituted 10% of the cell media. The first two assay repeats assessing fibroblast ATP levels following 24 hour incubation with UA and UCA loaded nanoparticles were kindly performed by Dr. H.M. Mortiboys. Drug formulations were applied to fibroblasts by Mr. G.M. Yealland in all instances.

UDCA loaded polymersomes were also characterised and tested in fibroblasts, however no measurable effect on intracellular ATP levels was found at the concentrations tested, using PMPC₂₅–PDPA₆₅ nanoparticles or 0.1% DMSO formulations. A third patient derived *parkin* mutant fibroblast (PD2) was also tested, however this failed to demonstrate a deficiency in cellular ATP levels relative to control. This is contrary to previous evidence and possibly the result of the late passages at which the fibroblasts and controls were available (passage 11-13).

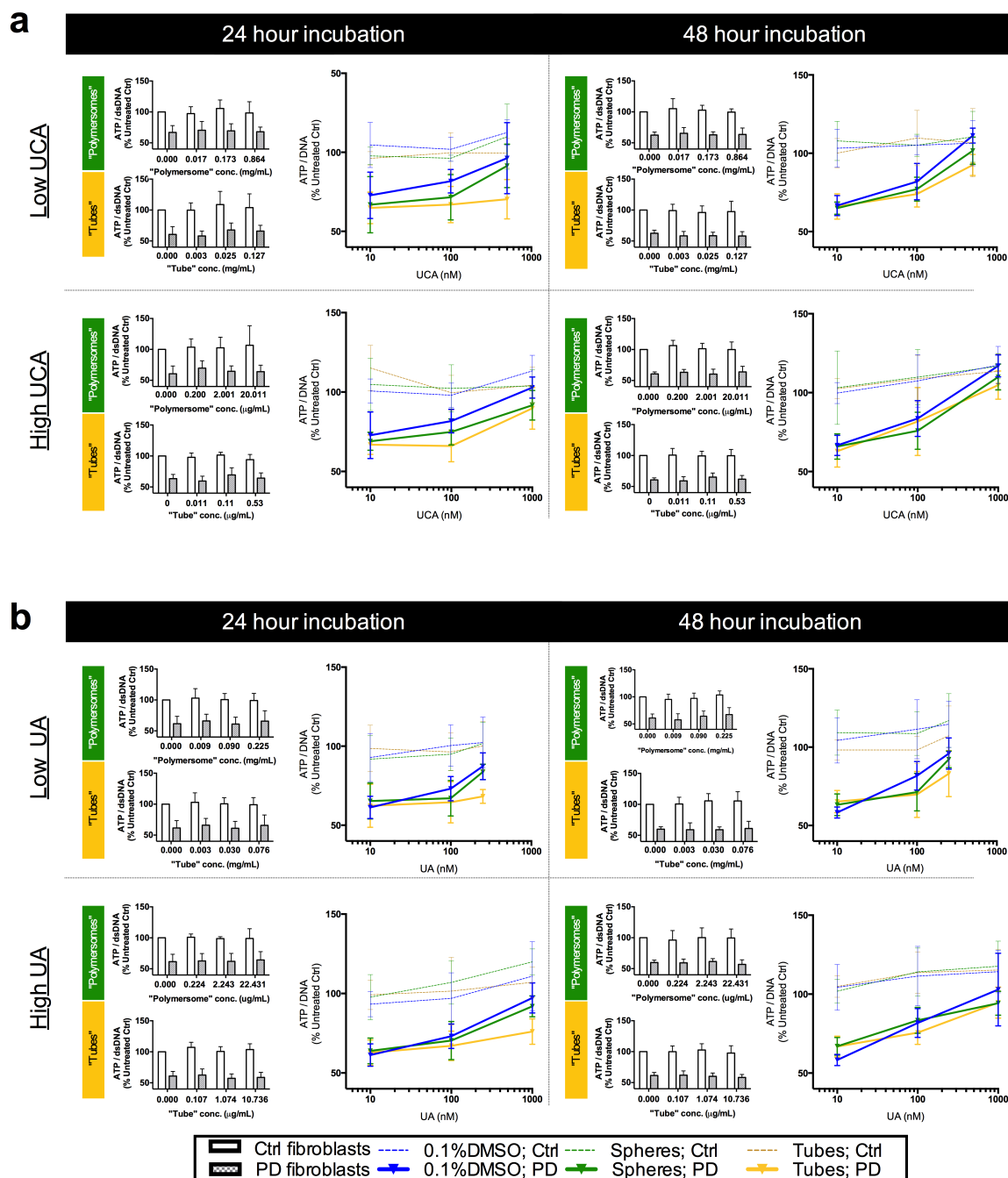


FIGURE 5.2: Cellular ATP of healthy and *parkin* mutant fibroblasts following incubation with drug loaded PMPC₂₅–PDPA₆₅ nanoparticles: Intracellular ATP levels of *parkin* mutant fibroblasts plus matched controls were measured following incubation UCA (a) or UA (b) formulated in “polymersomes” (green), “tubes” (yellow) or 0.1% DMSO (blue). High or low drug loads in nanoparticles are indicated on the side, and incubation periods along the top. The effect of empty nanoparticles at concentrations matched to drug loaded nanoparticles are shown in accompanying bar graphs (graphs depict the mean of two sets of *parkin* mutant fibroblast plus age and sex matched controls, PD1, PD4, Ctrl1 and Ctrl4, n = 3 for each; error bars = SD)

Therapeutic effect of UCA Formulations					Therapeutic effect of UA Formulations							
		PD1 - % ATP		PD4 - % ATP				PD1 - % ATP		PD4 - % ATP		
UCA (nM)		24hr	48hr	24hr	48hr	UA (nM)		24hr	48hr	24hr	48hr	
Low drug load	P.somes (10% PBS)	0	55.6	63.9	65.5	61.1	P.somes (10% PBS)	0	62.0	58.6	61.1	60.5
		10	71.1	66.8	62.7	63.2		10	66.1	62.9	64.5	63.6
		100	73.4	77.6	69.8	76.7		100	66.8	77.0	67.3	65.6
		500	*** 95.2	* 86.9	* 87.5	*** 96.6		250	* 83.0	**** 96.2	* 84.4	** 88.1
	Tubes (10% PBS)	0	55.6	63.9	65.5	61.1	Tubes (10% PBS)	0	62.0	58.6	60.3	58.0
		10	63.6	65.2	66.1	66.8		10	65.1	64.7	59.5	65.8
		100	64.2	73.9	69.6	74.0		100	66.5	71.8	62.6	67.8
		500	64.3	**** 106.6	76.3	**** 98.1		250	69.2	** 84.9	67.3	* 81.25
	0.1% DMSO	0	55.6	63.9	65.5	61.1	0.1% DMSO	0	62.0	58.6	61.1	60.5
		10	70.9	70.0	74.7	63.2		10	59.9	56.8	62.6	59.7
		100	77.9	* 87.8	* 85.5	76.0		100	70.2	* 84.0	76.0	79.5
		500	**** 104.7	**** 111.0	**** 100.3	**** 111.5		250	** 88.2	**** 101.9	** 86.4	*** 89.8
High drug load	P.somes (10% PBS)	0	65.8	60.0	65.5	61.1	P.somes (10% PBS)	0	60.7	62.1	61.1	60.9
		10	69.8	62.8	68.3	69.0		10	58.7	70.6	69.0	63.2
		100	69.0	71.0	80.8	80.8		100	62.7	*** 90.1	80.8	76.7
		1000	**** 96.9	**** 110.7	* 86.4	**** 109.0		1000	** 87.3	**** 97.4	**** 96.5	*** 90.1
	Tubes (10% PBS)	0	65.8	60.0	65.5	61.1	Tubes (10% PBS)	0	60.7	62.1	61.1	60.9
		10	64.6	62.4	69.0	63.4		10	62.1	69.8	63.4	63.9
		100	61.2	71.5	70.8	** 91.9		100	63.5	* 81.1	70.6	70.0
		1000	84.5	**** 99.4	*** 94.9	**** 110.1		1000	72.4	**** 99.3	79.7	** 89.0
	0.1% DMSO	0	55.6	63.9	65.5	61.1	0.1% DMSO	0	60.7	62.1	61.1	60.9
		10	70.9	70.0	74.7	63.2		10	59.9	56.8	62.6	59.7
		100	77.9	** 91.1	* 85.6	76.0		100	70.2	84.0	76.0	79.5
		1000	**** 103.2	**** 113.93	**** 102.3	**** 120.7		1000	**** 92.0	**** 114.2	**** 102.4	*** 91.6

TABLE 5.1: Intracellular ATP levels of PD1 and PD4 (expressed a % of untreated matched controls), following UA and UCA treatment for 24 or 48 hours when formulated in PMPC₂₅–PDPA₆₅ “polymersomes” (green), “tubes” (yellow) or 0.1% DMSO (blue). Blue figures indicate ATP levels significantly different from untreated controls (n=3; statistics performed by two way ANOVA with bonferoni corrected multiple comparisons, * = p ≤ 0.05, ** = p ≤ 0.01, *** = p ≤ 0.001, **** = p ≤ 0.0001)

UA and UCA formulated within 0.1%DMSO demonstrated increases to *parkin* mutant fibroblast ATP levels following 24 and 48 hours incubation (figure 5.2). The dose response curve appears to be linear or just entering the linear phase, in keeping with previous evidence [198]. Formulation within PMPC₂₅–PDPA₆₅ nanoparticles also elicited similar increases to *parkin* mutant fibroblast ATP levels, though formulation in 0.1% DMSO consistently showed the strongest therapeutic effect. At 24 hours, the therapeutic effect of UA and UCA loaded “tubes” is notably weaker than the other two formulations, particularly at low drug loads. Longer incubation periods tended to yield improved therapeutic effects in *parkin* mutant fibroblasts. High drug loads produced marginally greater, though non-significant, gains in intracellular ATP levels relative to low drug loads. Significant increases in the ATP levels relative to untreated *parkin* mutant fibroblasts were seen at concentrations $\geq 100\text{nM}$ (indicated in blue in table 5.1).

5.4 Delivery efficiency of steroid like compounds by PMPC₂₅–PDPA₆₅ polymersomes

5.4.1 Characterisation of DHE loaded polymersomes

Delivery efficiency of steroid like compound to fibroblasts was assessed using rhodamine labelled polymersomes loaded with DHE, a naturally occurring fluorescent steroid [486] (figure 5.3). DHE is a close analogue of cholesterol, and reliably mimics the membrane altering properties of cholesterol within lipid bilayers [486]. It is used here as a representative steroid like compound, to model their delivery to fibroblasts when formulated in PMPC₂₅–PDPA₆₅ nanoparticles or DMSO. Fluorescent polymersomes were made from thin films of 5% (w/w) R.6G-PMPC-PDPA (ex. 432-582nm, peak at 505nm; em. 532-682nm, peak at 566nm) and DHE (ex. 250-360nm, peak at 325nm; em. 340-550nm, peak at 375nm), the fluorescence spectra of which show no overlap in excitation or

emission, allowing polymersome entry and cargo delivery to be measured independently and simultaneously [415, 487].

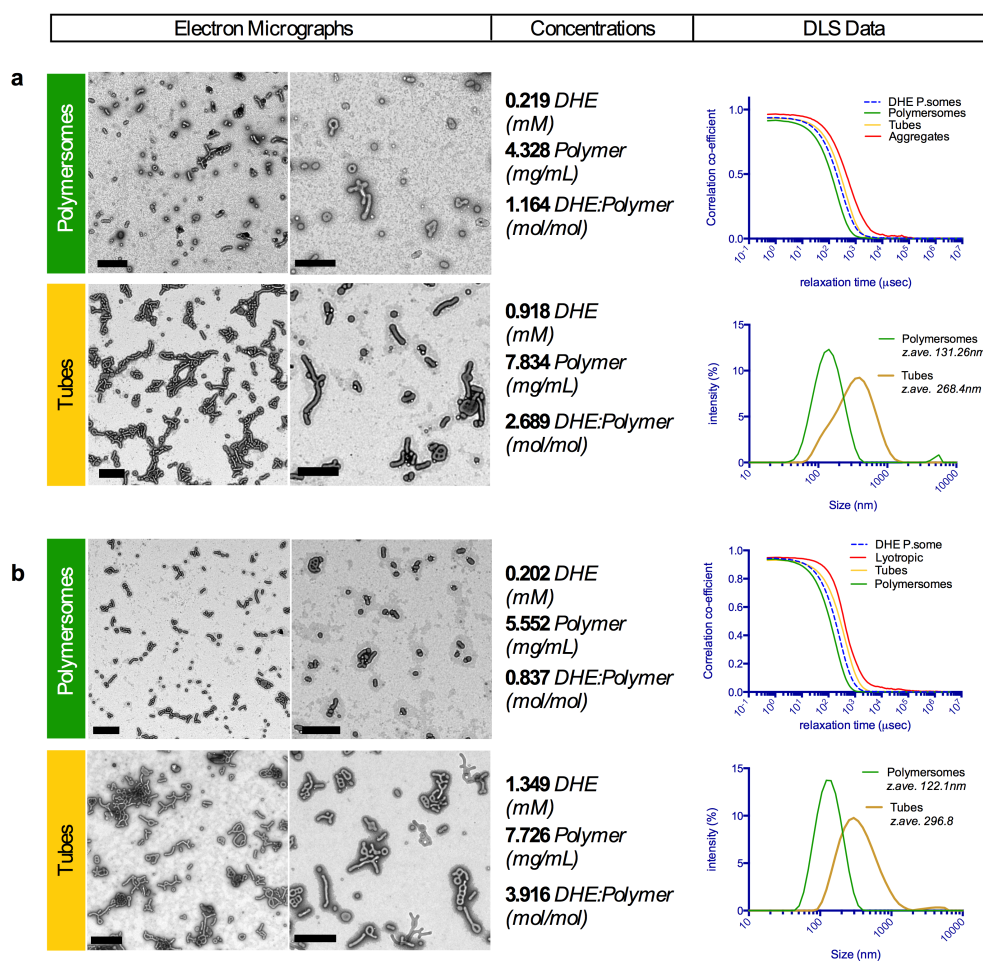


FIGURE 5.3: **DHE loaded nanoparticle characterisation:** (a, b) From left to right; two representative fields of view from EMs supporting DHE loaded “polymersomes” or “tubes”, their DHE and PMPC₂₅–PDPA₆₅ concentrations in PBS plus the ratio between these, and their DLS correlation functions and size distributions for two separate DHE loaded nanoparticle batches.

5.4.2 Polymersome mediated DHE delivery to fibroblasts

The ability of DHE loaded polymersomes to accumulate and deliver DHE to fibroblasts was assessed by flow cytometry. Pilot data indicated DHE and R.6G-PMPC-PDPA signal was weak below 10 μ M DHE load (0.198 and 0.121 mg/mL

“polymersomes” and “tubes” respectively, figure 5.3a), likely due to the non-optimal excitation of DHE at 355nm, close to its absorption extinction and unfortunately the lowest excitation wavelength available to the equipment used [487]. Concentrations of 10, 25 and 50 μM were subsequently chosen for investigation (0.198, 0.495 and 0.99mg/mL “Polymersomes”, and 0.121, 0.303, 0.605 mg/mL “Tubes”). No fluorescence bleed through was seen between DHE and R.6G-PMPC-PDPA fluorescence channels (figure 5.4a). Fibroblasts derived from *parkin* mutant patients plus controls were incubated with polymersome and tubular fractions (figure 5.3a) for 24 and 48 hours in galactose media (figure 5.5, 5.4b).

Fluorescence gating revealed that approximately all cells demonstrated R.6G-PMPC₂₅-PDPA₇₀ and DHE fluorescence greater than maximal basal fluorescence, at all concentrations studied, following 24 hours incubation with “polymersomes” or “tubes” (table 5.2). Both were delivered in a time and concentration dependent manner (figure 5.5a-d). While polymer accumulation from the tubular fraction is less than from “polymersomes”, both deliver an amount of DHE comparable to 0.1% DMSO. At higher concentrations, “polymersomes” deliver the highest DHE concentrations, followed by “tubes” and then DMSO, a trend seen in all cells tested. This is less clear at 10 μM DHE, and may be a result of the low fluorescent signal drawn from the non-optimal excitation of DHE. Both DHE and R.6G-PMPC-PDPA signal showed good linearity to concentration.

The DHE:R.6G-PMPC-PDPA ratio reveals that “tubes” deliver more DHE per unit polymer, likely a reflection of the higher DHE loading in these particles. Normalisation by the DHE load within nanoparticles (DHE:PMPC-PDPA ratio, figure 5.3) revealed “polymersomes” deliver slightly more DHE load once nanoparticle cargo load is accounted for. However it should be noted that DHE quantification accounts for its load within a polydisperse fraction of nanoparticles, and that the tubular fraction possesses a greater size distribution, possibly explaining this discrepancy. In all instances, the DHE:R.6G ratio declines with increasing

nanoparticle/DHE concentration, indicating either decreasing DHE delivery or a declining DHE signal.

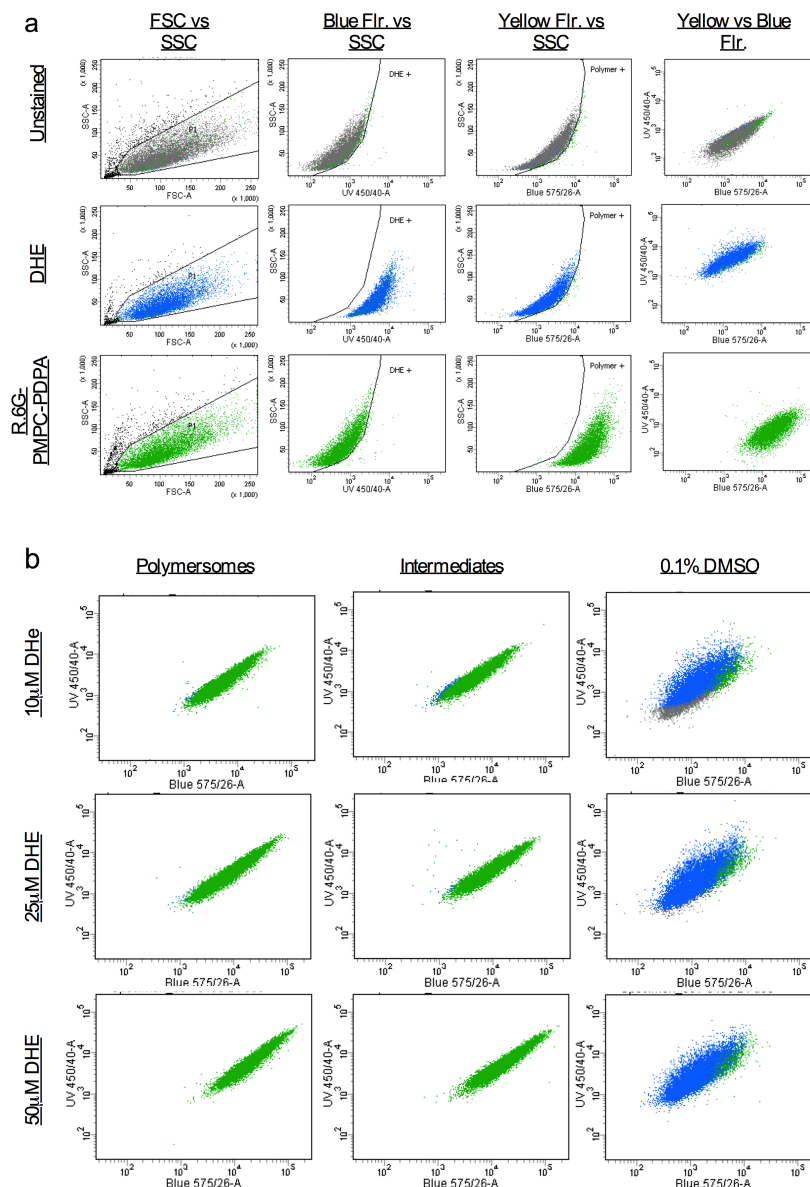


FIGURE 5.4: **Flow cytometry settings for DHE delivery experiments:** (a) DHE plus R.6G-PMPC-PDPA fluorescence (ex.355nm em.450nm and ex.488nm em.575nm respectively) was measured by flow cytometry (BD™ LSRII) following 72 hour incubation with galactose media alone (top), 50 μM DHE (middle), or 1mg/mL R.6G polymersomes (bottom). Gating for fibroblasts (left, grey), DHE positive cells (middle, blue), and R.6G positive cells (right, green) are indicated. DHE was excited by a (b) Dot plots from Ctrl1 fibroblasts following 24 hour incubation with 10, 25 and 50 μM DHE formulated in “polymersomes”, “intermediate structures” and 0.1% DMSO.

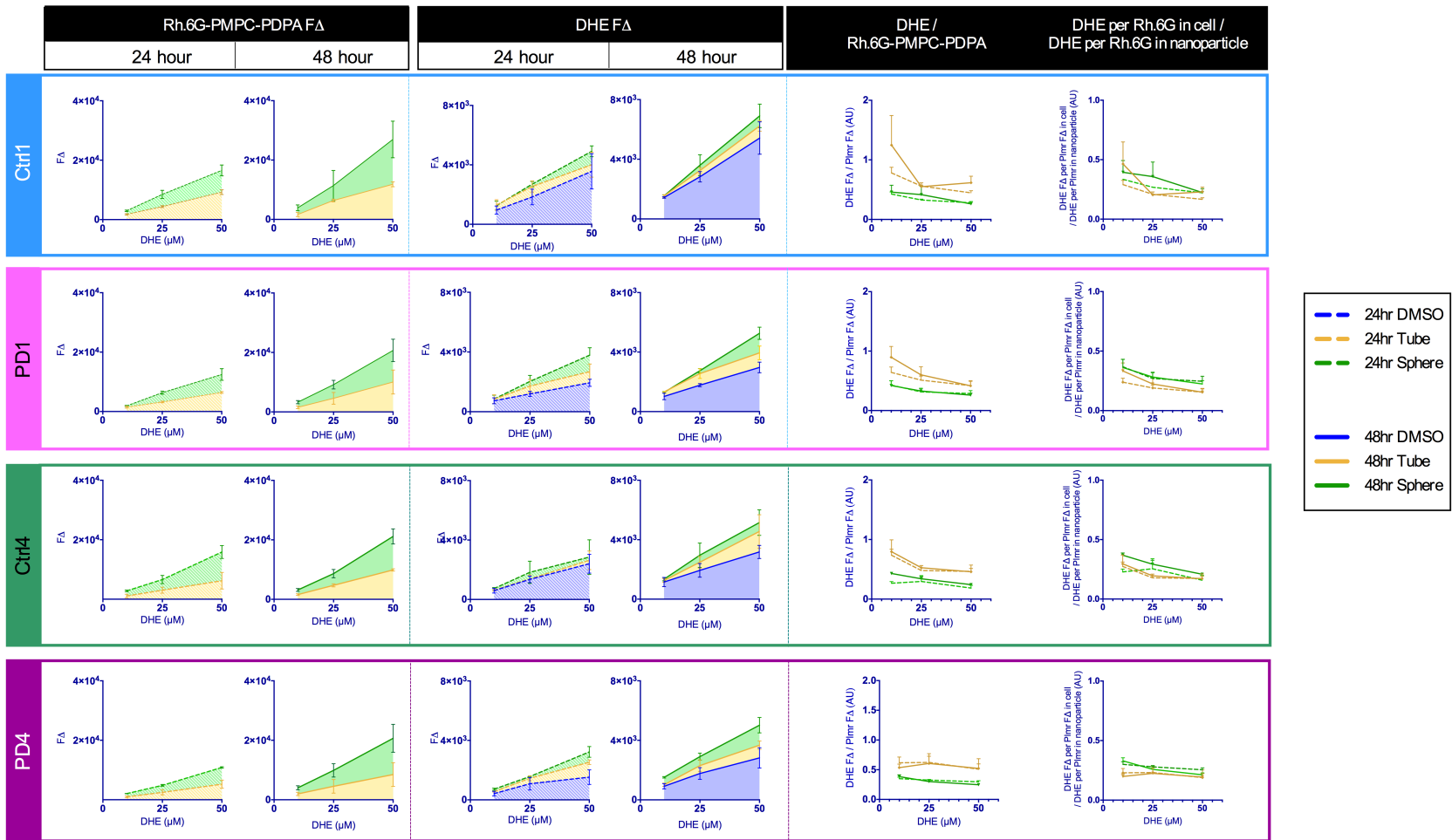


FIGURE 5.5: Delivery efficiency of polymersome formulated DHE to fibroblasts following 24 and 48 incubation: Fibroblasts were incubated for 24 and 48 hours with rhodamine labelled and DHE loaded “polymersomes” and “tubes” (figure 5.3a) in a galactose media. Background subtracted Rh.6G-PMPC₂₅–PDPA₇₀ and DHE fluorescence was assessed by flow cytometry. Graphs are arranged by fibroblasts in rows. From left to right, graphs represent; Rh.6G-PMPC₂₅–PDPA₇₀ fluorescence, DHE fluorescence, DHE fluorescence per Rh.6G-PMPC-PDA fluorescence (DHE:R.6G), and DHE:R.6G in fibroblasts divided by DHE:PMPC-PDPA in relevant nanoparticles (all error bars = SD).

PMPC-PDPA (mg/mL)		DHE (uM)	Ctrl 24hr	Ctrl 48hr	PD1 24hr	PD1 48hr	Ctrl4 24hr	Ctrl4 48hr	PD4 24hr	PD4 48hr
"Polymersomes"	R _h .6G F%	0	2.1	2.1	0.8	0.8	1.1	1.1	3.0	3.0
		0.198	96.9	98.5	98.1	99.1	88.4	92.4	82.7	88.1
		0.494	99.9	99.9	100.0	100.0	98.6	99.2	99.7	99.9
		0.988	100.0	100.0	100.0	100.0	100.0	99.9	100.0	99.9
		0	0	0.5	0.5	1.7	1.7	0.6	0.6	0.2
"Tubes"	R _h .6G F%	0	2.1	2.1	0.8	0.8	1.1	1.1	3.0	3.0
		0.085	92.4	83.4	95.9	89.6	90.2	80.3	82.2	78.4
		0.213	99.6	99.9	99.9	99.8	94.4	96.0	93.8	94.4
		0.427	100.0	100.0	100.0	100.0	97.8	99.1	99.6	99.7
		0	0	0.5	0.5	1.7	1.7	0.6	0.6	0.2
0.1% DMSO	DHE F%	0	0.5	0.5	1.7	1.7	0.6	0.6	0.2	0.2
		NA	80.8	97.0	94.1	99.2	88.8	92.4	83.8	80.6
		NA	98.5	98.7	99.8	100.0	95.6	99.8	97.7	95.5
		NA	99.4	100.0	99.1	100.0	99.5	99.9	98.7	99.7
		NA	0	0.5	0.5	1.7	1.7	0.6	0.6	0.2

TABLE 5.2: Percentage of cells demonstrating R.6G-PMPC-PDPA and DHE fluorescence greater than maximum endogenous levels, as assessed in untreated controls, following 24 or 48 hour incubation with DHE loaded PMPC₂₅–PDPA₆₅ nanoparticles. Blue indicates percentages greater than 90% (n = 3).

A separate batch of DHE loaded polymersomes (figure 5.3 b) was used to assess DHE delivery by “polymersomes” and “tubes” when PMPC₂₅–PDPA₆₅ concentrations were matched (figure 5.6). At matched polymer concentrations, “tubes” delivered a greater DHE load than “polymersomes”, again showing greater DHE delivery per unit R.6G-PMPC-PDPA in fibroblasts. While the accumulation of polymer is linear with concentration, DHE accumulation saturates at higher concentrations. This indicates either less DHE is delivered when there are more “intermediate” nanoparticles, or DHE signal is decreasing due to cell metabolism, efflux or quenching fluorescence signal.

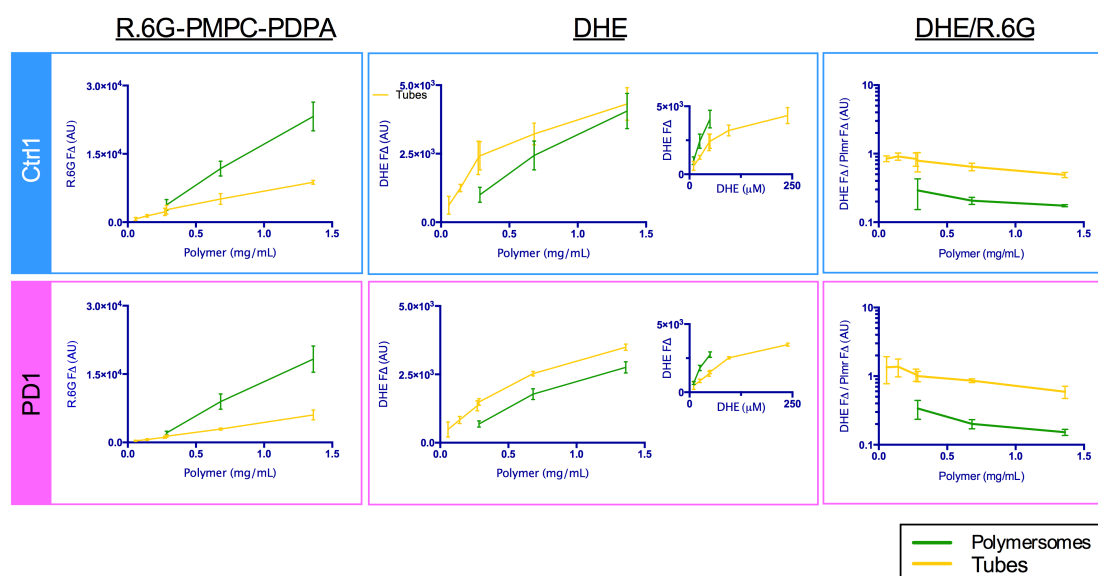


FIGURE 5.6: **Comparison of “Polymersome” and “Tubular” fractions efficiency in delivering DHE:** Healthy and *parkin* mutant fibroblasts were incubated with DHE loaded “polymersomes” and “tubes” (figure 5.3b) for 48 hours, at matched polymer and DHE concentrations. Fibroblasts were passed through a flow cytometer and median R.6G-PMPC-PDPA and DHE fluorescence per cell assessed. Graphs are arranged by fibroblast in rows. From left to right graphs show accumulation of R.6G-PMPC-PDPA with increasing polymer concentration, DHE accumulation with increasing polymer and DHE concentration, and R.6G-PMPC-PDPA:DHE ratios with increasing polymer concentration (n = 3 ; error bars = SD).

5.4.3 Discussion

UA and UCA loaded “polymersomes” and “tubes” elicited dose dependent increases in the intracellular ATP levels of *parkin* mutant fibroblasts. Their effect was comparable to 0.1% DMSO formulations. In keeping PMPC₂₅–PDPA₆₅ nanoparticles and 0.1% DMSO showed similar delivery efficiencies of DHE, a highly hydrophobic cholesterol analogue with strong structural similarities to UA and UCA. It is notable that the therapeutic responses detailed here, whilst similar in trend, are less potent than those previously reported [198], possibly a consequence of the late passages at which fibroblasts were used. Drug decomposition within nanoparticles is also a possibility given the long duration of formation, however DMSO formulated drugs were prepared fresh prior to the first experimental repeat. Increased incubation periods yielded both improved

therapeutic effect and increased delivery of hydrophobic cargoes in all three formulations. Similar increases in physiological action have previously been reported for UA with increased incubation periods [488].

Though both UA and UCA are known to activate at least one extracellular receptor, TGR5 [231, 232], the data here would suggest their therapeutic effects on intracellular ATP can still be elicited following direct intracellular delivery, though it is notable that DMSO consistently proved the most efficacious formulation. Future work investigating the effect of polymersome encapsulation on the discrete pleiotropic effects of UA and UCA would be of interest. This may also hold some therapeutic relevance, as certain side effects may be connected to activation of TGR5, gastrointestinal problems for instance [226, 282, 489].

PMPC₂₅–PDPA₆₅ nanoparticles did not show increased therapeutic effect over DMSO formulated drugs. Other work has demonstrated increased *in vitro* efficacy of compounds with typical dose responses when delivered by nanoparticles, something believed to result from the simultaneous delivery of many drug molecules, temporarily creating regions of high drug concentration within the cell [341, 366]. A pertinent example would be UA loaded mPEG-PCL polymersomes, which showed greatly enhanced apoptotic induction in a gastric cancer cell line over “free” UA, though it is of note the polymer itself evoked some alterations in cellular viability [447]. Comparisons with this study are difficult to make due to differences in cell type, UA concentrations, and the physiological effect studied. Perhaps of particular relevance, fibroblasts are known for slow internalisation of PMPC-PDPA nanoparticles relative to other cell types, so likely receive less therapeutic compound when delivered by these vectors [339, 341]. Cells which are known to endocytose nanoparticles more rapidly may demonstrate enhanced therapeutic effects compared with those seen here. Another study showed moderately decreased hydrophobic drug efficacy when formulated within polymersomes, which was speculated to result from reduced intracellular concentrations relative to free drug [490].

The DHE loaded PMPC₂₅–PDPA₆₅ nanoparticles used here possess similar sizes, morphologies and cargo loads to UA and UCA loaded nanoparticles used in experiments measuring ATP recovery (figures 5.1, 5.3). As DHE possesses a hydrophobicity, structure and size close to UCA and similar to UA, it may be considered a representative model for the delivery of high UA and UCA loads by “polymersome” and “tubes”. In all cells, DHE was delivered most effectively by “polymersomes”, then “tubes” and least effectively by 0.1% DMSO at matched DHE concentrations (figures 5.5, 5.6). The higher DHE delivery by nanoparticles may be a result of the non-fouling properties of PMPC-PDPA, wherein this formulation shields DHE from adsorption to the polystyrene wells in which the uptake assay was performed and serum proteins within the cell media [491]. In this regard it is notable that DHE formulated within DMSO shows increased accumulation within the cell with increased incubation periods. It must however also be noted that where DHE uptake assays were performed in 12 well plates, ATP assays were performed in 96 well plates, and that the differences in surface area may have affected the delivery efficiencies from all three formulations between the two assay sets, though perhaps DMSO formulations in particular.

Drug formulated within “polymersomes” and DMSO produced greater therapeutic effects than “tubes” following 24 hour incubation, though these were approximately equivalent by 48 hours. Where PMPC₂₅–PDPA₆₅ “polymersomes” enter cells with a single saturating exponent (figure 4.2) [341, 435] “tubular” particles have been shown to enter cells only after an appreciable dwelling time on the cell surface (figure 4.6) [435]. Following this, it is possible a significant proportion of the drug delivered to fibroblasts by “tubes” remains sequestered within nanoparticles bound to, but not yet internalised by the cell. Future experiments that distinguish between bound and internalised polymersomes/cargo would help resolve this point.

The ratio of DHE to R.6G-PMPC-PDPA delivered by DHE loaded nanoparticles was approximately the same between all fibroblasts studied, where “tubes” delivered more DHE per unit polymer than “polymersomes”. Though “tubes” entered fibroblasts less readily than “polymersomes”, the higher drug load in

the tubular fraction would require fewer particles to enter the cell to deliver an equivalent DHE load (figure 5.3). Indeed, at matched polymer concentrations, “intermediate particles” delivered more hydrophobic cargo than the more readily internalised “polymersomes”. Normalisation of the DHE delivered to the cell per unit R.6G-PMPC-PDPA, by the DHE load within the nanoparticles themselves demonstrated the latter can account for the much of the difference in delivery efficiency between the two particle morphologies. “Polymersomes” were slightly more effective in this, however this difference might be explained by the tendency of larger oblate particles to less readily enter fibroblasts [340, 435] (Chapter 4), and the greater size distribution seen in the “intermediate” fraction. Cholesterol like molecules have been shown stabilise and concentrate in larger PMPC₂₅–PDPA₆₅ assemblies during the TFR method of formation, so it is probable the DHE:Polymer ratio increases with particle size (Chapter 3). As particles of smaller size and lesser DHE loads are likely to enter fibroblasts more rapidly, normalisation of DHE delivery by DHE load will be most accurate where a nanoparticle size distribution is smaller, and DHE loads show less deviation from the populations average, as quantified by UV-HPLC.

At high concentrations, the DHE delivered by “intermediate” nanoparticles began to saturate, while delivery of R.6G-PMPC-PDPA remained linear (figure 5.6). Again it is unlikely that particles with greater DHE loads enter into fibroblasts more rapidly, as they concentrate within larger tubular particles (figure 5.3). Loss of DHE fluorescence by cellular metabolisation and/or excretion are possibilities, such as previously seen with polymersome mediated delivery of Rhodamine B to fibroblasts [404]. However DHE:R.6G ratios in fibroblasts were not greatly altered between 24 and 48 hours, which suggests this is not the case unless DHE delivery and processing remains constant over this duration (figure 5.5). The non-linearity of DHE fluorescence in the cell is another possibility. DHE fluorescence is auto-quenched at high concentrations and dilution within lipid or cell membranes is known to ameliorate this [492, 493]. DHE fluorescence emission is also known to under go a blue-shift on incorporation within lipid membranes [492]. Thus, saturation of DHE signal might occur due

to heightened quenching or altered emission spectra whilst concentrated and encapsulated within PMPC₂₅–PDPA₆₅ nanoparticles, compared to its relative dilution on cellular distribution. This assumes a greater proportion of bound but non-internalised particles are present at higher polymersome concentrations, for which there is evidence (Chapter 4; figure 4.6).

A representative model of UA and UCA delivery to fibroblasts at low concentrations within “polymersomes” and “tubes” was not investigated. Given the lower drug to polymer ratios present in this formulation, a greater number of particles must be internalised to deliver drug concentrations equivalent to nanoparticles with higher drug loads. It has been demonstrated that uptake of mixed populations of “polymersomes” and “tubes” is linear with concentration following 1 minute, 24 or 48 hour incubation up to 1 mg/mL in fibroblasts cultured in galactose media (figure 4.2). This suggests both that polymersome receptor occupancy is not saturated by PMPC₂₅–PDPA₆₅ nanoparticles below 1mg/mL, and that subsequent internalisation is linear to this. Though drug concentration was lower per particle, the increased particle number should lead to greater receptor occupancy and internalisation. Concordantly high and low drug loaded PMPC₂₅–PDPA₆₅ nanoparticles produced approximately equivalent therapeutic responses, though high loads were marginally more effective, suggesting a possible effect of increased drug concentration per particle.

The uptake of empty and drug loaded polymersomes was not compared here, though this may be of interest as there are lines of evidence that might suggest UA interacts with class B scavenger receptors and alter PKC activity which in turn affects endocytosis [477, 488, 494]. Further, alterations to PMPC-PDPA membrane properties by blending with steroid like components may alter their cellular interactions [436].

5.5 Conclusions

UA and UCA loaded “polymersomes” and “tubes” increase *parkin* mutant fibroblast ATP levels in a dose dependent manner comparable to DMSO formulations. Whilst the polymersome fraction enters fibroblasts more rapidly than the tubular fraction, and subsequently give faster therapeutic responses, the higher drug loads present in “intermediates” elicit similar therapeutic effects at matched drug concentrations following 48 hours incubation. At matched polymer concentrations below 2mg/mL, the tubular fraction deliver more hydrophobic compound to cell. This may be of particular interest, as ligand functionalised tubular particles are known to show enhanced targeting specificity *in vivo*.

Chapter 6

Discussion & future directions

6.1 Project findings

PMPC-PDPA nanoparticles formed by TFR were shown to produce a mixture of morphologies consisting of large planar structures, branched and high genus morphologies, elongated tubes and vesicles. The average size of these mixtures decreased over time with the continuing application of exogenous energy, suggesting the large lyotropic structures were metastable. However these metastable structures were also extremely long lived, failing to reach morphological uniformity after eight weeks of mechanical stirring and 30 minutes of sonication. This is likely the result of the exceptionally slow chain kinetics within the semi-fluid membranes of large MW block copolymer membranes [321, 410]. Particles were successfully separated on the basis of size and density by centrifugation, producing fractions enriched with vesicles, tubes and larger lyotropic aggregates. Quantification of their relative mass over time further demonstrated the progression from larger to smaller structures over time.

PMPC-PDPA nanoparticles were able to successfully encapsulate UA, UCA and UDCA with high efficiency, at low and high compound to copolymer ratios. The particles proved stable over time, with no marked alteration to size distribution, or apparent loss of encapsulated compound after six months. Fractionation and

quantification of these and cholesterol loaded nanoparticles revealed encapsulation of hydrophobic sterol like compounds altered the formation pathway of nanoparticles, apparently enhancing and/or stabilising the formation of the tubular fraction. Morphological analysis indicated cholesterol loaded particles, were of a larger average length, and more branched than unloaded particles. The presence of sterol like compounds within large copolymer bulks may act as plasticiser, easing their initial transition into genus and tubular structures. However their presence within the membrane may also act to increase the hydrophobic volume without concomitant increases in the hydrophilic brush of the nanoparticles, resulting in a modification to copolymer packing.

PMPC-PDPA nanoparticles of mixed morphologies were shown to enter into fibroblasts derived from patients possessing a form of PD caused by compound heterozygous mutations in *parkin*. These have been shown to possess defective mitochondrial function akin to that seen in patient neurons [95, 96], a factor believed to at least in part underly the disease pathogenesis [23, 71]. The nanoparticles were able to enter fibroblasts without detriment to MMP, cellular ATP levels or viability under conditions of heavy mitochondrial activity. This suggests PMPC-PDPA nanoparticles do not aggravate existing mitochondrial dysfunction, and could also potentially also be used in cells with more marked mitochondrial dependance, in particular neurons.

Nanoparticles entered into fibroblasts in a time- and concentration- dependent fashion. Mixed vesicular and tubular morphologies demonstrated long initial surface dwelling times, the magnitude of which correlated to their eventual internalisation kinetics, suggesting variation in nanoparticle uptake was related to receptor expression. A possible uptake deficiency in fibroblasts possessing homozygous mutations in *parkin's* second exon was also highlighted, and appeared to relate to receptor expression, in keeping with other research [469]. Uptake was also affected by the sugar substrate in which fibroblasts were cultured, a clear saturation in the uptake of spherical particles being seen in galactose, but not glucose media. Galactose media forces fibroblasts to utilise mitochondrial OXPHOS to a much greater degree [107]. However, the physiological

relevance of saturating uptake is difficult to interpret as galactose may alter gene expression and receptor signalling independently of its effect on mitochondrial activity [477]. Spherical particles also entered fibroblasts more rapidly than particle populations of mixed spherical and tubular morphology.

UA and UCA loaded PMPC-PDPA nanoparticles taken from the polymersome and tubular fraction demonstrated a therapeutic effect on *parkin* mutant fibroblasts, similar though marginally weaker than drug administered in a co-solvent, 0.1% DMSO. This suggested that the mode of action by which these compounds exert their mitochondrial effects was compatible with nanoparticle mediated delivery. Longer incubation with drug loaded nanoparticles or DMSO formulated compounds resulted in higher efficacy. Higher drug to copolymer ratio did not result in significantly improved therapeutic effect. Previous work has shown improved therapeutic effects are associated with delivering drugs to cells in large payloads relative to simple diffusion. The absence of this effect here may result either from the mode of drug action, or slower drug delivery to fibroblasts by nanoparticles.

Polymersome and tubular fractions of PMPC-PDPA nanoparticles loaded with a fluorescent cholesterol analogue successfully entered into fibroblasts along with their cargo. This was both time and concentration dependent. The tubular fraction accumulated on and in fibroblasts more slowly than polymersomes, but delivered a similar amount of cargo at cargo matched concentrations, by merit of their greater cargo loading efficiency. At polymer matched concentrations, the tubular fraction delivered greater cargo loads at lower concentrations, though this effect saturated toward higher concentrations, again likely due to their slower internalisation. Both sets of nanoparticles delivered a greater concentration of cargo to the cell than when the cargo was formulated in 0.1% DMSO. However a distinction between surface bound and truly internalised nanoparticles was not made, making it difficult to interpret how this relates to intracellular delivery and subsequent therapeutic effects.

6.2 Implications for the treatment of Parkinson's Disease

6.2.1 Therapeutic effect *in vitro*

Highly hydrophobic sterol-like compounds were successfully delivered to fibroblasts where they elicited therapeutic effects. UA and UCA's therapeutic effect on mitochondria thus seem to be elicited from a location accessible either from within the cell membrane or elsewhere in the cell. The precise sub-cellular location of these nanoparticles during internalisation was not investigated. Previous work has shown that purely spherical PMPC-PDPA enter into the endosome, where they rapidly disassemble permitting access to the rest of the cell [339, 392]. Elsewhere tubular particles have been shown to enter the cell apparently intact, at least initially suggesting a separate mechanism of internalisation. Both however appear compatible with the therapeutic effects of steroid like compounds. It is also interesting that the tubular fraction also produced similar therapeutic effects to polymersomes despite their slower entry. This was likely due to the higher drug loading efficiency seen in the tubes. However it is also notable that the polymersome fraction also possessed some particles of greater aspect ratio which may have had a negative impact on overall particle uptake.

Whilst an enhanced therapeutic effect was not seen when the drugs were delivered as encapsulated "packets", this may be due to do with the particularly slow internalisation of PMPC-PDPA polymersomes seen in fibroblasts, something which will likely have been enhanced by the presence of particles of higher aspect ratio, found in both the tubular and polymersome fractions [326]. This may not be true of other less dormant cell types such as BBB endothelia and neurons, where more rapid uptake of "drug packets" could yield enhanced efficacy. It is however notable that UA at least has been shown to induce toxicity at low μM concentrations in at least some cell types [258, 488, 495], possibly by merit of its cell membrane altering properties [260]. It is therefore possible

that delivery of large drug “packets” could enhance cellular toxicity at certain concentrations. Similarly, very hydrophobic bile acids demonstrate cellular toxicity, again possibly attributable to their membrane altering properties [496]. This may be of relevance for UCA given its very high hydrophobicity and structural likeness to these. UDCA has been shown not to alter membrane ordering [496], and is well tolerated *in vitro* up to 500 μM [209].

That PMPC-PDPA nanoparticle alone prove innocuous to the viability and mitochondrial function of PD fibroblasts derived directly from PD patients is promising. It is also promising for their therapeutic use in other diseases with a mitochondrially related pathology. As these cells are human and possess the same, or at least highly similar extent of ageing and genetic background found in the respective individual, these results are likely to be at least partially transferable. However fibroblasts are also a very different cell to those of the CNS and BBB. Further, studies here only tested viability over a relatively short time. Though previous work has indicated that PMPC-PDPA nanoparticles are well tolerated in human fibroblasts for up to a week [404], the effect a PD causing *parkin* mutant phenotype may have on this is unknown. It will also be essential to assess the long term toxicological profile of copolymer particles in neurons of the CNS prior to their potential therapeutic application here. In particular, though requiring both *in vitro* and *in vivo* studies, consideration should be given to the potential for microglial activation, the primary immune cells of the CNS. Though rarely addressed in brain delivery studies to date, microglial activation is associated with enhanced cell death, and indeed already implicated in the pathogenesis of many neurodegenerative diseases.

It is interesting that a deficiency in particle uptake may be present in certain *parkin* mutant phenotypes [469]. If this were tissue specific, it may be that PMPC-PDPA polymersomes show preferential entry to certain cells within this phenotype. It may also translate to decreased uptake in all cell types, from which extended circulation times *in vivo* could result.

6.2.2 Therapeutic effect *in vivo*

6.2.2.1 Potential of UA, UCA and UDCA in the treatment of Parkinson's Disease

UA, UCA and UDCA possess chemical characters which suggest they may be able to cross the BBB to some extent [267, 497]. However as highly hydrophobic compounds, they will also rapidly accumulate into many other non-polar environments, meaning the use of formulations that enhance their distribution to the brain are desirable. Further, strong accumulation into regions other than the brain would require increasing dosage to deliver therapeutically effective doses of these compounds to the brain, from which adverse systemic effects may result. Thus appropriate formulation may dictate whether UA, UCA and UDCA are viable for use in PD. Whilst the therapeutic use of UCA has received little attention, UA and UDCA have been extensively studied for use in a number of conditions and some information is known of their toxicological profiles as well as brain penetrance.

UA administered orally to mice has been shown to distribute to the brain in small amounts relative to other tissues, in particular the liver, colon and kidneys [271]. Neuroprotective actions have been ascribed to orally administered UA in murine models, though it is difficult to discern whether this is a result of systemic actions or brain delivery [216, 217, 279]. As a potential anti-cancer agent the safety and tolerability of intravenously administered, liposomally formulated UA was recently assessed in a phase I clinical study [282]. Whilst UA was generally well tolerated, the duration of its use was relatively short, and hepatotoxicity and diarrhoea were encountered in humans after single doses $\geq 74\text{mg/mL}$, with a maximum tolerable dose of 98mg/mL [281, 282]. As noted before, there is evidence of UA induced toxicity at low μM concentrations in some [258, 488, 495], though not all cell types [216, 498]. Research has also shown UA is an activator of the TGR5, an extracellular GPCR that in mice has been shown to

induce defecation, which could possibly underlie the occurrence of diarrhoea in patients [231, 232, 489].

UDCA, as an endogenously synthesised bile acid, is better tolerated in humans, showing no toxicity up to 500 μ M *in vitro* [209]. Oral formulations such as URDOX are known to accumulate well within the liver, and UDCA is currently approved by the FDA and MHRA for therapeutic use against primary biliary cirrhosis [209]. There are however certain safety concerns with its use at high and/or prolonged use including; increased incidence of colorectal cancer and hepatocellular carcinoma, liver failure, digestive tract varices, diarrhoea, and immune complications such as hepatitis and cholangitis [210, 283, 499]. These could result from the actions of UDCA, or its metabolites lithocholic acid and chenodeoxycholic acid, which UDCA is converted to by intestinal bacteria [209]. Both are more hydrophobic than UDCA and shows higher *in vitro* toxicity [200]. Lithocholic acid can also be reabsorbed into blood flow. They also, unlike UDCA, are TGR5 activators [230]. It is also notable that a fraction of UDCA is conjugated to glycine or taurine in the liver. This increases its solubility but limits its ability to permeate cell membranes and the BBB. True evidence of UDCA distribution to the brain in humans is presently lacking [272, 275]. Whilst there is evidence of distribution to the brain of rat models of stroke following intravenous administration [277, 278], BBB permeability is enhanced within this condition [500].

Formulations of UA, UCA and UDCA that both limit their accumulation within non-disease tissue, and increase their distribution to disease affected tissue could make the difference in their clinical viability. Encapsulation within a nanoparticle may have further benefits such as preventing extracellular-drug interactions, for instance with the TGR5 receptor, and limiting drug metabolism to toxic by-products as seen with UDCA. Drug loaded spherical and tubular PMPC-PDPA nanoparticles were able to successfully deliver hydrophobic cargo into cells, and produce a therapeutic effect in *parkin* mutant fibroblasts. However to elicit a therapeutic effect in PD, these must be able to deliver their cargo to the brain ISF or effected cells directly. By attaching ligands targeting

transcytotic receptors on the BBB to nanoparticles, improvements in brain delivery from intravenous administration have been reported [296, 343]. However these improvements are still relatively modest in light of high nanoparticle distribution elsewhere in the body. The use of particle designs may however be able to resolve this [330].

6.2.2.2 Potential of tubular nanoparticles to enhance drug distribution to the brain

Ligand functionalised nanoparticles have shown significantly enhanced targeting specificity when particle shape is elongated, both in static conditions [331] and within blood- or blood like- flow [324, 329]. Notably, intravenous injection of nano-rods functionalised with antibodies against the transferrin receptor distributed to the brain of mice more than seven times as effectively as functionalised nano-spheres [330]. Modelling studies have shown the increased surface area of these particles provides a greater contact area over which specific ligand-receptor interactions can be made with target cells resulting in enhanced binding avidity [323]. Elongated particles have also demonstrated a tendency for lateral drift within flow, resulting in the marginalisation of particles at the endothelial lining where they lie parallel, further enhancing their ability to interact with endothelial cells [323, 324]. At the same time, the shear stress exerted on particles of longer aspect ratios is greater in flow, helping to destabilise weak interactions. In keeping, intravenous administration of unfunctionalised, long copolymer filomicelles circulate within the blood for approximately ten times longer than any currently used spherical particle, an effect which scaled with particle length and improved with particle flexibility [322, 501]. Both the filomicelles and tubular PMPC-PDPA particles possess similar mean diameters, $\sim 60\text{nm}$ and $\sim 65\text{nm}$ respectively [322, 502]. Functionalisation of long filomicelles against endothelial receptors resulted in an enhancement to specific *in vivo* binding, similar to that seen with functionalised spheres [329]. Though the latter accumulated to greater extents within the endothelia, this is in

close keeping with the greater forces hydrodynamic flow exerts on longer particles, which itself is believed to at least in part underly there extended circulation times.

Thus, the creation and separation of tubular particles produced by TFR of PMPC-PDPA may be advantageous to the purposes of brain delivery. However, whilst tube like particles may show enhanced targeting specificity, they also enter cells less readily. Though greater interaction strengths between a particle and a cell favours internalisation [382, 388], increasing aspect ratios result in greater energetic cost to membrane wrapping [325, 326]. Subsequently, a variety of cells demonstrate reduced uptake of elongated particles [328, 387, 435]. Certain particle features may possibly be able to overcome this however. For instance, spherical particles of increasing size show reduced cellular internalisation [339, 340]. However, there is evidence that incorporating “patches” of a chemistry known to interact more strongly with the cell surface into the nanoparticle surface can overcome the effect of size, resulting in uptake kinetics independent of particle diameter [339, 340]. Careful design of particle shape, and target interaction strength could thus be tailored to optimise adherence and internalisation within a given endothelial surface.

Though many lengths of unbranched tubes were seen among TFR formed PMCP-PDPA nanoparticles, these were mixed among branched and high genus morphologies as well. Optimisation of both formation method and separation technique could help increase the prevalence and isolation of long or short single branched tubes. For instance, optimisation of copolymer film thickness and homogeneity prior TFR may improve the yield of tubes, as may pre-templating techniques. Recent work from the Battaglia lab has made use of density gradients to improve the resolution of separation by centrifugal fractionation and from which tubes of specific lengths can be more effectively isolated. In designing ligand functionalised tubular vectors to target the BBB endothelia, striking a balance between particle length, which is shown to decrease binding to endothelial surface, and strength of ligand receptor interaction, which enhances

tissue specific interactions, could be used to greatly improve targeting fidelity and limit off target accumulation [322, 329, 330].

The ability of cyclic molecules such as UA, UCA, UDCA and cholesterol to modulate membrane properties of copolymer self assemblies may be of future interest. They are relatively cheap and here were shown to increase the proportion of tubular, branched and high genus morphologies. Though their effects will undoubtedly vary with method of formation and copolymer used [436], the ability to modulate particle morphology may be of benefit to the production of therapeutically relevant particle morphologies.

As PMPC-PDPA polymersomes have recently been shown to target class B scavenger receptors, their therapeutic applications may be best suited to those tissues that express these in relatively high amounts, such as immune cells, adipocytes and a number of cancer cells [341]. Other copolymer chemistries may thus be more suitable to BBB targeting, POEGMA-PDPA polymersomes for instance possess a highly PEG'ylated surface chemistry known to circulate for long times and enter cells slowly [340, 356]. Further, POEGMA-PDPA polymersomes functionalised with ligands against the BBB transcytotic receptor LRP have also shown effective penetrance into the brain ISF from blood circulation [356, in preparation]. However, it is presently unknown if this chemistry will, like PMPC-PDPA, produce tubular assemblies from TFR. Both possess PDPA blocks, and it has been hypothesised that tubes result from the unique ordering of PMPC-PDPA within dry thin films. The presence of PDPA may be sufficient to exert a similar effect in POEGMA-PDPA films. It is still possible that tubular PMPC-PDPA assemblies may be more resistant to uptake than polymersomes, and that appropriate functionalisation of the particle surface may be able to displace PMPC-scavenger receptor interactions. However, use of a longer circulating copolymer chemistry would seem the more logical first step. Another option available to the delivery of hydrophobic compounds would be packaging them within solid worm like micelles, which can readily be achieved use particular ratios hydrophilic to hydrophobic block lengths in diblock copolymers [322, 329].

Packaging UA, UCA and UDCA within tubular nanoparticles functionalised against transcytotic receptors could both improve brain delivery and reduce off target effects and toxicity from intravenous administration, both by lowering the therapeutically effective dose, and limiting non-brain specific drug distribution. One alternate consideration would be to use a route of administration that avoids exposing the drugs to non-nervous tissue. For instance, some promising results for drug delivery to brain following an intra-nasal administration of wheat-germ agglutinin functionalised copolymer nanoparticles have been reported. Indeed there is evidence this strategy can yield therapeutic effects at the SN of a toxin induced rat models of PD [363–365]. Research in this area is still however relatively new and the relevance to other intra-nasal therapies in humans has previously been called into question [361, 362].

A mentionable advantage to packaging drugs within nanoparticles is their applicability to combination therapies. By packaging two or more compounds that have complimentary therapeutic effects within a targeted nanoparticle, their simultaneous delivery to a destination can be assured. The hollow nature of both polymersomes [358] and polymer tubes [435] allows them to encapsulate large soluble entities. If such nanoparticles possessed the ability to cross into the brain, therapeutic avenues would be opened for larger hydrophobic compounds such as CoQ10 [167] and more soluble compounds such as neurotrophic peptides [14].

Finally, though un-functionalised PMPC-PDPA nanoparticles loaded with UA, UCA or UDCA may not be directly applicable to PD, they may have applications in other diseases. UA for instance has proposed used against colorectal and skin cancer, diabetes, inflammation, forms of atherosclerosis, muscle wasting and oxidant injury in heart tissue [252, 280, 503–506]. Similarly bile acids and their derivatives are under investigation for therapeutic use in liver diseases, cancer, metabolic disorders, and extrahepatic inflammatory disorders [227]. Packaging these within PMPC-PDPA nanoparticles of particular size and shape may alter their distribution within the body and subsequently enhance and detriment particular tissue specific effects.

6.3 Conclusion

Mitochondrial dysfunction has been identified as a major common feature within the many forms of Parkinson's [23], as well as other neurodegenerative diseases [507]. Several mitochondrially related therapies have shown promising results in early clinical trials [160, 161], whilst others have fallen short despite promising pre-clinical results [160, 167]. One possible explanation for this is the limited ability of certain therapeutics to reach the the brain at effective concentrations, owing to barriers between the CNS and its external environment [267].

Ursolic acid, ursocholanic acid and ursodeoxycholic acid have all demonstrated positive effects on the mitochondrial function of cell's possessing deficient Parkin activity, a known cause of Parkinson's disease [198]. It is presently unknown whether these can produce disease modifying effects within Parkinson's sufferers. It is probable that, to elicit a therapeutic effect in Parkinson's, these compounds must exert their effects in those cells affected within the patient brain. It would follow that methods which enable, or improve, their ability to distribute here will enhance *in vivo* efficacy, as well as reduce dosage and off-target effects.

Aqueous nanoparticles self assembled from PMPC-PDPA and other PDPA based diblock copolymers are able to encapsulate hydrophobic, amphiphilic and soluble compounds and retain them until they are exposed to mildly acidic environments. Many morphologies are able to enter the cell using endocytic pathways and release their cargo therein, and enhanced therapeutic efficacies relative to other forms of drug delivery have been reported [339, 341, 435]. Nanoparticles functionalised with ligands against specific endothelial surfaces have been used to improve the tissue specific delivery of drugs, and elongated morphologies have recently been shown to enhance these effects. Targeting transcytosis mediating receptors of the blood brain barrier has shown increase brain penetration of such nanoparticles and their cargo.

Ursolic acid, ursocholanic and ursodeoxycholic acid loaded PMPC-PDPA nanoparticles formed by thin film rehydration possessed high loading efficiencies and produced a range of vesicular, tubular, branched and high genus morphologies. The tubular particles in particular would lend themselves well to ligand based targeting of the blood brain barrier. Morphologies were successfully separated using centrifugation, and were able to enter *parkin* mutant cells without adverse effects. Drug loaded nanoparticles successfully delivered hydrophobic cargos to *parkin* mutant cells and produced therapeutic effects. Given the high levels of customisation available to copolymer based nanoparticles, drug formulation within these presents an ideal platform from which drug specific drug distribution to the brain may be enabled or enhanced towards that of clinical relevance.

Unique formulations of pre-existing drugs are patentable. This, and the strong potential synthetic copolymers possess for large scale manufacture, would aid in drawing attention from the pharmaceutical industry towards otherwise unprofitable naturally occurring compounds which could aid in bringing such therapies to the clinic.

Bibliography

- [1] E. R. Dorsey, R. Constantinescu, J. P. Thompson, K. M. Biglan, R. G. Holloway, K. Kieburtz, F. J. Marshall, B. M. Ravina, G. Schifitto, A. Siderowf, and C. M. Tanner, "Projected number of people with Parkinson disease in the most populous nations, 2005 through 2030.," *Neurology*, vol. 68, pp. 384–6, Jan. 2007.
- [2] M. M. Hoehn and M. D. Yahr, "Parkinsonism: onset, progression and mortality.," *Neurology*, vol. 17, pp. 427–42, May 1967.
- [3] P. Riederer and S. Wuketich, "Time course of nigrostriatal degeneration in parkinson's disease. A detailed study of influential factors in human brain amine analysis.," *Journal of neural transmission (Vienna, Austria : 1996)*, vol. 38, pp. 277–301, Jan. 1976.
- [4] E. C. Hirsch, "Biochemistry of Parkinson's disease with special reference to the dopaminergic systems.," *Molecular neurobiology*, vol. 9, pp. 135–42, Jan. 1994.
- [5] H. Braak, U. Rüb, W. P. Gai, and K. Del Tredici, "Idiopathic Parkinson's disease: Possible routes by which vulnerable neuronal types may be subject to neuroinvasion by an unknown pathogen," *Journal of Neural Transmission*, vol. 110, pp. 517–536, May 2003.
- [6] J. E. Ahlskog, "Parkin and PINK1 parkinsonism may represent nigral mitochondrial cytopathies distinct from Lewy body Parkinson's disease.," *Parkinsonism & related disorders*, vol. 15, pp. 721–7, Dec. 2009.
- [7] I. McKeith, J. Mintzer, D. Aarsland, D. Burn, H. Chiu, J. Cohen-Mansfield, D. Dickson, B. Dubois, J. E. Duda, H. Feldman, S. Gauthier, G. Halliday, B. Lawlor, C. Lippa, O. L. Lopez, J. Carlos Machado, J. O'Brien, J. Playfer, and W. Reid, "Dementia with Lewy bodies," *Lancet Neurology*, vol. 3, pp. 19–28, Jan. 2004.
- [8] No Authors Listed, "Practice parameters: initial therapy of Parkinson's disease (summary statement). Report of the Quality Standards Subcommittee of the American Academy of Neurology.," *Neurology*, vol. 43, pp. 1296–1297, July 1993.
- [9] S. Tsouli and S. Konitsiotis, "How should we treat a patient with early Parkinson's disease?," *International journal of clinical practice*, vol. 64, pp. 1210–9, Aug. 2010.
- [10] S. Fahn, D. Oakes, I. Shoulson, K. Kieburtz, A. Rudolph, A. Lang, C. W. Olanow, C. Tanner, and K. Marek, "Levodopa and the progression of Parkinson's disease.," *The New England journal of medicine*, vol. 351, pp. 2498–508, Dec. 2004.

- [11] O. Lindvall and A. Björklund, "Cell therapy in Parkinson's disease.," *NeuroRx : the journal of the American Society for Experimental NeuroTherapeutics*, vol. 1, pp. 382–93, Oct. 2004.
- [12] P. Brundin, J.-Y. Li, J. L. Holton, O. Lindvall, and T. Revesz, "Research in motion: the enigma of Parkinson's disease pathology spread.," *Nature reviews. Neuroscience*, vol. 9, pp. 741–5, Oct. 2008.
- [13] E. Emmanouilidou, K. Melachroinou, T. Roumeliotis, S. D. Garbis, M. Ntzouni, L. H. Margaritis, L. Stefanis, and K. Vekrellis, "Cell-produced alpha-synuclein is secreted in a calcium-dependent manner by exosomes and impacts neuronal survival.," *The Journal of neuroscience : the official journal of the Society for Neuroscience*, vol. 30, pp. 6838–51, May 2010.
- [14] S. Ramaswamy and J. H. Kordower, "Are growth factors the answer?," *Parkinsonism & related disorders*, vol. 15 Suppl 3, pp. S176–80, Dec. 2009.
- [15] Y. Ai, W. Markesbery, Z. Zhang, R. Grondin, D. Elseberry, G. A. Gerhardt, and D. M. Gash, "Intrapatamenal infusion of GDNF in aged rhesus monkeys: distribution and dopaminergic effects.," *The Journal of comparative neurology*, vol. 461, pp. 250–61, June 2003.
- [16] N. K. Patel and S. S. Gill, "GDNF delivery for Parkinson's disease," *Acta Neurochirurgica, Supplementum*, vol. 97, pp. 135–154, Jan. 2007.
- [17] A. Whone, S. Gill, N. Barua, D. Cronin, S. Mani, L. Mooney, E. Mohr, M. Luz, L. Barclay, E. Coulthard, A. Lawrence, and G. Johnson, "A Placebo-Controlled, Randomised, Double-Blind Trial to Assess the Safety and Efficacy of Intermittent Bilateral Intraputamenal Glial Cell Line-Derived Neurotrophic Factor (GDNF) Infusions Administered via Convection Enhanced Delivery (CED) in Subjects with," *EU Clinical Trials Register*, 2012.
- [18] F. P. Manfredsson and R. J. Mandel, "Development of gene therapy for neurological disorders.," *Discovery medicine*, vol. 9, pp. 204–11, Mar. 2010.
- [19] R. T. Bartus, M. S. Weinberg, and R. J. Samulski, "Parkinson's disease gene therapy: success by design meets failure by efficacy.," *Molecular therapy : the journal of the American Society of Gene Therapy*, vol. 22, pp. 487–97, Mar. 2014.
- [20] P. J. Mulcahy, K. Iremonger, E. Karyka, S. Herranz-Martín, K.-T. Shum, J. K. V. Tam, and M. Azzouz, "Gene therapy: a promising approach to treating spinal muscular atrophy.," *Human gene therapy*, vol. 25, pp. 575–86, July 2014.
- [21] S. Palfi, J. M. Gurruchaga, G. Scott Ralph, H. Lepetit, S. Lavisse, P. C. Buttery, C. Watts, J. Miskin, M. Kelleher, S. Deeley, H. Iwamuro, J. P. Lefaucheur, C. Thiriez, G. Fenelon, C. Lucas, P. Brugières, I. Gabriel, K. Abhay, X. Drouot, N. Tani, A. Kas, B. Ghaleh, P. Le Corvoisier, P. Dolphin, D. P. Breen, S. Mason, N. V. Guzman, N. D. Mazarakis, P. A. Radcliffe, R. Harrop, S. M. Kingsman, O. Rascol, S. Naylor, R. A. Barker, P. Hantraye, P. Remy, P. Cesaro, and K. A. Mitrophanous, "Long-term safety and tolerability of ProSavin, a lentiviral vector-based gene therapy for Parkinson's disease: A dose escalation, open-label, phase 1/2 trial," *The Lancet*, vol. 383, pp. 1138–1146, Mar. 2014.

- [22] I. Martin, V. L. Dawson, and T. M. Dawson, "Recent advances in the genetics of Parkinson's disease.," *Annual review of genomics and human genetics*, vol. 12, pp. 301–325, June 2011.
- [23] N. Exner, A. K. Lutz, C. Haass, and K. F. Winklhofer, "Mitochondrial dysfunction in Parkinson's disease: molecular mechanisms and pathophysiological consequences," *The EMBO Journal*, vol. 31, pp. 3038–3062, July 2012.
- [24] D. C. Wallace, "A mitochondrial paradigm of metabolic and degenerative diseases, aging, and cancer: a dawn for evolutionary medicine.," *Annual review of genetics*, vol. 39, pp. 359–407, Jan. 2005.
- [25] H. Chen and D. C. Chan, "Mitochondrial dynamics-fusion, fission, movement, and mitophagy-in neurodegenerative diseases," *Human Molecular Genetics*, vol. 18, pp. R169–76, Oct. 2009.
- [26] J. Bereiter-Hahn and M. Vöth, "Dynamics of mitochondria in living cells: shape changes, dislocations, fusion, and fission of mitochondria.," *Microscopy research and technique*, vol. 27, pp. 198–219, Mar. 1994.
- [27] A. G. M. Tielens, C. Rotte, J. J. Van Hellemond, and W. Martin, "Mitochondria as we don't know them," *Trends in Biochemical Sciences*, vol. 27, pp. 564–572, Nov. 2002.
- [28] B. B. Lowell and B. M. Spiegelman, "Towards a molecular understanding of adaptive thermogenesis.," *Nature*, vol. 404, pp. 652–660, Apr. 2000.
- [29] P. F. Chinnery, D. C. Samuels, J. Elson, and D. M. Turnbull, "Accumulation of mitochondrial DNA mutations in ageing, cancer, and mitochondrial disease: Is there a common mechanism?," *Lancet*, vol. 360, pp. 1323–1325, Oct. 2002.
- [30] C. Richter, V. Gogvadze, R. Laffranchi, R. Schlapbach, M. Schweizer, M. Suter, P. Walter, and M. Yaffee, "Oxidants in mitochondria: from physiology to diseases.," *Biochimica et biophysica acta*, vol. 1271, pp. 67–74, May 1995.
- [31] P. Smits, S. Mattijssen, E. Morava, M. van den Brand, F. van den Brandt, F. Wijburg, G. Pruijn, J. Smeitink, L. Nijtmans, R. Rodenburg, and L. van den Heuvel, "Functional consequences of mitochondrial tRNA Trp and tRNA Arg mutations causing combined OXPHOS defects.," *European journal of human genetics : EJHG*, vol. 18, pp. 324–329, Mar. 2010.
- [32] E. Cadenas and A. Boveris, "Mitochondrial Free Radical Production , Antioxidant Defenses and Cell Signaling," *Environmental Chemistry*, vol. 2, pp. 219–234, Jan. 2005.
- [33] R. J. Mailloux and M. E. Harper, "Mitochondrial proticity and ROS signaling: Lessons from the uncoupling proteins," *Trends in Endocrinology and Metabolism*, vol. 23, pp. 451–458, Sept. 2012.
- [34] R. J. Mailloux and M.-E. Harper, "Uncoupling proteins and the control of mitochondrial reactive oxygen species production.," *Free radical biology & medicine*, vol. 51, pp. 1106–1115, Sept. 2011.

- [35] I. Shabalina and J. Nedergaard, "Mitochondrial (mild) uncoupling and ROS production: physiologically relevant or not?," *Biochemical Society Transactions*, vol. 39, pp. 1305–1309, Oct. 2011.
- [36] D. E. Clapham, "Calcium Signaling," *Cell*, vol. 131, pp. 1047–1058, Dec. 2007.
- [37] C. Franzini-Armstrong, "ER-mitochondria communication. How privileged?," *Physiology (Bethesda, Md.)*, vol. 22, pp. 261–268, Aug. 2007.
- [38] F. M. Lasorsa, P. Pinton, L. Palmieri, G. Fiermonte, R. Rizzuto, and F. Palmieri, "Recombinant expression of the Ca(2+)-sensitive aspartate/glutamate carrier increases mitochondrial ATP production in agonist-stimulated Chinese hamster ovary cells.," *The Journal of biological chemistry*, vol. 278, pp. 38686–38692, Oct. 2003.
- [39] N. Demaurex and C. Distelhorst, "Cell biology. Apoptosis—the calcium connection.," *Science (New York, N.Y.)*, vol. 300, pp. 65–67, Apr. 2003.
- [40] M. R. Duchen, "Contributions of mitochondria to animal physiology: from homeostatic sensor to calcium signalling and cell death.," *The Journal of physiology*, vol. 516, pp. 1–17, Apr. 1999.
- [41] D. Spierings, G. McStay, M. Saleh, C. Bender, J. Chipuk, U. Maurer, and D. R. Green, "Connected to death: the (unexpurgated) mitochondrial pathway of apoptosis.," *Science (New York, N.Y.)*, vol. 310, pp. 66–67, Oct. 2005.
- [42] J. C. Martinou and R. J. Youle, "Mitochondria in Apoptosis: Bcl-2 Family Members and Mitochondrial Dynamics," *Developmental Cell*, vol. 21, pp. 92–101, July 2011.
- [43] S. M. Kilbride and J. H. M. Prehn, "Central roles of apoptotic proteins in mitochondrial function," *Oncogene*, vol. 32, pp. 2703–11, May 2012.
- [44] G. Twig, B. Hyde, and O. S. Shirihai, "Mitochondrial fusion, fission and autophagy as a quality control axis: The bioenergetic view," *Biochimica et Biophysica Acta - Bioenergetics*, vol. 1777, pp. 1092–1097, Sept. 2008.
- [45] D. Safiulina and A. Kaasik, "Energetic and Dynamic: How Mitochondria Meet Neuronal Energy Demands," *PLoS Biology*, vol. 11, p. e1001755, Dec. 2013.
- [46] G. Ashrafi and T. L. Schwarz, "The pathways of mitophagy for quality control and clearance of mitochondria," *Cell Death and Differentiation*, vol. 20, pp. 31–42, Jan. 2012.
- [47] M. B. Hock and A. Kralli, "Transcriptional control of mitochondrial biogenesis and function.," *Annual review of physiology*, vol. 71, pp. 177–203, Jan. 2009.
- [48] J. A. Calvo, T. G. Daniels, X. Wang, A. Paul, J. Lin, B. M. Spiegelman, S. C. Stevenson, and S. M. Rangwala, "Muscle-specific expression of PPARgamma coactivator-1alpha improves exercise performance and increases peak oxygen uptake.," *Journal of applied physiology (Bethesda, Md. : 1985)*, vol. 104, pp. 1304–1312, May 2008.

- [49] C. J. Lelliott, G. Medina-Gomez, N. Petrovic, A. Kis, H. M. Feldmann, M. Bjursell, N. Parker, K. Curtis, M. Campbell, P. Hu, D. Zhang, S. E. Litwin, V. G. Zaha, K. T. Fountain, S. Boudina, M. Jimenez-Linan, M. Blount, M. Lopez, A. Meirhaeghe, M. Bohlooly-Y, L. Storlien, M. Strömstedt, M. Snaith, M. Orešič, E. D. Abel, B. Cannon, and A. Vidal-Puig, "Ablation of PGC-1 β results in defective mitochondrial activity, thermogenesis, hepatic function, and cardiac performance," *PLoS Biology*, vol. 4, pp. 2042–2056, Nov. 2006.
- [50] R. C. Scarpulla, "Nuclear control of respiratory chain expression by nuclear respiratory factors and PGC-1-related coactivator," *Annals of the New York Academy of Sciences*, vol. 1147, pp. 321–334, Dec. 2008.
- [51] V. K. Mootha, C. Handschin, D. Arlow, X. Xie, J. St Pierre, S. Sihag, W. Yang, D. Altshuler, P. Puigserver, N. Patterson, P. J. Willy, I. G. Schulman, R. A. Heyman, E. S. Lander, and B. M. Spiegelman, "Erralpha and Gabpa/b specify PGC-1alpha-dependent oxidative phosphorylation gene expression that is altered in diabetic muscle.," *Proceedings of the National Academy of Sciences of the United States of America*, vol. 101, pp. 6570–6575, Apr. 2004.
- [52] Y. Zhang, G. Uguccioni, V. Ljubcic, I. Irrcher, S. Iqbal, K. Singh, S. Ding, and D. a. Hood, "Multiple signaling pathways regulate contractile activity-mediated PGC-1 α gene expression and activity in skeletal muscle cells.," *Physiological reports*, vol. 2, pp. 1–12, May 2014.
- [53] S. Anderson, A. T. Bankier, B. G. Barrell, M. H. de Bruijn, A. R. Coulson, J. Drouin, I. C. Eperon, D. P. Nierlich, B. A. Roe, F. Sanger, P. H. Schreier, A. J. Smith, R. Staden, and I. G. Young, "Sequence and organization of the human mitochondrial genome.," *Nature*, vol. 290, pp. 457–465, Apr. 1981.
- [54] R. M. Andrews, I. Kubacka, P. F. Chinnery, R. N. Lightowlers, D. M. Turnbull, and N. Howell, "Reanalysis and revision of the Cambridge reference sequence for human mitochondrial DNA.," *Nature genetics*, vol. 23, p. 147, Oct. 1999.
- [55] O. Schmidt, N. Pfanner, and C. Meisinger, "Mitochondrial protein import: from proteomics to functional mechanisms.," *Nature reviews. Molecular cell biology*, vol. 11, pp. 655–667, Sept. 2010.
- [56] J. W. Langston, P. Ballard, J. W. Tetrud, and I. Irwin, "Chronic Parkinsonism in humans due to a product of meperidine-analog synthesis.," *Science (New York, N.Y.)*, vol. 219, pp. 979–980, Feb. 1983.
- [57] W. J. Nicklas, I. Vyas, and R. E. Heikkila, "Inhibition of NADH-linked oxidation in brain mitochondria by 1-methyl-4-phenyl-pyridine, a metabolite of the neurotoxin, 1-methyl-4-phenyl-1,2,5,6-tetrahydropyridine," *Life Sciences*, vol. 36, pp. 2503–2508, July 1985.
- [58] A. Schapira, J. Cooper, D. Dexter, J. Clark, P. Jenner, and C. Marsden, "Mitochondrial Complex I Deficiency in Parkinsons-Disease," *Lancet*, vol. 1, no. 8649, p. 1269, 1990.
- [59] W. D. Parker, J. K. Parks, and R. H. Swerdlow, "Complex I deficiency in Parkinson's disease frontal cortex," *Brain Research*, vol. 1189, pp. 215–218, Jan. 2008.

- [60] P. M. Keeney, J. Xie, R. A. Capaldi, and J. P. Bennett, "Parkinson's disease brain mitochondrial complex I has oxidatively damaged subunits and is functionally impaired and misassembled.," *The Journal of neuroscience : the official journal of the Society for Neuroscience*, vol. 26, pp. 5256–5264, May 2006.
- [61] A. Priyadarshi, S. A. Khuder, E. A. Schaub, and S. S. Priyadarshi, "Environmental risk factors and Parkinson's disease: a metaanalysis.," *Environmental research*, vol. 86, pp. 122–127, June 2001.
- [62] A. Lannuzel, G. U. Höglinger, P. Champy, P. P. Michel, E. C. Hirsch, and M. Ruberg, "Is atypical parkinsonism in the Caribbean caused by the consumption of Annonaceae?," *Journal of neural transmission. Supplementum*, pp. 153–157, Jan. 2006.
- [63] A. H. Schapira, "Mitochondria in the aetiology and pathogenesis of Parkinson's disease," *The Lancet Neurology*, vol. 7, pp. 97–109, Jan. 2008.
- [64] G. Ambrosi, C. Ghezzi, S. Sepe, C. Milanese, C. Payan-Gomez, C. R. Bombardieri, M. T. Armentero, R. Zangaglia, C. Pacchetti, P. G. Mastroberardino, and F. Blandini, "Bioenergetic and proteolytic defects in fibroblasts from patients with sporadic Parkinson's disease," *Biochimica et Biophysica Acta - Molecular Basis of Disease*, vol. 1842, pp. 1385–1394, May 2014.
- [65] C. B. Park and N.-G. Larsson, "Mitochondrial DNA mutations in disease and aging.," *The Journal of cell biology*, vol. 193, pp. 809–818, May 2011.
- [66] D. Orsucci, E. Caldarazzo Ienco, M. Mancuso, and G. Siciliano, "POLG1-related and other "mitochondrial parkinsonisms": An overview," *Journal of Molecular Neuroscience*, vol. 44, pp. 17–24, May 2011.
- [67] S. D. Ryan, N. Dolatabadi, S. F. Chan, X. Zhang, M. W. Akhtar, J. Parker, F. Soldner, C. R. Sunico, S. Nagar, M. Talantova, B. Lee, K. Lopez, A. Nutter, B. Shan, E. Molokanova, Y. Zhang, X. Han, T. Nakamura, E. Masliah, J. R. Yates, N. Nakanishi, A. Y. Andreyev, S. Okamoto, R. Jaenisch, R. Ambasudhan, and S. A. Lipton, "Isogenic Human iPSC Parkinson's Model Shows Nitrosative Stress-Induced Dysfunction in MEF2-PGC1 a Transcription," *Cell*, vol. 155, pp. 1351–64, Dec. 2013.
- [68] A. Bender, K. J. Krishnan, C. M. Morris, G. a. Taylor, A. K. Reeve, R. H. Perry, E. Jaros, J. S. Hersheson, J. Betts, T. Klopstock, R. W. Taylor, and D. M. Turnbull, "High levels of mitochondrial DNA deletions in substantia nigra neurons in aging and Parkinson disease.," *Nature genetics*, vol. 38, pp. 515–517, May 2006.
- [69] Y. Kraytsberg, E. Kudryavtseva, A. C. McKee, C. Geula, N. W. Kowall, and K. Khrapko, "Mitochondrial DNA deletions are abundant and cause functional impairment in aged human substantia nigra neurons.," *Nature genetics*, vol. 38, pp. 518–520, May 2006.
- [70] D. G. Nicholls and S. L. Budd, "Mitochondria and neuronal survival.," *Physiological reviews*, vol. 80, pp. 315–360, Jan. 2000.
- [71] C. Perier and M. Vila, "Mitochondrial biology and Parkinson's disease," *Cold Spring Harbor Perspectives in Medicine*, vol. 2, p. a009332, Feb. 2013.

- [72] E. K. Pissadaki and J. P. Bolam, "The energy cost of action potential propagation in dopamine neurons: clues to susceptibility in Parkinson's disease.," *Frontiers in computational neuroscience*, vol. 7, p. 13, Jan. 2013.
- [73] A. Cheng, R. Wan, J.-L. Yang, N. Kamimura, T. G. Son, X. Ouyang, Y. Luo, E. Okun, and M. P. Mattson, "Involvement of PGC-1 α in the formation and maintenance of neuronal dendritic spines.," *Nature communications*, vol. 3, p. 1250, Jan. 2012.
- [74] N. C. Harris, C. Webb, and S. A. Greenfield, "A possible pacemaker mechanism in pars compacta neurons of the guinea-pig substantia nigra revealed by various ion channel blocking agents.," *Neuroscience*, vol. 31, pp. 355–362, Jan. 1989.
- [75] M. Puopolo, E. Raviola, and B. P. Bean, "Roles of subthreshold calcium current and sodium current in spontaneous firing of mouse midbrain dopamine neurons.," *The Journal of neuroscience : the official journal of the Society for Neuroscience*, vol. 27, pp. 645–656, Jan. 2007.
- [76] P. S. Brookes, Y. Yoon, J. L. Robotham, M. W. Anders, and S.-S. Sheu, "Calcium, ATP, and ROS: a mitochondrial love-hate triangle.," *American journal of physiology. Cell physiology*, vol. 287, pp. C817–C833, Oct. 2004.
- [77] C. S. Chan, J. N. Guzman, E. Ilijic, J. N. Mercer, C. Rick, T. Tkatch, G. E. Meredith, and D. J. Surmeier, "'Rejuvenation' protects neurons in mouse models of Parkinson's disease.," *Nature*, vol. 447, pp. 1081–1086, June 2007.
- [78] J. N. Guzman, J. Sanchez-Padilla, D. Wokosin, J. Kondapalli, E. Ilijic, P. T. Schumacker, and D. J. Surmeier, "Oxidant stress evoked by pacemaking in dopaminergic neurons is attenuated by DJ-1.," *Nature*, vol. 468, pp. 696–700, Nov. 2010.
- [79] J. Meiser, D. Weindl, and K. Hiller, "Complexity of dopamine metabolism.," *Cell communication and signaling : CCS*, vol. 11, p. 34, Jan. 2013.
- [80] W. M. Caudle, J. R. Richardson, M. Z. Wang, T. N. Taylor, T. S. Guillot, A. L. McCormack, R. E. Colebrooke, D. A. Di Monte, P. C. Emson, and G. W. Miller, "Reduced vesicular storage of dopamine causes progressive nigrostriatal neurodegeneration.," *The Journal of neuroscience : the official journal of the Society for Neuroscience*, vol. 27, pp. 8138–8148, July 2007.
- [81] S. S. Park, E. M. Schulz, and D. Lee, "Disruption of dopamine homeostasis underlies selective neurodegeneration mediated by α -synuclein," *European Journal of Neuroscience*, vol. 26, pp. 3104–3112, Dec. 2007.
- [82] W.-S. Choi, R. D. Palmiter, and Z. Xia, "Loss of mitochondrial complex I activity potentiates dopamine neuron death induced by microtubule dysfunction in a Parkinson's disease model.," *The Journal of cell biology*, vol. 192, pp. 873–882, Mar. 2011.
- [83] F. H. Sterky, A. F. Hoffman, D. Milenkovic, B. Bao, A. Paganelli, D. Edgar, R. Wibom, C. R. Lupica, L. Olson, and N. G. Larsson, "Altered dopamine metabolism and increased vulnerability to MPTP in mice with partial deficiency of mitochondrial complex I in dopamine neurons," *Human Molecular Genetics*, vol. 21, pp. 1078–1089, Mar. 2012.

- [84] E. M. Valente, P. M. Abou-Sleiman, V. Caputo, M. M. K. Muqit, K. Harvey, S. Gispert, Z. Ali, D. Del Turco, A. R. Bentivoglio, D. G. Healy, A. Albanese, R. Nussbaum, R. González-Maldonado, T. Deller, S. Salvi, P. Cortelli, W. P. Gilks, D. S. Latchman, R. J. Harvey, B. Dallapiccola, G. Auburger, and N. W. Wood, "Hereditary early-onset Parkinson's disease caused by mutations in PINK1.," *Science (New York, N.Y.)*, vol. 304, pp. 1158–1160, May 2004.
- [85] C. A. Gautier, T. Kitada, and J. Shen, "Loss of PINK1 causes mitochondrial functional defects and increased sensitivity to oxidative stress.," *Proceedings of the National Academy of Sciences of the United States of America*, vol. 105, pp. 11364–11369, Aug. 2008.
- [86] A. Rakovic, A. Grünewald, P. Seibler, A. Ramirez, N. Kock, S. Orolicki, K. Lohmann, and C. Klein, "Effect of endogenous mutant and wild-type PINK1 on Parkin in fibroblasts from Parkinson disease patients," *Human Molecular Genetics*, vol. 19, pp. 3124–3137, Aug. 2010.
- [87] A. W. Greene, K. Grenier, M. A. Aguilera, S. Muise, R. Farazifard, M. E. Haque, H. M. McBride, D. S. Park, and E. A. Fon, "Mitochondrial processing peptidase regulates PINK1 processing, import and Parkin recruitment," *EMBO reports*, vol. 13, pp. 378–385, Apr. 2012.
- [88] N. Matsuda, S. Sato, K. Shiba, K. Okatsu, K. Saisho, C. A. Gautier, Y. S. Sou, S. Saiki, S. Kawajiri, F. Sato, M. Kimura, M. Komatsu, N. Hattori, and K. Tanaka, "PINK1 stabilized by mitochondrial depolarization recruits Parkin to damaged mitochondria and activates latent Parkin for mitophagy," *Journal of Cell Biology*, vol. 189, pp. 211–221, Apr. 2010.
- [89] C. Meissner, H. Lorenz, A. Weihofen, D. J. Selkoe, and M. K. Lemberg, "The mitochondrial intramembrane protease PARL cleaves human Pink1 to regulate Pink1 trafficking," *Journal of Neurochemistry*, vol. 117, pp. 856–867, July 2011.
- [90] M. E. Haque, M. P. Mount, F. Safarpour, E. Abdel-Messih, S. Callaghan, C. Maze-rolle, T. Kitada, R. S. Slack, V. Wallace, J. Shen, H. Anisman, and D. S. Park, "Inactivation of Pink1 gene in Vivo sensitizes dopamine-producing neurons to 1-methyl-4-phenyl-1,2,3,6-tetrahydropyridine (MPTP) and can be rescued by autosomal recessive Parkinson disease genes, Parkin or DJ-1," *Journal of Biological Chemistry*, vol. 287, pp. 23162–23170, July 2012.
- [91] V. S. Burchell, D. E. Nelson, A. Sanchez-Martinez, M. Delgado-Camprubi, R. M. Ivatt, J. H. Pogson, S. J. Randle, S. Wray, P. A. Lewis, H. Houlden, A. Y. Abramov, J. Hardy, N. W. Wood, A. J. Whitworth, H. Laman, and H. Plun-Favreau, "The Parkinson's disease-linked proteins Fbxo7 and Parkin interact to mediate mitophagy.," *Nature neuroscience*, vol. 16, pp. 1257–65, Sept. 2013.
- [92] T. Kitada, S. Asakawa, N. Hattori, H. Matsumine, Y. Yamamura, S. Minoshima, M. Yokochi, Y. Mizuno, and N. Shimizu, "Mutations in the parkin gene cause autosomal recessive juvenile parkinsonism.," *Nature*, vol. 392, pp. 605–8, Apr. 1998.
- [93] V. Bonifati, P. Rizzu, M. J. van Baren, O. Schaap, G. J. Breedveld, E. Krieger, M. C. J. Dekker, F. Squitieri, P. Ibanez, M. Joosse, J. W. van Dongen, N. Vanacore, J. C. van Swieten, A. Brice, G. Meo, C. M. van Duijn, B. A. Oostra, and

- P. Heutink, "Mutations in the DJ-1 gene associated with autosomal recessive early-onset parkinsonism.," *Science (New York, N.Y.)*, vol. 299, pp. 256–259, Jan. 2003.
- [94] A. Di Fonzo, M. C. J. Dekker, P. Montagna, A. Baruzzi, E. H. Yonova, L. Correia Guedes, A. Szczerbinska, T. Zhao, L. O. M. Dubbel-Hulsman, C. H. Wouters, E. de Graaff, W. J. G. Oyen, E. J. Simons, G. J. Breedveld, B. A. Oostra, M. W. Horstink, and V. Bonifati, "FBXO7 mutations cause autosomal recessive, early-onset parkinsonian-pyramidal syndrome.," *Neurology*, vol. 72, pp. 240–245, Jan. 2009.
- [95] H. Mortiboys, K. J. Thomas, W. J. H. Koopman, S. Klaffke, P. Abou-Sleiman, S. Olpin, N. W. Wood, P. H. G. M. Willems, J. A. M. Smeitink, M. R. Cookson, and O. Bandmann, "Mitochondrial function and morphology are impaired in parkin-mutant fibroblasts.," *Annals of neurology*, vol. 64, pp. 555–65, Nov. 2008.
- [96] A. Grünewald, L. Voges, A. Rakovic, M. Kasten, H. Vandebona, C. Hemmelmann, K. Lohmann, S. Orolicki, A. Ramirez, A. H. V. Schapira, P. P. Pramstaller, C. M. Sue, and C. Klein, "Mutant parkin impairs mitochondrial function and morphology in human fibroblasts," *PLoS ONE*, vol. 5, p. e12962, Jan. 2010.
- [97] C. Pacelli, D. De Rasmio, A. Signorile, I. Grattagliano, G. di Tullio, A. D'Orazio, B. Nico, G. P. Comi, D. Ronchi, E. Ferranini, D. Pirolo, P. Seibel, S. Schubert, A. Gaballo, G. Villani, and T. Cocco, "Mitochondrial defect and PGC-1?? dysfunction in parkin-associated familial Parkinson's disease," *Biochimica et Biophysica Acta - Molecular Basis of Disease*, vol. 1812, pp. 1041–1053, Aug. 2011.
- [98] H. E. Moon, S. H. Yoon, Y. S. Hur, H. W. Park, J. Y. Ha, K.-H. Kim, J. H. Shim, S. H. Yoo, J. H. Son, S. L. Paek, I. K. Kim, J. H. Hwang, D. G. Kim, H.-J. Kim, B. S. Jeon, S. S. Park, and S. H. Paek, "Mitochondrial dysfunction of immortalized human adipose tissue-derived mesenchymal stromal cells from patients with Parkinson's disease.," *Experimental neurobiology*, vol. 22, pp. 283–300, Dec. 2013.
- [99] C. Wang, H. S. Ko, B. Thomas, F. Tsang, K. C. M. Chew, S.-P. Tay, M. W. L. Ho, T.-M. Lim, T.-W. Soong, O. Pletnikova, J. Troncoso, V. L. Dawson, T. M. Dawson, and K.-L. Lim, "Stress-induced alterations in parkin solubility promote parkin aggregation and compromise parkin's protective function.," *Human molecular genetics*, vol. 14, pp. 3885–97, Dec. 2005.
- [100] M. J. LaVoie, B. L. Ostaszewski, A. Weihofen, M. G. Schlossmacher, and D. J. Selkoe, "Dopamine covalently modifies and functionally inactivates parkin.," *Nature medicine*, vol. 11, pp. 1214–1221, Nov. 2005.
- [101] A. C. Pawlyk, B. I. Giasson, D. M. Sampathu, F. a. Perez, K. L. Lim, V. L. Dawson, T. M. Dawson, R. D. Palmiter, J. Q. Trojanowski, and V. M. Y. Lee, "Novel Monoclonal Antibodies Demonstrate Biochemical Variation of Brain Parkin with Age," *Journal of Biological Chemistry*, vol. 278, pp. 48120–48128, Nov. 2003.
- [102] D. Yao, Z. Gu, T. Nakamura, Z.-Q. Shi, Y. Ma, B. Gaston, L. A. Palmer, E. M. Rockenstein, Z. Zhang, E. Masliah, T. Uehara, and S. A. Lipton, "Nitrosative stress linked to sporadic Parkinson's disease: S-nitrosylation of parkin regulates its E3 ubiquitin ligase activity.," *Proceedings of the National Academy of Sciences of the United States of America*, vol. 101, pp. 10810–10814, July 2004.

- [103] D. Narendra, A. Tanaka, D. F. Suen, and R. J. Youle, "Parkin is recruited selectively to impaired mitochondria and promotes their autophagy," *Journal of Cell Biology*, vol. 183, pp. 795–803, Dec. 2008.
- [104] C. Vives-Bauza, C. Zhou, Y. Huang, M. Cui, R. L. A. de Vries, J. Kim, J. May, M. A. Tocilescu, W. Liu, H. S. Ko, J. Magrané, D. J. Moore, V. L. Dawson, R. Grailhe, T. M. Dawson, C. Li, K. Tieu, and S. Przedborski, "PINK1-dependent recruitment of Parkin to mitochondria in mitophagy.," *Proceedings of the National Academy of Sciences of the United States of America*, vol. 107, pp. 378–383, Jan. 2010.
- [105] P. Seibler, J. Graziotto, H. Jeong, F. Simunovic, C. Klein, and D. Krainc, "Mitochondrial Parkin recruitment is impaired in neurons derived from mutant PINK1 induced pluripotent stem cells.," *The Journal of neuroscience : the official journal of the Society for Neuroscience*, vol. 31, pp. 5970–5976, Apr. 2011.
- [106] V. S. Van Laar, B. Arnold, S. J. Cassady, C. T. Chu, E. A. Burton, and S. B. Berman, "Bioenergetics of neurons inhibit the translocation response of Parkin following rapid mitochondrial depolarization," *Human Molecular Genetics*, vol. 20, pp. 927–940, Mar. 2011.
- [107] V. M. Gohil, S. A. Sheth, R. Nilsson, A. P. Wojtovich, J. H. Lee, F. Perocchi, W. Chen, C. B. Clish, C. Ayata, P. S. Brookes, and V. K. Mootha, "Nutrient-sensitized screening for drugs that shift energy metabolism from mitochondrial respiration to glycolysis.," *Nature biotechnology*, vol. 28, pp. 249–255, Mar. 2010.
- [108] A. P. Joselin, S. J. Hewitt, S. M. Callaghan, R. H. Kim, Y. H. Chung, T. W. Mak, J. Shen, R. S. Slack, and D. S. Park, "ROS-dependent regulation of parkin and DJ-1 localization during oxidative stress in neurons," *Human Molecular Genetics*, vol. 21, pp. 4888–4903, Nov. 2012.
- [109] X. Wang, D. Winter, G. Ashrafi, J. Schlehe, Y. L. Wong, D. Selkoe, S. Rice, J. Steen, M. J. Lavoie, and T. L. Schwarz, "PINK1 and Parkin target miro for phosphorylation and degradation to arrest mitochondrial motility," *Cell*, vol. 147, pp. 893–906, Nov. 2011.
- [110] S. Liu, T. Sawada, S. Lee, W. Yu, G. Silverio, P. Alapatt, I. Millan, A. Shen, W. Saxton, T. Kanao, R. Takahashi, N. Hattori, Y. Imai, and B. Lu, "Parkinson's disease-associated kinase PINK1 regulates miro protein level and axonal transport of mitochondria," *PLoS Genetics*, vol. 8, p. e1002537, Jan. 2012.
- [111] E. S. Vincow, G. Merrihew, R. E. Thomas, N. J. Shulman, R. P. Beyer, M. J. MacCoss, and L. J. Pallanck, "The PINK1-Parkin pathway promotes both mitophagy and selective respiratory chain turnover in vivo.," *Proceedings of the National Academy of Sciences of the United States of America*, vol. 110, pp. 6400–5, Apr. 2013.
- [112] N. Exner, B. Treske, D. Paquet, K. Holmström, C. Schiesling, S. Gispert, I. Carballo-Carbajal, D. Berg, H.-H. Hoepken, T. Gasser, R. Krüger, K. F. Winklhofer, F. Vogel, A. S. Reichert, G. Auburger, P. J. Kahle, B. Schmid, and C. Haass, "Loss-of-function of human PINK1 results in mitochondrial pathology and can be rescued by parkin.," *The Journal of neuroscience : the official journal of the Society for Neuroscience*, vol. 27, pp. 12413–8, Nov. 2007.

- [113] J. H. Shin, H. S. Ko, H. Kang, Y. Lee, Y. I. Lee, O. Pletinkova, J. C. Troconso, V. L. Dawson, and T. M. Dawson, "PARIS (ZNF746) repression of PGC-1 α contributes to neurodegeneration in parkinson's disease," *Cell*, vol. 144, pp. 689–702, Mar. 2011.
- [114] R. C. Scarpulla, "Metabolic control of mitochondrial biogenesis through the PGC-1 family regulatory network," *Biochimica et Biophysica Acta - Molecular Cell Research*, vol. 1813, pp. 1269–1278, July 2011.
- [115] D. Skowyra, K. L. Craig, M. Tyers, S. J. Elledge, and J. W. Harper, "F-box proteins are receptors that recruit phosphorylated substrates to the SCF ubiquitin-ligase complex," *Cell*, vol. 91, pp. 209–219, Oct. 1997.
- [116] M. R. Cookson, "DJ-1, PINK1, and their effects on mitochondrial pathways," *Movement Disorders*, vol. 25, pp. S44–8, Jan. 2010.
- [117] P. J. Kahle, J. Waak, and T. Gasser, "DJ-1 and prevention of oxidative stress in Parkinson's disease and other age-related disorders," *Free Radical Biology and Medicine*, vol. 47, pp. 1354–1361, Nov. 2009.
- [118] I. Irrcher, H. Aleyasin, E. L. Seifert, S. J. Hewitt, S. Chhabra, M. Phillips, a. K. Lutz, M. W. C. Rousseaux, L. Bevilacqua, a. Jahani-Asl, S. Callaghan, J. G. MacLaurin, K. F. Winklhofer, P. Rizzu, P. Rippstein, R. H. Kim, C. X. Chen, E. a. Fon, R. S. Slack, M. E. Harper, H. M. McBride, T. W. Mak, and D. S. Park, "Loss of the Parkinson's disease-linked gene DJ-1 perturbs mitochondrial dynamics," *Human Molecular Genetics*, vol. 19, pp. 3734–3746, Oct. 2010.
- [119] K. J. Thomas, M. K. McCoy, J. Blackinton, A. Beilina, M. van der Brug, A. Sandebring, D. Miller, D. Maric, A. Cedazo-Minguez, and M. R. Cookson, "DJ-1 acts in parallel to the PINK1/parkin pathway to control mitochondrial function and autophagy," *Human Molecular Genetics*, vol. 20, pp. 40–50, Oct. 2011.
- [120] M. H. Polymeropoulos, C. Lavedan, E. Leroy, S. E. Ide, A. Dehejia, A. Dutra, B. Pike, H. Root, J. Rubenstein, R. Boyer, E. S. Stenroos, S. Chandrasekharappa, A. Athanassiadou, T. Papapetropoulos, W. G. Johnson, A. M. Lazzarini, R. C. Duvoisin, G. Di Iorio, L. I. Golbe, and R. L. Nussbaum, "Mutation in the alpha-synuclein gene identified in families with Parkinson's disease.," *Science (New York, N.Y.)*, vol. 276, pp. 2045–7, June 1997.
- [121] R. Krüger, W. Kuhn, T. Müller, D. Voitalla, M. Graeber, S. Kösel, H. Przuntek, J. T. Epplen, L. Schöls, and O. Riess, "Ala30Pro mutation in the gene encoding alpha-synuclein in Parkinson's disease.," *Nature genetics*, vol. 18, pp. 106–108, Feb. 1998.
- [122] A. B. Singleton, M. Farrer, J. Johnson, A. Singleton, S. Hague, J. Kachergus, M. Hulihan, T. Peuralinna, A. Dutra, R. Nussbaum, S. Lincoln, A. Crawley, M. Hanson, D. Maraganore, C. Adler, M. R. Cookson, M. Muenter, M. Baptista, D. Miller, J. Blancato, J. Hardy, and K. Gwinn-Hardy, "alpha-Synuclein locus triplication causes Parkinson's disease.," *Science (New York, N.Y.)*, vol. 302, p. 841, Oct. 2003.

- [123] J. Simón-Sánchez, C. Schulte, J. M. Bras, M. Sharma, J. R. Gibbs, D. Berg, C. Paisan-Ruiz, P. Lichtner, S. W. Scholz, D. G. Hernandez, R. Krüger, M. Federoff, C. Klein, A. Goate, J. Perlmutter, M. Bonin, M. A. Nalls, T. Illig, C. Gieger, H. Houlden, M. Steffens, M. S. Okun, B. A. Racette, M. R. Cookson, K. D. Foote, H. H. Fernandez, B. J. Traynor, S. Schreiber, S. Arepalli, R. Zonozi, K. Gwinn, M. van der Brug, G. Lopez, S. J. Chanock, A. Schatzkin, Y. Park, A. Hollenbeck, J. Gao, X. Huang, N. W. Wood, D. Lorenz, G. Deuschl, H. Chen, O. Riess, J. A. Hardy, A. B. Singleton, and T. Gasser, "Genome-wide association study reveals genetic risk underlying Parkinson's disease.," *Nature genetics*, vol. 41, pp. 1308–1312, Dec. 2009.
- [124] M. A. Nalls, V. Plagnol, D. G. Hernandez, M. Sharma, U. M. Sheerin, M. Saad, J. Simón-Sánchez, C. Schulte, S. Lesage, S. Sveinbjörnsdóttir, K. Stefánsson, M. Martinez, J. Hardy, P. Heutink, A. Brice, T. Gasser, A. B. Singleton, and N. W. Wood, "Imputation of sequence variants for identification of genetic risks for Parkinson's disease: A meta-analysis of genome-wide association studies," *The Lancet*, vol. 377, pp. 641–649, Feb. 2011.
- [125] C. M. Lill, J. T. Roehr, M. B. McQueen, F. K. Kavvoura, S. Bagade, B. M. M. Schjeide, L. M. Schjeide, E. Meissner, U. Zauft, N. C. Allen, T. Liu, M. Schilling, K. J. Anderson, G. Beecham, D. Berg, J. M. Biernacka, A. Brice, A. L. DeStefano, C. B. Do, N. Eriksson, S. A. Factor, M. J. Farrer, T. Foroud, T. Gasser, T. Hamza, J. A. Hardy, P. Heutink, E. M. Hill-Burns, C. Klein, J. C. Latourelle, D. M. Maraganore, E. R. Martin, M. Martinez, R. H. Myers, M. A. Nalls, N. Pankratz, H. Payami, W. Satake, W. K. Scott, M. Sharma, A. B. Singleton, K. Stefansson, T. Toda, J. Y. Tung, J. Vance, N. W. Wood, C. P. Zabetian, P. Young, R. E. Tanzi, M. J. Houry, F. Zipp, H. Lehrach, J. P. A. Ioannidis, and L. Bertram, "Comprehensive research synopsis and systematic meta-analyses in Parkinson's disease genetics: The PDgene database," *PLoS Genetics*, vol. 8, p. e1002548, Jan. 2012.
- [126] W. S. Davidson, A. Jonas, D. F. Clayton, and J. M. George, "Stabilization of α -Synuclein secondary structure upon binding to synthetic membranes," *Journal of Biological Chemistry*, vol. 273, pp. 9443–9449, Apr. 1998.
- [127] M. G. Spillantini, M. L. Schmidt, V. M. Lee, J. Q. Trojanowski, R. Jakes, and M. Goedert, "Alpha-synuclein in Lewy bodies.," *Nature*, vol. 388, pp. 839–40, Aug. 1997.
- [128] L. Zhang, C. Zhang, Y. Zhu, Q. Cai, P. Chan, K. Uéda, S. Yu, and H. Yang, "Semi-quantitative analysis of α -synuclein in subcellular pools of rat brain neurons: An immunogold electron microscopic study using a C-terminal specific monoclonal antibody," *Brain Research*, vol. 1244, pp. 40–52, Dec. 2008.
- [129] P. K. Auluck, G. Caraveo, and S. Lindquist, " α -Synuclein: membrane interactions and toxicity in Parkinson's disease.," *Annual review of cell and developmental biology*, vol. 26, pp. 211–233, Jan. 2010.
- [130] V. M. Nemani, W. Lu, V. Berge, K. Nakamura, B. Onoa, M. K. Lee, F. A. Chaudhry, R. A. Nicoll, and R. H. Edwards, "Increased Expression of α -Synuclein Reduces Neurotransmitter Release by Inhibiting Synaptic Vesicle Reclustering after Endocytosis," *Neuron*, vol. 65, pp. 66–79, Jan. 2010.

- [131] M. R. Cookson, "alpha-Synuclein and neuronal cell death.," *Molecular neurodegeneration*, vol. 4, p. 9, Jan. 2009.
- [132] L. A. Volpicelli-Daley, K. C. Luk, T. P. Patel, S. A. Tanik, D. M. Riddle, A. Stieber, D. F. Meaney, J. Q. Trojanowski, and V. M. Y. Lee, "Exogenous alpha-Synuclein Fibrils Induce Lewy Body Pathology Leading to Synaptic Dysfunction and Neuron Death," *Neuron*, vol. 72, pp. 57–71, Oct. 2011.
- [133] K. Nakamura, V. M. Nemani, F. Azarbal, G. Skibinski, J. M. Levy, K. Egami, L. Munishkina, J. Zhang, B. Gardner, J. Wakabayashi, H. Sesaki, Y. Cheng, S. Finkbeiner, R. L. Nussbaum, E. Masliah, and R. H. Edwards, "Direct membrane association drives mitochondrial fission by the Parkinson disease-associated protein α -synuclein," *Journal of Biological Chemistry*, vol. 286, pp. 20710–20726, June 2011.
- [134] F. Kamp, N. Exner, A. K. Lutz, N. Wender, J. Hegermann, B. Brunner, B. Nuscher, T. Bartels, A. Giese, K. Beyer, S. Eimer, K. F. Winklhofer, and C. Haass, "Inhibition of mitochondrial fusion by α -synuclein is rescued by PINK1, Parkin and DJ-1.," *The EMBO journal*, vol. 29, pp. 3571–3589, Oct. 2010.
- [135] H. Chen, M. Vermulst, Y. E. Wang, A. Chomyn, T. A. Prolla, J. M. McCaffery, and D. C. Chan, "Mitochondrial fusion is required for mtdna stability in skeletal muscle and tolerance of mtDNA mutations," *Cell*, vol. 141, pp. 280–289, Apr. 2010.
- [136] C. C. Stichel, X. R. Zhu, V. Bader, B. Linnartz, S. Schmidt, and H. Lübbert, "Mono- and double-mutant mouse models of Parkinson's disease display severe mitochondrial damage," *Human Molecular Genetics*, vol. 16, pp. 2377–2393, Oct. 2007.
- [137] G. Liu, C. Zhang, J. Yin, X. Li, F. Cheng, Y. Li, H. Yang, K. Uéda, P. Chan, and S. Yu, " α -Synuclein is differentially expressed in mitochondria from different rat brain regions and dose-dependently down-regulates complex I activity," *Neuroscience Letters*, vol. 454, pp. 187–192, May 2009.
- [138] S. J. Chinta, J. K. Mallajosyula, A. Rane, and J. K. Andersen, "Mitochondrial alpha-synuclein accumulation impairs complex I function in dopaminergic neurons and results in increased mitophagy in vivo," *Neuroscience Letters*, vol. 486, pp. 235–239, Dec. 2010.
- [139] C. Paisán-Ruíz, S. Jain, E. W. Evans, W. P. Gilks, J. Simón, M. Van Der Brug, A. L. De Munain, S. Aparicio, A. M. Gil, N. Khan, J. Johnson, J. R. Martinez, D. Nicholl, I. M. Carrera, A. S. Pea, R. De Silva, A. Lees, J. F. Martí-Massó, J. Pérez-Tur, N. W. Wood, and A. B. Singleton, "Cloning of the gene containing mutations that cause PARK8-linked Parkinson's disease," *Neuron*, vol. 44, pp. 595–600, Nov. 2004.
- [140] A. Zimprich, S. Biskup, P. Leitner, P. Lichtner, M. Farrer, S. Lincoln, J. Kachergus, M. Hulihan, R. J. Uitti, D. B. Calne, a. J. Stoessl, R. F. Pfeiffer, N. Patenge, I. C. Carbajal, P. Vieregge, F. Asmus, B. Müller-Myhsok, D. W. Dickson, T. Meitinger, T. M. Strom, Z. K. Wszolek, and T. Gasser, "Mutations in LRRK2 cause autosomal-dominant parkinsonism with pleomorphic pathology," *Neuron*, vol. 44, pp. 601–607, Nov. 2004.

- [141] J. Deng, P. A. Lewis, E. Greggio, E. Sluch, A. Beilina, and M. R. Cookson, "Structure of the ROC domain from the Parkinson's disease-associated leucine-rich repeat kinase 2 reveals a dimeric GTPase.," *Proceedings of the National Academy of Sciences of the United States of America*, vol. 105, pp. 1499–1504, Mar. 2008.
- [142] B. D. Lee, J. H. Shin, J. VanKampen, L. Petrucelli, A. B. West, H. S. Ko, Y.-I. Lee, K. a. Maguire-Zeiss, W. J. Bowers, H. J. Federoff, V. L. Dawson, and T. M. Dawson, "Inhibitors of leucine-rich repeat kinase-2 protect against models of Parkinson's disease.," *Nature medicine*, vol. 16, pp. 998–1000, Sept. 2010.
- [143] Z. Liu, S. Hamamichi, B. D. Lee, D. Yang, A. Ray, G. A. Caldwell, K. A. Caldwell, T. M. Dawson, W. W. Smith, and V. L. Dawson, "Inhibitors of LRRK2 kinase attenuate neurodegeneration and Parkinson-like phenotypes in *Caenorhabditis elegans* and *Drosophila* Parkinson's disease models," *Human Molecular Genetics*, vol. 20, pp. 3933–3942, Oct. 2011.
- [144] H. Mortiboys, K. K. Johansen, J. O. Aasly, and O. Bandmann, "Mitochondrial impairment in patients with Parkinson disease with the G2019S mutation in LRRK2," *Neurology*, vol. 75, pp. 2017–2020, Nov. 2010.
- [145] S. Biskup, D. J. Moore, F. Celsi, S. Higashi, A. B. West, S. a. Andrabi, K. Kurkinen, S. W. Yu, J. M. Savitt, H. J. Waldvogel, R. L. M. Faull, P. C. Emson, R. Torp, O. P. Ottersen, T. M. Dawson, and V. L. Dawson, "Localization of LRRK2 to membranous and vesicular structures in mammalian brain," *Annals of Neurology*, vol. 60, pp. 557–569, Nov. 2006.
- [146] X. Wang, M. H. Yan, H. Fujioka, J. Liu, A. Wilson-delfosse, S. G. Chen, G. Perry, G. Casadesus, and X. Zhu, "LRRK2 regulates mitochondrial dynamics and function through direct interaction with DLP1," *Human Molecular Genetics*, vol. 21, pp. 1931–1944, May 2012.
- [147] S. Hindle, F. Afsari, M. Stark, C. Adam Middleton, G. J. O. Evans, S. T. Sweeney, and C. J. H. Elliott, "Dopaminergic expression of the Parkinsonian gene LRRK2-G2019S leads to non-autonomous visual neurodegeneration, accelerated by increased neural demands for energy," *Human Molecular Genetics*, vol. 22, pp. 2129–2140, June 2013.
- [148] V. Bonifati, "Genetics of Parkinson's disease—state of the art, 2013.," *Parkinsonism & related disorders*, vol. 20, pp. S23–8, Jan. 2014.
- [149] K. Marder, G. Levy, E. D. Louis, H. Mejia-Santana, L. Cote, H. Andrews, J. Harris, C. Waters, B. Ford, S. Frucht, S. Fahn, and R. Ottman, "Familial aggregation of early- and late-onset Parkinson's disease," *Annals of Neurology*, vol. 54, pp. 507–513, Oct. 2003.
- [150] D. P. Huynh, D. R. Scoles, D. Nguyen, and S. M. Pulst, "The autosomal recessive juvenile Parkinson disease gene product, parkin, interacts with and ubiquitinates synaptotagmin XI," *Human Molecular Genetics*, vol. 12, pp. 2587–2597, Oct. 2003.
- [151] N.-N. Li, E.-K. Tan, X.-L. Chang, X.-Y. Mao, J.-H. Zhang, D.-M. Zhao, Q. Liao, W.-J. Yu, and R. Peng, "Genetic association study between STK39 and CCDC62/HIP1R and Parkinson's disease.," *PloS one*, vol. 8, p. e79211, Jan. 2013.

- [152] J. Neumann, J. Bras, E. Deas, S. S. O'sullivan, L. Parkkinen, R. H. Lachmann, A. Li, J. Holton, R. Guerreiro, R. Paudel, B. Segarane, A. Singleton, A. Lees, J. Hardy, H. Houlden, T. Revesz, and N. W. Wood, "Glucocerebrosidase mutations in clinical and pathologically proven Parkinson's disease," *Brain*, vol. 132, pp. 1783–1794, July 2009.
- [153] G. A. Grabowski, "Phenotype, diagnosis, and treatment of Gaucher's disease," *The Lancet*, vol. 372, pp. 1263–1271, Oct. 2008.
- [154] M. E. Gegg, D. Burke, S. J. R. Heales, J. M. Cooper, J. Hardy, N. W. Wood, and A. H. V. Schapira, "Glucocerebrosidase deficiency in substantia nigra of parkinson disease brains," *Annals of Neurology*, vol. 72, pp. 455–463, Sept. 2012.
- [155] L. D. Osellame, A. a. Rahim, I. P. Hargreaves, M. E. Gegg, A. Richard-Londt, S. Brandner, S. N. Waddington, A. H. V. Schapira, and M. R. Duchen, "Mitochondria and quality control defects in a mouse model of Gaucher disease—links to Parkinson's disease.," *Cell metabolism*, vol. 17, pp. 941–53, June 2013.
- [156] T. S. Bürklen, U. Schlattner, R. Homayouni, K. Gough, M. Rak, A. Szeghalmi, and T. Wallimann, "The creatine kinase/creatine connection to alzheimer's disease: CK-inactivation, APP-CK complexes and focal creatine deposits," *Journal of Biomedicine and Biotechnology*, vol. 2006, p. 35936, Jan. 2006.
- [157] P. J. Adhietty and M. F. Beal, "Creatine and its potential therapeutic value for targeting cellular energy impairment in neurodegenerative diseases," *NeuroMolecular Medicine*, vol. 10, pp. 275–290, Jan. 2008.
- [158] R. T. Matthews, R. J. Ferrante, P. Klivenyi, L. Yang, A. M. Klein, G. Mueller, R. Kaddurah-Daouk, and M. F. Beal, "Creatine and cyclocreatine attenuate MPTP neurotoxicity," *Experimental neurology*, vol. 157, pp. 142–149, May 1999.
- [159] R. H. Andres, A. D. Ducray, A. Pérez-Bouza, U. Schlattner, A. W. Huber, S. H. Krebs, R. W. Seiler, T. Wallimann, and H. R. Widmer, "Creatine supplementation improves dopaminergic cell survival and protects against MPP+ toxicity in an organotypic tissue culture system," *Cell Transplantation*, vol. 14, pp. 537–550, Jan. 2005.
- [160] Investigators NINDS NET-PD, "A pilot clinical trial of creatine and minocycline in early Parkinson disease: 18-month results.," *Clinical neuropharmacology*, vol. 31, no. 3, pp. 141–150, 2008.
- [161] J. J. Elm, "Design innovations and baseline findings in a long-term Parkinson's trial: The national institute of neurological disorders and stroke exploratory trials in Parkinson's Disease Long-Term Study-1," *Movement Disorders*, vol. 27, pp. 1513–1521, Oct. 2012.
- [162] L. Ernster and G. Dallner, "Biochemical, physiological and medical aspects of ubiquinone function," *Biochimica et Biophysica Acta - Molecular Basis of Disease*, vol. 1271, pp. 195–204, May 1995.
- [163] Y. Moon, K. H. Lee, J. H. Park, D. Geum, and K. Kim, "Mitochondrial membrane depolarization and the selective death of dopaminergic neurons by rotenone: Protective effect of coenzyme Q10," *Journal of Neurochemistry*, vol. 93, pp. 1199–1208, June 2005.

- [164] M. F. Beal, "Therapeutic Effects of Coenzyme Q10 in Neurodegenerative Diseases," *Methods in Enzymology*, vol. 382, pp. 473–487, Jan. 2004.
- [165] T. L. Horvath, S. Diano, C. Leranth, L. M. Garcia-Segura, M. A. Cowley, M. Shanabrough, J. D. Elsworth, P. Sotonyi, R. H. Roth, E. H. Dietrich, R. T. Matthews, C. J. Barnstable, and D. E. Redmond, "Coenzyme Q induces nigral mitochondrial uncoupling and prevents dopamine cell loss in a primate model of Parkinson's disease," *Endocrinology*, vol. 144, pp. 2757–2760, July 2003.
- [166] C. W. Shults, D. Oakes, K. Kieburtz, M. F. Beal, R. Haas, S. Plumb, J. L. Juncos, J. Nutt, I. Shoulson, J. Carter, K. Kompoliti, J. S. Perlmutter, S. Reich, M. Stern, R. L. Watts, R. Kurlan, E. Molho, M. Harrison, and M. Lew, "Effects of coenzyme Q10 in early Parkinson disease: evidence of slowing of the functional decline," *Archives of neurology*, vol. 59, pp. 1541–1550, Oct. 2002.
- [167] A. Storch, W. H. Jost, P. Vieregge, J. Spiegel, W. Greulich, J. Durner, T. Müller, A. Kupsch, H. Henningsen, W. H. Oertel, G. Fuchs, W. Kuhn, P. Niklowitz, R. Koch, B. Herting, and H. Reichmann, "Randomized, double-blind, placebo-controlled trial on symptomatic effects of coenzyme Q(10) in Parkinson disease," *Archives of neurology*, vol. 64, pp. 938–944, July 2007.
- [168] H. Pajouhesh and G. R. Lenz, "Medicinal chemical properties of successful central nervous system drugs," *NeuroRx : the journal of the American Society for Experimental NeuroTherapeutics*, vol. 2, no. October, pp. 541–553, 2005.
- [169] G. F. Kelso, C. M. Porteous, C. V. Coulter, G. Hughes, W. K. Porteous, E. C. Ledgerwood, R. A. J. Smith, and M. P. Murphy, "Selective targeting of a redox-active ubiquinone to mitochondria within cells: Antioxidant and antiapoptotic properties," *Journal of Biological Chemistry*, vol. 276, pp. 4588–4596, Feb. 2001.
- [170] S. Rodriguez-Cuenca, H. M. Cochemé, A. Logan, I. Abakumova, T. A. Prime, C. Rose, A. Vidal-Puig, A. C. Smith, D. C. Rubinsztein, I. M. Fearnley, B. A. Jones, S. Pope, S. J. R. Heales, B. Y. H. Lam, S. G. Neogi, I. McFarlane, A. M. James, R. A. J. Smith, and M. P. Murphy, "Consequences of long-term oral administration of the mitochondria-targeted antioxidant MitoQ to wild-type mice," *Free Radical Biology and Medicine*, vol. 48, pp. 161–172, Jan. 2010.
- [171] M. E. Solesio, T. a. Prime, A. Logan, M. P. Murphy, M. del Mar Arroyo-Jimenez, J. Jordán, and M. F. Galindo, "The mitochondria-targeted anti-oxidant MitoQ reduces aspects of mitochondrial fission in the 6-OHDA cell model of Parkinson's disease," *Biochimica et Biophysica Acta - Molecular Basis of Disease*, vol. 1832, pp. 174–182, Jan. 2013.
- [172] R. A. J. Smith and M. P. Murphy, "Animal and human studies with the mitochondria-targeted antioxidant MitoQ," *Annals of the New York Academy of Sciences*, vol. 1201, pp. 96–103, July 2010.
- [173] B. J. Snow, F. L. Rolfe, M. M. Lockhart, C. M. Frampton, J. D. O'Sullivan, V. Fung, R. a. J. Smith, M. P. Murphy, and K. M. Taylor, "A double-blind, placebo-controlled study to assess the mitochondria-targeted antioxidant MitoQ as a disease-modifying therapy in Parkinson's disease.," *Movement disorders : official journal of the Movement Disorder Society*, vol. 25, pp. 1670–1674, Aug. 2010.

- [174] A. Mordente, G. E. Martorana, G. Minotti, and B. Giardina, "Antioxidant properties of 2,3-dimethoxy-5-methyl-6-(10-hydroxydecyl)-1,4-benzoquinone (idebenone).," *Chemical research in toxicology*, vol. 11, pp. 54–63, Jan. 1998.
- [175] M. H. Parkinson, J. B. Schulz, and P. Giunti, "Co-enzyme Q10 and idebenone use in Friedreich's ataxia," *Journal of Neurochemistry*, vol. 126, pp. 125–141, Aug. 2013.
- [176] K.-K. Tai, L. Pham, and D. D. Truong, "Idebenone Induces Apoptotic Cell Death in the Human Dopaminergic Neuroblastoma SHSY-5Y Cells.," *Neurotoxicity research*, vol. 20, pp. 321–328, Nov. 2011.
- [177] K. Schoonjans, B. Staels, and J. Auwerx, "The peroxisome proliferator activated receptors (PPARS) and their effects on lipid metabolism and adipocyte differentiation.," *Biochimica et biophysica acta*, vol. 1302, pp. 93–109, July 1996.
- [178] J. Vamecq and N. Latruffe, "Medical significance of peroxisome proliferator-activated receptors," *Lancet*, vol. 354, pp. 141–148, July 1999.
- [179] C. De Nuccio, A. Bernardo, R. De Simone, E. Mancuso, V. Magnaghi, S. Visentin, and L. Minghetti, "Peroxisome Proliferator-Activated Receptor γ Agonists Accelerate Oligodendrocyte Maturation and Influence Mitochondrial Functions and Oscillatory Ca^{2+} Waves," *Journal of Neuropathology and Experimental Neurology*, vol. 70, pp. 900–912, Oct. 2011.
- [180] T. Dehmer, M. T. Heneka, M. Sastre, J. Dichgans, and J. B. Schulz, "Protection by pioglitazone in the MPTP model of Parkinson's disease correlates with I kappa B alpha induction and block of NF kappa B and iNOS activation.," *Journal of neurochemistry*, vol. 88, pp. 494–501, Jan. 2004.
- [181] C. R. Swanson, V. Joers, V. Bondarenko, K. Brunner, H. A. Simmons, T. E. Ziegler, J. W. Kemnitz, J. A. Johnson, and M. E. Emborg, "The PPAR- γ agonist pioglitazone modulates inflammation and induces neuroprotection in parkinsonian monkeys.," *Journal of neuroinflammation*, vol. 8, p. 91, Jan. 2011.
- [182] Y. Miyazaki, A. Mahankali, M. Matsuda, S. Mahankali, J. Hardies, K. Cusi, L. J. Mandarino, and R. A. DeFronzo, "Effect of pioglitazone on abdominal fat distribution and insulin sensitivity in type 2 diabetic patients.," *The Journal of clinical endocrinology and metabolism*, vol. 87, pp. 2784–2791, June 2002.
- [183] E. Palombo, L. J. Porrino, K. S. Bankiewicz, A. M. Crane, I. J. Kopin, and L. Sokoloff, "Administration of MPTP acutely increases glucose utilization in the substantia nigra of primates.," *Brain research*, vol. 453, pp. 227–234, June 1988.
- [184] J. C. Strum, R. Shehee, D. Virley, J. Richardson, M. Mattie, P. Selley, S. Ghosh, C. Nock, A. Saunders, and A. Roses, "Rosiglitazone induces mitochondrial biogenesis in mouse brain.," *Journal of Alzheimer's disease : JAD*, vol. 11, pp. 45–51, Mar. 2007.
- [185] A. L. Goldberg and F. S. Boches, "Oxidized proteins in erythrocytes are rapidly degraded by the adenosine triphosphate-dependent proteolytic system.," *Science (New York, N.Y.)*, vol. 215, pp. 1107–1109, Feb. 1982.

- [186] H. Atamna, A. Nguyen, C. Schultz, K. Boyle, J. Newberry, H. Kato, and B. N. Ames, "Methylene blue delays cellular senescence and enhances key mitochondrial biochemical pathways.," *The FASEB journal : official publication of the Federation of American Societies for Experimental Biology*, vol. 22, pp. 703–712, Mar. 2008.
- [187] Y. Wen, W. Li, E. C. Poteet, L. Xie, C. Tan, L. J. Yan, X. Ju, R. Liu, H. Qian, M. A. Marvin, M. S. Goldberg, H. She, Z. Mao, J. W. Simpkins, and S. H. Yang, "Alternative mitochondrial electron transfer as a novel strategy for neuroprotection," *Journal of Biological Chemistry*, vol. 286, pp. 16504–16515, May 2011.
- [188] R. O'Lone, K. Knorr, I. Z. Jaffe, M. E. Schaffer, P. G. V. Martini, R. H. Karas, J. Binkowska, M. E. Mendelsohn, and U. Hansen, "Estrogen receptors alpha and beta mediate distinct pathways of vascular gene expression, including genes involved in mitochondrial electron transport and generation of reactive oxygen species.," *Molecular endocrinology (Baltimore, Md.)*, vol. 21, pp. 1281–1296, June 2007.
- [189] J. W. Simpkins, S. H. Yang, S. N. Sarkar, and V. Pearce, "Estrogen actions on mitochondria-Physiological and pathological implications," *Molecular and Cellular Endocrinology*, vol. 290, pp. 51–59, Aug. 2008.
- [190] L. Dong, W. Wang, F. Wang, M. Stoner, J. C. Reed, M. Harigai, I. Samudio, M. P. Kladde, C. Vyhlidal, and S. Safe, "Mechanisms of transcriptional activation of bcl-2 gene expression by 17beta-estradiol in breast cancer cells.," *The Journal of biological chemistry*, vol. 274, pp. 32099–32107, Nov. 1999.
- [191] C. J. Pike, "Estrogen modulates neuronal Bcl-x(L) expression and ??-amyloid-induced apoptosis: Relevance to Alzheimer's disease," *Journal of Neurochemistry*, vol. 72, pp. 1552–1563, Apr. 1999.
- [192] M. Singh, G. Sétáló, X. Guan, M. Warren, and C. D. Toran-Allerand, "Estrogen-induced activation of mitogen-activated protein kinase in cerebral cortical explants: convergence of estrogen and neurotrophin signaling pathways.," *The Journal of neuroscience : the official journal of the Society for Neuroscience*, vol. 19, pp. 1179–1188, Feb. 1999.
- [193] P. S. G. P. Investigators., "A randomized pilot trial of estrogen replacement therapy in post-menopausal women with Parkinsons disease," *Parkinsonism & Related Disorders*, vol. 17, pp. 757–760, Dec. 2011.
- [194] K. M. Smith and N. Dahodwala, "Sex differences in Parkinson's disease and other movement disorders," *Experimental Neurology*, vol. 259C, pp. 44–56, Sept. 2014.
- [195] M. Bourque, D. E. Dluzen, and T. Di Paolo, "Signaling pathways mediating the neuroprotective effects of sex steroids and SERMs in Parkinson's disease," *Frontiers in Neuroendocrinology*, vol. 33, pp. 169–178, Apr. 2012.
- [196] N. M. Gatto, D. Deapen, S. Stoyanoff, R. Pinder, S. Narayan, Y. Bordelon, and B. Ritz, "Parkinsonism and Related Disorders Lifetime exposure to estrogens and Parkinson ' s disease in California teachers," *Parkinsonism and Related Disorders*, vol. 20, pp. 1149–1156, Aug. 2014.

- [197] M. S. Okun, H. H. Fernandez, R. L. Rodriguez, J. Romrell, M. Suelter, S. Munson, E. D. Louis, T. Mulligan, P. S. Foster, B. V. Shenal, S. J. Armaghani, C. Jacobson, S. Wu, and G. Crucian, "Testosterone therapy in men with Parkinson disease: results of the TEST-PD Study," *Archives of neurology*, vol. 63, pp. 729–735, May 2006.
- [198] H. Mortiboys, J. Aasly, and O. Bandmann, "Ursocholic acid rescues mitochondrial function in common forms of familial Parkinson's disease," *Brain*, vol. 136, pp. 3038–3050, Sept. 2013.
- [199] G. Auburger, M. Klinkenberg, J. Drost, K. Marcus, B. Morales-Gordo, W. S. Kunz, U. Brandt, V. Broccoli, H. Reichmann, S. Gispert, and M. Jendrach, "Primary skin fibroblasts as a model of Parkinson's disease," *Molecular Neurobiology*, vol. 46, pp. 20–27, Aug. 2012.
- [200] A. F. Hofmann, "Detoxification of lithocholic acid, a toxic bile acid: relevance to drug hepatotoxicity," *Drug metabolism reviews*, vol. 36, pp. 703–722, Oct. 2004.
- [201] R. E. Poupon, R. Poupon, and B. Balkau, "Ursodiol for the long-term treatment of primary biliary cirrhosis. The UDCA-PBC Study Group.," *The New England journal of medicine*, vol. 330, pp. 1342–1347, May 1994.
- [202] H. S. Chun and W. C. Low, "Ursodeoxycholic acid suppresses mitochondria-dependent programmed cell death induced by sodium nitroprusside in SH-SY5Y cells," *Toxicology*, vol. 292, pp. 105–112, Feb. 2012.
- [203] S. D. Kunkel, M. Suneja, S. M. Ebert, K. S. Bongers, D. K. Fox, S. E. Malmberg, F. Alipour, R. K. Shields, and C. M. Adams, "mRNA expression signatures of human skeletal muscle atrophy identify a natural compound that increases muscle mass," *Cell Metabolism*, vol. 13, pp. 627–638, June 2011.
- [204] H. Leis, A. Page, A. Ramírez, A. Bravo, C. Segrelles, J. Paramio, D. Baretino, J. L. Jorcano, and P. Pérez, "Glucocorticoid Receptor Counteracts Tumorigenic Activity of Akt in Skin through Interference with the Phosphatidylinositol 3-Kinase Signaling Pathway.," *Molecular endocrinology (Baltimore, Md.)*, vol. 18, pp. 303–311, Feb. 2004.
- [205] S. Arancibia, D. Benítez, L. E. Núñez, C. M. Jewell, P. Langjahr, E. Candia, G. Zapata-Torres, J. A. Cidlowski, M. J. González, and M. A. Hermoso, "Phosphatidylinositol 3-kinase interacts with the glucocorticoid receptor upon TLR2 activation," *Journal of Cellular and Molecular Medicine*, vol. 15, pp. 339–349, Feb. 2011.
- [206] S. Solá, M. M. Aranha, C. J. Steer, and C. M. P. Rodrigues, "Game and players: Mitochondrial apoptosis and the therapeutic potential of ursodeoxycholic acid," *Current Issues in Molecular Biology*, vol. 9, pp. 123–138, July 2007.
- [207] J. Haller, E. Mikics, and G. B. Makara, "The effects of non-genomic glucocorticoid mechanisms on bodily functions and the central neural system. A critical evaluation of findings," *Frontiers in Neuroendocrinology*, vol. 29, pp. 273–291, May 2008.

- [208] Y. Ikeda, A. Murakami, and H. Ohigashi, "Ursolic acid: an anti- and pro-inflammatory triterpenoid.," *Molecular nutrition & food research*, vol. 52, pp. 26–42, Jan. 2008.
- [209] R. Poupon, "Ursodeoxycholic acid and bile-acid mimetics as therapeutic agents for cholestatic liver diseases: An overview of their mechanisms of action," *Clinics and Research in Hepatology and Gastroenterology*, vol. 36, pp. S3–12, Sept. 2012.
- [210] T. Khare and S. Khare, "Controversies in Chemoprevention of Colorectal Cancer with Ursodeoxycholic Acid," *JSM Gastroenterology and Hepatology*, vol. 2, pp. 2–5, 2014.
- [211] L. Deng, R. Zhang, F. Tang, C. Li, Y. Y. Xing, and T. Xi, "Ursolic acid induces U937 cells differentiation by PI3K/Akt pathway activation," *Chinese Journal of Natural Medicines*, vol. 12, pp. 15–19, Jan. 2014.
- [212] X. Ou, M. Liu, H. Luo, L. Q. Dong, and F. Liu, "Ursolic acid inhibits leucine-stimulated mTORC1 signaling by suppressing mTOR localization to lysosome," *PLoS ONE*, vol. 9, p. e95393, Jan. 2014.
- [213] L. Qiao, A. Yacoub, E. Studer, S. Gupta, X. Y. Pei, S. Grant, P. B. Hylemon, and P. Dent, "Inhibition of the MAPK and PI3K pathways enhances UDCA-induced apoptosis in primary rodent hepatocytes," *Hepatology*, vol. 35, pp. 779–789, Apr. 2002.
- [214] S. Arisawa, K. Ishida, N. Kameyama, J. Ueyama, A. Hattori, Y. Tatsumi, H. Hayashi, M. Yano, K. Hayashi, Y. Katano, H. Goto, K. Takagi, and S. Wakisawa, "Ursodeoxycholic acid induces glutathione synthesis through activation of PI3K/Akt pathway in HepG2 cells," *Biochemical Pharmacology*, vol. 77, pp. 858–866, Mar. 2009.
- [215] X.-S. Liu and J. Jiang, "Induction of apoptosis and regulation of the MAPK pathway by ursolic acid in human leukemia K562 cells.," *Planta medica*, vol. 73, pp. 1192–1194, Sept. 2007.
- [216] Y. H. Shih, Y. C. Chein, J. Y. Wang, and Y. S. Fu, "Ursolic acid protects hippocampal neurons against kainate-induced excitotoxicity in rats," *Neuroscience Letters*, vol. 362, pp. 136–140, May 2004.
- [217] J. Lu, Y.-L. Zheng, D.-M. Wu, L. Luo, D.-X. Sun, and Q. Shan, "Ursolic acid ameliorates cognition deficits and attenuates oxidative damage in the brain of senescent mice induced by D-galactose.," *Biochemical pharmacology*, vol. 74, pp. 1078–90, Oct. 2007.
- [218] J. Liobikas, D. Majiene, S. Trumbeckaite, L. Kursvietiene, R. Masteikova, D. M. Kopustinskiene, A. Savickas, and J. Bernatoniene, "Uncoupling and antioxidant effects of ursolic acid in isolated rat heart mitochondria," *Journal of Natural Products*, vol. 74, pp. 1640–1644, June 2011.
- [219] X. Tang, J. Gao, J. Chen, F. Fang, Y. Wang, H. Dou, Q. Xu, and Z. Qian, "Inhibition of ursolic acid on calcium-induced mitochondrial permeability transition and release of two proapoptotic proteins," *Biochemical and Biophysical Research Communications*, vol. 337, pp. 320–324, Nov. 2005.

- [220] R. M. Ramalho, R. J. S. Viana, W. C. Low, C. J. Steer, and C. M. P. Rodrigues, "Bile acids and apoptosis modulation: an emerging role in experimental Alzheimer's disease," *Trends in Molecular Medicine*, vol. 14, pp. 54–62, Feb. 2008.
- [221] P. B. Hylemon, H. Zhou, W. M. Pandak, S. Ren, G. Gil, and P. Dent, "Bile acids as regulatory molecules.," *Journal of lipid research*, vol. 50, pp. 1509–1520, Aug. 2009.
- [222] T. Maruyama, Y. Miyamoto, T. Nakamura, Y. Tamai, H. Okada, E. Sugiyama, T. Nakamura, H. Itadani, and K. Tanaka, "Identification of membrane-type receptor for bile acids (M-BAR)," *Biochemical and Biophysical Research Communications*, vol. 298, pp. 714–719, Nov. 2002.
- [223] Y. Kawamata, R. Fujii, M. Hosoya, M. Harada, H. Yoshida, M. Miwa, S. Fukusumi, Y. Habata, T. Itoh, Y. Shintani, S. Hinuma, Y. Fujisawa, and M. Fujino, "A G protein-coupled receptor responsive to bile acids," *Journal of Biological Chemistry*, vol. 278, pp. 9435–9440, Mar. 2003.
- [224] M. Watanabe, S. M. Houten, C. Matak, M. a. Christoffolete, B. W. Kim, H. Sato, N. Messaddeq, J. W. Harney, O. Ezaki, T. Kodama, K. Schoonjans, A. C. Bianco, and J. Auwerx, "Bile acids induce energy expenditure by promoting intracellular thyroid hormone activation.," *Nature*, vol. 439, pp. 484–489, Jan. 2006.
- [225] V. Keitel, B. Görg, H. J. Bidmon, I. Zemtsova, L. Spomer, K. Zilles, and D. Häussinger, "The bile acid receptor TGR5 (Gpbar-1) acts as a neurosteroid receptor in brain," *Glia*, vol. 58, pp. 1794–1805, Nov. 2010.
- [226] F. Alemi, E. Kwon, D. P. Poole, T. Lieu, V. Lyo, F. Cattaruzza, F. Cevikbas, M. Steinhoff, R. Nassini, S. Materazzi, R. Guerrero-Alba, E. Valdez-Morales, G. S. Cottrell, K. Schoonjans, P. Geppetti, S. J. Vanner, N. W. Bunnett, and C. U. Corvera, "The TGR5 receptor mediates bile acid-induced itch and analgesia," *Journal of Clinical Investigation*, vol. 123, pp. 1513–1530, Apr. 2013.
- [227] F. G. Schaap, M. Trauner, and P. L. M. Jansen, "Bile acid receptors as targets for drug development.," *Nature reviews. Gastroenterology & hepatology*, vol. 11, pp. 55–67, Jan. 2014.
- [228] A. Macchiarulo, A. Gioiello, C. Thomas, T. W. H. Pols, R. Nuti, C. Ferrari, N. Giacchè, F. De Franco, M. Pruzanski, J. Auwerx, K. Schoonjans, and R. Pellicciari, "Probing the Binding Site of Bile Acids in TGR5.," *ACS medicinal chemistry letters*, vol. 4, pp. 1158–62, Oct. 2013.
- [229] C. Thomas, A. Gioiello, L. Noriega, A. Strehle, J. Oury, G. Rizzo, A. Macchiarulo, H. Yamamoto, C. Matak, M. Pruzanski, R. Pellicciari, J. Auwerx, and K. Schoonjans, "TGR5-Mediated Bile Acid Sensing Controls Glucose Homeostasis," *Cell Metabolism*, vol. 10, pp. 167–177, Sept. 2009.
- [230] T. W. H. Pols, L. G. Noriega, M. Nomura, J. Auwerx, and K. Schoonjans, "The bile acid membrane receptor TGR5: A valuable metabolic target," *Digestive Diseases*, vol. 29, pp. 37–44, Jan. 2011.

- [231] H. Sato, A. Macchiarulo, C. Thomas, A. Gioiello, M. Une, A. F. Hofmann, R. Saladin, K. Schoonjans, R. Pellicciari, and J. Auwerx, "Novel potent and selective bile acid derivatives as TGR5 agonists: Biological screening, structure-activity relationships, and molecular modeling studies," *Journal of Medicinal Chemistry*, vol. 51, pp. 1831–1841, Mar. 2008.
- [232] C. Genet, A. Strehle, C. Schmidt, G. Boudjelal, A. Lobstein, K. Schoonjans, M. Souchet, J. Auwerx, R. Saladin, and A. Wagner, "Structure-activity relationship study of betulinic acid, a novel and selective TGR5 agonist, and its synthetic derivatives: potential impact in diabetes.," *Journal of medicinal chemistry*, vol. 53, pp. 178–190, Jan. 2010.
- [233] D. P. Poole, C. Godfrey, F. Cattaruzza, G. S. Cottrell, J. G. Kirkland, J. C. Pelayo, N. W. Bunnett, and C. U. Corvera, "Expression and function of the bile acid receptor GpBAR1 (TGR5) in the murine enteric nervous system," *Neurogastroenterology and Motility*, vol. 22, pp. 814–25, e227–8, July 2010.
- [234] Y. Iguchi, T. Nishimaki-Mogami, M. Yamaguchi, F. Teraoka, T. Kaneko, and M. Une, "Effects of chemical modification of ursodeoxycholic acid on TGR5 activation.," *Biological & pharmaceutical bulletin*, vol. 34, pp. 1–7, Jan. 2011.
- [235] J. H. Robben, M. L. A. Kortenoeven, M. Sze, C. Yae, G. Milligan, V. M. Oorschot, J. Klumperman, N. V. A. M. Knoers, and P. M. T. Deen, "Intracellular activation of vasopressin V2 receptor mutants in nephrogenic diabetes insipidus by nonpeptide agonists.," *Proceedings of the National Academy of Sciences of the United States of America*, vol. 106, pp. 12195–12200, July 2009.
- [236] J. Lee, S. Sharma, J. Kim, R. J. Ferrante, and H. Ryu, "Mitochondrial nuclear receptors and transcription factors: Who's minding the cell?," *Journal of Neuroscience Research*, vol. 86, pp. 961–971, Apr. 2008.
- [237] A. M. G. Psarra and C. E. Sekeris, "Steroid and thyroid hormone receptors in mitochondria," *IUBMB Life*, vol. 60, pp. 210–223, Apr. 2008.
- [238] H. J. Cha, M. T. Park, H. Y. Chung, N. D. Kim, H. Sato, M. Seiki, and K. W. Kim, "Ursolic acid-induced down-regulation of MMP-9 gene is mediated through the nuclear translocation of glucocorticoid receptor in HT1080 human fibrosarcoma cells.," *Oncogene*, vol. 16, pp. 771–778, Feb. 1998.
- [239] E. Kassi, Z. Papoutsi, H. Pratsinis, N. Aligiannis, M. Manoussakis, and P. Moutsatsou, "Ursolic acid, a naturally occurring triterpenoid, demonstrates anticancer activity on human prostate cancer cells," *Journal of Cancer Research and Clinical Oncology*, vol. 133, pp. 493–500, July 2007.
- [240] E. Kassi, T. G. Sourlingas, M. Spiliotaki, Z. Papoutsi, H. Pratsinis, N. Aligiannis, and P. Moutsatsou, "Ursolic acid triggers apoptosis and Bcl-2 downregulation in MCF-7 breast cancer cells.," *Cancer investigation*, vol. 27, pp. 723–733, Aug. 2009.
- [241] J. S. Torday and V. K. Rehan, "A cell-molecular approach predicts vertebrate evolution," *Molecular Biology and Evolution*, vol. 28, pp. 2973–2981, Nov. 2011.

- [242] V. Haridas, Z. X. Xu, D. Kitchen, A. Jiang, P. Michels, and J. U. Gutterman, "The anticancer plant triterpenoid, avicin d, regulates glucocorticoid receptor signaling: Implications for cellular metabolism," *PLoS ONE*, vol. 6, p. e28037, Jan. 2011.
- [243] V. Haridas, X. Li, T. Mizumachi, M. Higuchi, V. V. Lemeshko, M. Colombini, and J. U. Gutterman, "Avicins, a novel plant-derived metabolite lowers energy metabolism in tumor cells by targeting the outer mitochondrial membrane," *Mitochondrion*, vol. 7, pp. 234–240, May 2007.
- [244] H. Tanaka, Y. Makino, T. Miura, F. Hirano, K. Okamoto, K. Komura, Y. Sato, and I. Makino, "Ligand-independent activation of the glucocorticoid receptor by ursodeoxycholic acid. Repression of IFN-gamma-induced MHC class II gene expression via a glucocorticoid receptor-dependent pathway.," *Journal of immunology (Baltimore, Md. : 1950)*, vol. 156, pp. 1601–1608, Feb. 1996.
- [245] T. Miura, R. Ouchida, N. Yoshikawa, K. Okamoto, Y. Makino, T. Nakamura, C. Morimoto, I. Makino, and H. Tanaka, "Functional Modulation of the Glucocorticoid Receptor and Suppression of NF- κ B-dependent Transcription by Ursodeoxycholic Acid," *Journal of Biological Chemistry*, vol. 276, pp. 47371–47378, Dec. 2001.
- [246] S. Solá, J. D. Amaral, R. E. Castro, R. M. Ramalho, P. M. Borralho, B. T. Kren, H. Tanaka, C. J. Steer, and C. M. P. Rodrigues, "Nuclear translocation of UDCA by the glucocorticoid receptor is required to reduce TGF-beta1-induced apoptosis in rat hepatocytes.," *Hepatology (Baltimore, Md.)*, vol. 42, pp. 925–934, Oct. 2005.
- [247] C. Weitzel, D. Stark, F. Kullmann, J. Schölmerich, A. Holstege, and W. Falk, "Ursodeoxycholic acid induced activation of the glucocorticoid receptor in primary rat hepatocytes.," *European journal of gastroenterology & hepatology*, vol. 17, pp. 169–177, Feb. 2005.
- [248] S. Solá, R. E. Castro, B. T. Kren, C. J. Steer, and C. M. P. Rodrigues, "Modulation of nuclear steroid receptors by ursodeoxycholic acid inhibits TGF-beta1-induced E2F-1/p53-mediated apoptosis of rat hepatocytes.," *Biochemistry*, vol. 43, pp. 8429–8438, July 2004.
- [249] C. M. Rodrigues, G. Fan, X. Ma, B. T. Kren, and C. J. Steer, "A novel role for ursodeoxycholic acid in inhibiting apoptosis by modulating mitochondrial membrane perturbation.," *The Journal of clinical investigation*, vol. 101, pp. 2790–9, June 1998.
- [250] L. Lim, V. Jackson-Lewis, L. C. Wong, G. H. Shui, A. X. H. Goh, S. Kesavapany, A. M. Jenner, M. Fivaz, S. Przedborski, and M. R. Wenk, "Lanosterol induces mitochondrial uncoupling and protects dopaminergic neurons from cell death in a model for Parkinson's disease," *Cell Death and Differentiation*, vol. 19, pp. 416–427, Mar. 2012.
- [251] K. M. Ko, T. Y. Y. Leon, D. H. F. Mak, P. Y. Chiu, Y. Du, and M. K. T. Poon, "A characteristic pharmacological action of 'Yang-invigorating' Chinese tonifying herbs: Enhancement of myocardial ATP-generation capacity," *Phytomedicine*, vol. 13, pp. 636–642, Nov. 2006.

- [252] J. Chen and K. M. Ko, "Ursolic-acid-enriched herba cynomorii extract protects against oxidant injury in H9c2 cells and rat myocardium by increasing mitochondrial ATP generation capacity and enhancing cellular glutathione redox cycling, possibly through mitochondrial uncoupling," *Evidence-based Complementary and Alternative Medicine*, vol. 2013, p. 924128, Jan. 2013.
- [253] J. Chen, H. S. Wong, and K. M. Ko, "Ursolic acid-enriched Herba Cynomorii extract induces mitochondrial uncoupling and glutathione redox cycling through mitochondrial reactive oxygen species generation: Protection against menadione cytotoxicity in H9c2 cells," *Molecules*, vol. 19, pp. 1576–1591, Jan. 2014.
- [254] J. Du, Y. Wang, R. Hunter, Y. Wei, R. Blumenthal, C. Falke, R. Khairova, R. Zhou, P. Yuan, R. Machado-Vieira, B. S. McEwen, and H. K. Manji, "Dynamic regulation of mitochondrial function by glucocorticoids," *Proceedings of the National Academy of Sciences of the United States of America*, vol. 106, pp. 3543–3548, Mar. 2009.
- [255] A. N. Murphy, "Ca(2+)-mediated mitochondrial dysfunction and the protective effects of Bcl-2," *Annals of the New York Academy of Sciences*, vol. 893, pp. 19–32, Jan. 1999.
- [256] G. Talabér, F. Boldizsár, D. Bartis, L. Pálinkás, M. Szabó, G. Berta, G. Sétáló, P. Németh, and T. Berki, "Mitochondrial translocation of the glucocorticoid receptor in double-positive thymocytes correlates with their sensitivity to glucocorticoid-induced apoptosis," *International Immunology*, vol. 21, pp. 1269–1276, Nov. 2009.
- [257] S. R. Lee, H. K. Kim, I. S. Song, J. Youm, L. A. Dizon, S. H. Jeong, T. H. Ko, H. J. Heo, K. S. Ko, B. D. Rhee, N. Kim, and J. Han, "Glucocorticoids and their receptors: Insights into specific roles in mitochondria," *Progress in Biophysics and Molecular Biology*, vol. 112, pp. 44–54, May 2013.
- [258] K. Jilani, M. Abed, C. Zelenak, E. Lang, S. M. Qadri, and F. Lang, "Triggering of erythrocyte cell membrane scrambling by ursolic acid," *Journal of Natural Products*, vol. 74, pp. 2181–2186, Oct. 2011.
- [259] M. M. A. Elsayed and G. Cevc, "The vesicle-to-micelle transformation of phospholipid-cholate mixed aggregates: A state of the art analysis including membrane curvature effects," *Biochimica et Biophysica Acta - Biomembranes*, vol. 1808, pp. 140–153, Jan. 2011.
- [260] J. Prades, O. Vögler, R. Alemany, M. Gomez-Florit, S. S. Funari, V. Ruiz-Gutiérrez, and F. Barceló, "Plant pentacyclic triterpenic acids as modulators of lipid membrane physical properties," *Biochimica et Biophysica Acta - Biomembranes*, vol. 1808, pp. 752–760, Mar. 2011.
- [261] C. A. Lipinski, "Lead- and drug-like compounds: the rule-of-five revolution," *Drug discovery today. Technologies*, vol. 1, pp. 337–41, Dec. 2004.
- [262] C. A. Lipinski, F. Lombardo, B. W. Dominy, and P. J. Feeney, "Experimental and computational approaches to estimate solubility and permeability in drug discovery and development settings," *Advanced Drug Delivery Reviews*, vol. 64, pp. 4–17, Mar. 2012.

- [263] N. J. Abbott, L. Rönnbäck, and E. Hansson, "Astrocyte-endothelial interactions at the blood-brain barrier.," *Nature reviews. Neuroscience*, vol. 7, pp. 41–53, Jan. 2006.
- [264] K. E. Schlageter, P. Molnar, G. D. Lapin, and D. R. Groothuis, "Microvessel organization and structure in experimental brain tumors: microvessel populations with distinctive structural and functional properties.," *Microvascular research*, vol. 58, pp. 312–328, Nov. 1999.
- [265] M. Marroni, N. Marchi, L. Cucullo, N. J. Abbott, K. Signorelli, and D. Janigro, "Vascular and parenchymal mechanisms in multiple drug resistance: a lesson from human epilepsy.," *Current drug targets*, vol. 4, pp. 297–304, May 2003.
- [266] D. B. Stanimirovic and A. Friedman, "Pathophysiology of the neurovascular unit: disease cause or consequence?," *Journal of Cerebral Blood Flow & Metabolism*, vol. 32, pp. 1207–1221, July 2012.
- [267] W. M. Pardridge, "Drug transport across the bloodbrain barrier," *Journal of Cerebral Blood Flow & Metabolism*, vol. 32, pp. 1959–72, Nov. 2012.
- [268] S. J. Marrink, F. Jähnig, and H. J. Berendsen, "Proton transport across transient single-file water pores in a lipid membrane studied by molecular dynamics simulations.," *Biophysical journal*, vol. 71, pp. 632–647, Aug. 1996.
- [269] W. Stein, *The Movement of Molecules across Cell, Membranes*, vol. 9. Elsevier Science, 1969.
- [270] W. M. Pardridge and L. J. Mietus, "Transport of steroid hormones through the rat blood-brain barrier. Primary role of albumin-bound hormone," *Journal of Clinical Investigation*, vol. 64, pp. 145–154, July 1979.
- [271] M. C. Yin, M. C. Lin, M. C. Mong, and C. Y. Lin, "Bioavailability, distribution, and antioxidative effects of selected triterpenes in mice," *Journal of Agricultural and Food Chemistry*, vol. 60, pp. 7697–7701, July 2012.
- [272] G. J. Parry, C. M. P. Rodrigues, M. M. Aranha, S. J. Hilbert, C. Davey, P. Kelkar, W. C. Low, and C. J. Steer, "Safety, tolerability, and cerebrospinal fluid penetration of ursodeoxycholic Acid in patients with amyotrophic lateral sclerosis.," *Clinical neuropharmacology*, vol. 33, pp. 17–21, Jan.
- [273] H. Reiber and K. Felgenhauer, "Protein transfer at the blood cerebrospinal fluid barrier and the quantitation of the humoral immune response within the central nervous system.," *Clinica chimica acta; international journal of clinical chemistry*, vol. 163, pp. 319–328, Mar. 1987.
- [274] W. H. Oldendorf, "Cerebrospinal fluid formation and circulation.," *Progress in nuclear medicine*, vol. 1, pp. 336–358, Jan. 1972.
- [275] J.-H. Min, Y.-H. Hong, J.-J. Sung, S.-M. Kim, J. B. Lee, and K.-W. Lee, "Oral Solubilized Ursodeoxycholic Acid Therapy in Amyotrophic Lateral Sclerosis: A Randomized Cross-Over Trial," *Journal of Korean Medical Science*, vol. 27, p. 200, Mar. 2012.

- [276] S. H. Yoo, "Dried Forms of Aqueous Solubilized Bile Acid Dosage Formulation: Preparation and Uses Thereof," *US Patent 2005/0158408 A1*, 2005.
- [277] C. M. P. Rodrigues, S. R. Spellman, S. Solá, A. W. Grande, C. Linehan-Stieers, W. C. Low, and C. J. Steer, "Neuroprotection by a bile acid in an acute stroke model in the rat.," *Journal of cerebral blood flow and metabolism : official journal of the International Society of Cerebral Blood Flow and Metabolism*, vol. 22, pp. 463–471, Apr. 2002.
- [278] S. H. Yoo, "Long Lasting Therapeutic Effects of Yoo's Solution for Ischemic Stroke (P1.144)," *Neurology*, vol. 82, p. P1.144, Apr. 2014.
- [279] J. Lu, D. M. Wu, Y. L. Zheng, B. Hu, W. Cheng, Z. F. Zhang, and Q. Shan, "Ursolic acid improves high fat diet-induced cognitive impairments by blocking endoplasmic reticulum stress and I κ B kinase β /nuclear factor- κ B-mediated inflammatory pathways in mice," *Brain, Behavior, and Immunity*, vol. 25, pp. 1658–1667, Nov. 2011.
- [280] D. M. Both, K. Goodtzova, D. B. Yarosh, and D. A. Brown, "Liposome-encapsulated ursolic acid increases ceramides and collagen in human skin cells.," *Archives of dermatological research*, vol. 293, pp. 569–75, Jan. 2002.
- [281] X.-H. Wang, S.-Y. Zhou, Z.-Z. Qian, H.-L. Zhang, L.-H. Qiu, Z. Song, J. Zhao, P. Wang, X.-S. Hao, and H.-Q. Wang, "Evaluation of toxicity and single-dose pharmacokinetics of intravenous ursolic acid liposomes in healthy adult volunteers and patients with advanced solid tumors.," *Expert opinion on drug metabolism & toxicology*, vol. 9, pp. 117–25, Feb. 2013.
- [282] Z. Zhu, Z. Qian, Z. Yan, C. Zhao, H. Wang, and G. Ying, "A phase I pharmacokinetic study of ursolic acid nanoliposomes in healthy volunteers and patients with advanced solid tumors," *International Journal of Nanomedicine*, vol. 8, pp. 129–136, Jan. 2013.
- [283] M. A. Kotb, "Molecular mechanisms of ursodeoxycholic acid toxicity & side effects: Ursodeoxycholic acid freezes regeneration & induces hibernation mode," *International Journal of Molecular Sciences*, vol. 13, pp. 8882–8914, Jan. 2012.
- [284] M. P. Moisan, A. M. Minni, G. Dominguez, J. C. Helbling, A. Foury, N. Henkous, R. Dorey, and D. Béracochéa, "Role of corticosteroid binding globulin in the fast actions of glucocorticoids on the brain," *Steroids*, vol. 81, pp. 109–115, Mar. 2014.
- [285] D. E. Henley and S. L. Lightman, "New insights into corticosteroid-binding globulin and glucocorticoid delivery," *Neuroscience*, vol. 180, pp. 1–8, Apr. 2011.
- [286] E. V. Sivukhina and G. F. Jirikowski, "Adrenal steroids in the brain: Role of the intrinsic expression of corticosteroid-binding globulin (CBG) in the stress response," *Steroids*, vol. 81, pp. 70–73, Mar. 2014.
- [287] R. E. Olson, "Discovery of the lipoproteins, their role in fat transport and their significance as risk factors.," *The Journal of nutrition*, vol. 128, pp. 439S–443S, Feb. 1998.

- [288] L. Zhang, J. Song, G. Cavigliolo, B. Y. Ishida, S. Zhang, J. P. Kane, K. H. Weisgraber, M. N. Oda, K.-A. Rye, H. J. Pownall, and G. Ren, "Morphology and structure of lipoproteins revealed by an optimized negative-staining protocol of electron microscopy," *Journal of lipid research*, vol. 52, pp. 175–184, Jan. 2011.
- [289] I. Björkhem, S. Meaney, and A. M. Fogelman, "Brain Cholesterol: Long Secret Life behind a Barrier," *Arteriosclerosis, Thrombosis, and Vascular Biology*, vol. 24, pp. 806–815, May 2004.
- [290] Z. Balazs, U. Panzenboeck, A. Hammer, A. Sovic, O. Quehenberger, E. Malle, and W. Sattler, "Uptake and transport of high-density lipoprotein (HDL) and HDL-associated alpha-tocopherol by an in vitro blood-brain barrier model," *Journal of Neurochemistry*, vol. 89, pp. 939–950, May 2004.
- [291] I. Kratzer, K. Wernig, U. Panzenboeck, E. Bernhart, H. Reicher, R. Wronski, M. Windisch, A. Hammer, E. Malle, A. Zimmer, and W. Sattler, "Apolipoprotein A-I coating of protamine-oligonucleotide nanoparticles increases particle uptake and transcytosis in an in vitro model of the blood-brain barrier," *Journal of Controlled Release*, vol. 117, pp. 301–311, Feb. 2007.
- [292] L. Zhang and a. Eisenberg, "Multiple Morphologies of "Crew-Cut" Aggregates of Polystyrene-b-poly(acrylic acid) Block Copolymers.," *Science (New York, N.Y.)*, vol. 268, pp. 1728–1731, June 1995.
- [293] B. M. Discher, Y. Y. Won, D. S. Ege, J. C. Lee, F. S. Bates, D. E. Discher, and D. A. Hammer, "Polymersomes: tough vesicles made from diblock copolymers.," *Science (New York, N.Y.)*, vol. 284, pp. 1143–1146, May 1999.
- [294] T. Smart, H. Lomas, M. Massignani, M. V. Flores-Merino, L. R. Perez, and G. Battaglia, "Block copolymer nanostructures," *Nano Today*, vol. 3, no. 3, pp. 38–46, 2008.
- [295] J. F. Le Meins, O. Sandre, and S. Lecommandoux, "Recent trends in the tuning of polymersomes' membrane properties," *European Physical Journal E*, vol. 34, pp. 1–17, Mar. 2011.
- [296] J. Nicolas, S. Mura, D. Brambilla, N. Mackiewicz, and P. Couvreur, "Design, functionalization strategies and biomedical applications of targeted biodegradable/biocompatible polymer-based nanocarriers for drug delivery.," *Chemical Society reviews*, vol. 42, pp. 1147–235, Feb. 2013.
- [297] J. Hrkach, D. Von Hoff, M. M. Ali, E. Andrianova, J. Auer, T. Campbell, D. De Witt, M. Figa, M. Figueiredo, a. Horhota, S. Low, K. McDonnell, E. Peeke, B. Retnarajan, a. Sabnis, E. Schnipper, J. J. Song, Y. H. Song, J. Summa, D. Tompsett, G. Troiano, T. Van Geen Hoven, J. Wright, P. LoRusso, P. W. Kantoff, N. H. Bander, C. Sweeney, O. C. Farokhzad, R. Langer, and S. Zale, "Preclinical Development and Clinical Translation of a PSMA-Targeted Docetaxel Nanoparticle with a Differentiated Pharmacological Profile," *Science Translational Medicine*, vol. 4, pp. 128ra39–128ra39, Apr. 2012.
- [298] M. E. Davis, J. E. Zuckerman, C. H. J. Choi, D. Seligson, A. Tolcher, C. A. Alabi, Y. Yen, J. D. Heidel, and A. Ribas, "Evidence of RNAi in humans from systemically administered siRNA via targeted nanoparticles.," *Nature*, vol. 464, pp. 1067–1070, Apr. 2010.

- [299] D. E. Owens and N. A. Peppas, "Opsonization, biodistribution, and pharmacokinetics of polymeric nanoparticles," *International Journal of Pharmaceutics*, vol. 307, pp. 93–102, Jan. 2006.
- [300] M. P. Monopoli, D. Walczyk, A. Campbell, G. Elia, I. Lynch, F. Baldelli Bombelli, and K. A. Dawson, "Physical-Chemical aspects of protein corona: Relevance to in vitro and in vivo biological impacts of nanoparticles," *Journal of the American Chemical Society*, vol. 133, pp. 2525–2534, Mar. 2011.
- [301] S. M. Moghimi, I. Hamad, T. L. Andresen, K. Jørgensen, and J. Szebeni, "Methylation of the phosphate oxygen moiety of phospholipid-methoxy(polyethylene glycol) conjugate prevents PEGylated liposome-mediated complement activation and anaphylatoxin production.," *The FASEB journal : official publication of the Federation of American Societies for Experimental Biology*, vol. 20, pp. 2591–2593, Dec. 2006.
- [302] I. Hamad, C. A. Hunter, K. J. Rutt, Z. Liu, H. Dai, and M. S. Moghimi, "Complement activation by PEGylated single-walled carbon nanotubes is independent of C1q and alternative pathway turnover," *Molecular Immunology*, vol. 45, pp. 3797–3803, Aug. 2008.
- [303] A. Vonarbourg, C. Passirani, P. Saulnier, and J. P. Benoit, "Parameters influencing the stealthiness of colloidal drug delivery systems," *Biomaterials*, vol. 27, pp. 4356–4373, Aug. 2006.
- [304] R. K. Jain and T. Stylianopoulos, "Delivering nanomedicine to solid tumors.," *Nature reviews. Clinical oncology*, vol. 7, pp. 653–664, Nov. 2010.
- [305] P. J. Photos, L. Bacakova, B. Discher, F. S. Bates, and D. E. Discher, "Polymer vesicles in vivo: Correlations with PEG molecular weight," *Journal of Controlled Release*, vol. 90, pp. 323–334, July 2003.
- [306] S. Chen, L. Li, C. Zhao, and J. Zheng, "Surface hydration: Principles and applications toward low-fouling/nonfouling biomaterials," *Polymer*, vol. 51, pp. 5283–5293, Oct. 2010.
- [307] J. M. Harris and R. B. Chess, "Effect of pegylation on pharmaceuticals.," *Nature reviews. Drug discovery*, vol. 2, pp. 214–221, Mar. 2003.
- [308] M. C. Woodle, "Surface-modified liposomes: assessment and characterization for increased stability and prolonged blood circulation.," *Chemistry and physics of lipids*, vol. 64, pp. 249–262, Sept. 1993.
- [309] A. L. Lewis, "Phosphorylcholine-based polymers and their use in the prevention of biofouling," *Colloids and Surfaces B: Biointerfaces*, vol. 18, pp. 261–275, Oct. 2000.
- [310] Y. Iwasaki and K. Ishihara, "Cell membrane-inspired phospholipid polymers for developing medical devices with excellent biointerfaces," *Science and Technology of Advanced Materials*, vol. 13, p. 064101, Dec. 2012.
- [311] A. L. Klibanov, K. Maruyama, V. P. Torchilin, and L. Huang, "Amphipathic polyethyleneglycols effectively prolong the circulation time of liposomes.," *FEBS letters*, vol. 268, pp. 235–237, July 1990.

- [312] F. Alexis, E. Pridgen, L. K. Molnar, and O. C. Farokhzad, "Factors affecting the clearance and biodistribution of polymeric nanoparticles.," *Molecular pharmaceutics*, vol. 5, pp. 505–15, July 2008.
- [313] R. P. Brinkhuis, K. Stojanov, P. Laverman, J. Eilander, I. S. Zuhorn, F. P. J. T. Rutjes, and J. C. M. van Hest, "Size dependent biodistribution and SPECT imaging of (111)In-labeled polymersomes.," *Bioconjugate chemistry*, vol. 23, pp. 958–65, May 2012.
- [314] R. A. Petros and J. M. DeSimone, "Strategies in the design of nanoparticles for therapeutic applications.," *Nature reviews. Drug discovery*, vol. 9, pp. 615–627, July 2010.
- [315] J. R. Margit Pavelka, *Functional Ultrastructure An Atlas of Tissue Biology and Pathology*, vol. 59. 2005.
- [316] H. S. Choi, W. Liu, P. Misra, E. Tanaka, J. P. Zimmer, B. Itty Ipe, M. G. Bawendi, and J. V. Frangioni, "Renal clearance of quantum dots.," *Nature biotechnology*, vol. 25, pp. 1165–1170, Oct. 2007.
- [317] S. Mitragotri and J. Lahann, "Physical approaches to biomaterial design.," *Nature materials*, vol. 8, pp. 15–23, Jan. 2009.
- [318] L. Ilium, S. Davis, C. Wilson, N. Thomas, M. Frier, and J. Hardy, "Blood clearance and organ deposition of intravenously administered colloidal particles. The effects of particle size, nature and shape," *International Journal of Pharmaceutics*, vol. 12, pp. 135–146, Oct. 1982.
- [319] A. E. Nel, L. Mädler, D. Velegol, T. Xia, E. M. V. Hoek, P. Somasundaran, F. Klaessig, V. Castranova, and M. Thompson, "Understanding biophysicochemical interactions at the nano-bio interface.," *Nature materials*, vol. 8, pp. 543–557, July 2009.
- [320] K. Maruyama, T. Yuda, A. Okamoto, S. Kojima, A. Suginaka, and M. Iwatsuru, "Prolonged circulation time in vivo of large unilamellar liposomes composed of distearoyl phosphatidylcholine and cholesterol containing amphipathic poly(ethylene glycol).," *Biochimica et biophysica acta*, vol. 1128, pp. 44–49, Sept. 1992.
- [321] D. E. Discher and F. Ahmed, "Polymersomes.," *Annual review of biomedical engineering*, vol. 8, pp. 323–341, Jan. 2006.
- [322] Y. Geng, P. Dalhaimer, S. Cai, R. Tsai, M. Tewari, T. Minko, and D. E. Discher, "Shape effects of filaments versus spherical particles in flow and drug delivery.," *Nature nanotechnology*, vol. 2, pp. 249–255, Apr. 2007.
- [323] P. Decuzzi and M. Ferrari, "The adhesive strength of non-spherical particles mediated by specific interactions," *Biomaterials*, vol. 27, pp. 5307–5314, Oct. 2006.
- [324] S. Y. Lee, M. Ferrari, and P. Decuzzi, "Shaping nano-/micro-particles for enhanced vascular interaction in laminar flows.," *Nanotechnology*, vol. 20, p. 495101, Dec. 2009.

- [325] H. Gao, W. Shi, and L. B. Freund, "Mechanics of receptor-mediated endocytosis.," *Proceedings of the National Academy of Sciences of the United States of America*, vol. 102, pp. 9469–9474, July 2005.
- [326] P. Decuzzi and M. Ferrari, "The receptor-mediated endocytosis of nonspherical particles.," *Biophysical journal*, vol. 94, pp. 3790–3797, May 2008.
- [327] J. A. Champion and S. Mitragotri, "Role of target geometry in phagocytosis.," *Proceedings of the National Academy of Sciences of the United States of America*, vol. 103, pp. 4930–4934, Mar. 2006.
- [328] J. A. Champion and S. Mitragotri, "Shape induced inhibition of phagocytosis of polymer particles," *Pharmaceutical Research*, vol. 26, pp. 244–249, Jan. 2009.
- [329] V. V. Shuvaev, M. A. Ilies, E. Simone, S. Zaitsev, Y. Kim, S. Cai, A. Mahmud, T. Dziubla, S. Muro, D. E. Discher, and V. R. Muzykantov, "Endothelial targeting of antibody-decorated polymeric filomicelles," *ACS Nano*, vol. 5, pp. 6991–6999, Sept. 2011.
- [330] P. Kolhar, A. C. Anselmo, V. Gupta, K. Pant, B. Prabhakarpandian, E. Ruoslahti, and S. Mitragotri, "Using shape effects to target antibody-coated nanoparticles to lung and brain endothelium.," *Proceedings of the National Academy of Sciences of the United States of America*, vol. 110, pp. 10753–8, June 2013.
- [331] S. Barua, J.-W. Yoo, P. Kolhar, A. Wakankar, Y. R. Gokarn, and S. Mitragotri, "Particle shape enhances specificity of antibody-displaying nanoparticles.," *Proceedings of the National Academy of Sciences of the United States of America*, vol. 110, pp. 3270–5, Feb. 2013.
- [332] R. Sinha, G. J. Kim, S. Nie, and D. M. Shin, "Nanotechnology in cancer therapeutics: bioconjugated nanoparticles for drug delivery.," *Molecular cancer therapeutics*, vol. 5, pp. 1909–1917, Aug. 2006.
- [333] A. Gabizon, H. Shmeeda, A. T. Horowitz, and S. Zalipsky, "Tumor cell targeting of liposome-entrapped drugs with phospholipid-anchored folic acid-PEG conjugates," *Advanced Drug Delivery Reviews*, vol. 56, pp. 1177–1192, Apr. 2004.
- [334] E. Ruoslahti, S. N. Bhatia, and M. J. Sailor, "Targeting of drugs and nanoparticles to tumors," *Journal of Cell Biology*, vol. 188, pp. 759–768, Mar. 2010.
- [335] B. S. Jacobson, D. B. Stolz, and J. E. Schnitzer, "Identification of endothelial cell-surface proteins as targets for diagnosis and treatment of disease.," *Nature medicine*, vol. 2, pp. 482–484, Apr. 1996.
- [336] E. A. Murphy, B. K. Majeti, L. a. Barnes, M. Makale, S. M. Weis, K. Lutu-Fuga, W. Wrasidlo, and D. A. Cheresh, "Nanoparticle-mediated drug delivery to tumor vasculature suppresses metastasis.," *Proceedings of the National Academy of Sciences of the United States of America*, vol. 105, pp. 9343–9348, July 2008.
- [337] D. Simberg, T. Duza, J. H. Park, M. Essler, J. Pilch, L. Zhang, A. M. Derfus, M. Yang, R. M. Hoffman, S. Bhatia, M. J. Sailor, and E. Ruoslahti, "Biomimetic amplification of nanoparticle homing to tumors.," *Proceedings of the National Academy of Sciences of the United States of America*, vol. 104, pp. 932–936, Jan. 2007.

- [338] M. F. Renschler, R. R. Bhatt, W. J. Dower, and R. Levy, "Synthetic peptide ligands of the antigen binding receptor induce programmed cell death in a human B-cell lymphoma.," *Proceedings of the National Academy of Sciences of the United States of America*, vol. 91, pp. 3623–3627, Apr. 1994.
- [339] M. Massignani, C. Lopresti, A. Blanazs, J. Madsen, S. P. Armes, A. L. Lewis, and G. Battaglia, "Controlling cellular uptake by surface chemistry, size, and surface topology at the nanoscale," *Small*, vol. 5, pp. 2424–2432, Nov. 2009.
- [340] C. Lopresti, M. Massignani, C. Fernyhough, A. Blanazs, A. J. Ryan, J. Madsen, N. J. Warren, S. P. Armes, A. L. Lewis, S. Chirasatitsin, A. J. Engler, and G. Battaglia, "Controlling polymersome surface topology at the nanoscale by membrane confined polymer/polymer phase separation," *ACS Nano*, vol. 5, pp. 1775–1784, Mar. 2011.
- [341] H. E. Colley, V. Hearnden, M. Avila-Olias, D. Cecchin, I. Canton, J. Madsen, S. MacNeil, N. Warren, K. Hu, J. A. McKeating, S. P. Armes, C. Murdoch, M. H. Thornhill, and G. Battaglia, "Polymersome-mediated delivery of combination anticancer therapy to head and neck cancer cells: 2D and 3D in vitro evaluation.," *Molecular pharmaceuticals*, vol. 11, pp. 1176–88, Apr. 2014.
- [342] A. Boullier, P. Friedman, R. Harkewicz, K. Hartvigsen, S. R. Green, F. Almazan, E. A. Dennis, D. Steinberg, J. L. Witztum, and O. Quehenberger, "Phosphocholine as a pattern recognition ligand for CD36.," *Journal of lipid research*, vol. 46, pp. 969–976, May 2005.
- [343] Z. Pang, W. Lu, H. Gao, K. Hu, J. Chen, C. Zhang, X. Gao, X. Jiang, and C. Zhu, "Preparation and brain delivery property of biodegradable polymersomes conjugated with OX26," *Journal of Controlled Release*, vol. 128, pp. 120–127, June 2008.
- [344] S. Méresse, C. Delbart, J. C. Fruchart, and R. Cecchelli, "Low-density lipoprotein receptor on endothelium of brain capillaries.," *Journal of neurochemistry*, vol. 53, pp. 340–345, Nov. 1989.
- [345] Z. M. Qian, H. Li, H. Sun, and K. Ho, "Targeted drug delivery via the transferrin receptor-mediated endocytosis pathway.," *Pharmacological reviews*, vol. 54, pp. 561–587, Dec. 2002.
- [346] J. Huwyler, D. Wu, and W. M. Pardridge, "Brain drug delivery of small molecules using immunoliposomes.," *Proceedings of the National Academy of Sciences of the United States of America*, vol. 93, pp. 14164–14169, Nov. 1996.
- [347] K. Hu, J. Li, Y. Shen, W. Lu, X. Gao, Q. Zhang, and X. Jiang, "Lactoferrin-conjugated PEG-PLA nanoparticles with improved brain delivery: In vitro and in vivo evaluations," *Journal of Controlled Release*, vol. 134, pp. 55–61, Feb. 2009.
- [348] Y. Hu, W. Lu, G. Chen, P. Wang, Z. Chen, Y. Zhou, M. Ogasawara, D. Trachootham, L. Feng, H. Pelicano, P. J. Chiao, M. J. Keating, G. Garcia-Manero, and P. Huang, "K-rasG12V transformation leads to mitochondrial dysfunction and a metabolic switch from oxidative phosphorylation to glycolysis," *Cell Research*, vol. 22, pp. 399–412, Aug. 2012.

- [349] A. Yu, Z. Pang, W. Lu, Q. Yin, H. Gao, and X. Jiang, "Self-assembled polymerosomes conjugated with lactoferrin as novel drug carrier for brain delivery," *Pharmaceutical Research*, vol. 29, pp. 83–96, Jan. 2012.
- [350] Z. Pang, L. Feng, R. Hua, J. Chen, H. Gao, S. Pan, X. Jiang, and P. Zhang, "Lactoferrin-conjugated biodegradable polymersome holding doxorubicin and tetrandrine for chemotherapy of glioma rats," *Molecular Pharmaceutics*, vol. 7, pp. 1995–2005, Dec. 2010.
- [351] Y. C. Chen, C. F. Chiang, L. F. Chen, S. C. Liao, W. Y. Hsieh, and W. L. Lin, "Polymerosomes conjugated with des-octanoyl ghrelin for the delivery of therapeutic and imaging agents into brain tissues," *Biomaterials*, vol. 35, pp. 2051–2065, Feb. 2014.
- [352] T. Pflanzner, M. C. Janko, B. André-Dohmen, S. Reuss, S. Weggen, A. J. M. Roebroek, C. R. W. Kuhlmann, and C. U. Pietrzik, "LRP1 mediates bidirectional transcytosis of amyloid- β across the blood-brain barrier," *Neurobiology of Aging*, vol. 32, pp. 2323.e1–11, Dec. 2011.
- [353] K. Shao, R. Huang, J. Li, L. Han, L. Ye, J. Lou, and C. Jiang, "Angiopep-2 modified PE-PEG based polymeric micelles for amphotericin B delivery targeted to the brain," *Journal of Controlled Release*, vol. 147, pp. 118–126, Oct. 2010.
- [354] M. Demeule, A. Régina, C. Ché, J. Poirier, T. Nguyen, R. Gabathuler, J.-P. Castaigne, and R. Béliveau, "Identification and design of peptides as a new drug delivery system for the brain.," *The Journal of pharmacology and experimental therapeutics*, vol. 324, pp. 1064–1072, Mar. 2008.
- [355] H. Xin, X. Sha, X. Jiang, W. Zhang, L. Chen, and X. Fang, "Anti-glioblastoma efficacy and safety of paclitaxel-loading Angiopep-conjugated dual targeting PEG-PCL nanoparticles," *Biomaterials*, vol. 33, pp. 8167–8176, Nov. 2012.
- [356] X. Tian, S. Nyberg, P. Sharp, J. Madsen, S. P. Armes, J. Berwick, M. Azzouz, N. J. Abbott, and G. Battaglia, "LRP1-mediated intracellular delivery of antibody to the Central Nervous System," *[In Preparation]*, 2014.
- [357] J. Du, Y. Tang, A. L. Lewis, and S. P. Armes, "pH-sensitive vesicles based on a biocompatible zwitterionic diblock copolymer," *Journal of the American Chemical Society*, vol. 127, pp. 17982–17983, Dec. 2005.
- [358] H. Lomas, M. Massignani, K. A. Abdullah, I. Canton, C. Lo Presti, S. MacNeil, J. Du, A. Blanazs, J. Madsen, S. P. Armes, A. L. Lewis, and G. Battaglia, "Non-cytotoxic polymer vesicles for rapid and efficient intracellular delivery.," *Faraday discussions*, vol. 139, pp. 143–59; discussion 213–28, 419–20, Jan. 2008.
- [359] Y. L. Hu, W. Qi, F. Han, J. Z. Shao, and J. Q. Gao, "Toxicity evaluation of biodegradable chitosan nanoparticles using a zebrafish embryo model.," *International journal of nanomedicine*, vol. 6, pp. 3351–3359, Jan. 2011.
- [360] Z. H. Wang, Z. Y. Wang, C. S. Sun, C. Y. Wang, T. Y. Jiang, and S. L. Wang, "Trimethylated chitosan-conjugated PLGA nanoparticles for the delivery of drugs to the brain," *Biomaterials*, vol. 31, pp. 908–915, Feb. 2010.

- [361] W. Ying, "The nose may help the brain: intranasal drug delivery for treating neurological diseases," *Future Neurology*, vol. 3, pp. 1–4, 2008.
- [362] F. W. H. M. Merkus and M. P. Van Den Berg, "Can nasal drug delivery bypass the blood-brain barrier? Questioning the direct transport theory," *Drugs in R and D*, vol. 8, pp. 133–144, Jan. 2007.
- [363] X. Gao, B. Wu, Q. Zhang, J. Chen, J. Zhu, W. Zhang, Z. Rong, H. Chen, and X. Jiang, "Brain delivery of vasoactive intestinal peptide enhanced with the nanoparticles conjugated with wheat germ agglutinin following intranasal administration," *Journal of Controlled Release*, vol. 121, pp. 156–167, Aug. 2007.
- [364] Q. Liu, Y. Shen, J. Chen, X. Gao, C. Feng, L. Wang, Q. Zhang, and X. Jiang, "Nose-to-brain transport pathways of wheat germ agglutinin conjugated PEG-PLA nanoparticles," *Pharmaceutical Research*, vol. 29, pp. 546–558, Feb. 2012.
- [365] Z. Wen, Z. Yan, K. Hu, Z. Pang, X. Cheng, L. Guo, Q. Zhang, X. Jiang, L. Fang, and R. Lai, "Odorranalectin-conjugated nanoparticles: Preparation, brain delivery and pharmacodynamic study on Parkinson's disease following intranasal administration," *Journal of Controlled Release*, vol. 151, pp. 131–138, Apr. 2011.
- [366] F. Ahmed, R. I. Pakunlu, A. Brannan, F. Bates, T. Minko, and D. E. Discher, "Biodegradable polymersomes loaded with both paclitaxel and doxorubicin permeate and shrink tumors, inducing apoptosis in proportion to accumulated drug," *Journal of Controlled Release*, vol. 116, pp. 150–158, Nov. 2006.
- [367] B. Alberts, A. Johnson, J. Lewis, R. Martin, R. Keith, and W. Peter, "Transport into the Cell from the Plasma Membrane: Endocytosis," in *Molecular Biology of the Cell: 4th Edition*, p. online edition ncbi.nlm.nih.gov/books/NBK26870/, Garland Science, 2002.
- [368] I. Canton and G. Battaglia, "Endocytosis at the nanoscale," *Chemical Society Reviews*, vol. 41, pp. 2718–2739, Apr. 2012.
- [369] J. A. Swanson, "Shaping cups into phagosomes and macropinosomes," *Nature reviews. Molecular cell biology*, vol. 9, pp. 639–649, Aug. 2008.
- [370] J. P. Lim and P. A. Gleeson, "Macropinocytosis: an endocytic pathway for internalising large gulps," *Immunology and Cell Biology*, vol. 89, pp. 836–843, Nov. 2011.
- [371] J. E. Heuser and T. S. Reese, "Evidence for recycling of synaptic vesicle membrane during transmitter release at the frog neuromuscular junction.," *Journal of Cell Biology*, vol. 57, pp. 315–344, May 1973.
- [372] M. Ehrlich, W. Boll, A. Van Oijen, R. Hariharan, K. Chandran, M. L. Nibert, and T. Kirchhausen, "Endocytosis by random initiation and stabilization of clathrin-coated pits," *Cell*, vol. 118, pp. 591–605, Sept. 2004.
- [373] J. Aggeler and Z. Werb, "Initial events during phagocytosis by macrophages viewed from outside and inside the cell: Membrane particle interactions and clathrin," *Journal of Cell Biology*, vol. 94, pp. 613–623, Sept. 1982.

- [374] P. Lajoie and I. R. Nabi, "Lipid rafts, caveolae, and their endocytosis," *International Review of Cell and Molecular Biology*, vol. 282, pp. 135–163, Jan. 2010.
- [375] P. G. Frank, S. Pavlides, and M. P. Lisanti, "Caveolae and transcytosis in endothelial cells: Role in atherosclerosis," *Cell and Tissue Research*, vol. 335, pp. 41–47, Jan. 2009.
- [376] Z. Wang, C. Tiruppathi, R. D. Minshall, and A. B. Malik, "Size and dynamics of caveolae studied using nanoparticles in living endothelial cells," *ACS Nano*, vol. 3, pp. 4110–4116, Dec. 2009.
- [377] X. Banquy, F. Suarez, A. Argaw, J.-M. Rabanel, P. Grutter, J.-F. Bouchard, P. Hildgen, and S. Giasson, "Effect of mechanical properties of hydrogel nanoparticles on macrophage cell uptake," *Soft Matter*, vol. 5, p. 3984, Oct. 2009.
- [378] S. E. a. Gratton, P. A. Ropp, P. D. Pohlhaus, J. C. Luft, V. J. Madden, M. E. Napier, and J. M. DeSimone, "The effect of particle design on cellular internalization pathways.," *Proceedings of the National Academy of Sciences of the United States of America*, vol. 105, pp. 11613–11618, Aug. 2008.
- [379] J. Rejman, V. Oberle, I. S. Zuhorn, and D. Hoekstra, "Size-dependent internalization of particles via the pathways of clathrin- and caveolae-mediated endocytosis.," *The Biochemical journal*, vol. 377, pp. 159–169, Jan. 2004.
- [380] T. Nakai, T. Kanamori, S. Sando, and Y. Aoyama, "Remarkably size-regulated cell invasion by artificial viruses. Saccharide-dependent self-aggregation of glycoviruses and its consequences in glycoviral gene delivery," *Journal of the American Chemical Society*, vol. 125, pp. 8465–8475, July 2003.
- [381] W. Jiang, B. Y. S. Kim, J. T. Rutka, and W. C. W. Chan, "Nanoparticle-mediated cellular response is size-dependent.," *Nature nanotechnology*, vol. 3, pp. 145–150, Mar. 2008.
- [382] H. Yuan, J. Li, G. Bao, and S. Zhang, "Variable nanoparticle-cell adhesion strength regulates cellular uptake," *Physical Review Letters*, vol. 105, Sept. 2010.
- [383] R. Lipowsky and H.-G. Döbereiner, "Vesicles in contact with nanoparticles and colloids," *Europhysics Letters (EPL)*, vol. 43, pp. 219–225, July 2007.
- [384] S. K. Banerji and M. A. Hayes, "Examination of nonendocytotic bulk transport of nanoparticles across phospholipid membranes," *Langmuir*, vol. 23, pp. 3305–3313, Mar. 2007.
- [385] O. Le Bihan, P. Bonnafous, L. Marak, T. Bickel, S. Trépout, S. Mornet, F. De Haas, H. Talbot, J. C. Taveau, and O. Lambert, "Cryo-electron tomography of nanoparticle transmigration into liposome," *Journal of Structural Biology*, vol. 168, pp. 419–425, Dec. 2009.
- [386] Y. Zhao, X. Sun, G. Zhang, B. G. Trewyn, I. I. Slowing, and V. S. Y. Lin, "Interaction of mesoporous silica nanoparticles with human red blood cell membranes: Size and surface effects," *ACS Nano*, vol. 5, pp. 1366–1375, Feb. 2011.

- [387] B. D. Chithrani, A. A. Ghazani, and W. C. W. Chan, "Determining the size and shape dependence of gold nanoparticle uptake into mammalian cells," *Nano Letters*, vol. 6, pp. 662–668, Apr. 2006.
- [388] A. Chaudhuri, G. Battaglia, and R. Golestanian, "The effect of interactions on the cellular uptake of nanoparticles," *Physical biology*, vol. 8, p. 046002, Aug. 2011.
- [389] A. V. Nicola, H. C. Aguilar, J. Mercer, B. Ryckman, and C. M. Wiethoff, "Virus entry by endocytosis," *Advances in Virology*, vol. 2013, pp. 803–33, Jan. 2013.
- [390] E. Leupold, H. Nikolenko, and M. Dathe, "Apolipoprotein E peptide-modified colloidal carriers: The design determines the mechanism of uptake in vascular endothelial cells," *Biochimica et Biophysica Acta - Biomembranes*, vol. 1788, pp. 442–449, Feb. 2009.
- [391] E. Hutter, S. Boridy, S. Labrecque, M. Lalancette-Hébert, J. Kriz, F. M. Winnik, and D. Maysinger, "Microglial response to gold nanoparticles," *ACS Nano*, vol. 4, pp. 2595–2606, May 2010.
- [392] I. Canton, M. Massignani, N. Patikarnmonthon, L. Chierico, J. Robertson, S. A. Renshaw, N. J. Warren, J. P. Madsen, S. P. Armes, A. L. Lewis, and G. Battaglia, "Fully synthetic polymer vesicles for intracellular delivery of antibodies in live cells," *FASEB Journal*, vol. 27, pp. 98–108, Jan. 2013.
- [393] M. Massignani, *Polymersomes for intracellular delivery: Mechanism of action and applications*. PhD thesis, The University of Sheffield, 2011.
- [394] Y. Zeng, N. Tao, K. N. Chung, J. E. Heuser, and D. M. Lublin, "Endocytosis of Oxidized Low Density Lipoprotein through Scavenger Receptor CD36 Utilizes a Lipid Raft Pathway That Does Not Require Caveolin-1," *Journal of Biological Chemistry*, vol. 278, pp. 45931–45936, Nov. 2003.
- [395] E. Blanchard, S. Belouzard, L. Goueslain, T. Wakita, J. Dubuisson, C. Wychowski, and Y. Rouillé, "Hepatitis C virus entry depends on clathrin-mediated endocytosis," *Journal of virology*, vol. 80, pp. 6964–6972, July 2006.
- [396] L. Shen, J. Du, S. P. Armes, and S. Liu, "Kinetics of pH-induced formation and dissociation of polymeric vesicles assembled from a water-soluble zwitterionic diblock copolymer," *Langmuir*, vol. 24, pp. 10019–10025, Sept. 2008.
- [397] F. Ahmed, R. I. Pakunlu, G. Srinivas, A. Brannan, F. Bates, M. L. Klein, T. Minko, and D. E. Discher, "Shrinkage of a rapidly growing tumor by drug-loaded polymersomes: pH-triggered release through copolymer degradation," *Molecular Pharmaceutics*, vol. 3, pp. 340–350, Jan. 2006.
- [398] Y. Kim, M. Tewari, J. D. Pajeroski, S. Cai, S. Sen, J. Williams, S. Sirsi, G. Lutz, and D. E. Discher, "Polymersome delivery of siRNA and antisense oligonucleotides," *Journal of Controlled Release*, vol. 134, pp. 132–140, Mar. 2009.
- [399] F. Najafi and M. N. Sarbolouki, "Biodegradable micelles/polymersomes from fumaric/sebacic acids and poly(ethylene glycol)," *Biomaterials*, vol. 24, pp. 1175–1182, Mar. 2003.

- [400] F. Ahmed and D. E. Discher, "Self-porating polymersomes of PEG-PLA and PEG-PCL: Hydrolysis-triggered controlled release vesicles," *Journal of Controlled Release*, vol. 96, pp. 37–53, Apr. 2004.
- [401] A. Napoli, M. Valentini, N. Tirelli, M. Müller, and J. a. Hubbell, "Oxidation-responsive polymeric vesicles.," *Nature materials*, vol. 3, pp. 183–189, Mar. 2004.
- [402] M. Massignani, H. Lomas, and G. Battaglia, "Polymersomes: A synthetic biological approach to encapsulation and delivery," *Advances in Polymer Science*, vol. 229, pp. 115–154, 2010.
- [403] G. Battaglia, A. J. Ryan, and S. Tomas, "Polymeric vesicle permeability: A facile chemical assay," *Langmuir*, vol. 22, pp. 4910–4913, May 2006.
- [404] M. Massignani, I. Canton, T. Sun, V. Hearnden, S. MacNeil, A. Blanzs, S. P. Armes, A. Lewis, and G. Battaglia, "Enhanced fluorescence imaging of live cells by effective cytosolic delivery of probes," *PLoS ONE*, vol. 5, p. e10459, Jan. 2010.
- [405] E. E. Meyer, K. J. Rosenberg, and J. Israelachvili, "Recent progress in understanding hydrophobic interactions.," *Proceedings of the National Academy of Sciences of the United States of America*, vol. 103, pp. 15739–15746, Oct. 2006.
- [406] J. N. Israelachvili, *Intermolecular and Surface Forces*. Academic Press; 3 edition, 2011.
- [407] G. Battaglia and A. J. Ryan, "Effect of amphiphile size on the transformation from a lyotropic gel to a vesicular dispersion," *Macromolecules*, vol. 39, pp. 798–805, Jan. 2006.
- [408] S. Jain and F. S. Bates, "Consequences of Nonergodicity in Aqueous Binary PEO-PB Micellar Dispersions," *Macromolecules*, vol. 37, pp. 1511–1523, Feb. 2004.
- [409] G. Battaglia and A. J. Ryan, "The evolution of vesicles from bulk lamellar gels.," *Nature materials*, vol. 4, pp. 869–876, Nov. 2005.
- [410] G. Battaglia and A. J. Ryan, "Bilayers and interdigitation in block copolymer vesicles," *Journal of the American Chemical Society*, vol. 127, pp. 8757–8764, June 2005.
- [411] J. C. Lee, M. Santore, F. S. Bates, and D. E. Discher, "From Membranes to Melts, Rouse to Reptation: Diffusion in Polymersome versus Lipid Bilayers," *Macromolecules*, vol. 35, pp. 323–326, Jan. 2002.
- [412] G. Battaglia and A. J. Ryan, "Pathways of polymeric vesicle formation," *Journal of Physical Chemistry B*, vol. 110, pp. 10272–10279, June 2006.
- [413] C. Pegoraro, D. Cecchin, L. S. Gracia, N. Warren, J. Madsen, S. P. Armes, A. Lewis, S. MacNeil, and G. Battaglia, "Enhanced drug delivery to melanoma cells using PMPC-PDPA polymersomes," *Cancer Letters*, vol. 334, pp. 328–337, Feb. 2013.

- [414] Y. Ma, Y. Tang, N. C. Billingham, S. P. Armes, A. L. Lewis, A. W. Lloyd, and J. P. Salvage, "Well-defined biocompatible block copolymers via atom transfer radical polymerization of 2-methacryloyloxyethyl phosphorylcholine in protic media," *Macromolecules*, vol. 36, pp. 3475–3484, May 2003.
- [415] J. Madsen, N. J. Warren, S. P. Armes, and A. L. Lewis, "Synthesis of rhodamine 6G-based compounds for the ATRP synthesis of fluorescently labeled biocompatible polymers," *Biomacromolecules*, vol. 12, pp. 2225–2234, June 2011.
- [416] P. R. Berne J.B., *Dynamic Light Scattering: With Applications to Chemistry, Biology, and Physics*. Courier Dover Publications, 2000.
- [417] S. W. Provencher, "Contin: A general purpose constrained regularization program for inverting noisy linear algebraic and integral equations," *Computer Physics Communications*, vol. 35, pp. C–818–C–819, 1984.
- [418] S.-G. Huang, "Development of a High Throughput Screening Assay for Mitochondrial Membrane Potential in Living Cells," *Journal of Biomolecular Screening*, vol. 7, pp. 383–389, Aug. 2002.
- [419] B. Ehrenberg, V. Montana, M. D. Wei, J. P. Wuskell, and L. M. Loew, "Membrane potential can be determined in individual cells from the nernstian distribution of cationic dyes.," *Biophysical journal*, vol. 53, pp. 785–794, May 1988.
- [420] L. J. Jones, M. Gray, S. T. Yue, R. P. Haugland, and V. L. Singer, "Sensitive determination of cell number using the CyQUANT?? cell proliferation assay," *Journal of Immunological Methods*, vol. 254, pp. 85–98, Aug. 2001.
- [421] S. Information, "CyQUANT NF Cell Proliferation Assay Kit," 2006.
- [422] Perkin Elmer, "Luminescence ATP Detection Assay System," 2002.
- [423] C. Thomas, R. Pellicciari, M. Pruzanski, J. Auwerx, and K. Schoonjans, "Targeting bile-acid signalling for metabolic diseases.," *Nature reviews. Drug discovery*, vol. 7, pp. 678–693, Aug. 2008.
- [424] A. Dalpiaz, C. Contado, L. Mari, D. Perrone, B. Pavan, G. Paganetto, M. Hanusková, E. Vighi, and E. Leo, "Development and characterization of PLGA nanoparticles as delivery systems of a prodrug of zidovudine obtained by its conjugation with ursodeoxycholic acid.," *Drug delivery*, vol. 7544, pp. 1–12, Oct. 2013.
- [425] J. H. Park, S. Kwon, J. O. Nam, R. W. Park, H. Chung, S. B. Seo, I. S. Kim, I. C. Kwon, and S. Y. Jeong, "Self-assembled nanoparticles based on glycol chitosan bearing 5 β -cholanic acid for RGD peptide delivery," *Journal of Controlled Release*, vol. 95, pp. 579–588, Mar. 2004.
- [426] L. Yang, Z. Sun, Y. Zu, C. Zhao, X. Sun, Z. Zhang, and L. Zhang, "Physicochemical properties and oral bioavailability of ursolic acid nanoparticles using supercritical anti-solvent (SAS) process," *Food Chemistry*, vol. 132, pp. 319–325, May 2012.
- [427] S. K. Han, Y. I. Ko, S. J. Park, I. J. Jin, and Y. M. Kim, "Oleanolic acid and ursolic acid stabilize liposomal membranes," *Lipids*, vol. 32, pp. 769–773, July 1997.

- [428] B. Ruozi, R. Battini, M. Montanari, A. Mucci, G. Tosi, F. Forni, and M. A. Vandelli, "DOTAP/UDCA vesicles: novel approach in oligonucleotide delivery," *Nanomedicine: Nanotechnology, Biology, and Medicine*, vol. 3, pp. 1–13, Mar. 2007.
- [429] S. Güldütuna, B. Deisinger, A. Weiss, H. J. Freisleben, G. Zimmer, P. Sipos, and U. Leuschner, "Ursodeoxycholate stabilizes phospholipid-rich membranes and mimics the effect of cholesterol: Investigations on large unilamellar vesicles," *Biochimica et Biophysica Acta - Biomembranes*, vol. 1326, pp. 265–274, June 1997.
- [430] R. T. Pearson, N. J. Warren, A. L. Lewis, S. P. Armes, and G. Battaglia, "Effect of pH and Temperature on PMPCPDPA Copolymer Self-Assembly," *Macromolecules*, vol. 46, pp. 1400–1407, Feb. 2013.
- [431] G. Battaglia, S. Tomas, and A. J. Ryan, "Lamellarsomes: metastable polymeric multilamellar aggregates," *Soft Matter*, vol. 3, p. 470, Mar. 2007.
- [432] S. Jain and F. S. Bates, "On the origins of morphological complexity in block copolymer surfactants.," *Science (New York, N.Y.)*, vol. 300, pp. 460–464, Apr. 2003.
- [433] R. Dimova, U. Seifert, and B. Pouligny, "Hyperviscous diblock copolymer vesicles," *The European Physical Journal E*, vol. 250, pp. 241–250, Mar. 2002.
- [434] S. J. Holder and N. A. J. M. Sommerdijk, "New micellar morphologies from amphiphilic block copolymers: disks, toroids and bicontinuous micelles," *Polymer Chemistry*, vol. 2, p. 1018, Apr. 2011.
- [435] J. D. Robertson, G. Yealland, M. Avila-Olias, L. Chierico, O. Bandmann, S. A. Renshaw, and G. Battaglia, "PH-sensitive tubular polymersomes: Formation and applications in cellular delivery," *ACS Nano*, vol. 8, pp. 4650–4661, Apr. 2014.
- [436] S. Winzen, M. Bernhardt, D. Schaeffel, A. Koch, M. Kappl, K. Koynov, K. Landfester, and A. Kroeger, "Submicron hybrid vesicles consisting of polymerlipid and polymercholesterol blends," *Soft Matter*, vol. 9, p. 5883, June 2013.
- [437] D. a. Mannock, R. N. A. H. Lewis, T. P. W. McMullen, and R. N. McElhaney, "The effect of variations in phospholipid and sterol structure on the nature of lipid-sterol interactions in lipid bilayer model membranes," *Chemistry and Physics of Lipids*, vol. 163, pp. 403–448, June 2010.
- [438] R. Crawford, B. Dogdas, E. Keough, R. M. Haas, W. Wepukhulu, S. Krotzer, P. A. Burke, L. Sepp-Lorenzino, A. Bagchi, and B. J. Howell, "Analysis of lipid nanoparticles by Cryo-EM for characterizing siRNA delivery vehicles," *International Journal of Pharmaceutics*, vol. 403, pp. 237–244, Jan. 2011.
- [439] A. Sharma and R. Khanna, "Pattern Formation in Unstable Thin Liquid Films," *Physical Review Letters*, vol. 81, pp. 3463–3466, Oct. 1998.
- [440] P. F. Green and R. Limary, "Block copolymer thin films: Pattern formation and phase behavior," *Advances in Colloid and Interface Science*, vol. 94, pp. 53–81, Nov. 2001.

- [441] H.-G. Döbereiner, *Perspectives in Supramolecular Chemistry*, vol. 6 of *Perspectives in Supramolecular Chemistry*. Chichester, UK: John Wiley & Sons, Ltd., Nov. 1999.
- [442] H. Igimi and M. C. Carey, "pH-Solubility relations of chenodeoxycholic and ursodeoxycholic acids: physical-chemical basis for dissimilar solution and membrane phenomena.," *Journal of lipid research*, vol. 21, pp. 72–90, Jan. 1980.
- [443] Y. Moroi, M. Kitagawa, and H. Itoh, "Aqueous solubility and acidity constants of cholic, deoxycholic, chenodeoxycholic, and ursodeoxycholic acids.," *Journal of lipid research*, vol. 33, pp. 49–53, 1992.
- [444] T. Hisadome, T. Nakama, H. Itoh, and T. Furusawa, "Physical-chemical properties of chenodeoxycholic acid and ursodeoxycholic acid.," *Gastroenterologia Japonica*, vol. 15, pp. 257–263, Jan. 1980.
- [445] M. E. Haberland and J. A. Reynolds, "Self-association of cholesterol in aqueous solution.," *Proceedings of the National Academy of Sciences of the United States of America*, vol. 70, pp. 2313–2316, Aug. 1973.
- [446] H. Martinez-Seara, T. Róg, M. Pasenkiewicz-Gierula, I. Vattulainen, M. Karttunen, and R. Reigada, "Interplay of unsaturated phospholipids and cholesterol in membranes: effect of the double-bond position.," *Biophysical journal*, vol. 95, pp. 3295–3305, Oct. 2008.
- [447] H. Zhang, X. Li, J. Ding, H. Xu, X. Dai, Z. Hou, K. Zhang, K. Sun, and W. Sun, "Delivery of ursolic acid (UA) in polymeric nanoparticles effectively promotes the apoptosis of gastric cancer cells through enhanced inhibition of cyclooxygenase 2 (COX-2).," *International Journal of Pharmaceutics*, vol. 441, pp. 261–268, Jan. 2013.
- [448] X. Li, R. Li, X. Qian, Y. Ding, Y. Tu, R. Guo, Y. Hu, X. Jiang, W. Guo, and B. Liu, "Superior antitumor efficiency of cisplatin-loaded nanoparticles by intratumoral delivery with decreased tumor metabolism rate," *European Journal of Pharmaceutics and Biopharmaceutics*, vol. 70, pp. 726–734, Nov. 2008.
- [449] G. Battaglia and A. J. Ryan, "Neuron-like tubular membranes made of diblock copolymer amphiphiles," *Angewandte Chemie - International Edition*, vol. 45, pp. 2052–2056, Mar. 2006.
- [450] W.-C. Hung, M.-T. Lee, F.-Y. Chen, and H. W. Huang, "The condensing effect of cholesterol in lipid bilayers.," *Biophysical journal*, vol. 92, pp. 3960–3967, June 2007.
- [451] E. Falck, M. Patra, M. Karttunen, M. T. Hyvönen, and I. Vattulainen, "Lessons of slicing membranes: interplay of packing, free area, and lateral diffusion in phospholipid/cholesterol bilayers.," *Biophysical journal*, vol. 87, pp. 1076–1091, Aug. 2004.
- [452] D. A. Fahey, M. C. Carey, and J. M. Donovan, "Bile acid/phosphatidylcholine interactions in mixed monomolecular layers: differences in condensation effects but not interfacial orientation between hydrophobic and hydrophilic bile acid species.," *Biochemistry*, vol. 34, pp. 10886–10897, Aug. 1995.

- [453] B. Beaumelle, M. Alami, and C. R. Hopkins, "ATP-dependent translocation of ricin across the membrane of purified endosomes," *Journal of Biological Chemistry*, vol. 268, pp. 23661–23669, Nov. 1993.
- [454] B. L. Fredericksen, B. L. Wei, J. Yao, T. Luo, and J. V. Garcia, "Inhibition of endosomal/lysosomal degradation increases the infectivity of human immunodeficiency virus," *Journal of virology*, vol. 76, pp. 11440–6, Nov. 2002.
- [455] P. A. Conrad, E. J. Smart, Y. S. Ying, R. G. W. Anderson, and G. S. Bloom, "Caveolin cycles between plasma membrane caveolae and the Golgi complex by microtubule-dependent and microtubule-independent steps," *Journal of Cell Biology*, vol. 131, pp. 1421–1433, Dec. 1995.
- [456] R. F. Collins, N. Touret, H. Kuwata, N. N. Tandon, S. Grinstein, and W. S. Trimble, "Uptake of oxidized low density lipoprotein by CD36 occurs by an actin-dependent pathway distinct from macropinocytosis," *Journal of Biological Chemistry*, vol. 284, pp. 30288–30297, Oct. 2009.
- [457] R. F. Murphy, "Maturation models for endosome and lysosome biogenesis," *Trends in cell biology*, vol. 1, pp. 77–82, Oct. 1991.
- [458] D. M. Sipe, A. Jesurum, and R. F. Murphy, "Absence of Na⁺,K⁺-ATPase regulation of endosomal acidification in K562 erythroleukemia cells: Analysis via inhibition of transferrin recycling by low temperatures," *Journal of Biological Chemistry*, vol. 266, pp. 3469–3474, Feb. 1991.
- [459] J. Madsen, I. Canton, N. J. Warren, E. Themistou, A. Blanz, B. Ustbas, X. Tian, R. Pearson, G. Battaglia, A. L. Lewis, and S. P. Armes, "Nile blue-based nano-sized pH sensors for simultaneous far-red and near-infrared live bioimaging," *Journal of the American Chemical Society*, vol. 135, pp. 14863–14870, Sept. 2013.
- [460] M. Neu, D. Fischer, and T. Kissel, "Recent advances in rational gene transfer vector design based on poly(ethylene imine) and its derivatives," *Journal of Gene Medicine*, vol. 7, pp. 992–1009, Aug. 2005.
- [461] S. Ranary, A. S. Hoffman, and P. S. Stayton, "Antigen delivery with poly(propylacrylic acid) conjugation enhances MHC-1 presentation and T-Cell activation," *Bioconjugate Chemistry*, vol. 20, pp. 241–248, Feb. 2009.
- [462] B. H. Robinson, R. Petrova-Benedict, J. R. Buncic, and D. C. Wallace, "Nonviability of cells with oxidative defects in galactose medium: A screening test for affected patient fibroblasts," *Biochemical Medicine and Metabolic Biology*, vol. 48, pp. 122–126, Oct. 1992.
- [463] G. Hofhaus, D. R. Johns, O. Hurko, G. Attardi, and A. Chomyn, "Respiration and growth defects in transmittochondrial cell lines carrying the 11778 mutation associated with Leber's hereditary optic neuropathy," *The Journal of biological chemistry*, vol. 271, pp. 13155–61, May 1996.
- [464] R. Rossignol, R. Gilkerson, R. Aggeler, K. Yamagata, S. J. Remington, and R. a. Capaldi, "Energy Substrate Modulates Mitochondrial Structure and Oxidative Capacity in Cancer Cells," *Cancer Research*, vol. 64, pp. 985–993, Feb. 2004.

- [465] S. L. Fink and B. T. Cookson, "Apoptosis, pyroptosis, and necrosis: mechanistic description of dead and dying eukaryotic cells.," *Infection and immunity*, vol. 73, pp. 1907–16, Apr. 2005.
- [466] T. L. Riss and R. A. Moravec, "Use of multiple assay endpoints to investigate the effects of incubation time, dose of toxin, and plating density in cell-based cytotoxicity assays.," *Assay and drug development technologies*, vol. 2, pp. 51–62, Feb. 2004.
- [467] R. C. Scaduto and L. W. Grotyohann, "Measurement of mitochondrial membrane potential using fluorescent rhodamine derivatives.," *Biophysical journal*, vol. 76, pp. 469–477, Jan. 1999.
- [468] I. A. Cree and P. E. Andreotti, "Measurement of cytotoxicity by ATP-based luminescence assay in primary cell cultures and cell lines.," *Toxicology in vitro : an international journal published in association with BIBRA*, vol. 11, pp. 553–6, Oct. 1997.
- [469] K.-Y. Kim, M. V. Stevens, M. H. Akter, S. E. Rusk, R. J. Huang, A. Cohen, A. Noguchi, D. Springer, A. V. Bocharov, T. L. Eggerman, D.-F. Suen, R. J. Youle, M. Amar, A. T. Remaley, and M. N. Sack, "Parkin is a lipid-responsive regulator of fat uptake in mice and mutant human cells.," *The Journal of clinical investigation*, vol. 121, pp. 3701–12, Sept. 2011.
- [470] J. Brooks, J. Ding, J. Simon-Sanchez, C. Paisan-Ruiz, A. B. Singleton, and S. W. Scholz, "Parkin and PINK1 mutations in early-onset Parkinson's disease: comprehensive screening in publicly available cases and control.," *Journal of medical genetics*, vol. 46, pp. 375–381, June 2009.
- [471] S. L. Schmid and L. L. Carter, "ATP is required for receptor-mediated endocytosis in intact cells," *Journal of Cell Biology*, vol. 111, pp. 2307–2318, Dec. 1990.
- [472] J. M. Larkin, W. C. Donzell, and R. G. Anderson, "Modulation of intracellular potassium and ATP: effects on coated pit function in fibroblasts and hepatocytes.," *Journal of cellular physiology*, vol. 124, pp. 372–378, Sept. 1985.
- [473] S. L. Acton, P. E. Scherer, H. F. Lodish, and M. Krieger, "Expression cloning of SR-BI, a CD36-related class B scavenger receptor," *Journal of Biological Chemistry*, vol. 269, pp. 21003–21009, Aug. 1994.
- [474] D. Rhinds, L. Falstrault, C. Tremblay, and L. Brissette, "Uptake and fate of class B scavenger receptor ligands in HepG2 cells.," *European journal of biochemistry / FEBS*, vol. 261, pp. 227–35, Apr. 1999.
- [475] S. Nishimura, S. Takahashi, H. Kamikatahira, Y. Kuroki, D. E. Jaalouk, S. O'Brien, E. Koivunen, W. Arap, R. Pasqualini, H. Nakayama, and A. Kuniyasu, "Combinatorial targeting of the macropinocytotic pathway in leukemia and lymphoma cells," *Journal of Biological Chemistry*, vol. 283, pp. 11752–11762, Apr. 2008.
- [476] K. J. Sandgren, J. Wilkinson, M. Miranda-Saksena, G. M. McInerney, K. Byth-Wilson, P. J. Robinson, and A. L. Cunningham, "A differential role for macropinocytosis in mediating entry of the two forms of vaccinia virus into dendritic cells.," *PLoS pathogens*, vol. 6, p. e1000866, Apr. 2010.

- [477] B. Play, S. Salvini, Z. Haikal, M. Charbonnier, A. Harbis, M. Roussel, D. Laron, and D. Jourdheuil-Rahmani, "Glucose and galactose regulate intestinal absorption of cholesterol," *Biochemical and Biophysical Research Communications*, vol. 310, pp. 446–451, Oct. 2003.
- [478] E. Griffin, a. Re, N. Hamel, C. Fu, H. Bush, T. McCaffrey, and a. S. Asch, "A link between diabetes and atherosclerosis: Glucose regulates expression of CD36 at the level of translation.," *Nature medicine*, vol. 7, pp. 840–846, July 2001.
- [479] H. Farhangkhoe, Z. A. Khan, Y. Barbin, and S. Chakrabarti, "Glucose-induced up-regulation of CD36 mediates oxidative stress and microvascular endothelial cell dysfunction," *Diabetologia*, vol. 48, pp. 1401–1410, July 2005.
- [480] Z. Ravid, M. Bendayan, E. Delvin, A. T. Sane, M. Elchebly, J. Lafond, M. Lambert, G. Mailhot, and E. Levy, "Modulation of intestinal cholesterol absorption by high glucose levels: impact on cholesterol transporters, regulatory enzymes, and transcription factors.," *American journal of physiology. Gastrointestinal and liver physiology*, vol. 295, pp. G873–85, Nov. 2008.
- [481] J. H. Xue, Z. Yuan, Y. Wu, Y. Liu, Y. Zhao, W. P. Zhang, Y. L. Tian, W. M. Liu, Y. Liu, and C. Kishimoto, "High glucose promotes intracellular lipid accumulation in vascular smooth muscle cells by impairing cholesterol influx and efflux balance," *Cardiovascular Research*, vol. 86, pp. 141–150, Apr. 2010.
- [482] K. H. Song, J. Park, and H. Ha, "High glucose increases mesangial lipid accumulation via impaired cholesterol transporters," *Transplantation Proceedings*, vol. 44, pp. 1021–1025, May 2012.
- [483] H. Lu, K. Yao, D. Huang, A. Sun, Y. Zou, J. Qian, and J. Ge, "High glucose induces upregulation of scavenger receptors and promotes maturation of dendritic cells.," *Cardiovascular diabetology*, vol. 12, p. 80, May 2013.
- [484] J. D. Robertson, *Polymersome mediated intracellular delivery: A tool for research and treatment of infectious and inflammatory diseases*. PhD thesis, University of Sheffield, 2014.
- [485] B. K. Smith, S. S. Jain, S. Rimbaud, A. Dam, J. Quadrilatero, R. Ventura-Clapier, A. Bonen, and G. P. Holloway, "FAT/CD36 is located on the outer mitochondrial membrane, upstream of long-chain acyl-CoA synthetase, and regulates palmitate oxidation.," *The Biochemical journal*, vol. 437, pp. 125–134, July 2011.
- [486] A. L. McIntosh, B. P. Atshaves, H. Huang, A. M. Gallegos, A. B. Kier, and F. Schroeder, "Fluorescence techniques using dehydroergosterol to study cholesterol trafficking," *Lipids*, vol. 43, pp. 1185–1208, Dec. 2008.
- [487] S. Mukherjee, X. Zha, I. Tabas, and F. R. Maxfield, "Cholesterol distribution in living cells: fluorescence imaging using dehydroergosterol as a fluorescent cholesterol analog.," *Biophysical journal*, vol. 75, pp. 1915–1925, Oct. 1998.
- [488] M. Wójciak-Kosior, R. Paduch, A. Matysik-Woźniak, P. Niedziela, and H. Donica, "The effect of ursolic and oleanolic acids on human skin fibroblast cells.," *Folia histochemica et cytobiologica / Polish Academy of Sciences, Polish Histochemical and Cytochemical Society*, vol. 49, pp. 664–9, Jan. 2011.

- [489] F. Alemi, D. P. Poole, J. Chiu, K. Schoonjans, F. Cattaruzza, J. R. Grider, N. W. Bunnett, and C. U. Corvera, "The receptor TGR5 mediates the prokinetic actions of intestinal bile acids and is required for normal defecation in mice," *Gastroenterology*, vol. 144, pp. 145–154, Jan. 2013.
- [490] H. Yin, H. C. Kang, K. M. Huh, and Y. H. Bae, "Effects of cholesterol incorporation on the physicochemical, colloidal, and biological characteristics of pH-sensitive AB2 miktoarm polymer-based polymersomes," *Colloids and Surfaces B: Biointerfaces*, vol. 116, pp. 128–137, Dec. 2014.
- [491] J. J. Palmgrén, J. Mönkkönen, T. Korjamo, A. Hassinen, and S. Auriola, "Drug adsorption to plastic containers and retention of drugs in cultured cells under in vitro conditions," *European Journal of Pharmaceutics and Biopharmaceutics*, vol. 64, pp. 369–378, Nov. 2006.
- [492] D. Wüstner, "Improved visualization and quantitative analysis of fluorescent membrane sterol in polarized hepatic cells," *Journal of Microscopy*, vol. 220, pp. 47–64, Oct. 2005.
- [493] S. Kametaka, K. Moriyama, P. V. Burgos, E. Eisenberg, L. E. Greene, R. Mattera, and J. S. Bonifacino, "Canonical interaction of cyclin G associated kinase with adaptor protein 1 regulates lysosomal enzyme sorting," *Molecular biology of the cell*, vol. 18, pp. 2991–3001, Aug. 2007.
- [494] K. Wilkinson, J. D. Boyd, M. Glicksman, K. J. Moore, and J. El Khoury, "A high content drug screen identifies ursolic acid as an inhibitor of amyloid ?? protein interactions with its receptor CD36," *Journal of Biological Chemistry*, vol. 286, pp. 34914–34922, Oct. 2011.
- [495] B. Messner, I. Zeller, C. Ploner, S. Frotschnig, T. Ringer, A. Steinacher-Nigisch, A. Ritsch, G. Laufer, C. Huck, and D. Bernhard, "Ursolic acid causes DNA-damage, P53-mediated, mitochondria- and caspase-dependent human endothelial cell apoptosis, and accelerates atherosclerotic plaque formation in vivo," *Atherosclerosis*, vol. 219, pp. 402–408, Dec. 2011.
- [496] J. Mello-Vieira, T. Sousa, A. Coutinho, A. Fedorov, S. D. Lucas, R. Moreira, R. E. Castro, C. M. P. Rodrigues, M. Prieto, and F. Fernandes, "Cytotoxic bile acids, but not cytoprotective species, inhibit the ordering effect of cholesterol in model membranes at physiologically active concentrations," *Biochimica et Biophysica Acta - Biomembranes*, vol. 1828, pp. 2152–2163, Sept. 2013.
- [497] C. A. Lipinski, F. Lombardo, B. W. Dominy, and P. J. Feeney, "Experimental and computational approaches to estimate solubility and permeability in drug discovery and developmental settings," *Advanced Drug Deliv. Rev.*, vol. 23, pp. 3–25, Jan. 1997.
- [498] S. Mitsuda, T. Yokomichi, J. Yokoigawa, and T. Kataoka, "Ursolic acid, a natural pentacyclic triterpenoid, inhibits intracellular trafficking of proteins and induces accumulation of intercellular adhesion molecule-1 linked to high-mannose-type glycans in the endoplasmic reticulum," *FEBS Open Bio*, vol. 4, pp. 229–239, Jan. 2014.

- [499] K. D. Lindor, K. V. Kowdley, V. A. C. Luketic, M. E. Harrison, T. McCashland, A. S. Befeler, D. Harnois, R. Jorgensen, J. Petz, J. Keach, J. Mooney, C. Sargeant, J. Braaten, T. Bernard, D. King, E. Miceli, J. Schmoll, T. Hoskin, P. Thapa, and F. Enders, "High-dose ursodeoxycholic acid for the treatment of primary sclerosing cholangitis.," *Hepatology (Baltimore, Md.)*, vol. 50, pp. 808–814, Sept. 2009.
- [500] D. Fernandez-Lopez, J. Faustino, R. Daneman, L. Zhou, S. Y. Lee, N. Derugin, M. F. Wendland, and Z. S. Vexler, "Blood-Brain Barrier Permeability Is Increased After Acute Adult Stroke But Not Neonatal Stroke in the Rat," *Journal of Neuroscience*, vol. 32, pp. 9588–9600, July 2012.
- [501] N. S. Oltra, J. Swift, A. Mahmud, K. Rajagopal, S. M. Loverde, and D. E. Discher, "Filomicelles in nanomedicine from flexible, fragmentable, and ligand-targetable drug carrier designs to combination therapy for brain tumors," *Journal of Materials Chemistry B*, vol. 1, p. 5177, Sept. 2013.
- [502] J. D. Robertson, G. Yealland, M. Avila-Olias, L. Chierico, O. Bandmann, S. a. Renshaw, and G. Battaglia, "PH-sensitive tubular polymersomes: Formation and applications in cellular delivery," *ACS Nano*, vol. 8, pp. 4650–4661, May 2014.
- [503] D. Camer, Y. Yu, A. Szabo, and X. F. Huang, "The molecular mechanisms underpinning the therapeutic properties of oleanolic acid, its isomer and derivatives for type 2 diabetes and associated complications," *Molecular Nutrition and Food Research*, vol. 58, pp. 1750–1759, Apr. 2014.
- [504] Y. Ikeda, A. Murakami, Y. Fujimura, H. Tachibana, K. Yamada, D. Masuda, K.-I. Hirano, S. Yamashita, and H. Ohigashi, "Aggregated ursolic acid, a natural triterpenoid, induces IL-1 β release from murine peritoneal macrophages: role of CD36.," *Journal of immunology (Baltimore, Md. : 1950)*, vol. 178, pp. 4854–4864, 2007.
- [505] H. Takeshita, E. Tsubota, H. Takatsuka, T. Kunito, and J. Fujihara, "Cytochrome P450 2J2*7 polymorphisms in Japanese, Mongolians and Ovambos.," *Cell biochemistry and function*, vol. 26, no. November 2011, pp. 813–816, 2008.
- [506] B. Messner, I. Zeller, C. Ploner, S. Frotschnig, T. Ringer, A. Steinacher-Nigisch, A. Ritsch, G. Laufer, C. Huck, and D. Bernhard, "Ursolic acid causes DNA-damage, P53-mediated, mitochondria- and caspase-dependent human endothelial cell apoptosis, and accelerates atherosclerotic plaque formation in vivo," *Atherosclerosis*, vol. 219, pp. 402–408, Dec. 2011.
- [507] A. Federico, E. Cardaioli, P. Da Pozzo, P. Formichi, G. N. Gallus, and E. Radi, "Mitochondria, oxidative stress and neurodegeneration," *Journal of the Neurological Sciences*, vol. 322, pp. 254–262, Nov. 2012.